DEVELOPMENT OF COMPUTATIONAL MODELS TO PREDICT THE TOXICITY OF ADVANCED MATERIALS

A Thesis Submitted to
the Graduate School of Engineering and Sciences of
İzmir Institute of Technology
in Partial Fulfillment of the Requirements for the Degree of

DOCTOR OF PHILOSOPHY

in Material Science and Engineering

by
Eyüp BİLGİ

December 2023
İZMİR

We approve the thesis of **Eyüp Bilgi**

Examining Committee Members

Asst. Prof. Dr. Ceyda ÖKSEL KARAKUŞ
Department of Bioengineering
İzmir Institute of Technology

Prof. Dr. Haldun SEVİNÇLİ
Department of Material Science and Engineering
İzmir Institute of Technology

Asst. Prof. Dr. Onur SERÇİNOĞLU
Department of Bioengineering
Gebze Technical University

Assoc. Prof. Dr. Utku Kürşat ERCAN
Department of Clinical Engineering
İzmir Kâtip Çelebi University

Assoc. Prof. Dr. Efe SEZGİN
Department of Food Engineering
İzmir Institute of Technology

05 December 2023

Asst. Prof. Dr. Ceyda ÖKSEL KARAKUŞ
Supervisor, Department of Bioengineering
İzmir Institute of Technology

Prof. Dr. Erdal BEDİR
Co-advisor, Department of Bioengineering, İzmir Institute of Technology

Prof. Dr. Sedat AKKURT
Head of the Department of Material Science and Engineering

Prof. Dr. Mehtap EANES
Dean of the Graduate School of Engineering and Sciences

ACKNOWLEDGEMENTS

Firstly, I would like to thank my supervisor, Asst. Prof. Dr. Ceyda ÖKSEL KARAKUŞ, for her help and guidance throughout my thesis study. Her willingness to assist me in all aspects has been a source of great encouragement and has significantly contributed to my personal and professional growth (much like how she can spot a statistically significant trend from a mile away, she was always able to identify my weak spots and guide me towards improvement). I would also like to express my gratitude to her esteemed husband Halil Karakuş, who has always been with me and supported me throughout this process.

I would also like to express my sincere gratitude to my co-advisor, Prof. Dr. Erdal BEDİR, for his invaluable help and guidance since the beginning of my academic journey in 2008. I also want to thank Prof. Dr. Haldun SEVİNÇLİ and Asst. Prof. Onur SERÇİNOĞLU for their valuable contributions throughout this thesis and I would like to thank examining committee members Assoc. Prof. Dr. Efe SEZGİN and Assoc. Prof. Dr. Utku Kürşat ERCAN for their constructive criticism and guiding questions.

Also, I would like to thank The Scientific and Technological Research Council of Turkey (TUBITAK) for providing financial support to this project with a grant number of 118C229.

I also want to thank Prof. Dr. Hasan ŞAHİN for his support and for always being open to collaboration.

I am also thankful to my lab mates of Bionanolab, Muhammet Semih BAŞLAR, Aysel TOMAK, MELİSA TÜNCER and Selin ÇEŞMELİ, and Bedir Lab. Members Gamze DOĞAN, Gülten KURU, Göklem ÜNER, Melis KÜÇÜKSOLAK and Mustafa Ünver KURT.

I would like to extend my thanks to all the friends and instructors, both past and present, at IZTECH Bioengineering.

In the journey of research and discovery, I have learned that success is often a collective effort. Sharing knowledge leads to successful outcomes, but equally important is the sharing of challenges, which builds the motivation needed to overcome them. In this spirit, I want to extend my deepest gratitude to my dear friends and colleagues,

Muhammet Semih BAŞLAR, Gülten KURU, Gamze DOĞAN, Alper ŞAHİN, Ekin KESTEVUR DOĞRU, and Öykü SARIGİL.

I also would like to thank to my family, my mother Kadriye BİLGİ, my father İsmail Hakkı BİLGİ, my sister Yasemin BİLGİ ERLER and my brother Mustafa BİLGİ for their endless support, love and motivation during this study and my life. I would also like to thank my niece and nephews, Zehra ERLER, Ali ERLER, and Tunahan BİLGİ, for the joy and happiness they bring to our family.

Finally, I wish to express my infinite gratitude to my beloved wife, Çiğdem BİLGİ. Her presence has been my greatest support during this challenging journey. I am deeply thankful for her love, unwavering support, and for constantly boosting my motivation.

ABSTRACT

DEVELOPMENT OF COMPUTATIONAL MODELS TO PREDICT THE TOXICITY OF ADVANCED MATERIALS

The aim of this study is to harness computational power to enhance existing knowledge on NM safety and to optimize the use of existing nanotoxicity data. The primary goal is to support the safe(r)-by-design concept, necessitating early integration of safety considerations into NM design through structural manipulation strategies. This thesis focuses on three case studies: zinc oxide, silver, and gold NP, using data manually collected from the literature.

Analyses with zinc oxide and silver NP revealed a correlation between their toxicity and both internal (intrinsic properties, size, shape, surface charge) and external (cell and analysis-related properties) factors. For zinc oxide, it was found that coating had significant influence on cell viability, with a critical threshold identified at 20 μg/ml concentration and 10 nm size. Similarly, for silver NPs, concentration, size, and exposure time were significant factors. Coating with organic macromolecules increased cell viability, whereas green-synthesized NPs (using bacteria, plant extracts, algae) decreased it. The gold NP study highlighted that ensemble methods were more effective in elucidating complex relationships, with cellular uptake linked to particle size, zeta potential, concentration, and exposure time.

Overall, this thesis contributes to safer-by-design strategies, crucial for developing commercially viable and safe NMs. The findings advocate for a broader toxicity evaluation approach, considering various physicochemical aspects and experimental procedures. The complex interactions observed suggest that advanced algorithms are necessary for accurate modeling, supporting the optimization of experimental parameters in NP engineering for biomedical applications.

ÖZET

İLERİ MALZEMELERİN TOKSİSİTESİNİN TAHMİNLENMESİ İÇİN BİLGİSAYIMSAL MODELLERİN GELİŞTİRİLMESİ

Bu çalışmanın amacı, nanomateryal güvenliğine ilişkin mevcut bilgiyi geliştirmek ve mevcut nanotoksisite verilerinin kullanımını optimize etmek için hesaplama gücünden yararlanmaktır. Birincil amaç, yapısal manipülasyon stratejileri yoluyla güvenlik hususlarının nanomalzeme tasarımına erken entegrasyonunu gerektiren tasarım-aşamasında-güvenlik konseptini desteklemektir. Bu tez, çinko oksit, gümüş ve altın nanoparçacıkları (NP) üzerine yapılan üç ayrı araştırmayı ele almaktadır, bu araştırmalar literatürden el ile toplanan verilere dayanmaktadır.

Çinko oksit ve gümüş nanopartiküller ile yapılan analizler, bunların toksisitesi ile hem iç (içsel özellikler, boyut, şekil, yüzey yükü) hem de harici (hücre ve analizle ilgili özellikler) parametreler arasında bir korelasyon olduğunu ortaya koymuştur. Çinko oksit için, kaplamanın hücre canlılığını etkilediği, 20 µg/ml konsantrasyon, 12 saat maruziyet ve 10 nm boyutunun kritik bir eşik değerleri olduğu tespit edilmiştir. Benzer şekilde gümüş NP için konsantrasyon, boyut ve maruz kalma süresi önemli faktörler olarak belirlenmiştir. Organik makromoleküllerle kaplama hücre canlılığını artırırken, yeşil sentezlenen NPlerde (bakteri, bitki özleri, algler kullanılarak) canlılık azalmıştır. Altın NP çalışması, topluluk öğrenmesi yöntemlerinin, parçacık boyutuna, zeta potansiyeline, konsantrasyona ve maruz kalma süresine bağlı hücresel alımın karmaşık ilişkilerini açıklamada daha etkili olduğu gösterilmiştir.

Genel olarak bu tez, ticari olarak uygulanabilir ve güvenli nanomateryallerin geliştirilmesi için hayati önem taşıyan tasarım açısından daha güvenli stratejilere katkıda bulunmaktadır. Bulgular, çeşitli fizikokimyasal yönleri ve deneysel prosedürleri dikkate alan daha geniş bir toksisite değerlendirme yaklaşımını desteklemektedir. Gözlemlenen karmaşık etkileşimler, biyomedikal uygulamalar için nanopartikül mühendisliğinde deneysel parametrelerin optimizasyonunu destekleyen, doğru modelleme için gelişmiş algoritmaların gerekli olduğunu göstermektedir.

TABLE OF CONTENTS

LIST OF FIGURES

Figure **Page**

Figure **Page**

LIST OF TABLES

LIST OF ABBREVIATIONS

Abbreviation	Definition
1D	One Dimensional
2D	Two Dimensional
3D	Three Dimensional
ANN	Artificial Neural Network
ANOVA	ANalysis Of VAriance
AOP	Adverse Outcome Pathway
ATP	Adenosine TriPhosphate
Au	Gold
AUC	Area Under Curve
BA	Bootstrap Aggregation
BPNN	BackPropagation Neural Network
CART	Classification And Regression Tree
CAS	Chemical Abstracts Service
CLP	Classification, Labelling and Packaging
CNT	Carbon NanoTube
Conc.	Concentration
CT	Computed Tomography
Cu	Copper
DLS	Dynamic Light Scattering
DNA	DeoxyriboNucleic Acid
DoC	Declaration of Conformity
DT	Decision Tree
EC	European Commission
ECHA	European Chemicals Agency
EHS	Environmental, Health, and Safety
ELISA	Enzyme-Linked ImmunoSorbent Assay
EMA	European Medicines Agency
EPA	Environmental Protection Agency
EU	European Union
FDA	Food and Drug Administration

Abbreviation	Definition
FN	False Negative
FP	False Positive
GB	Gradient Boosting
GNB	Gaussian Naive Bayes
GNP	Gold NanoParticle
HSD	Honest Significant Difference
ICP	Inductively Coupled Plasma
InChI	International Chemical Identifier
ISO	International Organization for Standardization
KNN	K-Nearest Neighbor
LDH	Lactate DeHydrogenase
LightGBM	Light Gradient Boosting
LR	Logistic Regression
MAE	Mean Absolute Error
MIE	Molecular Initiating Event
MLR	Multiple Linear Regression
MRI	Magnetic Resonance Imaging
MTT	3-(4,5-diMethylThiazol-2-yl)-2,5-diphenylTetrazolium Bromide
NM	NanoMaterial
NP	NanoParticle
NT	NanoTube
OECD	Organization for Economic Cooperation and Development
PBPK	Physiologically Based PharmacoKinetics
PCA	Principal Component Analysis
PEG	PolyEthylene Glycol
PET	Positron Emission Tomography
PLS	Partial Least Squares
PMA	Pre-Market approval
PQA	Production Quality Assurance
PV	Production Verification
QMS	Quality Management System
QSAR	Quantitative Structure Activity Relationship

Abbreviation	Definition
REACH	Registration, Evaluation, Authorisation and Restriction of Chemicals
RF	Random Forest
RMSE	Root Mean Square Error
SAR	Structure Activity Relationship
SbyD	Safe by Design
SEM	Scanning Electron Microscopy
SMILES	Simplified Input Line Entry System
SPECT	Single-Photon Emission Computed Tomography
SPION	Superparamagnetic Iron Oxide Nanoparticle
SPR	Surface Plasmon Resonance
SS_{effect}	Sum of Squares of an effect
SS_{total}	Total Sum of Squares
SVM	Support Vector Machine
SVR	Support Vector Regression
TD	Technical Documentation
TE	Type Examination
TEM	Transmission Electron Microscopy
TN	True Negative
TP	True Positive
TUBITAK	The Scientific and Technological Research Council of Turkey
US	United States
UV	UltraViolet
w/wo	with or without
WST-1	Water-Soluble Tetrazolium
XGBoost	eXtreme Gradient Boosting
ZnO	Zinc Oxide

CHAPTER 1

INTRODUCTION

Nanomaterials (NM) are one of the most important double-edged swords of our modern age. Nanomaterials are characterized by having at least one external dimension in the 1-100nm range. This definition is widely accepted across various scientific bodies, including the European Commission, which further specifies that at least half of the particles in a nanomaterial should have a size of 100nm or below. At the nanoscale, materials exhibit unique physical and chemical properties that differ significantly from their larger-scale counterparts. These include variations in strength, electrical conductivity, reactivity, and optical properties. For instance, nanomaterials can have enhanced magnetic, electrical, optical, mechanical, and catalytic characteristics. These properties are not just a function of their size but can also be influenced by the shape, synthesis conditions, and functionalization of the nanomaterials. One of the key aspects of nanomaterials is their increased specific surface area compared to the same material at a larger scale. This increased surface area can lead to different behaviors and interactions with other materials or environments, which is a fundamental aspect of their unique properties. The definition and understanding of nanomaterials are crucial for a broad range of applications, from medical therapies and drug delivery systems to renewable energy technologies and advanced materials for electronics. The unique properties of nanomaterials at the nanoscale offer innovative solutions and enhancements in these fields, making their study and application a pivotal aspect of modern science and technology. The nanoscale materials exhibit a range of unique properties that are different from their bulk counterparts. For example, the physical (melting point, strength, hardness, reactivity, etc.), chemical (catalytic activity, optical properties, chemical stability, etc.), and biological (cellular uptake, viability, clearance, genotoxicity, etc.) properties may change at the nanoscale due to the increased surface area and the quantum effects (quantum confinement, quantum tunnelling, superparamagnetism, superconductivity etc.) that may occur in that scale. After a basic overview of nanomaterials and their wide-range applications in various industries, this thesis focuses on arguably the most critical

aspect of nanotechnology: the assessment and prediction of the toxicity of nanotechnology-enabled materials. Recognizing the dual nature of nanomaterials and promoting a balanced perspective on their revolutionary and potentially hazardous nature, the main goal of this work is to develop robust computational models that can accurately predict the toxicity of these materials. This effort is vital not only to advance the safe use of nanotechnology but also to reduce the potential health and environmental risks associated with these materials. This thesis aims to bridge the gap between the rapid development of nanomaterials and the understanding of their safety implications by providing a comprehensive approach to toxicity prediction. This will involve the investigation of various computational methods, including machine learning algorithms, to analyze and predict the toxicological profiles of advanced nanomaterials. The ultimate aim is to establish a predictive framework that can be used by scientists and industry professionals to assess the safety of novel nanomaterials, thus ensuring their responsible and sustainable application in various sectors.

1.1. Basic Terms and Definitions Associated with Nano

Although there is still no consensus on the definition of nanomaterials but yet their potential risks, it would be useful to make basic definitions of nanomaterials before delving into their possible risks [1-4].

Nano: One billionth of a meter (10^{-9}m) [5].

Nanoscale: The size range of the nanomaterials is generally accepted from 1 to 100 nm, but all submicron (≤1000 nm) could be accepted by some fields [6].

Nanoscience: The science and technologies comprise the study of phenomena and manipulation of materials at atomic, molecular, and macromolecular scales where properties differ significantly from those at larger scales, and the understanding of the fundamental physics, chemistry, biology, and technology of nanoscale objects [7, 8].

Nanotechnology: The branch of science that covers the development and application of materials, devices, and systems by controlling shape and size at the

nanometer scale. It is the field of science that aims to translate the knowledge and techniques obtained from different sciences into practice [9].

Nanomanufacturing: Any manufacturing phenomenon performed at the nanoscale. It comprises both top-down and bottom-up manufacturing approaches.

Nanomaterial (NM): A class of materials of which at least one dimension is sized between 1 and 100 nm.

Engineered NM: A subsection of NM that comprises the intentionally produced NMs [10].

Incidental NM: A subset of NMs that come into existence as a result of natural events (may also be named natural NMs) or incidental human activities rather than being engineered or manufactured with specific properties in mind [11].

Advanced materials: The materials that are designed or produced with the aim of adding or improving superior properties to existing materials, reducing production costs, or encouraging the development of new technologies and applications [12].

Nanoparticle: a particle that operates at the nanoscale, usually with all three dimensions in the range of 1 to 100 nm [13].

Nanorod: A type of nanoparticle characterized by its elongated shape in one dimension. Typically, nanorods have a significantly longer dimension than the other two, but the longest dimension remains within the nanoscale.

Nanoplate: A flat NP where one dimension (thickness) is significantly smaller compared to the other two but remains within the nanoscale range. They resemble small plates or discs and may have unique properties due to their geometry.

Nanofiber: an extremely thin fiber with a diameter in the nm range.

Nanostar: An NP with multiple points or arms extending from a central core reminiscent of the shape of a star.

Nanotubes: Cylindrical nanostructures with a diameter on the nanoscale. The most well-known are carbon nanotubes (CNTs), which are sheets of carbon that are one atom thick, rolled into a tube. Nanotubes can be single-walled or multi-walled. NTs can also be formed via lipids [14].

Nanowires: Extremely thin wires with a diameter on the nanoscale. They can be composed of various materials, including metals, semiconductors, or insulators.

Quantum Dots: Nanoscale semiconductor particles that exhibit quantum mechanical properties. They are distinctive in that they can emit different colors of light when excited, depending on their size.

Nanosphere: Spherical particles where all three dimensions are on the nanoscale.

Nanocone: A cone-shaped nanostructure with a circular base that tapers to a point.

Nanoshell: An NP consisting of a dielectric core coated with a thin metallic outer layer.

Nanoring: Ring-shaped nanostructures that may have magnetic properties distinct from those of linear nanostructures due to their closed-loop geometry.

Nanodisc: Disc-shaped NPs with a flat, circular shape whose height is significantly less than their diameter.

1.2. Common Machine Learning Algorithms Used in This Thesis

XGBoost: Stands for eXtreme Gradient Boosting. It is a scalable and efficient implementation of the gradient boosting framework by Tianqi Chen and Carlos Guestrin. XGBoost provides a parallel tree boosting that solves many data science problems quickly and accurately.

Random Forest (RF): A versatile machine learning method capable of performing regression and classification tasks. It uses multiple decision trees and outputs the class, which is the mode of the classes (classification) or mean prediction (regression) of the individual trees.

Bootstrap Aggregation (Bagging): A method that involves training the same algorithm many times using different subsets sampled from the training data. It improves the accuracy and stability of machine learning algorithms.

Light Gradient Boosting (LightGBM): A gradient boosting framework that uses tree-based learning algorithms. It is designed for distributed and efficient training.

Gradient Boosting (GB): A machine learning technique for regression and classification problems that produces a prediction model in the form of an ensemble of weak prediction models, typically decision trees.

Decision Tree (DT): A decision support tool that uses a tree-like model of decisions and their possible consequences, including chance event outcomes, resource costs, and utility.

K-Nearest Neighbors: A non-parametric method used for classification and regression. In both cases, the input consists of the k closest training examples in the feature space.

BPNN (ReLu, 4 neurons in hidden layer): A backpropagation neural network with the ReLu activation function in the hidden layer introduces non-linearity to the model.

Support Vector Regression (RBF kernel): An extension of Support Vector Machines (SVMs) to regression problems, it uses the same principles as SVM for classification but with a different loss function.

AdaBoost: A machine learning meta-algorithm that can be used with many other learning algorithms to improve performance..

Bayesian Ridge: Implements Bayesian ridge regression, a linear regression with a probabilistic approach.

Stochastic Gradient Descent: A simple yet very efficient approach to fitting linear classifiers and regressors under convex loss functions such as (linear) Support Vector Machines and Logistic Regression.

Ridge Regression with Cross-Validation: A way to perform Ridge Regression, a type of linear least squares with l2 regularization, with built-in cross-validation of the alpha parameter.

Generalized Additive Models: A statistical model that is a non-parametric extension of generalized linear models, allowing for flexibility in modeling.

Huber Regression: A type of robust regression that is less sensitive to outliers in data than traditional regression methods.

Support Vector Regression (linear kernel): Similar to SVR with RBF kernel, it uses a linear kernel to predict the values of a new dataset.

Poisson Regression: A regression model is used when the dependent variables are count data.

Tweedie Regression: A type of regression useful for modeling positive continuous data with exact zeroes.

Theil-Sen Regression: A non-parametric regression method that chooses the median slope among all lines through pairs of two-dimensional sample points.

An artificial neural network (ANN): A computational model that mimics the structure and functioning of the human brain to process information and generate outcomes. It consists of layers of interconnected nodes, called neurons, with each

connection representing a synapse that can transmit signals between neurons. ANNs are capable of learning from data through a process called training, where the weights of the connections are adjusted to minimize the difference between the actual output and the predicted output by the network.

1.3. Non-testing Approaches for Regulatory Testing

Traditional methods for assessing chemical toxicity rely largely on *in vivo* animal testing. This practice requires significant financial and temporal resources as well as ethical concerns regarding animal welfare [15]. Rapid advances in innovative technologies, such as nanotechnology, are causing a large number of NMs to appear on the market rapidly. In addition, changes in existing technologies such as biotechnology require the urgent adoption of alternative evaluation methods that avoid (or at least reduce the use of) animal testing [16]. Although practitioners and regulators clearly express the need for these methods, and the incentives in this direction are increasing day by day, the developments do not yet coincide with the targets [17]. However, the numerous advantages inherent in non-testing methods are widely recognized, and they have significant potential in many fields, including the hazard assessment of NMs.

The concept of "non-testing" for hazard assessment encompasses the use of computational technologies, molecular modeling, and chemical databases to inform risk management decisions with greater efficiency and precision [18]. This approach prioritizes the safe production and use of products, protecting not only people and the environment but also manufacturers by reducing possible negative impacts, as it significantly reduces the time and financial resources required from design to market [19]. Since NMs are highly researched products, non-assay methods offer significant opportunities to leverage these available data effectively and facilitate early-stage safety assessments of new materials [20]. The main misconception about these methods is that they will eliminate the need for current experimental approaches and nullify the use of animals in experiments. On the contrary, *in silico* methods provide invaluable support in making sense of existing data and elucidating possible mechanisms of toxicity, making it possible to identify missing data sets and what additional experiments need to be performed - with the minimum

number of experiments possible that will allow meaningful conclusions to be drawn [21, 22]. Despite all their potential, the main reason why these methods are not widely used in the industry is that common and clear rules have not been fully established by the industry and regulators. In order to demonstrate the usability of these methods for hazard assessment, reliability, and compliance, studies must be carried out in a transparent manner and documented in regulatory contexts [23].

It is possible to divide non-testing methods into three main types, namely grouping and read-across approaches, structure-activity relationship methods, and expert systems. These categories are interconnected as they all operate on the premise that structurally similar compounds will exhibit similar biological activities [24]. The data they examine vary in their complexity, involving analytical processes, expert judgments, and mechanistic interpretations.

These methods are particularly promising in terms of effectively using available data, providing mechanistic explanations for priority setting, and filling data gaps necessary for categorization, classification, labeling, and risk assessment processes [25]. In this thesis, the potential applications of various computer-aided methods in risk assessment will be highlighted, including their roles in establishing categories, identifying hazards, filling regulatory data gaps, and prioritizing NMs for further testing.

Despite the advantages of non-testing methods in chemical safety assessments, the difficulties in integrating these alternative methods into regulatory frameworks are complex enough in their current state. The situation becomes more challenging when elements that have very complex interactions with biological systems, such as NMs, are added to the models being developed. The first two chapters of this thesis aim to review how these methods can contribute to hazard and risk assessment and risk reduction in a regulatory context.

Non-testing methods hold considerable promise for making the best possible use of existing data, providing mechanistic interpretation for priority setting, and filling data gaps required for categorization, classification, labeling, and risk assessment processes. The potential use of different computer-assisted methods in risk assessment is summarised in Table 1.1.

Table 1.1. Potential use of non-testing methods in risk assessment

Non-Testing Method	Potential Use in Risk Assessment
GROUPING AND READ-ACROSS APPROACHES	Chemical category formation Hazard identification Filling data gaps for regulatory purposes Prioritisation of chemicals for further testing
MACHINE LEARNING AND STATISTICAL APPROACHES CORRELATING ACTIVITY WITH THE STRUCTURE	Chemical category formation Hazard identification Identification of toxicity-related properties Hazard minimization through safe-by-design Prioritisation of chemicals for further testing
PHYSIOLOGICALLY-BASED PHARMACOKINETIC MODELS	Prediction of internal-dose at a target organ Risk assessment extrapolations (inter/intra-species, high-low doses, route to route)
ADVERSE OUTCOME PATHWAYS	Chemical category formation Prioritisation of chemicals for further testing Providing mechanistic explanations Integration of testing strategies

1.3.1. Grouping – Category Formation

Risk assessment processes can be simplified by grouping chemicals or NMs with common properties relevant to safety and environmental impact based on physical, chemical, optical, electromagnetic, and biological similarities. In this way, it is possible to predict the behavior of non-tested compounds within the groups and reduces the need for new individual tests. Considerations related to creating strong categories and strengthening the existing ones are explained below [26-28]:

- Defining the Category: Inclusion criteria within the category should be determined, and these criteria should facilitate grouping.

- Data Collection: For each member in the categories, the largest possible amount of data that can be related to the endpoint should be collected (physical, chemical, biological).
- Determination of Common Features: Common features within the collected data should be revealed.
- Classification: Each member should be placed into appropriate categories based on common characteristics.

To establish and enhance categories effectively, several key considerations are outlined below [28, 29]:

- ✓ Maximum Category Size: Placing all possible individuals in the data set into a certain category can increase the power of predictions for untested products.
- ✓ Recognize Member Variability: Understand that while members share common features, their behaviors might differ. Consider these differences in making predictions.
- ✓ Document Expert Judgment: Since forming categories often involves expert opinions, document the data and reasoning behind the categorization decisions thoroughly.

In addition to the primary considerations for establishing and enhancing categories, there are important guidelines and requirements provided by international organizations that should be taken into account:

- o OECD (The Organization for Economic Cooperation and Development) Guidance: The OECD offers detailed guidance documents on the principles and methodologies for chemical grouping.
- o ECHA Information Requirements: ECHA's guidance on information requirements and chemical safety assessment provides insights into data needs for forming categories.

1.3.2. Read-Across

Read-across facilitates the estimation of missing data for untested items (target) by utilizing information from similar, well-studied items (source). This technique plays an important role in fulfilling regulatory requirements, filling data gaps, and making informed decisions when it is impractical to test each item individually [28, 30]. Figure 1.1. summarize the potential benefits of the read-across strategies.

Fundamental similarities are considered: Similarities between substances include structure, physicochemical properties (e.g., solubility, ionization state) [31], activity/ mode of action (e.g., (eco)toxicological effects, fate) [32], reactivity (e.g., chemical or biological) and metabolic pathways (e.g., formation of common metabolites) [33]. In the assessment of substances for safety and regulatory purposes, there are primarily two approaches employed to make predictions:

- *Analog approach*: Uses data from a single source compound to make predictions. While convenient, data-rich categories are generally favored due to increased confidence in predictions [25].
- *Category approach*: Uses data from multiple source compounds within a defined category, offering higher confidence and more reliable generalizations due to the larger pool of data [34].
-

Ensuring a robust implementation of read-across involves several critical steps, which are [35]*:*

- ✓ Identify a group of substances with common characteristics.
- ✓ Establish a strong rationale for the similarity between source and target substances using multiple lines of evidence (e.g., structural, physicochemical, mechanistic).
- ✓ Use experimental data from source substances to predict the unknown value for the target substance.
- ✓ Extend the justification with additional mechanistic data to strengthen confidence in the predictions.

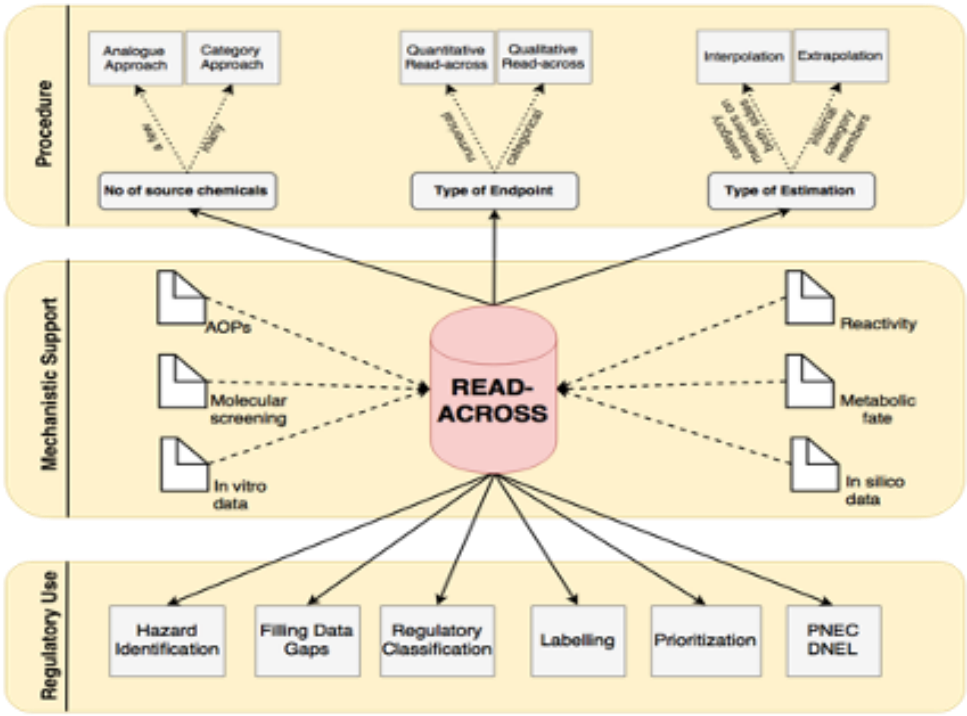

Figure 1.1. Read-across approach.

Uncertainty in the data directly affects forecast accuracy, so data quality assessment is crucial. The first step to address uncertainty for regulatory acceptance [36-38] is to ensure the adequacy and quality of the data sets used for prediction. In Figure 1.2. the relation between the source and type of uncertainty is summarized [37]. There is a need to go beyond structural similarities and include bioavailability, reactivity, metabolic profiles, and mechanistic information for a more comprehensive similarity assessment.

Another important issue is to provide clear and comprehensive documentation to demonstrate the robustness of the read-across process and results. Lack of transparency and incompleteness may hinder acceptance by regulatory agencies.

Figure 1.2. The interrelationships between the sources and types of uncertainty in a read-across [37].

Additional considerations for greater trust are preferred data-rich categories over analog approaches for greater confidence [38-40].

- Interpolation rather than extrapolation where possible as it carries lower uncertainty due to staying within data boundaries.
- Complementary evidence: Combine *in vitro, in silico*, omics, and adverse outcome pathway (AOP) information to strengthen predictions and provide mechanistic links.
- Transparent and defensible presentation of read-across hypotheses and findings to increase regulatory acceptance.

While read-across inherently involves some subjectivity and uncertainty, these can be minimized by the practices outlined above. By utilizing additional supporting data, a greater number of substances, multiple rationales, and transparent documentation, read-across can significantly contribute to effective and reliable chemical safety assessments and thus promote informed regulatory decision-making.

Integrating the concept of Adverse Outcome Pathways (AOPs) into NM grouping represents a future direction with considerable potential to enhance read-across predictions and lessen the regulatory burden for nanomaterials (NMs). AOPs detailing the biological steps from an NP-specific initiating event to an adverse outcome could increase confidence in predictions by ensuring that grouped NMs likely share similar toxicity pathways[41]. This approach requires consideration of how AOPs can be systematically related to NM properties and potentially involves new types of data analysis and interpretation [42].

Validation of read-across assumptions and similarity rules should go beyond traditional physicochemical comparisons [35]. By combining data from multiple sources, such as high-throughput analyses, *in silico* methods, and molecular screening specifically designed for NMs, a more comprehensive view of NM similarity can be obtained, and prediction accuracy can be improved [43-45]. However, this approach involves integrating various types of data, which can present unique challenges in terms of data compatibility and analysis [46].

Developing a reliability indicator specifically for NM read-across predictions would provide a quantitative measure of the uncertainty involved [47]. Such an indicator would assist regulators in assessing whether predictions are sufficiently robust for decision-making and help bridge the gap between scientific analysis and regulatory requirements [23].

1.4. Application of Machine Learning and Statistical Modelling Approaches to Structure-Activity Relationships (SAR) for NMs

The use of machine learning and statistical modeling in NM SAR analysis is a powerful tool for predicting NMs based on their properties and biological effects [48]. NM

SAR is a mathematical model that links the biological activities or properties of NMs to their physicochemical and structural properties [49]. The field of nanotoxicology relies heavily on this approach, which evolves continuously through ongoing modifications and advancements [50].

In NM SAR models, the biological activity of NMs is related to their properties, a relationship that can be expressed quantitatively by mathematical equations. This requires a dataset of NMs with well-characterized biological effects and corresponding physico-chemical and structural descriptors [50]. Machine learning and statistical methods ranging from simple data visualization tools to complex techniques such as random forests, decision trees, and neural networks are used to develop these mathematical models [51, 52]. The focus here is to assess the suitability of these methods for NM SAR modeling and to investigate how they can further improve the reliability and applicability of predictions of the *in silico* models.

Improving read-across predictions through advanced methodologies is a key focus for the future development of approaches to nanomaterials (NMs). The integration of SAR and AOP concepts. By combining these approaches with machine learning and statistical modeling, a more holistic and accurate system for predicting NM behavior and toxicity can be developed [52]. This would include not only an in-depth understanding of NM properties and biological activities, but also a comprehensive assessment of the pathways leading to adverse outcomes [53].

Such integrative approaches can support a more efficient, accurate, and ethically responsible evaluation of data obtained by traditional testing methods. The main challenge encountered at this point is to create regulatory contexts for these methodologies on NMs, which have many ambiguities (which will be detailed in the next chapter). Ongoing research and collaboration among scientists, regulators, and industry stakeholders are crucial to achieving this goal.

General information about the approaches that can potentially be used in the hazard assessment of NMs is explained below.

1.4.1. Decision Trees

Decision trees (DTs), powerful machine learning methods, have great potential in the field of NM risk assessment and regulatory decision-making [54]. DTs are created based on existing data, and tree-like decision-making structures are created by separating them first into branches and then into leaves, according to data characteristics [55]. These structures can be used predictively to classify and measure the toxicity of NMs [55]. In general, DTs stand out in the following areas, contributing to overcoming the difficulties in assessing the toxicity of NMs.

1. Ability to reveal underlying causes: DTs help to automatically scan data, determine the parameters that are effective in revealing the mechanisms underlying the toxic effects of NMs, and manufacture safer materials from the information obtained about these descriptors.

2. Diversity Recognition: It allows data, that is not evenly distributed, to be processed properly [56].

3. Transparency in Decisions [57]: Regulatory choices must be reliable, repeatable, clear and well explained. DTs make decisions within the framework of simple rules. In this way, it contributes to the transparency of the decisions and evaluations made by both researchers and regulators.

1.4.2. Multiple Linear Regression (MLR)

MLR models, which include algorithms with unique advantages such as Lasso Regression, Elastic Net Regression, Ordinary Least Squares, Least Angle Regression, Principal Component Regression, Partial Least Squares Regression, and Bayesian Linear Regression, are important tools for hazard assessment of NMs [58]. These approaches reveal simple relationships between NM properties and the possible toxic effects of these properties.

The main factor that limits their widespread use in the impact evaluation of structures that have complex interactions with biological systems, such as NMs, is that

these models are insensitive to complex and nonlinear interactions and operate on the assumption of linearity. Additionally, since these methods require a specific data-variable ratio, model-building studies can be difficult.

Methods such as principal component analysis (PCA) can be used to improve the success of MLR outputs [59]. However, it would still be a rational approach to use more complex machine learning algorithms to accurately predict the complex effects of NMs and reveal nonlinear relationships.

1.4.3. Partial Least Squares (PLS)

PLS is a linear regression approach; it has the potential to be used in modeling the toxicity of NMs as it has the capacity to expand the information revealed by traditional MLR and DTs [60-62]. PLS can expand the usage area of DTs by contributing to the management of the complexity in large and overlapping data sets encountered in NM studies and allows for overcoming the linearity limitation of MLR methods [63]. The feature of being robust in the presence of noise also makes this method ahead of others. PLS is also a powerful approach to detecting parameters affecting the endpoint, enabling a more holistic evaluation.

Unlike the simplicity of classical MLR models, PLS creates latent variables to capture important interactions within the dataset, thereby enhancing the stability and accuracy of the predictive model. Its ease of implementation and interpretation has broadened its application in various scientific fields. PLS's compatibility with the rule-based logic characteristic of decision trees, along with its transparency, makes its results particularly valuable. These features also facilitate the use of PLS models within the decision-making mechanisms of regulatory institutions. Despite its strengths, PLS, primarily focused on linear relationships like other MLR models, may not fully succeed in capturing the complex nonlinear interactions between NMs and biological systems.

To address this limitation, there are ongoing studies focused on developing extensions to PLS using decision trees (DTs), kernel methods, and artificial neural networks, which are good at modeling nonlinear relationships [64-66]. These innovative methodologies could play an important role in unraveling the complex interactions

between NMs and biological systems. The decision-making clarity provided by DTs, combined with the inherently simple structure of these advanced PLS models, makes them a promising approach to assessing the hazard of NMs. Consequently, these versatile approaches are leading to the development of ensemble methods, which integrate the principles of various methods for more comprehensive analysis.

1.4.4. Artificial Neural Networks

Artificial Neural Networks (ANNs) are computational models that simulate human brain processes such as data input, thought, decision-making, memory, reasoning, and action for problem-solving. By integrating statistical methods and machine learning, ANNs have the capability to produce highly accurate and quantifiable predictions based on the models they create using existing data sets [67]. Despite their complex internal structure, often referred to as a 'black box,' which can complicate practical applications, ANNs are increasingly utilized due to their superior performance in QSAR studies [68-71]. A significant advantage of ANNs is their ability to reveal both linear and nonlinear interactions between variables in the data set and endpoints, as well as to provide insights into hidden variables that may have been overlooked. They are often perceived as black-box models because the relationship they model between output and input can be challenging to interpret [72]. However, with the use of genetic algorithm-based feature selection, it is possible to eliminate redundant variables. Sensitivity analysis can be employed to reduce data sizes and to elucidate the significance of different inputs on the model's results [73].

ANNs, in assessing the human health and environmental impacts of NMs, offer significant contributions to risk assessors, regulators, end-users, and even manufacturers [74, 75]. These methods not only analyze existing data but also identify gaps within datasets, highlighting the need for further experiments. This approach facilitates the acquisition of more comprehensive data through fewer experiments.

Ensuring the reliability of these models through experimental verification is crucial. Such verifications can demonstrate the models' effectiveness and potentially lead to their acceptance by regulatory bodies and manufacturers. For this process to be

efficient, it is important to report the results and functionalities of the models in a detailed manner [76]. A clear presentation of all parameters and hyperparameters is essential for experimentally verifying the reliability of the models [77].

In summary, the integration of machine learning and statistical modeling, especially ANNs, into QSAR analysis is an important step forward in toxicological research. It shifts the focus from individual assessments to an integrated hazard screening approach that can predict chemical toxicity based on structural and physical properties. These computational methods play an important role in bringing new chemicals to market more efficiently and effectively. However, the regulatory acceptance of QSAR models, especially for complex NMs and nanosystems, is still a matter of ongoing debate. Given the diversity and complexity of NM classes, the acceptance of *in silico* models is likely to be determined on a case-by-case basis. The use of existing data with computational tools also offers opportunities for designing inherently safer NMs through structural modifications. Integrating safety into the design of nanoscale materials is one of the most effective risk reduction strategies, but its implementation faces challenges in maintaining the desired properties and commercial viability of materials during product design changes.

1.5. PBPK Modeling for NM Risk Assessment

In the field of traditional risk assessment, the process typically consists of four stages: identification of hazards, assessment of dose-response relationships, assessment of exposure, and characterization of risk. Dose-response evaluation involves determining the highest exposure dose at which a recognized hazard does not produce adverse effects. Originally developed to track the concentration of exogenous substances (chemicals) in the body over time, Physiologically Based Pharmacokinetics (PBPK) modeling holds significant potential for evaluating the effects of NMs [78]. PBPK models contribute to more accurate modeling of NM exposure consequences by focusing on the internal dose that remains after excretion rather than the external dose. The inclusion of factors such as different organisms, dose levels, and exposure routes in these models is leading to the widespread use of a cumulative approach in NM hazard assessment [78, 79]. The data

obtained from these models significantly aid in the evaluation, reporting, and establishment of appropriate regulations.

1.6. Adverse Outcome Pathways

The Adverse Outcome Pathway (AOP) is an approach that seeks to explain the sequence of events, starting from the interactions of NMs at the molecular level (known as the Molecular Initiating Event, or MIE), leading to the adverse outcomes resulting from these interactions [80]. Rather than focusing solely on the endpoint, it aims to understand the underlying reasons for these outcomes. As such, AOP is recognized as one of the leading methods in NM hazard assessment, noted for its comprehensiveness and ability to provide detailed and clear explanations.

AOPs typically consist of three key elements: MIE, a series of intermediate events, and the final adverse outcome [81]. The MIE represents the beginning of the interaction between an NM and a biological target, followed by key events leading to a toxic response. Potential applications of AOPs in regulatory environments for NMs include [82];

- Setting priorities for additional testing focused on specific targets,
- Helping to establish chemical categories relevant to NMs,
- Providing mechanistic justification for cross-reading predictions in nanotoxicology,
- Informing comprehensive testing strategies,
- Predicting overall toxicity outcomes at the organismal level.

The level of validation and precision required for effective implementation of AOPs depends on their specific use. Criteria specific to each application are required for AOPs to be accepted by regulatory authorities, especially if they replace conventional testing. It is crucial to quantify the variability and uncertainty in downstream events in the AOP framework to increase trust among stakeholders. Setting realistic expectations

about the capabilities and limitations of AOPs is crucial as it will contribute to strengthening scientific and regulatory confidence in AOPs. This approach supports the transition from traditional, costly, and ethically challenging animal testing in chemical safety assessment for NMs to alternative testing methods more suitable for regulatory purposes [83].

1.7. Perspectives on *In Silico* Methods

Assessment of chemical and biological safety is crucial for making informed decisions about substances humans encounter, particularly in the context of NMs. Traditionally, this evaluation has heavily relied on animal testing, relying on the assumption that data from animals can predict potential human side effects. However, due to the often insufficient correlation of these data with human outcomes and rising ethical concerns, the use of animal experiments has been restricted or even banned in many areas, like the cosmetics industry. This shift has encouraged the development of non-animal testing methods. The common features expected from these methods can be summarized as follows: they should yield faster results, not cause ethical concerns, be cost-effective, and be easily applied and interpreted.

In silico methods, increasingly utilized in conjunction with data from *in vivo* and *in vitro* experimental approaches in NM hazard assessment, hold significant potential in this concept. These methods do not claim to eliminate the need for experimental data. Rather, they can enhance the analysis of existing data, yielding clearer and more interpretable results. They can identify gaps in datasets, suggest minimal additional experimental setups required, and provide mechanistic insights or predictions about biological effects. Consequently, *in silico* methods have the potential to bridge the gap between *in vitro* studies and *in vivo* research, leading to more accurate results with reduced reliance on animal testing.

The shift to integrated hazard screening encouraged by policymakers and regulatory agencies aims to replace individual animal-based toxicity testing with more comprehensive and humane approaches. However, this shift is hindered by the lack of clear guidelines for the application of non-testing methods in a standardized regulatory

context, resulting in limited acceptance in regulatory and industrial circles. The reliability of these computational models for predicting NM toxicity depends on their validation against real-world results and acceptance by the scientific community, manufacturers, and regulatory authorities.

Addressing nanoscale applications, especially in assessing NM cytotoxicity and cellular uptake, introduces additional complexity due to the diverse nature of NMs. As the field of nanotoxicology continues to develop, the use of predictive models for evaluating newly produced NMs is still in an evolution phase and demands further research. This effort involves collecting and standardizing a vast array of existing literature data on NMs to enable effective analysis through machine learning algorithms. By employing a spectrum of models, ranging from simple to complex and linear to nonlinear, we can significantly enhance our understanding and prediction of NM behavior. The success of this approach depends on interdisciplinary collaboration, which requires open communication and understanding between academic experts (such as experimenters, toxicologists, and modelers) and industry and regulatory professionals.

Utilizing the power of accumulated data and advanced machine learning techniques documented in the literature enables the pioneering of a 'safer by design' approach in NM manufacturing. This strategy not only enhances NM safety but also facilitates responsible development and utilization of nanotechnologies, aligning with ethical standards and regulatory requirements. This paradigm shift, enabled by *in silico* methods, signifies a critical advancement in the development of NMs that are safe for both human health and the environment.

CHAPTER 2

BIOMEDICAL NANOMATERIALS: APPLICATIONS, TOXICOLOGICAL CONCERNS AND REGULATORY NEEDS

2.1. Background

Advances in cutting-edge technologies such as nano- and biotechnology have created an opportunity for re-engineering existing materials and generating new nano-scale products that can function beyond the limits of conventional ones. While the step change in the properties and functionalities of these new materials opens up new possibilities for a broad range of applications, it also calls for structural modifications to existing safety assessment processes that are primarily focused on bulk material properties. Decades after the need to modify existing risk management practices to include nano-specific behaviors and exposure pathways was recognized, relevant policies for evaluating and controlling health risks of nano-enabled materials is still lacking. This review provides an overview of current progress in the field of nanobiotechnology rather than intentions and aspirations, summarizes long-recognized but still unresolved issues surrounding materials safety at the nanoscale, and discusses key barriers preventing generation and integration of reliable data in bio/nano-safety domain. Particular attention is given to nanostructured materials that are commonly used in biomedical applications.

2.2. Introduction

Advanced materials that operate at the nano-bio interface exhibit novel or enhanced characteristics not observed in the bulk. While these unprecedented properties

of nanostructured materials make them promising candidates for diverse applications, these scale-specific properties may also trigger undesirable health or environmental consequences [84]. Although the health and safety risks of NMs (NMs) and their effective regulation has been given a great deal of attention over the past decades [85-88], science has not yet provided clear answers to the questions surrounding the safety of NMs.

Increasing evidence confirms that the main principles of traditional risks assessment also apply to NMs, so scientists and regulators have shifted their focus from developing a *completely new* risk assessment methodology to *modifying* existing practices to encompass the unique features of nanoscale materials [89]. However, as NMs are very complex systems and are still a relatively new technology, tailoring existing regulations to properly address nano-scale risks is yet to be completed.

While many questions still need to be answered in nano-safety research, a growing number of NMs continue to attract attention because of the potential benefits they provide to a wide range of industries and markets. In particular, nanostructured biomaterials in medicine promise to improve many key aspects of disease prevention, diagnosis, and treatment [90-92]. The nanomedicine industry is on the cusp of a major revolution and is expected to grow to $350 billion by 2025 [93]. While the growth potential of nano-enabled products in nanomedical industries is undeniably high, exaggerating potential benefits (the well-known Gartner technology hype cycle) is as problematic as overstating potential health risks as it contributes to public distrust of nanotechnologies [94].

Here, we discuss potential factors hampering effective assessment of health and safety risks of NMs within the regulatory context. We start by highlighting the long-standing but still unresolved problems in nano-safety research, and the key issues leading to data artefacts and controversies in nanotoxicology. We then discuss the latest medical applications of NMs, and how to assess the associated health risks given the lack of technical standards, consensus and legal frameworks.

2.3. Ambiguities Around Nano

NMs are structures having one or more dimensions smaller than 100 nm, with surface to volume ratios orders of magnitude larger than bulk materials that may trigger

specific hazardous properties. While the link between hazard and particle size alone is still unclear, the scientific evidence to date [95-98] suggests a growing controversy about the effects of long-term exposure to NMs, intensified by lack of standardized terminologies and methodologies [99, 100]. In particular, precise definitions and class labels are needed to avoid regional or sectoral differences in how NMs are defined, and to define sub-classes to which specific attention and regulatory assessment is more urgent. Despite many committees, reports and recommendations [101-104], the question of how to define, categorize and regulate NMs remains mostly controversial (Figure 2.1).

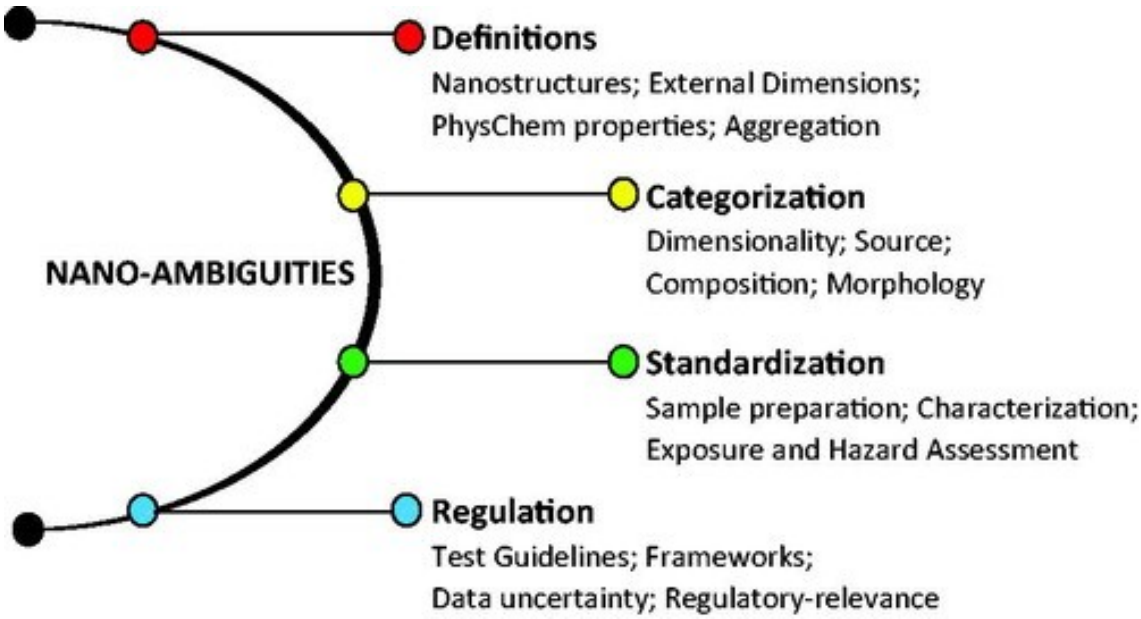

Figure 2.1. Ambiguities in NMs.

2.3.1. Ambiguity 1: Defining NMs

The problem with nano starts with definition, which have been a roadblock in deciding whether a material is a *NM* for which special legal requirements may apply. The European Commission's (EC) definition of NM, *a natural, incidental or manufactured material containing particles, in an unbound state or as an aggregate or as an agglomerate and where, for 50% or more of the particles in the number size distribution,*

one or more external dimensions is in the size range 1-100nm, is based on particles' external dimensions and does not cover nanoscale internal/surface structures. The International Organization for Standardization (ISO) includes nanostructures in its definition of NMs, *material with any external dimension in the nanoscale or having internal structure or surface structure in the nanoscale*, where nanoscale is defined as the size range from approximately 1–100 nm. The European Cosmetics Regulation provides an independent definition that incorporates insolubility and/or (bio)persistence, *insoluble or biopersistent and intentionally manufactured material with one or more external dimensions, or an internal structure, on the scale from 1 to 100 nm*.

Definition problems are exacerbated by the fact that NMs cannot simply be defined by their formula, and their characteristics cannot be represented by a single value. Moreover, size-dependent changes also occur in bulk properties of different materials at sizes above 100 nm. However, we stress that while conceptual ambiguity in the definition of NMs still persists (and likely always will), the definition itself serves as a guide for differentiating NMs from their bulk equivalents, not for separating hazardous materials from non-hazardous ones [105]. Clearly, as materials properties do not undergo a sudden, dramatic change once one dimension falls below 100 nm, definitions of what constitute NMs will never be completely precise. The current definitions of different types of NMs are likely to be useful and workable in the future.

2.3.2. Ambiguity 2: Categorizing NMs

Categorization of NMs is another area of research that has received considerable attention, but more work is needed [106-108]. A chemical category represents a group of chemicals sharing at least one similar physical, chemical and/or biological feature relevant to risk assessment. Category formation through grouping chemicals with common behaviour or consistent trends into distinct classes is usually intended to streamline the risk assessment and decision-making process. To date, several distinct categories of NMs have been defined according to their source (natural or synthetic), dimensionality (1D, 2D and 3D), composition (carbon-based, inorganic, organic and composite/hybrid) and morphology (high aspect ratio and low aspect ratio) [109]. Despite

the concerted efforts to establish science-based grouping approaches for NMs, there is still no consensus on how to apply, validate and report nano-specific grouping concepts in a regulatory context [34]. In particular, in order to group NMs according to their risk potential to eliminate the need to test every NM for every endpoint, we need improved understanding of the factors that control biological effects at the nanoscale.

When considering similar NMs as a group and applying grouping concepts for regulatory risk assessment purposes, special attention must be given to (1) justifying grouping criteria on multiple bases to validate initial category hypothesis, (2) forming information-rich categories with the highest possible number of potential members, (3) describing the logic of and data defining category formation, and (4) reporting the posterior probability that each group member follows the biological profile of reference substances.

The similarity principle has been used by chemical regulatory bodies, allowing simplified labelling of chemicals likely to have similar risk and hazard profiles. For NMs, recent developments in experimental and computational characterization of NM structures and other physicochemical properties and the relative success of read across methods have opened the door to similar categorization (labelling) of NM with similar risk and hazard profile in the future.

2.3.3. Ambiguity 3: Nanometrology and Standardization

NMs can generate new toxicological risks that are poorly understood or are contradictory, leading to greater uncertainty than the well-known risks of bulk materials or industrial chemicals. Lack of standardization of experimental procedures and methods involved in the preparation, characterization, and toxicological evaluation of NMs [110] is a major contributor to inconsistency and uncertainty in the field. This is particularly relevant for complex NMs whose physicochemical and toxicological properties are highly variable, environment-specific, and difficult to test.

Regulatory and standardization communities (e.g. FDA, EPA, ECHA, ISO and OECD) are strongly committed to development of validated methods for characterizing as-received intrinsic properties and medium-dependent extrinsic properties of NMs, and

to identifying the exposure/hazard posed by NMs to humans and the environment. Compared with the measurement of pristine properties free of the influence of biological environments, assessing properties of NMs that change over time or in different biological fluids is less standardized and more technically challenging.

This ambiguity is more difficult to address as it bears on how NMs are recognized by cells and other biological systems. The 'sizes' or NMs clearly depend on the environments in which they impact biological systems, depending on corona properties and how these modulate biological uptake. Pristine NM sizes are useful to characterize the initial average sizes and size distributions of NMs but we need to become better at predicting the change in NM size and surface composition in different environments. Lack of knowledge of the dynamic changes that occur when NMs are in biological or environmental compartments blunts our ability to understand and predict how NMs are taken up by cells. As the characterization of corona composition and its evolution in biological systems improve, we will gain increasing confidence in predicting the 'biological relevant entity' that ultimately affects the biological responses to NMs. Once the methods and procedures for NM testing in appropriate environments are developed and fully validated, they need to be converted into regulatory-relevant, practical recommendations.

2.3.4. Ambiguity 4: Regulating NMs

Nanotechnology was at an early stage of development when the EU's REACH Regulations came into force in 2007 [111]. These regulations aimed to ensure safe production, use and import of substances. The developments in nanotechnology triggered a need for modification of the EU's existing chemical legislation to cover nanoscale forms of materials. This was partly addressed by amending the REACH Regulation annexes [112] and corresponding ECHA guidance [113]. However, these changes have been based on knowledge from relatively simple NMs (e.g. metal oxides and carbon-based materials) that are smaller versions of familiar bulk substances. The capability of updated REACH annexes and guidance documents to estimate and manage potential impacts of more complex, functional NMs already in medical use remains to be tested.

These four ambiguities (i.e. definitions, categorization, standardization and regulation) add to the existing complexity in nano-EHS (Environmental, Health, and Safety) issues. Firstly, difficulties in finding a universally agreed definition and classification of a NM differentiated from its bulk correspondent present serious challenges for the nano-safety research and the safe use of NMs outside the research environment. Secondly, identifying the most important NM properties and functions contributing to their toxicity is only possible with the availability of reliable and extensive characterisation are available; this is currently limited by methodological complexities. Lastly, the uncertainties about regulatory requirements for NMs have direct impact on selecting relevant toxicity endpoints for risk assessment and judging the acceptability of measured risks on the basis of risk-benefit considerations for each NM. Resolving these ambiguities by generating new data, developing new tools to learn from the data and discovering new ways of interpreting the data would directly benefit nanosafety research in multiple ways. For example, the ability to group NMs based on structural/physicochemical similarity would enable regulators to focus their limited testing resources on NMs of high toxicity concern, and to fill data gaps without requiring additional time and cost-intensive animal studies. Moreover, having clear frameworks and guidelines detailing what qualifies as NM and what properties/endpoints need to be tested as part of regulatory risk assessment would help incorporate safety into the design stage and ensure regulatory clarity that improves compliance. In order to resolve remaining ambiguities in nanoscience, it is essential to establish an international network of scientists with multi-disciplinary expertise, policymakers and industry leaders fully committed to ensuring safer nanotechnology and nano-enabled products.

2.4. Regulatory Hazard Assessment of NMs

It is now generally agreed that [89, 114] nanotoxicity is not as *specific* as it was first thought to be, so it is unlikely that completely new risk assessment protocols will be required. However, there are additional issues that apply specifically to NMs, such as interference with toxicity assays [115] and formation of the protein corona [116, 117]. Questions like ‘which tests are reliable for identifying potential health effects of NMs’ and ‘how to

translate the acquired knowledge into a regulatory context' need to be clarified in order to avoid false positives or negatives and misinterpretation of toxicity data in nano-safety research. Key steps to consider for hazard assessment of NMs are summarized in Figure 2.2.

The paucity of faster methods of synthesis and characterization means that we are exploring a minute fraction of possible NMs. This in turn means that data that could be used to train ML models of NM structure-activity and structure-property relationships is sparse. The models are therefore less predictive and even those that perform well have small domains of applicability, limiting their use to leverage existing experimental data into new regions of NM space. Clearly, expanding the scale of synthesis and characterization will provide greater insight into the properties of NM that can be used to design improvements, and will have the added benefit of substantially improving the predictivity and applicability of ML models of NM properties. If these models are more predictive and more widely applicable, it makes possible more rational 'safe-by-design' NMs.

The inability to predict *in vivo* impacts of NMs is largely due to the cost and ethical limitations of animal testing, and the relatively poor correlations between *in vitro* assessments of the biological effects of NMs and their *in vivo* effects. Use of organ-specific cell lines derived by regenerative medicine techniques, and a better understanding of how NM impacts on biological systems as assessed by omics technologies inform toxicity mechanisms, should allow *in vivo* effects of NMs to be more accurately predicted without substantially increasing animal testing. All of these developments will provide much better tools for regulatory agencies to assess or even predict the likely risk and hazard of new NMs, allowing appropriate regulation.

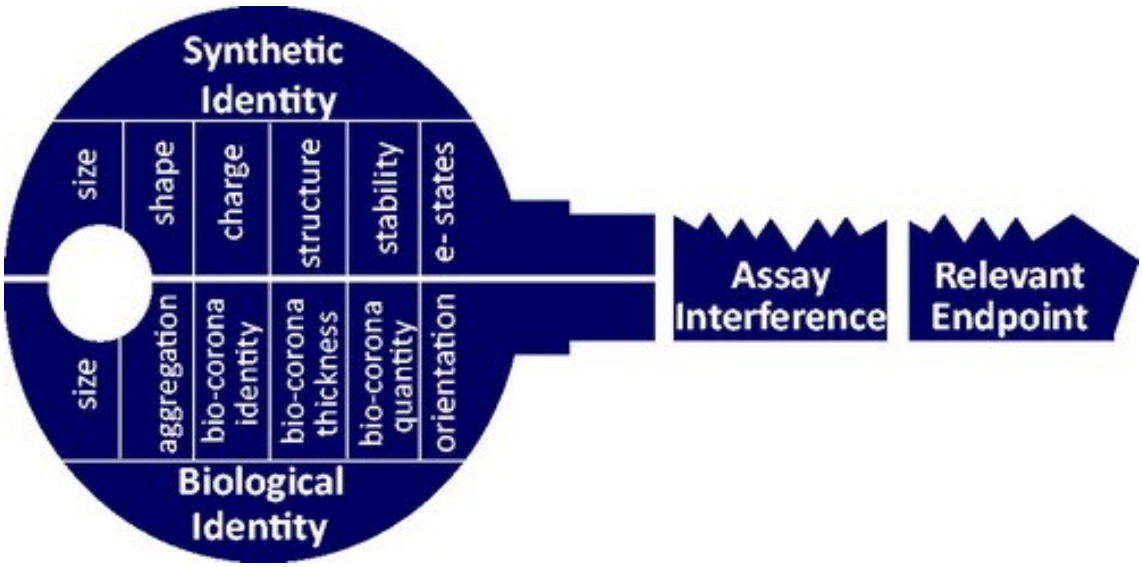

Figure 2.2. Key aspects associated NMs' hazard assessment.

2.4.1. Understanding the Physicochemical Identity of NMs

A thorough understanding of the *physicochemical* and the *biologically-relevant entities* is critical for linking biological activity to intrinsic materials properties, and to allow toxicity to be predicted for untested materials using these structure-activity relationships [118]. This knowledge can be also be used to reduce the toxicity of substances through structural modifications and to *design-out* hazards without compromising performance (so-called safety-by-design) [119]. In addition to designing out toxicity during the development of new NMs, the knowledge of toxicity-driven nano-scale properties would further assist in understanding the mechanisms by which NMs interact with biological systems and prioritizing which NMs should be subject to extensive experimental investigation.

There is still no scientific consensus on the minimum set of relevant characteristics for toxicological evaluation. The key physicochemical features considered important in the majority of cases [120-122] include: morphological characteristics (particle size, shape and their distribution); surface characteristics (chemistry, charge, and modifications); solubility; and colloidal stability and state of agglomeration. Numerous studies in recent years have shown that NMs may display size-dependent [123-126], shape-

dependent [127-130] and surface-dependent [131-133] toxicity. Table 2.1 lists the key toxicity-related physicochemical parameters of NMs.

Table 2.1. The key toxicity-related physical, chemical, and behavioral parameters of NMs

Property Type	**Key Property**
Physical Properties	Particle size (mean and distribution)
	Particle shape (dimensions and aspect ratio)
	Specific surface area
	Density
	Porosity
	Roughness
	Viscosity
Chemical Properties	Composition (core, surface, overall)
	Surface properties (charge, coating, affinity)
	Functionalization
	Purity/impurities
	Chemical Structure
	Crystallinity/defects
	Redox activity
Behavioural Properties	Solubility
	Dispersibility
	Corrosivity
	Dissolution rate
	Degradation rate
	Dustiness
	Hydrophobicity
	Surface reactivity
	Aggregation/agglomeration

The key considerations when characterizing NMs prior to toxicological evaluation are:

(1) measuring not only 'as-received' intrinsic properties but also properties in relevant media;

(2) quantifying a single characteristic over an extended period of time using multiple techniques, especially when a priori knowledge on the parameter of interest is unavailable for the test material;

(3) providing detailed information (metadata) on measurement conditions, such as sample preparation, pH value, and concentration [134].

2.4.2. Understanding the Biologically Relevant NM Identity

In biological fluids, the surfaces of NMs are immediately coated by a layer of adsorbed proteins (the protein corona) and ions. These materials have high affinity for biomolecules and ions resulting in their physicochemical identity being transformed into a biological one (the biologically relevant entity). This is a dynamic process in which the composition of the corona changes in different biological fluids, and over time as more abundant lower affinity proteins are replaced by less abundant higher affinity proteins. Since the toxic potential of NMs depends on their size and surface characteristics [133, 135, 136], the risk they pose may also change accordingly when they are aggregated or coated with other molecules in biological environments. Moreover, biological entities such as cells interact with the entire NM-corona complex (Figure 2.3), not just with the core NM. Therefore, it is critically important to investigate protein corona formation and its structure prior to toxicity testing [116]. Such knowledge may help understand the true correlation between structural features and biological effects and explain some of the inconsistencies in *in vitro* and *in vivo* studies.

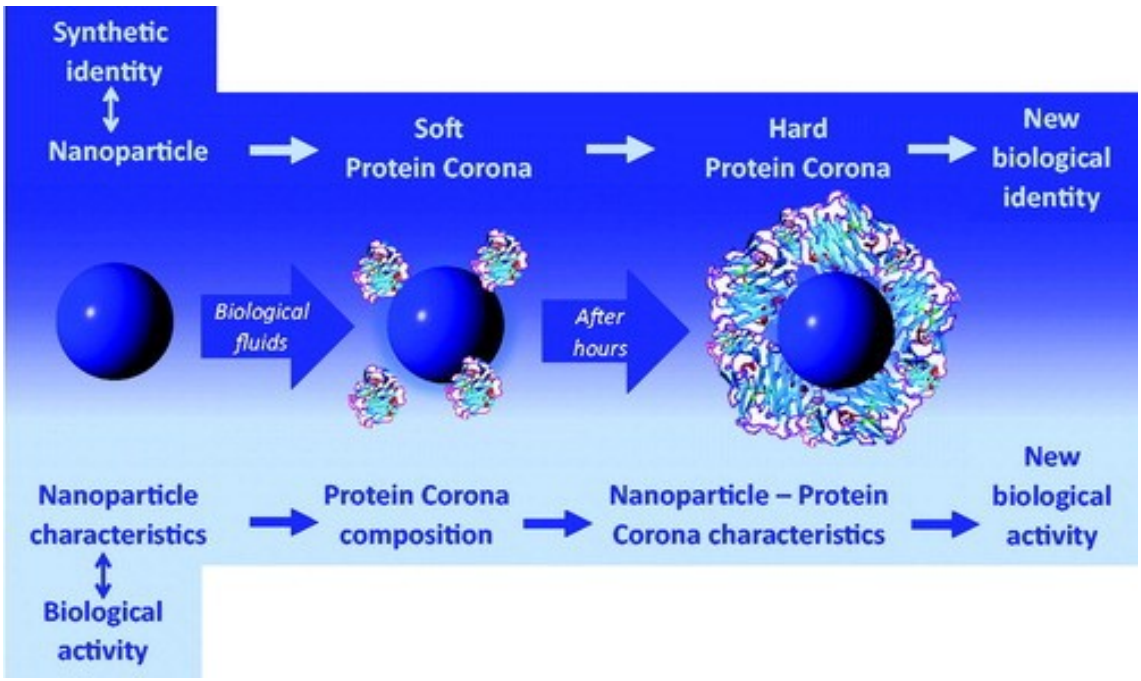

Figure 2.3. NM-corona complex formation steps

Currently, the main concern in nanotechnology-related EHS research is not only to identify which physicochemical or biological properties are responsible for toxicological effects but also to link hazard with toxicity-related features in a quantitative way. Altering the biological activity by modifying toxicity-related properties is only possible if the relationship between physicochemical characteristics, toxicity and the desired functionality is mathematically defined. The field of computational nanotoxicology has emerged to meet this need but it is challenged by lack of sizeable and consistent datasets, the complexity of nanostructures, and a need for more multidisciplinary trained researchers in this new field. More data on *in vitro* and *in vivo* effects of well-characterized NMs are needed for data-driven methods to reach their full potential and to fully decode the relationship between physicochemical structure and biological activity.

2.4.3. Understanding the Main Entry Routes of NMs

NMs may enter the human body by inhalation, ingestion or skin contact, and travel in the bloodstream to internal organs where they can cause harm. The main routes by which NMs can enter the body are shown in Figure 2.4.

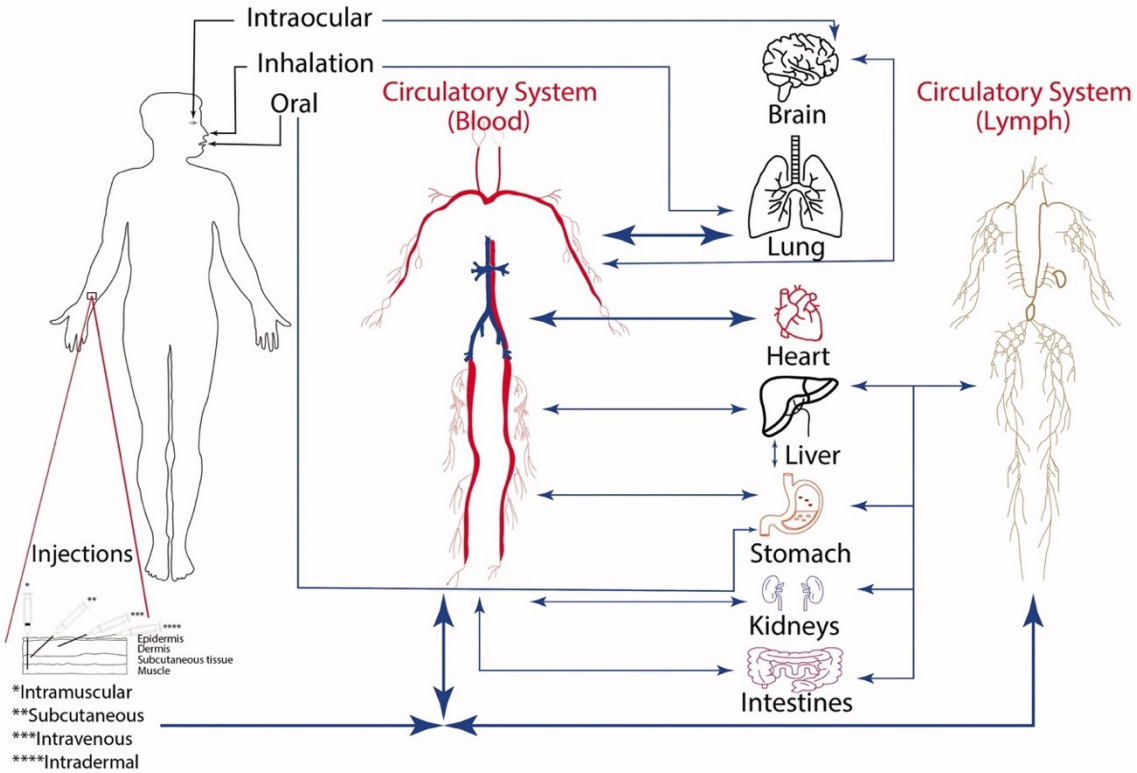

Figure 2.4. The main routes that can NMs enter the body.

It is now well known that the majority of non-targeted NMs tend to accumulate in the liver or spleen [137]. Most preliminary studies have shown that a large fraction of uncoated NMs that are distributed to major organs such as liver are cleared by the immune system within a short period of time [138]. However, accumulation in secondary organs following long-term exposures and the biological mechanism by which NMs are immunologically sequestered from the body need further investigation. While no vital danger has been proven, scientific evidence so far provides incomplete picture of the

organ distribution and clearance of NMs (and their agglomerates) from the body [139]. Such understanding is important for not only predicting the potential toxicological implications of accumulated NMs in human tissues and organs, but also controlling the biodistribution of NMs with the ultimate aim of targeting unhealthy cells (e.g. tumours) while leaving the healthy ones intact [140].

2.4.4. Understanding How NMs Affect Testing Systems

Reliability of existing *in vitro* approaches for the assessment of NMs health hazard potential has been a subject of continued debate for the past two decades. Although the question of 'which tests can be safely used to assess the hazard of NMs' continues to arouse controversy, expert consensus favours the use of testing systems with minimum interference potential (e.g. interference of NMs with nanotoxicology assays or assay reagents) to avoid under- or over-estimation of toxicity.

An important technical limitation of conventional assays is caused by putative interference between NMs and the assay system [115]. While assay interference is not a new phenomenon, specific properties of NMs (e.g. increased surface area, catalytic activity, optical and magnetic characteristics) can interfere with assays that rely on changes in absorbance or fluorescence to provide information on cellular activities. Several recent studies have exemplified NM interference with *in vitro* systems [141-143], generating both false positive or false negative results. For example, NMs have been shown to absorb analytes, react with assay components, release chemical species and cause side reactions [144]. Therefore, systematic evaluation of possible NM-assay interferences under realistic conditions is essential to ensure valid interpretation of test results. This will lead to necessary protocol modifications and nano-specific interference controls. As most of the traditional *in vitro* methods exist for the identification of toxicological hazards have not been specifically validated for each NM class, possible interferences and solutions given in Table 2.2, are more general in nature and not specific to any NM.

The ways in which potential assay interferences depend on particular physicochemical properties, working conditions of the assay, and the loading/exposure protocols applied makes drawing general conclusions about the reliability of certain tests

for all NMs very difficult. With so many factors contributing to assay interference, a paucity of knowledge on possible interference mechanisms, and the fact that NMs exhibit novel physicochemical properties, confidence in the results of toxicity testing can only be achieved by validating each assay for each NM formulation, and using complementary assays for common endpoints, especially if doubt exists. It is also advisable to use appropriate controls, realistic concentrations, and maintain a high level of suspicion when inspecting test results so as to detect and control interferences that may lead to erroneously high or low results.

2.4.5. Testing Nano-Hazards

Conventional toxicity assessment relies primarily on animal testing that is very costly, slow, and ethically problematic. With the rapid development of new materials and strong growth in existing technologies (e.g. biotechnologies), the need for faster and cheaper non-animal test methods for regulatory applications has become urgent.

The term non-animal testing in the context of hazard assessment refers to the use of human cells/tissues (*in vitro*) and computer-modelling (*in silico*) methods as alternatives to *in vivo* animal testing. *In vitro* approaches are employed world-wide to detect adverse effects of NMs such as cytotoxicity [145, 146], immunotoxicity [147, 148] and genotoxicity [149-151]. In particular, the ability of NMs to trigger oxidative stress in biological systems is the most frequently reported cause of nanotoxicity [152, 153]. However, the oxidative potential should be seen as a toxicological parameter rather than the main mechanism of nanotoxicity as the observed link could be a *consequence* of NM-induced toxicity, not necessarily the *cause* [154]. While conventional *in vitro* assays are an important first step toward assessing the potential risks of NMs, there is a need to establish fully validated test systems and procedures to bring old practices in line with the products of new technologies. In particular, the correlation between *in vitro* and *in vivo* responses needs to be made more robust if *in vitro* methods are to be used as viable surrogate assays to replace animal testing.

Table 2.2. Assay-specific interferences and possible solutions

Assay	Test	Potential Interference	Potential Solution
Cell Viability	LDH	Optical interference Inactivation/adsorption of LDH	Use lower concentrations Use cell-free controls
	Neutral Red	Dye adsorption Interference with readout system	Use lower concentrations Intensive washing steps
	Annexin V	Interaction with serum proteins	Confirm with other assays Use spike-in controls
	ATP	Optical interference	Avoid light emitting NMs
	TUNEL	Nonapoptotic DNA cleavage	Confirm with other assays Digest proteins
Metabolic Activity	MTT MTS XTT WST1	Optical quenching/interference Interaction with formazan salts, serum proteins or dye	Use lower concentrations Pre/post-spike controls Centrifugation Use modified salts Adapt cells to serum-free medium
Oxidative Stress	EPR ESR	Interaction with paramagnetic molecules	Use stable probes
	H_2DCF-DA	Optical quenching or interference	Thoroughly wash samples Confirm with other assays
Inflammation	ELISA	Interaction with Interleukins-cytokines	Careful design Pre-test using cell-free media
Genotoxicity	COMET	DNA fragmentation	Confirm with other assays Use lower concentrations Prevent agglomeration
	Micronucleus	Interference of cytochalasin-B	Careful design (serum, exposure time/order)

In silico approaches make much better use of the available experimental data on hazard, allowing new knowledge to be extracted that can be used to 'design in' safety for new materials without compromising desired functionality [155]. Clearly, most non-testing approaches are data driven, requiring experimental information to train them and cannot (yet) completely replace animal testing in toxicology. However, these methods are capable of making maximum use of often scarce and expensive experimental data,

providing insights into toxicity mechanisms, filling data gaps, prioritizing potentially problematic materials for testing, and reducing animal testing by eliminating non-critical experimental processes. The current state of research on the use of *in silico* methods and issues still to be addressed, are summarized in a recent review [156]. Although there is a profound interest among policy-makers and the scientific community to move from animal-based individual toxicity assessments toward a more integrated hazard screening approach, the lack of practical guidance on the harmonized use of non-animal testing methods in regulatory context has resulted in low regulatory and industrial acceptance so far [157]. The key to the successful uptake of alternative methods by scientists and regulators is to transparently demonstrate the reliability and relevance of their outcomes for hazard screening and assessment purposes.

2.4.6. Using Realistic Concentrations and Dose

The basic concept of toxicology, *the dose makes the poison*, has not been fully adopted in the field of nano-safety [158]. Selection of realistic exposure concentrations and physiologically relevant measures of dose is needed (and currently lacking) for meaningful comparison of *in vitro* outcomes with previously published *in vitro* data and *in vivo* biological responses [159]. Unlike conventional materials whose toxic doses can solely be described by administered mass or concentration, NMs requires a careful adaptation of traditional dose-metrics as mass alone is often not sufficient to describe their property-dependent dose-response relationship [160]. Earlier *in vitro* nanotoxicity studies have reported studied doses in mass units (μg/mL), ignoring surface- or number-related effects [161]. With the recognition of the need to move beyond mass-only metrics for NMs, various dose-metrics such as particle number, volume, surface area, and body burden have been suggested, each with some limitations. In the absence of universally agreed dose measures that can adequately reflect NM exposure, reporting concentrations in a range of dose metrics will allow for different interpretations of exposure. Special attention should be given to NM dispersion preparation and characterization to ensure accurate dosimetry and delivered to cell doses of particles [159].

2.4.7. Translating Knowledge into Regulatory Outcomes

Generating reliable nano-hazard data is one issue but translating these pre-normative research results into regulatory outcomes is an entirely different problem. In general, regulators' early concerns about lack of nanotoxicity data have been replaced by lack of regulatory-relevant data. Although large volumes of nanotoxicity data have been generated in the last two decades [162], the vast majority of these data suffer from consistency problems between replicate samples, methods, analysts, or laboratories. Much of this provides information of NM *hazard*, while modelling of the resulting *risk* when NMs are used in diverse workplaces and exposure scenarios, is less well developed. In the absence of reliable and consistent data needed to broaden the scope of existing laws to cover nano-specific issues, regulators take a precautionary approach or use the best available evidence to regulate NMs. However, overly cautious measures that are disproportionate to the real risk may stifle innovation, progress in the field of nanotechnology, and commercial applications. On the other hand, failing to properly address possible risks from nano-enabled products may have severe effects on public health and the environment, resulting in a backlash against NMs. The main risk management challenge under considerable uncertainty is to find the right balance between real risk and benefit.

Newly acquired information can only be applied to regulatory tasks if the key policymakers and legislators are able to translate, interpret and extrapolate it. Therefore, the key to the successful integration of new information and knowledge into regulatory frameworks and decision-making processes is to transparently demonstrate the reliability and relevance of their outcomes for regulatory purposes. To facilitate the flow of information from production to policy use, following barriers need to be addressed:

- providing an easy access to data,
- generating verifiable, consistent and high-quality data,
- fostering interdisciplinary and collaborative research,
- developing working relationships between policy making bodies, regulatory authorities and other relevant stakeholders,
- and increasing openness of regulatory bodies to new information and tools.

2.4.8. Comparison with Current FDA/EMA Regulations and Guidance in Related Fields

The Food and Drug Administration (FDA) and European Medicines Agency (EMA) have comprehensive regulations and guidance documents for drugs and medical devices, some of which provide insight into how biomedical NMs could be regulated. The FDA has classifications for ~1,700 different types of devices and has grouped them into 16 medical specialties (panels). Each type of device is assigned to one of three regulatory classes based on the level of control required to assure device safety and effectiveness:

(1) Class I General Controls e.g. nasal oxygen cannulas, manual stethoscopes, and hand splints represent a low risk to the patient.

(2) Class II General Controls and Special Controls represent the majority of medical devices e.g. tracheal tubes, bone plates, elbow joint radial prostheses. These are typically surgically implanted into the body or by some other medical intervention and represent a moderate risk to the patient.

(3) Class III General Controls and Premarket Approval e.g. aortic valves, constrained metal hip prostheses, and coronary stents with the highest patient risk.

The assigned class determines what premarketing submission/application is needed for FDA clearance to market. If your device is classified as Class I or II, and if it is not exempt, a 510k premarket notification is required.

The EMA regulates new drugs and medical devices. It evaluates the quality, safety and efficacy of marketing authorisation applications for drugs, medical devices and medical devices that also incorporate a medicinal product. As Table 3 shows, medical device classification and regulation in the US and EU are similar. The way these are regulated into three main classes provides possible guidance for streamlined regulation of NMs, as is suggested in Table 2.3.

In the EU, NMs are defined as any other substances under the both existing REACH and CLP regulations. An EU definition of a NMs is used to help harmonise how NMs are defined across REACH and CLP legal frameworks. Specific REACH legal

requirements apply to companies that manufacture or import nanoforms: characterisation of nanoforms or sets of nanoforms covered by the registration (Annex VI); chemical safety assessment (Annex I); registration information requirements (Annexes III and VII-XI); and downstream user obligations (Annex XII). Since REACH and CLP cover NMs, the European Chemicals Agency (ECHA) must carry out its tasks for nanoforms within the various REACH (e.g. registration, evaluation, authorisation and restrictions) and CLP processes (e.g. classification and labelling) as it would for any other form of a substance.

Miernicki et al. recently discussed the issues involved in regulation of NMs from an EU perspective [163]. They made the following recommendations for the regulation of NMs that would benefit not only European law, but other jurisdictions in which legal approaches to NMs are considered.

(1) NM definitions should be clarified by avoiding ill-defined terms and by including clear thresholds (e.g. for solubility in the Cosmetics Regulation) for the sake of legal certainty and workability of the regulations.

(2) Nano-specific regulations that are not workable in practice cannot fulfil their function, e.g. to protect humans and the environment, and thus need adaptation.

(3) Adaptation clauses should be harmonized and include clearer distinction between technical/scientific aspects to be adapted by the Commission and political/risk management aspects that should remain within the responsibility of the legislator.

(4) Product manufacturers should carry the burden of proof for the NMs' origin.

(5)The 50% by number threshold should be replaced by a threshold of 1% by weight to make definitions workable with current particle analysis methods, contributing to a more balanced cost–benefit relation in the regulatory nano-framework and its enforcement.

Table 2.3. A simplified summary of medical device classification and regulation in the EU and US and possible implications for NM regulation.

EU classifications and regulatory requirements		**US classifications and regulatory requirements**		**Possible implications for NM classifications and regulatory requirements**	
Class I	Declaration of conformity by manufacturer, registration of product	*Class I, largely external, low risk to patient*	Most devices exempt from FDA notification/regulation, and listing requirements apply	*Class I, low hazard materials, confined in matrices, negligible uptake by humans or environment, low risk*	Exempt from full notification, summary of NM properties and risk profile
Class I measuring or sterile	Notified Body approval is required to assess the sterility or measuring aspects of the device				
Class IIA	Conformity assessment by a Notified Body (QMS, TD for device category, PQA, PV, DoC)	*Class II, surgically or otherwise implanted, medium risk to patient.*	510(k) application for new/modified devices to demonstrate substantial equivalence to a predicate device. If not equivalent, PMA application	*Class II, medium or high hazard NMs in inert matrix, some potential for uptake during manufacture or disposal, medium risk*	Simplified registration as a new chemical under REACH/CLP and US EPA
Class IIB	Conformity assessment by a Notified Body (QMS, TE, TD for generic device group, PQA, PV, DoC)				
Class III	Conformity assessment by a Notified Body (QMS, TE, TD for every device, PQA, PV, Consultation, DoC)	*Class III, surgically implanted, high risk to patient*	PMA application to provide scientific evidence to support safety/efficacy, unless pre-amendment Class III device	*Class III, high hazard NMs, or medium risk used internally in man, high risk*	Full registration as a new chemical under REACH/CLP and US FDA/EPA

(QMS: Quality Management System; TD: Technical Documentation; PQA: Production Quality Assurance, PV: Production Verification; DoC: Declaration of Conformity; TE: Type Examination; FDA: Food and Drug Administration; PMA: Pre-market approval; REACH: Registration, Evaluation, Authorisation and Restriction of Chemicals; CLP: Classification, Labelling and Packaging; EPA: Environmental Protection Agency)

2.5. Biomedical Applications of NMs

Rapid developments in (bio)medical research and technology has contributed to increasing human life expectancy, which has resulted in an increase in the number of ageing patients requiring medical care [164]. NMs can play important role in early diagnosis and treatment of serious illnesses such as cancer. A short summary of biomedical technologies employing NPs are summarized below. Interested readers are referred to recent, comprehensive reviews in this field [165-173].

2.5.1. Contrast Enhancing Agents in Biomedical Imaging

NM selective accumulation in tumours, and their ease of functionalization, make them important contrast enhancing agents in biomedical imaging [174]. Dipeptide NPs [175], semiconductor quantum dots [176], thermosensitive fluorescent rhodamine 6G NPs [177], pyrene loaded supramolecular micelles [178], conjugated NPs [179] and functionalized fluorescent dyes (PEGylated C18-R) [180] have demonstrated enhanced emission, reduced non-specific binding, and better *in situ* stability [181]. Targeted paramagnetic NMs [182], superparamagnetic iron oxide NPs (SPION) [183], pH-sensitive calcium phosphate-PEG shell NPs [184], SPION loaded red blood cells [185], DNA plasmid loaded SPIONs [186] and fluorinated graphene oxide NPs [187] are recently developed MRI contrast agents with favourable superparamagnetic characteristics, biocompatibility, and ease of modification. Gold NPs are also important contrast agents for CT imaging due to their unique optical properties, high X-Ray attenuation, low toxicity, and ease of surface functionalization [188-193]. ^{18}F-, ^{64}Cu-, ^{199}Au- and ^{111}In-labelled NMs have been developed for PET and SPECT imaging [194-197]. NMs developed for biomedical imaging have superior performance to conventional agents, but few have been translated to the clinic [198].

2.5.2. Antimicrobial Agents

Some NPs exhibit high antimicrobial activity useful for treating surgical wound infections. Silver NMs accelerate wound healing [199] and fight post-surgical infections [200] due to broad-spectrum antimicrobial activity. Titanium-doped silver NPs prevent multidrug-resistant infections [201] while silver NP embedded titania nanotubes exhibit persistent antibacterial effect against pathogenic *Escherichia coli* and *Staphylococcus aureus* [202]. Nanoscale silver coatings are effective against implant-associated infections [203]. Copper, titanium, gold and zinc NPs have broad-spectrum antimicrobial activities due induction of oxidative stress [204].

2.5.3. Therapeutic NMs

Magnetic NMs are increasingly used for treatment of diseases, especially cancers. Magnetic NM clusters and colloidal crystals (nanobeads) have diameters 50–200 nm. They are very useful for tissue targeting, tissue ablation, and imaging [205-209]. Heating due to hysteresis losses, which occurs when a fluid containing magnetic NMs is exposed to an alternating external magnetic field, can selectively damage tumours It is particularly useful for hard-to-treat cancers like hepatocellular carcinomas.

2.5.4. Tissue Engineering

Tissue engineering research aims to develop biological constructs for repair, restoration, maintenance or improvement of tissue function [210]. Second generation biomaterials with biological and mechanical properties more similar to those of human tissues have evolved from first-generation biological substitutes [211]. Biomaterials can trigger immune responses because they do not mimic the highly complex extracellular matrix, leading to rejection of implanted materials [212, 213]. Tissue engineering at the

nanoscale allow design of new biologically inspired materials with properties that overcome the limitations of conventional tissue engineering materials [214-216]. A wide range of nano-scale biomaterials, including inorganic, ceramic, polymeric and metallic NPs, have been employed in tissue engineering applications, such as enhancement of cell proliferation rates, novel mechanical and electrical properties of scaffolds, gene deliver, and fabrication of 3D tissue engineered constructs [217]. For example, nanostructured calcium phosphates and nano-hydroxyapatite are used as bone substitutes due to their biocompatibility, osteoconductive properties, and bone regenerative capacity [218, 219]. Similarly, nano-scale bioprinting of 3D hydrogel scaffolds is an active area of research with enormous potential to resemble natural bone tissue and the cells' natural surrounding environment [220, 221].

2.5.5. Biosensors

Biosensors use biomolecules, tissues, and organisms to measure concentrations of specific biological analytes, a biological structure, or a microorganism [222]. They convert a molecular recognition event into a signal (e.g. optical, electrical or magnetic) that provides information about health and diseases, enabling earlier disease detection and more targeted therapies [223]. The small size and large surface-to-volume ratio of NMs make them well suited for medical biosensing applications where enhanced sensitivity and detection capability are essential. Nanostructured carbon materials e.g. nanotubes with high sensitivity and extremely low detection limits [224], have been used in biosensing applications for over two decades [225]. Their electronic/optical properties and permeability through biological membranes make them well-suited to minimally-invasive, *in vivo* optical biosensing applications [226]. Quantum dots are widely used in fluorescence-based medical biosensors [227]. Other nanobiosensors include gold nanorod- and graphene oxide-based electrochemical biosensors for early detection of cancer [228], inorganic nanocrystal-based sandwich immunoassays for multitarget detection of proteins [229], nanosized silica-based immunosensors for prostate cancer detection [230] and nanosilver-based plasmonic biosensing applications [231]. As the scientific evidence for the benefits of nanobiosensors grows, so too have concerns about their *in vitro* and *in vivo* biosafety. Clinical translation

of these systems hinges on understanding how the human body responds to, distributes, and eliminates biomedical NMs, with the ultimate aim of ensuring their safe use in biosensing applications.

2.6. Safety of Biomedical NMs

With the ever-increasing use of nanostructures in biomedical applications, human and environmental exposure to NMs has become inevitable. There are existing and robust regulatory processes in place for biomedical NMs used for diagnostic applications. There is also strict regulation of implantable and indwelling medical devices that increasingly contain nanostructured coatings. For example, the US FDA defines three risk classes for medical devices and devices that are not within a type marketed before are automatically classified into class III (high risk), a cautious approach that is suitable for NMs with unconventional properties. Review and approval of nanoscale drugs, coatings and devices is ongoing [232], e.g. the FDA has approved nano-formulations of paclitaxel and doxorubicin as new cancer drugs, of the immunosuppressant sirolimus, and of an oestradiol topical emulsion [92]. Regulation will need to be agile to deal with new technologies such as the use of microscale and nanoscale topographies to control biological responses such as microbial pathogen attachment, and modulation of immune responses by novel coatings [233].

2.7. Final Remarks

Advances in systems biology, chemistry, automation, and computer science have led to several paradigm shifts in regulatory safety assessment. These include use of animal data for estimating health impacts of chemicals on humans and the environment, development of faster and cheaper non-animal alternatives to animal tests, use of gene expression and other omics data, faster high capacity *in vitro* screens, and robust *in silico* methods. The ultimate aim is to accelerate safe manufacturing and use of products, while

reducing costs and the time from design to commercialization. Despite the growing interest among regulatory authorities in the development of time- and cost-effective methods to complement and extend traditional risk assessment methods, there are significant barriers to integrating such concepts into the practice of existing regulatory frameworks.

The safety evaluation of biomedical NMs requires input from multiple sources and disciplines. The successful adaptation of risk assessment procedures to NMs directly depends on the ability of experts in material science, toxicology, industry, and regulatory bodies to understand how their respective expertise complements that of the others. There is a clear recognition of the value of such cross-disciplinary collaboration for improving chemical risk assessment processes. However, only a few ideas have been reduced to practice so far, as scientists, regulators and industry work from different assumptions and are invested in their own points of view.

CHAPTER 3

MACHINE-LEARNING ASSISTED INSIGHTS INTO CYTOTOXICITY OF ZINC OXIDE NANOPARTICLES

3.1. Background

Zinc oxide NPs (ZnO NPs) are commercially used as an active ingredient or a color additive in foods, pharmaceuticals, sun protection lotions, and cosmetic products. While the use of ZnO NPs in everyday products has not been linked to any serious health issues so far, the scientific evidence generated for their safety is not conclusive and, in most cases, could not be validated further in *in vivo* settings. To settle controversies arising from inconsistent *in vitro* findings in previous research focusing on the toxicity ZnO NPs, we combined the results of 25+ independent studies. One way analysis of variance (ANOVA) and classification and regression tree (CART) algorithm were used to pinpoint intrinsic and extrinsic factors influencing cytotoxic potential of ZnO in nanoscale. Particle size was found to have the most significant impact on the cytotoxic potential of ZnO NPs, with 10 nm identified as a critical diameter below which cytotoxic effects were elevated. As expected, strong cell type-, exposure duration- and dose-dependency were observed in cytotoxic response of ZnO NPs, highlighting the importance of assay optimization for each cytotoxicity screening. Our findings also suggested that ≥12 hours exposure to NPs resulted in cytotoxic responses irrespective of the concentration. Considering the cumulative nature of research processes where advances are made through subsequent investigations over time, such meta-analytical approaches are critical to maximizing the use of accumulated data in nano-safety research.

3.1.1. Zinc Oxide Cytotoxicity

Nanoscience deals with the phenomena that occurs in the nanometer range which is one billionth of a meter. While the conceptual roots of nanoscience were planted in the late 1950s, it was not until early 1990s that nanotechnology advanced enough to design structures, devices and systems at atomic and molecular scales [234]. Nanoscale science and engineering is interdisciplinary in nature, requiring teams of researchers with different scientific backgrounds (e.g., physics, chemists, biologists, material scientists and engineers) working together to come up with new innovations and solutions to today's complex issues. The application of nanotechnology can span across different disciplines and research areas. Today, nanotechnology is explored in almost all existing domains ranging from high-strength materials and nanoscale sensors to electronic and opto-electronic devices [235]. In parallel, novel properties of nano-scale materials are enabling new commercial markets such as next generation batteries and intelligent drug delivery systems [236, 237].

NPs are commonly classified according to their origin (engineered or natural), dimensionality (0D, 1D, 2D or 3D), morphology (low or high aspect ratio), state (well-dispersed, aggregated etc.) or chemical composition (ceramic, polymeric, carbon-based or metallic) [238]. Among different metal-based NPs (NPs), zinc oxides (ZnO) stand out for their high UV-absorption capacity and solubility. They are commercially used as a bulking agent, filler or pigment in glass and ceramic products, foods, pharmaceuticals, sun protection lotions, and cosmetics [239]. One of the early uses of ZnO NPs was in sunscreens due to their intrinsic UV absorbing properties and transparent nature [240]. The use of nano-sized ZnO (and also titanium dioxide) as an effective ingredient in modern sunscreens has created a long-lasting debate over their safety [241, 242]. In early 2010s (and onwards), both the regulatory bodies and the public have become increasingly aware of the potential threat posed by sunscreens formulated with nano-ingredients. The early findings related to potential hazards of ZnO NPs were mostly inconsistent, making it impossible to conclude with high certainty that nano-sized ZnO is ultimately safe to use in skin-contacting products [242]. In the following years, it became clear that not all ZnO NPs should be treated the same from safety perspectives because physicochemical characteristics greatly affect cellular interactions and safety profiles of NPs [243].

Determining the potential harmful effects of NPs is critical to ensure that they are safe for human use. One effect of NPs that must primally be assessed is its cytotoxic potential, together with the factors contributing to their cytotoxicity [244]. After two decades of research and detailed investigations, there is still no consensus on the main physicochemical properties driving cytotoxicity of NPs [245-247]. In addition to intrinsic as-received properties of NPs and media-dependent surface characteristics, test conditions such as cell type, exposure concentration and duration have direct influence on the results of cytotoxicity assays. Figure 3.1 shows material- and assay- related parameters influencing different dimensions of NPs-protein and NPs-cell interactions.

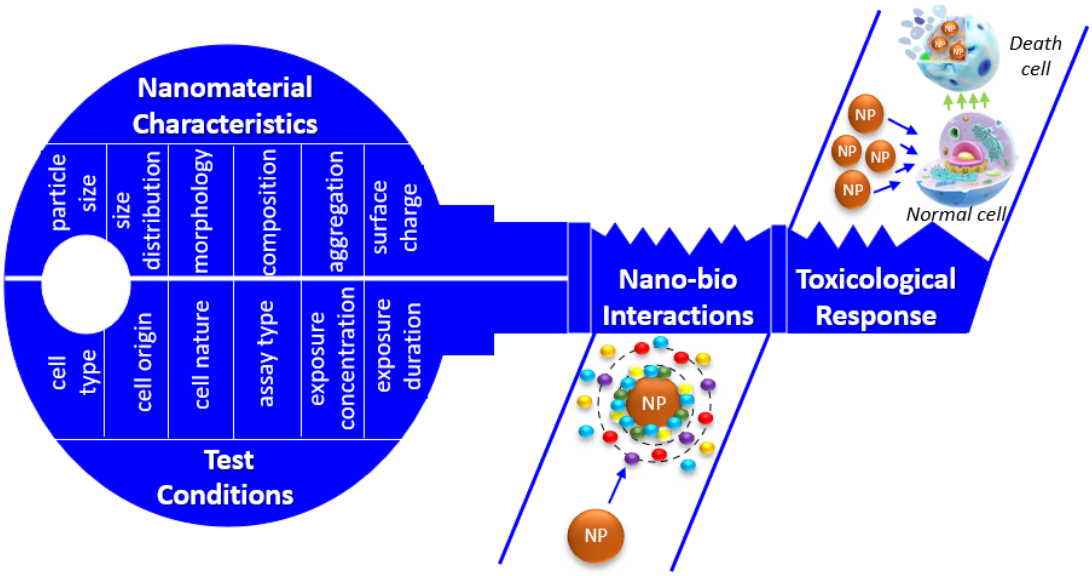

Figure 3.1. Key parameters affecting the toxicity of NPs.

ZnO NPs differ from their bulk counterparts in that their inherent complexity and medium-dependent characteristics make it very difficult to study their cellular interactions and effects. Moreover, the experimental differences in nano-hazard screening are directly reflected in test results, potentially leading to interexperimental inconsistencies. The aim of this study is to integrate published evidence on the cytotoxicity of ZnO NPs and to critically appraise bodies of evidence in their entirety.

3.2. Methods

3.2.1. Literature Search and Data Extraction

A systematic literature search was undertaken using the PubMed scientific search engine between 2010 and 2022. The following three terms were used for the initial article search: “zinc oxide”, “nanoparticle*” and “cytotoxic*”. The search returned 594 peer-reviewed research papers that were manually filtered according to the following inclusion criteria: (i) the core of the studied NPs must be zinc (and not a composite material); (ii) *in vitro* cytotoxicity data must be available and accessible; (iii) particle size data must be available; (iv) the unit of exposure concentration must be convertible to μg/mL; and (v) untreated cell control must be available. A total of 543 data points for 40 different ZnO NPs from the remaining 26 independent studies were included in the analysis.

3.2.2. Data Cleaning and Pre-processing

Data normalization (i.e., changing the values to a standard scale) is often used prior to statistical analysis when comparing features with different units or ranges. First, the units of measure were unified to minimize variability between different studies. The numeric data records describing the concentration were divided into ten subgroups. The cleaned data were randomly divided into training (75%) and test sets (25%), each involving a similar fraction of toxic and nontoxic groups.

3.2.3. Descriptive Statistics

One-way analysis of variance (ANOVA) was used to determine how strongly each of the categorical parameters describing NP, cell line, or assay characteristics was

related to cytotoxicity. The strength and direction of the relationship between pairs of continuous variables were measured by Pearson's correlation coefficients. A box plot was used to display the distribution and skewness of the cell viability data among different subcategories. Significance was reported at $p < 0.05$ and $p < 0.001$ levels.

3.2.4. Machine Learning

Classification and Regression Tree (CART) was applied to partition the pre-processed data using a series of binary decisions. The method was set to regression, as the endpoint was a numerical value (% cell viability). The *rpart* package in R version 4.2.0 was used to implement all CART analyses. Regression trees were pruned through a 10-fold cross-validation process to remove branches providing the least error reduction. Refer to more specialized publications for details on the CART algorithm [248-250]

3.3. Results and Discussion

Description of data included in analysis. After a systematic data search and excluding data points that did not meet the data inclusion criteria, a total of 543 data records from 26 independent studies remained for evaluation. Each data record corresponds to a cytotoxic evaluation of individual NP. Figure 3.2 summarizes the main characteristics of the collected data.

Effect Sizes and Heterogeneity. A series of one-way ANOVAs were conducted to assess the influence of NPs and assay parameters on cell viability (Table 3.1). As expected, a strong negative correlation was observed between exposure dose and cell viability ($p<0.001$), with concentrations ≥20 μg/mL killing at least half of the cells. Similarly, cytotoxic profiles were detected after >12h exposure to ZnO NPs, with shorter exposure durations not causing significant toxicity.

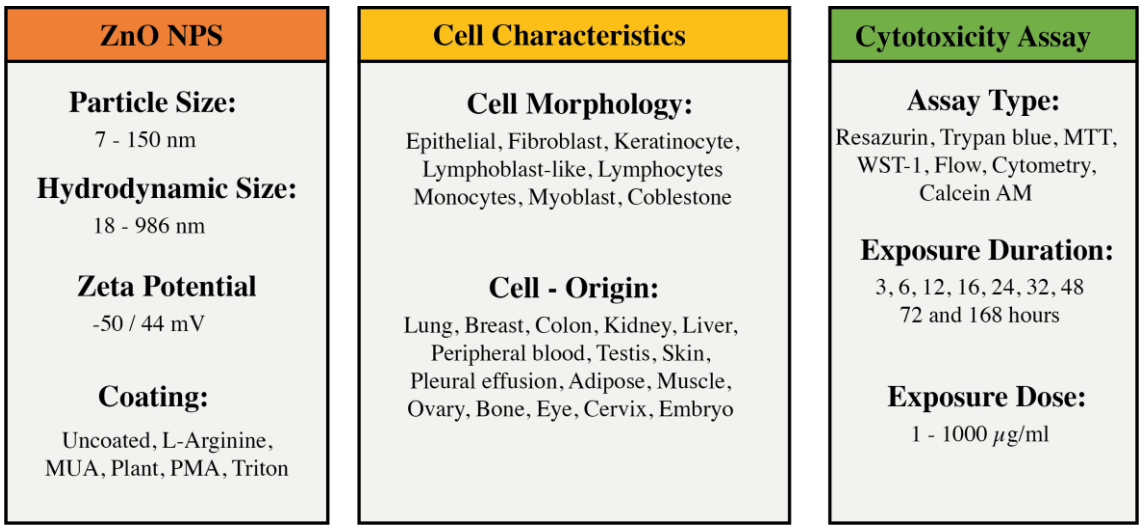

Figure 3.2. Dataset description

ANOVA also revealed that coating surfaces of NPs with amphiphilic polymers or thiol-containing acids could elevate its cytotoxicity, while green synthesis could help reduce the cytotoxic potential of ZnO NPs. These results highlight the importance of intrinsic materials characteristics and extrinsic experimental conditions on NP-induced cytotoxicity.

Table 3.1. One-way ANOVA results

Parameter	**n**	**Cell Viability (%)**	***p-value***
Coating (presence)			
Coated	110	47.4 ± 39.3	*<0.001*
Uncoated	433	60.5 ± 33.7	
Coating type			
Uncoated	433	60.5 ± 33.7	*<0.001*
PMA, amphiphilic polymer	26	39.7 ± 40.1	
L-Arginine	26	40.6 ± 39.4	
Mercaptoundecanoic acid	26	37.3 ± 42.4	
Plant extract	6	69.7 ± 24.0	
Triton X-100	26	67.0 ± 30.3	

(cont. on next page)

Table 3.1. (cont.)

Exposure concentration (dose)			
< 5 µg/mL	85	91.0 ± 10.8	*<0.001*
5 – 10 µg/mL	68	81.6 ± 27.2	
10 – 20 µg/mL	129	71.8 ± 31.0	
20 – 30 µg/mL	67	48.4 ± 31.3	
30 – 40 µg/mL	29	49.2 ± 20.0	
40 – 50 µg/mL	11	25.9 ± 15.5	
50 – 60 µg/mL	38	41.8 ± 25.0	
60 – 100 µg/mL	31	32.8 ± 24.0	
100 – 200 µg/mL	27	22.0 ± 18.9	
>200 µg/mL	58	12.8 ± 9.8	
Cell morphology			
Epithelial	152	58.6 ± 34.5	*0.002*
Epithelial-like	161	66.0 ± 37.0	
Fibroblast	163	49.4 ± 33.9	
Lymphocytes	5	59.1 ± 33.8	
Monocyte	5	48.4 ± 40.8	
Lymphoblast-like	5	41.6 ± 46.3	
Keratinocyte	22	69.7 ± 26.7	
Myoblast	11	42.3 ± 24.2	
Cobblestone	3	50.0 ± 25.0	
Cell source (organ/tissue)			
Skin	43	56.2 ± 29.7	
Lung	78	52.7 ± 33.2	*<0.001*
Cervix	57	58.0 ± 32.2	
Embryo	65	41.6 ± 38.5	
Peripheral Blood	26	55.8 ± 36.1	
Pleural effusion	5	48.4 ± 40.8	
Kidney	9	37.0 ± 34.0	
Liver	19	48.8 ± 32.8	
Adipose	43	50.4 ± 28.4	
Bone	9	53.7 ± 34.7	
Eye	30	72.5 ± 24.2	
Ovary	66	86.5 ± 31.0	
Colon	21	46.1 ± 37.8	
Testis	20	93.0 ± 12.2	
Breast	41	51.7 ± 35.6	
Muscle	11	42.3 ± 24.2	
Cytotoxicity assay			
MTT	324	63.1 ± 33.7	*<0.001*
WST-1	51	43.2 ± 33.9	
Resazurin	88	45.0 ± 41.2	
Flow cytometry	6	55.2 ± 34.6	
Calcein AM	8	80.6 ± 11.6	

(cont. on next page)

Table 3.1. (cont.)

Exposure duration				
	3_6 hours	30	89.3 ± 9.4	*<0.001*
	8_9 hours	13	68.8 ± 37.1	
	12 hours	28	70.1 ± 27.4	
	16 hours	5	47.6 ± 38.6	
	24 hours	345	53.6 ± 35.6	
	32 hours	5	36.8 ± 36.0	
	48 hours	88	56.6 ± 35.4	
	72 hours	26	74.2 ± 37.1	
	168 hours	3	30.0 ± 17.7	

A Pearson's correlation was run to assess the relationship between numeric parameters (particle size, hydrodynamic size, zeta potential, and concentration) and cell viability (%). The Pearson correlation coefficient of -0.22 suggested that cell viability and exposure concentration were moderately correlated in the opposite direction (Table 3.2). There was a positive correlation between particle size measured by TEM/SEM or DLS and cell viability, with NPs of larger diameter inducing less potent cell death. Interestingly, no direct correlation between zeta potential values and cell viability was observed.

Table 3.2. Pearson correlation results

	$d_{TEM/SEM}$	d_{DLS}	Zeta potential	Conc.	Viability
dTEM/SEM	---				
Zeta potential	0.14 (p=0.031)	-0.17 (p=0.021)	---		
Concentration	*-0.09* (p=0.028)	*-0.15* (p=0.026)	*-0.08* (p=0.026)	---	
Viability	***0.24***** (p<0.001)	***0.19** (p=0.005)	*-0.03* (p=0.696)	***-0.22***** (p<0.001)	---

Next, a box plot was constructed to show the distribution of cell viability among different exposure durations and doses (Figure 3.3). As expected, higher concentrations of NPs and longer exposure durations led to higher levels of cytotoxicity relative to untreated cell control. The effect of extended exposure on cell viability was more pronounced at higher exposure doses.

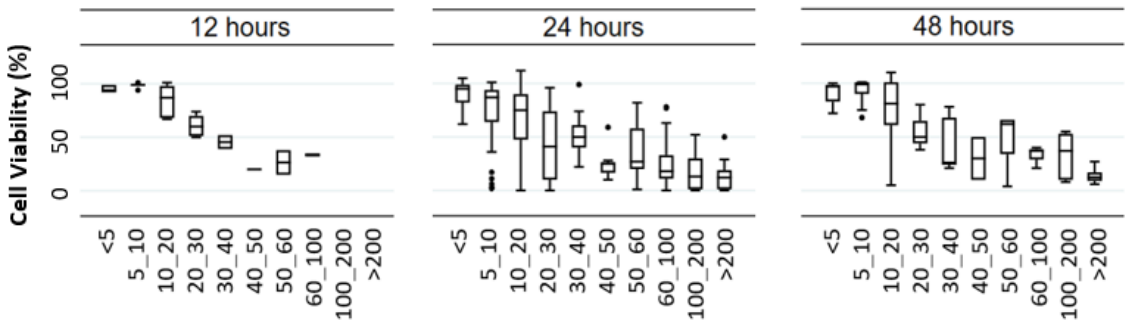

Figure 3.3. Box plot of changes in cell viability (%) as a function of exposure concentration (dose, μg/ml) category, grouped by exposure duration (h).

*Circles outside the plot represent outliers beyond the 10th and 90th percentiles.

Machine learning. To identify the influence of material characteristics and experimental factors on the cytotoxic potential of ZnO NPs, the CART recursive partitioning analysis was employed. The best-performing regression tree (Figure 3.4) was selected based on both cross-validation results and simplicity.

The zeta potential measurements were not included in the decision tree analysis due to a high number of missing values (57%). Cross-validation error minimized at a tree size of 5 branches. The best-performing regression tree given in Figure 3.4 included concentration, exposure duration, cell morphology, and particle size. The variable importance order was as follows: concentration > particle size > cell type > exposure duration > assay type > coating. In line with previous studies [251, 252], our analysis showed that the potency of ZnO NPs to induce cytotoxic response is particle size-dependent. In particular, the primary particle size of 10 nm was found to be critical below which elevated cytotoxicity was seen. As expected, a strong positive linear relationship was observed between exposure duration and cytotoxic response. The longer the duration that

cells are exposed to ZnO NPs, the greater the cytotoxicity. Most ZnO NPs were cytotoxic after 12 hours' exposure, especially at relatively higher doses (>20 µg/mL). As previously reported by Cierech et al., significant changes in cell viability were observed with increasing concentrations of ZnO NPs [253]. The identified relationships between exposure conditions and cell viability results are also very much in line with the earlier investigations in the field [254-257]. For example, Khan and co-workers evaluated the toxic effects of ZnO NPs at different concentrations and demonstrated the role of reactive oxygen species generation in NP-induced cytotoxicity and genotoxicity [258]. In another study, NP-induced DNA damage and cytotoxicity were evident after 6h exposure to 20 µg/mL of ZnO NPs [259]. Taken together, the accumulated evidence on the cytotoxic and genotoxic potential of ZnO NPs suggests that the safety of ZnO NPs should remain a critical concern for all parties involved, including regulators, academicians, and industrial people.

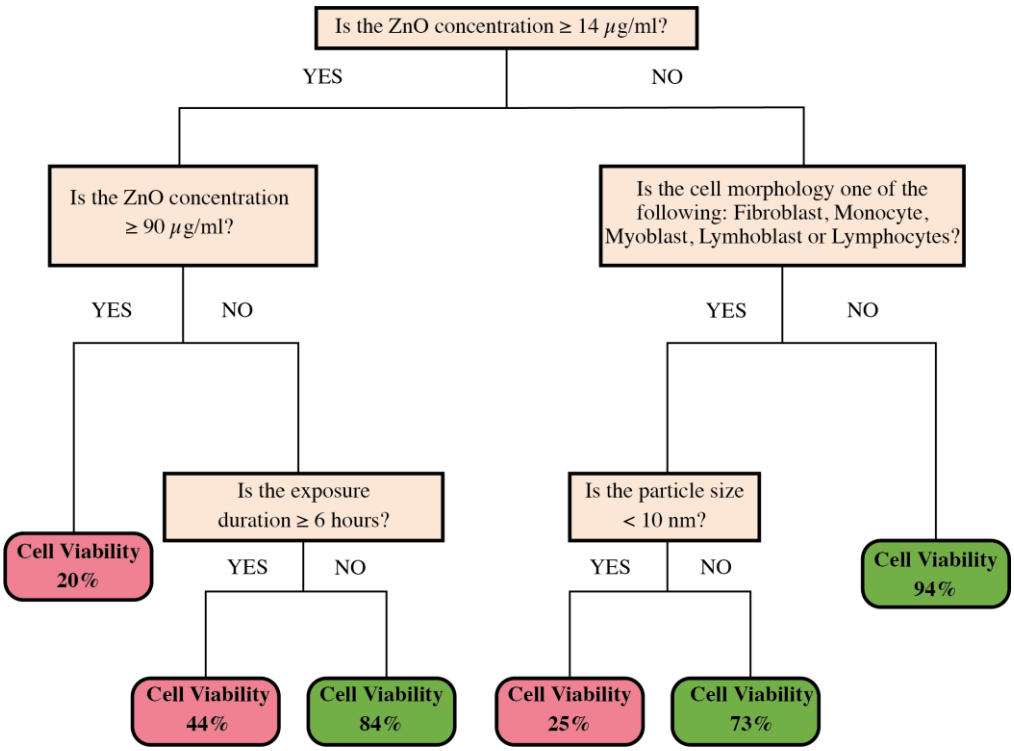

Figure 3.4. The best-performing regression tree predicting cell viability of ZnO NPs.

CHAPTER 4

MACHINE LEARNING-ASSISTED PREDICTION OF THE TOXICITY OF SILVER NANOPARTICLES: A META-ANALYSIS

4.1. Background

Silver nanoparticles are likely to be more dangerous than other forms of silver due to the intracellular release of silver ions upon dissolution and the formation of mixed ion-containing complexes. Such concerns have resulted in an ever-growing pile of scientific evaluations addressing the safety aspects of nanosilver with widely varying methodological approaches. The substantial differences in the conduct/design of nanotoxicity screening have led to the generation of conflicting findings that may be accurate in their narrative but fail to provide a complete picture. One strategy to maximize the use of individual risk assessments with potentially biased estimates of toxicological effects is to homogenize results across several studies and to increase the generalizability and human relevance of their findings. Here, we collected a large pool of data (n=162 independent studies) on the cytotoxicity of nanosilver and unrevealed potential triggers of toxicity. Two different machine learning approaches, decision tree (DT) and artificial neural network (ANN), were primarily employed to develop models that can predict the cytotoxic potential of nanosilver based on material- and assay-related parameters. Other machine learning algorithms (logistic regression, gaussian naive bayes, k-nearest neighbor, and random forest classifiers) were also applied. Among several attributes compared, exposure concentration, duration, zeta potential, particle size and coating were found to have the most substantial impact on nanotoxicity, with biomolecule- and microorganism-assisted surface modifications having the most beneficial and detrimental effects on cell survival, respectively. Such machine learning-assisted efforts are critical

to developing commercially viable and safe nanosilver-containing products in the ever-expanding nanobiomaterials market.

4.1.1. Silver Oxide Cytotoxicity

Nanotechnology is an interdisciplinary area of science and engineering that studies small feature sizes (in the range of 1-100 nm) with broad applications. The development of nanotechnology has been steadily gaining momentum since its early inception in the 1980s [234, 260, 261]. Over the next few decades, nanotechnology has been heavily incorporated in various fields, including medicine, electronics, agriculture, chemistry, physics, environment, material science, and engineering [235]. The application of nanotechnology in medicine (so-called *nanomedicine*) has led to the development of new diagnostic tools and treatment strategies with increased capabilities and success rates [23].

NPs used for medical applications can be broadly divided into three groups (1) inorganic NPs (metal, metal oxides, and quantum dots), (2) carbon-based NPs (graphene, fullerene, and carbon nanotubes), and (3) organic NPs (lipids and polymers) [262]. Among different NP formulations explicitly developed for biomedical applications, nanosilver-enriched materials are particularly suitable for implants, medical devices, coatings, and wound dressings due to their antioxidant, antibacterial, and antimicrobial properties [263]. While the antibacterial activity of silver has long been known and has found a wide range of applications, its production in nanoform results in additional benefits [264]. First, silver-core NPs enable bright particle tracking by providing fluorescence enhancement. The size of silver NPs can be easily controlled in the range of 4-150 nm, allowing customizable cellular internalization and targeted clinical interventions. Another advantage of nanosilver-based biomaterials is their high antimicrobial activity against multidrug-resistant microorganisms [265].

There is a risk that nanosilver not only destroys microorganisms but also damages healthy human organs. The unique properties that nano forms of silver exhibit relative to the bulk also raise concerns about their new biological identity and the physiological response triggered by them. Over the last decade, the nanosafety community has made a

substantial effort to determine the toxicological effects of silver NPs [266, 267]. The accumulated evidence suggests that nanosilver may exert toxic effects on mammalian cells (especially at high concentrations), attributed mainly to the release of Ag+ ions and the subsequent generation of reactive oxygen species [265, 268, 269].

Cytotoxicity (i.e., the quality of being toxic to cells) is the most common biosafety evaluation test. It is often the first step in determining whether a material is a viable candidate for biomedical applications [244, 270]. Most conventional *in vitro* cytotoxicity assays have been established long before the emergence of nanotechnology and hence, not particularly suitable for use in nanotoxicity testing. For example, the dyes used in the colorimetric MTT assay (i.e., the most widely applied method for assessing NP-induced cytotoxicity *in vitro,* Figure 4.1.) can interfere with silver NPs due to their unique optical properties [141, 271]. Similarly, the LDH release assay, another test commonly used for screening the cytotoxic potential of NPs (Figure 4.1.), is also repeatedly shown to suffer from cell-type specific NP-mediated interferences [272-274]. Another challenge for designing efficient *in vitro* nanotoxicity testing methods is NPs' large and dynamic physicochemical property space and the subsequent impacts of the variations in those characteristics on the toxicological behavior [267, 275].

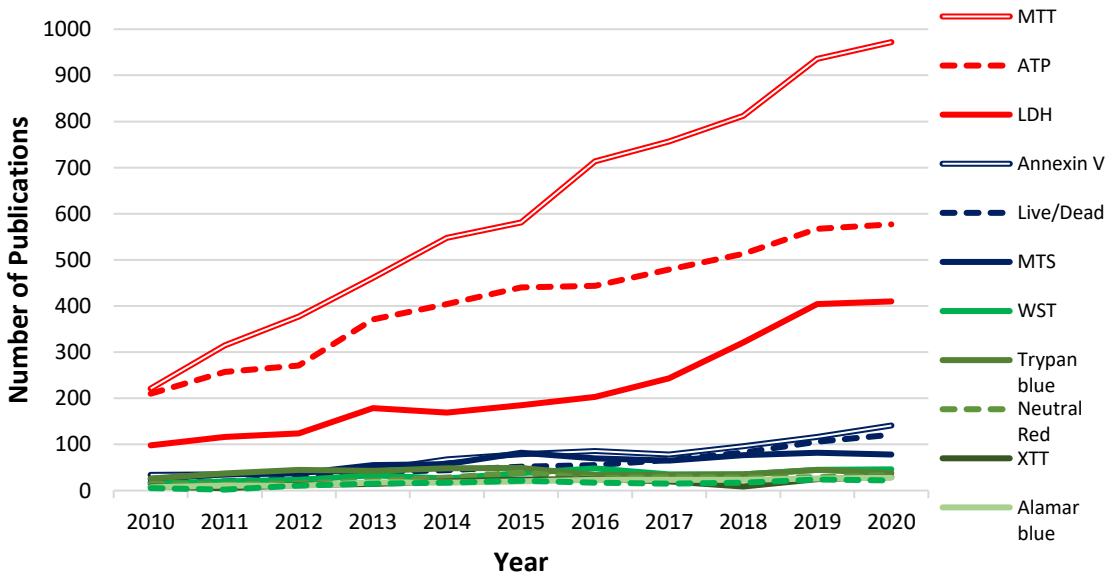

Figure 4.1. The relative increase in cumulative publications of in vitro assays commonly used to assess NP cytotoxicity.

Pubmed abstract search with the following terms: (MTT AND nano), (ATP AND nano*), (LDH AND nano*), (Annexin V AND nano*), (Live/Dead AND nano*), (MTS AND nano*), (WST AND nano*), (Trypan blue AND N-nano*), (Neutral AND nano*), (XTT AND nano*), (Alamar blue AND nano*), (Resazurin AND nano*).

The rapid increase in NP-containing biomedical materials and tools strengthens the need for a detailed investigation of their potential hazard to human health [276]. However, nanosilver is incorporated into commercial products much faster than mechanistic understanding relating to adverse health effects can be established. One strategy to fill the gap in nano-safety knowledge before it widens any further is to increase the generalizability of the findings coming from individual studies by conducting a meta-analysis [155, 243]. Meta-analysis can help solve the problem of the ever-growing body of data created through nanotoxicological studies and can enable the integration of the accumulated nanotoxicity data, which will ultimately boost the precision of conclusions drawn from it. Here, we present a meta-analysis of NP toxicity by combining published evidence on the cytotoxicity of silver NPs between 2007 and 2021. The central hypothesis here is that the cytotoxic potential of silver NPs can be estimated based on intrinsic material properties (e.g., particle size, concentration, zeta potential, and coating) and cytotoxicity test conditions (e.g., assay type, cell type and characteristics, and exposure duration). An exhaustive literature search yielded an initial pool of 338 studies, almost half of which were filtered down as per the inclusion/exclusion criteria and used in the meta-analysis.

4.2. Methods

4.2.1. Literature Search and Data Extraction

An iterative systematic literature search was undertaken using SCOPUS scientific search engine. Following terms were used for the article search: “silver” AND “nanoparticle” AND (“cytotoxicity” OR “toxicity” OR “ic50”) AND (“human” OR “cell”). The search returned 339 peer-reviewed research papers, which were manually

filtered according to the inclusion criteria outlined below. To be included in the metaanalysis, the following requirements had to be met: (i) the core of the studied NP must be silver, (ii) *in vitro* cytotoxicity data must be available, (iii) the particle size data measured by the electron microscopy and/or dynamic light scattering technique must be available, (iv) the unit of exposure concentration must be convertible to µg/ml, and (v) untreated cell control must be available. A total of 4477 data points for 255 individual silver-core NPs from the remaining 162 studies were included in the meta analysis (Figure 4.2).

4.2.2. Data Cleaning and Pre-processing

The raw dataset including a total of 4477 rows (each corresponding to a single cytotoxicity experiment) is provided in APPENDIX (barcode). First, the units of measures were unified to minimize variability between different studies. Surface-coated NPs were divided into one of the 13 categories according to the type of coating material (e.g., polymer, plant extract, surfactant, bacteria, fungi, etc.). Similarly, the numeric data records describing the concentration were divided into nine subgroups (0; 0-1; 1-10; 10-20; 20-40; 40-60; 60-100; 100-200 and >200 µg/mL). The quantitative cell viability data (% viability) was converted to binary (toxic or nontoxic) toxicity class variable based on a pre-defined threshold (<50%) widely applied in the scientific literature [277, 278]. The cleaned data were randomly divided into training (70%) and test sets (30%), each involving a similar fraction of toxic and nontoxic groups.

4.2.3. Descriptive Statistics

One-way analysis of variance (ANOVA) combined with Tukey's honest significant difference (HSD) test was used to determine how strongly each of the 10 categorical parameters describing NP, cell line, or assay characteristics was related to cytotoxicity. The strength and direction of the relationship between pairs of continuous

variables (particle size by SEM, TEM, or DLS, zeta potential, NP concentration, exposure duration, and cell viability) were measured by Pearson's correlation coefficients. A box plot was used to display the distribution and skewness of the cell viability data among different subcategories. ANOVA, Pearson correlation, and box plot visualization were performed using STATA/IC statistical software (version 16.1; StataCorp). Significance was reported at $p < 0.05$ and $p < 0.001$ levels.

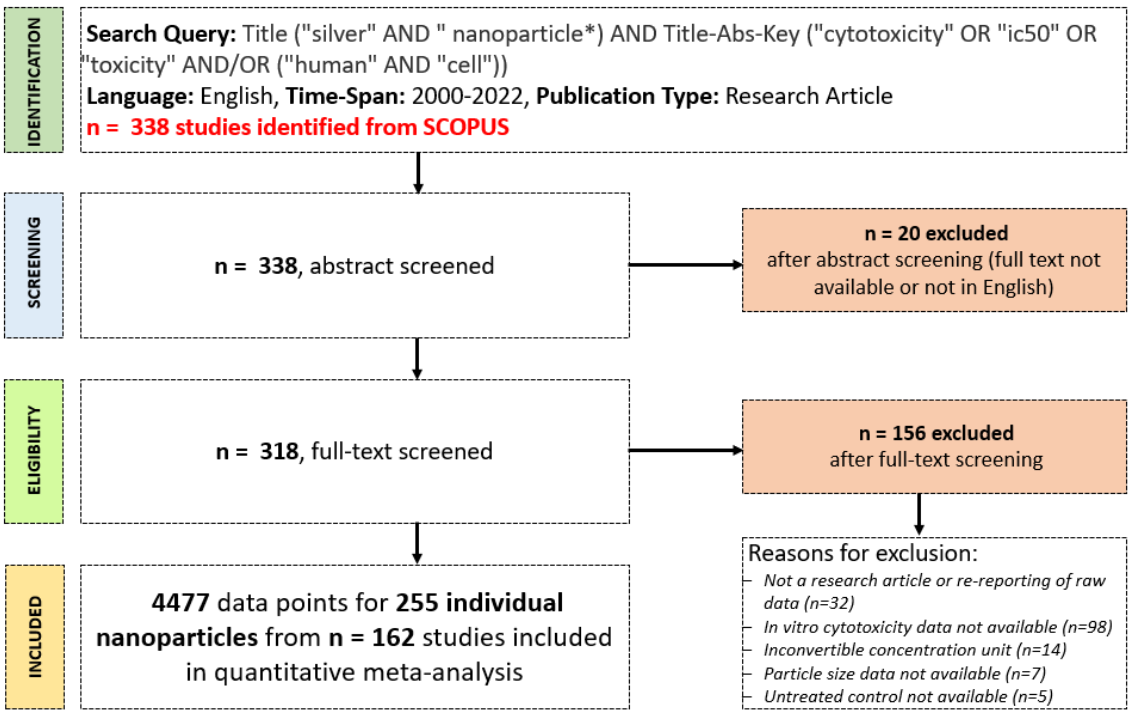

Figure 4.2. Data search and selection procedure.

4.2.4. Model Development

A Decision Tree (DT) is a non-parametric machine learning algorithm that can perform both classification and regression tasks. It has an inverted tree-like structure, where each node represents a predictor, each branch represents a decision on a predictor, and each leaf holds a class label [279, 280]. Here, DTs were developed using the Python-based scikit-learn classifier to predict whether a silver-core NP was toxic (cell viability < 50%) based on NP, cell, and assay characteristics [281, 282]. The best splits in DTs were selected

based on the Gini impurity index describing the likelihood of an incorrect classification [283]. The performance of DT models was compared with four different machine learning algorithms (logistic regression, gaussian naive bayes, k-nearest neighbor, and random forest classifiers) implemented in the Scikit-learn Python library. The versions were Python 3.8.10, Scikit-learn 1.0.2, Pandas 1.3.5, and Numpy 1.22.4.

Inspired by the biological neurons in the human brain, artificial neural networks (ANNs) take in data, train themselves to recognize the patterns in this data, and predict the output for a new set of similar data [284-286]. It is made up of layers of connected input and output units called *neurons*. The hidden layers that exist in between the input and output layers perform most of the computations required by ANN [287, 288]. In this study, the ANN models were designed, optimized, and tested using an advanced machine learning platform specializing in neural networks called *Neural Designer*. The *growing neurons* and *growing inputs* algorithms were used to select the optimum number of neurons and inputs. The aim here was to avoid the risk of both overfitting and underfitting and to develop high-performing ANN models capable of predicting the cytotoxicity of silver-core NPs based on material characteristics and hazard screening parameters.

4.2.5. Model Performance

The performance of machine learning models was assessed in terms of accuracy, precision, sensitivity, and specificity calculated based on the following equations:

$$Accuracy = \frac{TP+TN}{TP+TN+FP+FN} \quad (1)$$

$$Precision = \frac{TP}{TP+FP} \quad (2)$$

$$Sensitivity = \frac{TP}{TP+FN} \quad (3)$$

$$Specificity = \frac{TN}{TN+FP} \quad (4)$$

Where TP, FP, TN, and FN represent true positive, false positive, true negative, and false negative, respectively. The area under the receiver operating characteristic curve (AUC) and the ratio of misclassified instances (error rate) were also used to assess the performance of binary classification models.

4.3. Results

Description of data included in analysis. A total of 4477 data points for 255 individual NPs were collected from 162 independent studies and included in the meta-analysis (provided in Supplementary Material). Each data record represents an individual silver-core NP and the corresponding physicochemical characterization (size, zeta potential, and surface coating) and cytotoxicity data. The data search, extraction, and exclusion details are documented in the methods section. A short description of the data included in the meta-analysis is given in Table 4.1, whereas the frequency of collected data points per individual NP, coating category, exposure concentration, cell source, cell morphology, and assay type are summarized in Fig S1-7.

The missing data percentages given in Table 7 reveal that the variable with the highest number of missing cases is zeta-potential (38%). We further looked into missing data distribution between toxic and non-toxic classes and observed that ~ 31% of total cases with missing zeta potential values had a cell viability of < 50%. In the entire dataset (including missing and non-missing cases), approximately 28% of silver NPs were identified as toxic based on the pre-defined threshold (<50%). Considering the similarity in the fraction of cytotoxic NPs in both complete (547 cases out of 1706 data points) and incomplete cases (1280 cases out of 4477 data points), the missingness was deemed random, not significantly affecting the classification results. While the amount of missing data was not very small, the sample size was sufficiently large so we applied case-wise deletion (i.e., all silver NPs with missing zeta potential values were excluded from the analysis) and carried out a complete-case analysis as the primary method of missing data handling.

Table 4.1. Dataset description

Parameter	Type	Range	Missing
$NP_{Size\ by\ SEM/TEM}$	Numeric	2 – 275 nm	660
$NP_{Size\ by\ DLS}$	Numeric	3 – 534 nm	1601
$NP_{Zeta\ potential}$	Numeric	-56 – +89 mV	1706
$NP_{Concentration}$	Numeric	0.01 – 2000 μg/mL	0 (0%)

(cont. on next page)

Table 4.1. (cont.)

$NP_{Coating}$	Categorical	Coated or Uncoated	*0 (0%)*
$NP_{Coating\ type}$	Categorical	Bacteria, Surfactant, Polymer, Peptide, Protein, Plant, Algae, Fungi, Phospholipid, NP, Small molecule, or their combinations	0 (0%)
$Cell_{Viability}$	Numeric	0 – 206 %	0 (0%)
$Cell_{Nature}$	Categorical	Healthy or Cancer	6 (1%)
$Cell_{Origin}$	Categorical	Primary cells or Cell line	0 (0%)
$Cell_{Source}$	Categorical	Human, Mouse, Hamster, Rat, Bovine, Monkey, Pig, Dog	0 (0%)
$Cell_{Age}$	Categorical	Embryonic or Adult	0 (0%)
$Cell_{Morphology}$	Categorical	Endothelial, Epithelial, Fibroblast, Lymphoblast, and Neuronal	0 (0%)
$Cell_{Organ\_tissue}$	Categorical	Bone, Brain, Skin, Colon, Breast, Kidney, Lung, Liver, Embryo, Blood, Ascites, Urinary system, Others	0 (0%)
$Assay_{Indicator}$	Categorical	Resazurin reduction, Dye inclusion or exclusion, LDH activity, Tetrazolium salt	0 (0%)
$Assay_{Type}$	Categorical	Alamar blue, Apoptosis, ATP, CellTiter-Blue, LDH, Clonogenic assay, . blue, Crystal violet, DAPI, Image processing, Live/Dead, MMP, MTS, MTT, Neutral red, Presto blue, Resazurin, SRB, Trypan blue, WST-1/8, XTT	0 (0%)
$Exposure_{Duration}$	Numeric	1 – 504 hours	0 (0%)

A box plot was constructed to illustrate the distribution of cell viability among different exposure times and concentrations (Figure 4.3). As expected, higher NP concentrations and exposure duration led to higher levels of cytotoxicity relative to untreated cell control. The effect of extended exposure on cell viability was more pronounced at higher exposure doses (≥40 μg/mL).

A box plot diagram showing the percentage viability of cells exposed to silver-core NPs of different surface functionality at increasing doses confirmed that cell viability was significantly reduced when treated with algae-, bacteria-, fungi- or plant-extract-coated nanosilver, even at relatively lower exposure concentrations (Figure S8). It is worth noting that the microorganisms and plant extracts were not primarily used for coating purposes in these studies but rather for the synthesis of silver NPs. However, there was no additional step for removing these biological entities, suggesting that their residues remained on the surface of the synthesized nanosilver. Additionally, cells with lymphoblast morphology were more resistant to silver NPs, when compared to other cell lines (Figure S9).

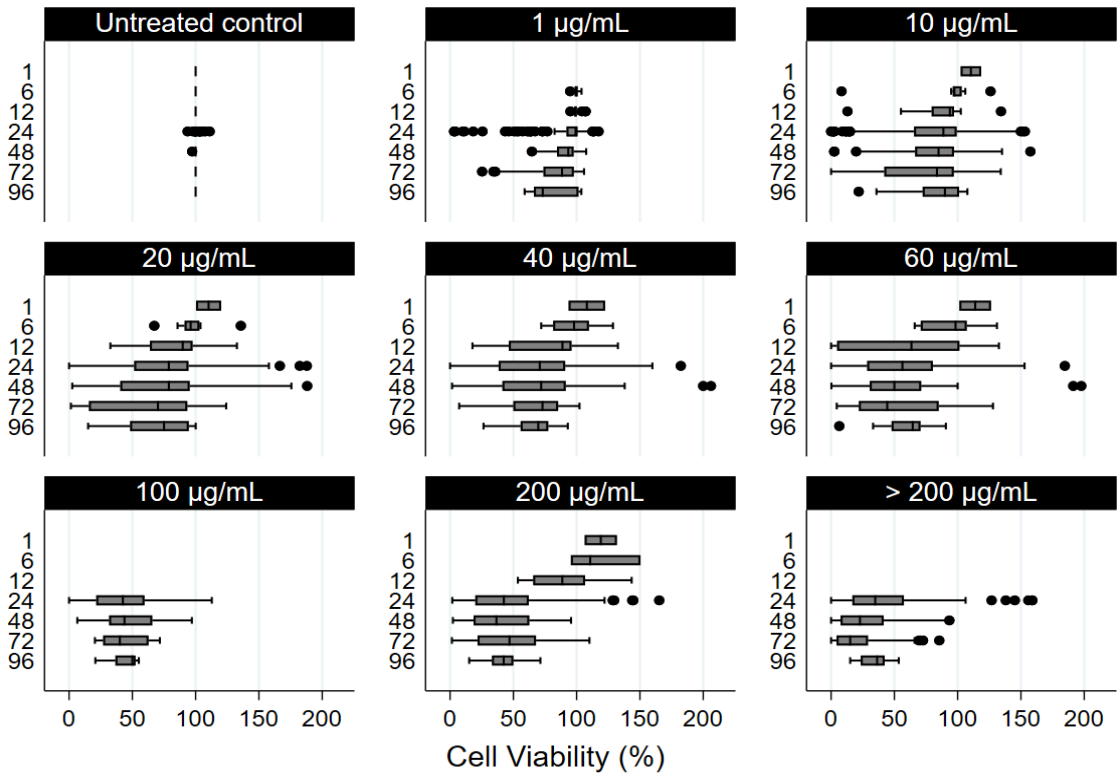

Figure 4.3. Box plot of changes in cell viability (%) as a function of exposure duration *(1, 6, 12, 24, 48, 72 and 96 hours)*, grouped by NP exposure concentrations. *(Untreated cell control; 1 µg/mL:0-1 µg/mL; 10 µg/mL:1-10 µg/mL; 20 µg/mL:10-20 µg/mL; 40 µg/mL:20-40 µg/mL; 60 µg/mL:40-60 µg/mL; 100 µg/mL:60-100 µg/mL; 200 µg/mL:100-200 µg/mL and >200 µg/mL)*. Circles outside the plot represent outliers beyond the 10th and 90th percentiles.

Effect Sizes and Heterogeneity. A series of one-way ANOVA was conducted to understand how each categorical variable given in Table 1 affected cell viability (Table 8). ANOVA revealed that there was a statistically significant difference between each category's mean cell viability value ($p<0.001$), except cell age (embryonic or adult) category. Coating the surface of silver NPs with biomolecules such as peptides, proteins, and DNA led to high cell viability values (95%). In contrast, microorganism-assisted (e.g., bacteria or algae) NP synthesis significantly reduced cell viability to 54%. The ANOVA analysis confirmed the negative correlation between exposure dose and cell viability, with concentrations ≥60 µg/mL killing almost half of the cells (Table 4.2). The silver NPs were slightly more toxic to cancer cells (68%) than normal cells (76%). The level of cytotoxicity caused by silver NPs was further influenced by the source and

morphology of cultured cells, as well as the type of assay used for toxicity screening ($p<0.001$).

Table 4.2. One-way ANOVA results

Parameter	n	Cell Viability (%) mean ± standard error	p-value
Coating (presence)			
Coated	3463	73.1 ± 33.4	*<0.001*
Uncoated	1014	65.6 ± 35.0	
Coating type			
Uncoated	1014	65.6 ± 35.0	
Bacteria	318	59.7 ± 33.7	
Fungi	258	70.8 ± 28.1	
Phospholipid	7	76.4 ± 25.4	
Plant extract	712	67.2 ± 31.6	
Polymer	635	70.9 ± 33.4	
Algae	75	53.6 ± 34.6	*<0.001*
Small molecule	736	78.5 ± 34.0	
Peptide, protein, or DNA	159	94.8 ± 33.4	
Surfactant w/wo* polymer	55	72.7 ± 25.6	
Nanoparticles w/wo* polymer	404	83.1 ± 30.6	
Small molecule w/wo* polymer	32	51.6 ± 32.2	
Small molecule mixture w/wo* nanoparticle	72	90.4 ± 23.9	
Nanoparticle exposure concentration			
0 µg/mL (untreated control)	702	100.0 ± 0.7	
0 – 1 µg/mL	381	91.2 ± 18.9	
1 – 10 µg/mL	1024	79.2 ± 27.7	
10 – 20 µg/mL	535	71.3 ± 34.1	
20 – 40 µg/mL	510	66.2 ± 33.5	*<0.001*
40 – 60 µg/mL	439	56.4 ± 35.5	
60 – 100 µg/mL	199	44.2 ± 24.6	
100 – 200 µg/mL	320	48.7 ± 32.4	
>200 µg/mL	367	34.5 ± 29.7	
Cell morphology			
Endothelial	56	77.5 ± 27.9	
Epithelial	3071	68.5 ± 33.4	
Fibroblast	759	74.9 ± 38.0	*<0.001*
Lymphoblast	506	83.0 ± 28.5	
Neuronal	85	73.7 ± 29.5	

(cont. on next page)

Table 4.2. (cont.)

Cell nature			
Healthy	1806	76.3 ± 35.3	*<0.001*
Cancer	2665	68.1 ± 32.7	
Cell origin			
Primary cells	143	90.5 ± 43.3	*<0.001*
Cell line	4334	70.8 ± 33.4	
Cell age			
Embryonic	251	72.9 ± 43.1	0.460
Adult	4226	71.3 ± 33.3	
Cell source (species)			
Human	3570	70.5 ± 33.6	*<0.001*
Mouse	654	76.6 ± 36.5	
Rat	175	71.1 ± 30.3	
Hamster	28	49.0 ± 35.2	
Bovine	11	53.9 ± 30.1	
Dog	3	99.4 ± 1.1	
Monkey	29	93.1 ± 14.7	
Pig	7	72.9 ± 18.4	
Cell source (organ/tissue)			
Ascites	129	88.5 ± 22.2	*<0.001*
Blood	214	85.7 ± 28.0	
Bone	250	79.4 ± 32.5	
Brain	109	73.9 ± 31.9	
Breast	513	61.9 ± 33.7	
Colon	289	72.0 ± 33.3	
Embryo	123	57.6 ± 36.3	
Kidney	138	76.1 ± 29.1	
Liver	415	72.4 ± 29.3	
Lung	605	75.9 ± 30.4	
Skin	668	67.4 ± 38.5	
Urinary systems	605	63.2 ± 36.0	
Others	337	81.5 ± 30.5	
Cytotoxicity assay			
MTT	2812	69.7 ± 33.1	*<0.001*
MTS	413	92.2 ± 32.7	
LDH	120	63.2 ± 33.5	
Dye-based	514	60.7 ± 34.2	
WST1/8	414	76.5 ± 32.6	
XTT	74	77.2 ± 23.9	
Presto Blue	97	71.2 ± 32.3	
Others	27	83.5 ± 16.4	

** w/wo: with or without*

To measure effect size, the eta-squared value describing the proportion of variance explained in an ANOVA model was calculated (Table S1). Large effects were only detected in the coating category (eta-squared: 0.33) based on the benchmark of 0.14 [289]. Next, Tukey's post-hoc test was performed to determine the significance of pairwise comparisons and to compare the means of groups that reached statistical significance (Table S2). A Pearson's correlation was run to assess the relationship between numeric parameters (mean particle size, hydrodynamic size, zeta potential, concentration, and exposure duration) and cell viability (%). The Pearson correlation coefficient of -0.37 suggested that cell viability and exposure concentration were moderately correlated in the opposite direction (Table S3).

Machine Learning Models. In the first attempts of machine learning modeling, all 16 features given in Table 1 were included, and the produced accuracy was around 20-40%. Suspecting that the collected data was too complex and heterogeneous for developing machine learning models with high predictive performance, we selected different sub-sets of features to generate *local* models. With the homogenized training data, the resulting DT models achieved an accuracy of 60-84%. The features included in the best-performing classification models and their predictive performance are summarized in Table 4.3.

Table 4.3. Performance of classification models built using different machine learning algorithms.

No. of data points and description	Features included	Algorithm	Accuracy	Precision	Sensitivity	AUC
3771 data points Complete and incomplete data without conc.= 0	Concentration Particle size Exposure time	DT	0.75	0.62	0.63	0.80
		LR	0.72	0.70	0.27	0.72
		GNB	0.71	0.69	0.25	0.65
		KNN	0.76	0.67	0.55	0.80
		RF	0.82	0.75	0.68	0.86
1515 data points Complete data without conc.= 0	Concentration Particle size Exposure time	DT	0.81	0.77	0.59	0.86
		LR	0.78	0.81	0.41	0.83
		GNB	0.79	0.82	0.43	0.81
		KNN	0.81	0.72	0.65	0.88
		RF	0.81	0.70	0.70	0.91
	Concentration Particle size Exposure time Zeta potential	**DT**	**0.84**	**0.89**	**0.56**	**0.86**
		LR	0.80	0.85	0.46	0.84
		GNB	0.79	0.78	0.47	0.79
		KNN	0.84	0.79	0.69	0.87
		RF	0.84	0.77	0.71	0.91

(cont. on next page)

Table 4.3. (cont.)

844 data points	Concentration	DT	0.82	0.79	0.73	0.88
	Particle size	LR	0.75	0.80	0.49	0.79
		GNB	0.72	0.79	0.41	0.75
Complete data	Exposure time	KNN	0.81	0.78	0.72	0.88
for uncoated nanosilver		RF	0.81	0.79	0.73	0.93
621 data points	Concentration	DT	0.82	0.67	0.62	0.79
		LR	0.74	0.56	0.1	0.73
	Particle size	GNB	0.74	0.58	0.14	0.74
Complete data	Exposure time	KNN	0.82	0.72	0.52	0.88
for small molecule		RF	0.82	0.72	0.56	0.90
289 data points	Concentration	DT	0.81	0.80	0.74	0.80
		LR	0.69	0.70	0.50	0.70
	Particle size	GNB	0.66	0.62	0.55	0.58
Complete data		KNN	0.76	0.72	0.74	0.82
for bacteria coated		RF	0.76	0.73	0.71	0.85
222 data points	Concentration	**DT**	**0.87**	**0.79**	**0.65**	**0.78**
	Particle size	LR	0.84	0.80	0.47	0.85
		GNB	0.84	0.80	0.47	0.76
Complete data	Exposure time	KNN	0.84	0.75	0.53	0.86
for fungi coated		RF	0.87	0.83	0.59	0.83
321 data points	Concentration	DT	0.86	0.63	0.63	0.74
		LR	0.85	0.64	0.47	0.77
	Particle size	GNB	0.86	0.63	0.63	0.74
Complete data		KNN	0.86	0.67	0.53	0.78
for nanoparticle coated		RF	0.88	0.77	0.53	0.89
125 data points	Particle size	DT	0.90	0.00	0.00	0.75
		LR	0.92	0.67	0.50	0.96
		GNB	0.92	0.67	0.50	0.97
Complete data for		KNN	0.89	0.00	0.00	0.93
peptide/protein/DNA		RF	0.95	1.00	0.50	0.96
589 data points	Concentration	DT	0.76	068	0.68	0.81
	Particle size	LR	0.66	0.67	0.21	0.63
		GNB	0.66	0.65	0.19	0.64
Complete data for plant	Exposure time	KNN	0.74	0.66	0.66	0.80
extract coated nanosilver		RF	0.82	0.78	0.74	0.86
545 data points	Concentration	DT	0.80	0.72	0.68	0.80
	Particle size	LR	0.73	0.84	0.28	0.77
		GNB	0.71	0.92	0.19	0.77
Complete data	Exposure time	KNN	0.82	0.81	0.61	0.81
for polymer coated		RF	0.76	0.68	0.60	0.86
381 data points	Particle size	DT	0.95	0.00	0.00	0.96
	Exposure time	LR	0.95	0.00	0.00	0.81
		GNB	0.95	0.00	0.00	0.72
Complete data	Coating	KNN	0.97	1.00	0.5	0.80
for conc. = 0-1 µg/mL	(binary)	RF	0.97	0.75	0.5	0.96
1024 data points		DT	0.86	0.75	0.18	0.85
	Particle size	LR	0.84	1.0	0.02	0.52
		GNB	0.83	0.4	0.04	0.61
Complete data	Exposure time	KNN	0.85	0.58	0.36	0.80
for conc. = 1-10 µg/mL		RF	0.87	0.63	0.44	0.85

(cont. on next page)

Table 4.3. (cont.)

535 data points Complete data for conc. = 10-20 µg/mL	Particle size Exposure time	DT	0.77	0.65	0.26	0.76
		LR	0.73	0.00	0.00	0.64
		GNB	0.75	0.62	0.12	0.64
		KNN	0.70	0.41	0.31	0.65
		RF	0.72	0.47	0.52	0.75
510 data points Complete data for conc. = 20-40 µg/mL	Particle size Exposure time	DT	0.65	0.44	0.43	0.73
		LR	0.69	0.00	0.00	0.48
		GNB	0.64	0.37	0.23	0.50
		KNN	0.69	0.50	0.47	0.66
		RF	0.71	0.53	0.49	0.73
439 data points Complete data for conc. = 40-60 µg/mL	Particle size Exposure time	DT	0.62	0.63	0.37	0.81
		LR	0.64	0.70	0.32	0.65
		GNB	0.59	0.61	0.24	0.59
		KNN	0.67	0.65	0.58	0.70
		RF	0.78	0.73	0.80	0.80
199 data points Complete data for conc. = 60-80 µg/mL	Particle size Exposure time	DT	0.63	0.64	0.89	0.77
		LR	0.60	0.60	1.00	0.38
		GNB	0.45	0.71	0.14	0.66
		KNN	0.58	0.65	0.67	0.60
		RF	0.68	0.74	0.72	0.76
320 data points Complete data for conc. = 80-100	Particle size Exposure time Coating (binary)	DT	0.67	0.67	0.82	0.74
		LR	0.51	0.55	0.78	0.60
		GNB	0.51	0.55	0.78	0.57
		KNN	0.72	0.71	0.85	0.73
		RF	0.72	0.72	0.81	0.79
364 data points Complete data for conc. > 100 µg/mL	Particle size Exposure time	**DT**	**0.82**	**0.85**	**0.93**	**0.92**
		LR	0.78	0.78	1.00	0.76
		GNB	0.78	0.78	1.00	0.76
		KNN	0.80	0.86	0.98	0.80
		RF	0.82	0.85	0.93	0.91

(DT: Decision Tree, LR: Logistic Regression, GNB: Gaussian Naive Bayes, KNN: K-Nearest Neighbor, RF: Random Forest) and different data subsets.

The DT model given in Figure 4.4 achieved an accuracy of 84% in predicting whether or not a silver-core NP is toxic. The dataset used to build the tree model included 1515 data points (i.e., case wise deletion was applied). Four features were selected based on their importance score, including concentration, zeta potential, particle size, and exposure time. Concentration was the best single predictor to start classification, with an importance score of 0.7. Early nodes were also formed by zeta potential, which had a feature importance score of 0.17. The relative importance of the remaining splitting variables, particle size, and exposure duration was less than 15% in total. The optimal decision tree model suggested a highly negative correlation between the concentration or

exposure time and cell viability, with increased NP concentrations and overlong exposures leading to an increase in the proportion of the toxic group.

Next, different machine learning models were developed for uncoated, small molecule-coated, bacteria-coated, fungi-coated, NP-coated, peptide/protein/ DNA-coated, plant extract-coated, or polymer-coated nanosilver (Table 4.3). Based on three parameters (concentration, exposure duration, and particle size), the highest prediction accuracy (87%) was achieved for fungi-coated nanosilver. Distinct models were also developed for each concentration category using different combinations of particle size, exposure duration, and the presence/absence of coating as predictors, with the highest prediction accuracy (82%) being achieved for the high concentration (≥100 μg/mL) class.

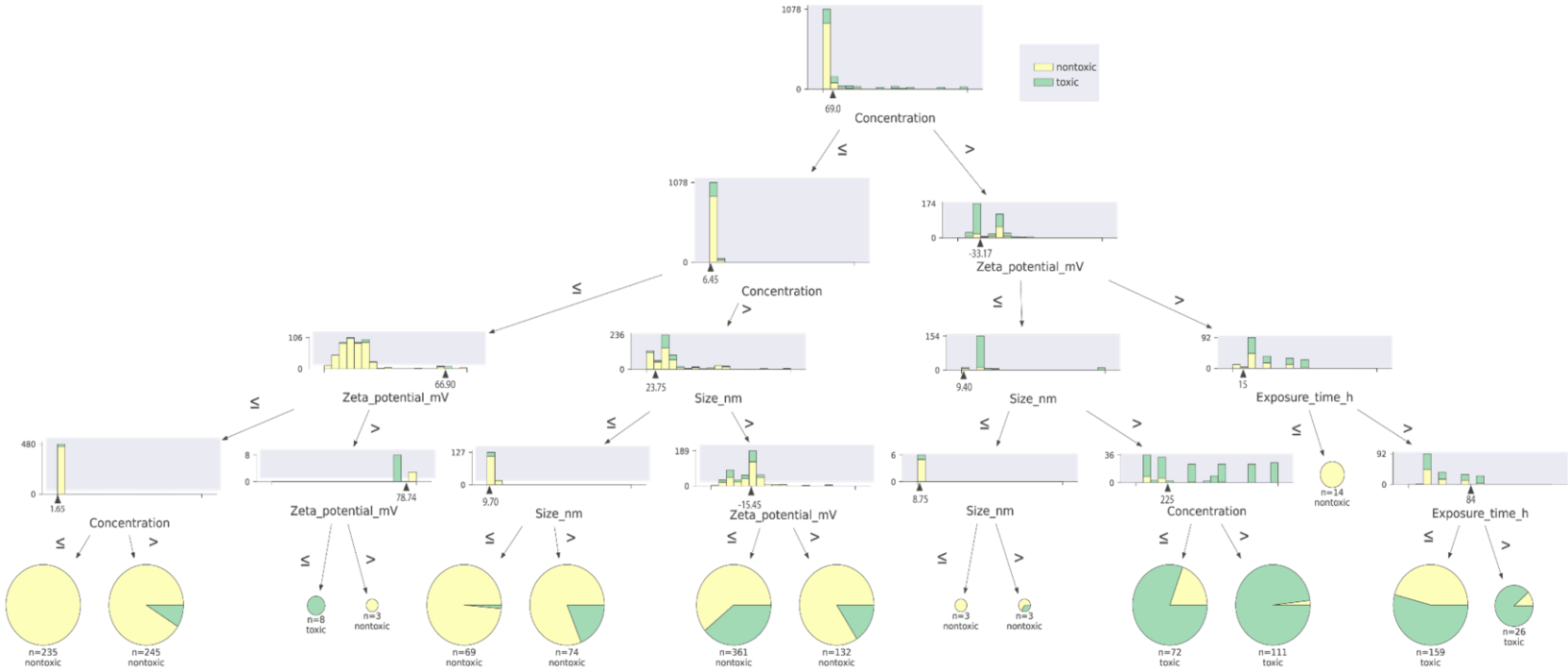

Figure 4.4. Optimal decision tree for predicting whether or not a silver-core nanoparticle is toxic.

A stacked histogram for splitting variables (colored according to cytotoxicity class) was provided at each node. The cut-off value for each splitting variable was shown with a small triangle (▲). The pie charts represent the proportion of toxic (green) and nontoxic (yellow) groups in terminal nodes.

Artificial Neural Network (ANN) Classifiers. For the ANN analysis, the dataset, including 1515 data points (after excluding con.= 0 and casewise deletion of missing data), was split into training (60%), test (20%), and validation (20%) sets. The ANN activation function was the hyperbolic tangent (tanh). The loss index used was the weighted squared error with L2 regularization [290]. The quasi-Newton method was used as an optimization algorithm. The charts in Figure 4.5 and 4.6 illustrate how the weighted squared error decreases with the increasing number of iterations and neurons, respectively.

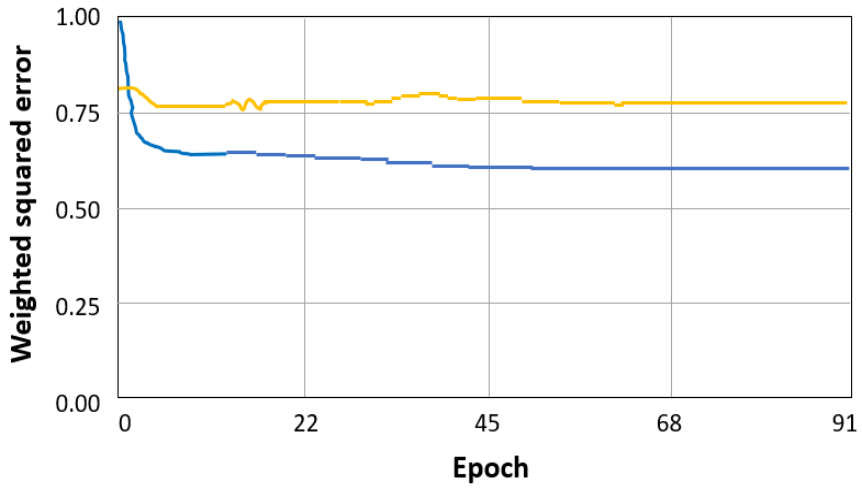

Figure 4.5. The training (blue) and selection (yellow) error as a function of the epoch (iteration) number

The network required approximately 10 epochs (iterations) of training to reach the minimum point (Fig 4.6). The optimal number of neurons was found to be 8 based on the training and selection error. The architecture of the final ANN model is given in Figure S10. The optimal ANN classification model included 4 inputs (particle size, NP concentration, zeta potential, and exposure duration) and 1 output (binary toxicity class). It consisted of a scaling layer, a perceptron layer with 8 neurons, and a probabilistic layer (Figure S10). It achieved an accuracy of 0.82, a sensitivity of 0.81, and a specificity of 0.83 (Table S4). The area under the curve was calculated as 0.88, indicating a great

performance. The relative importance of chosen input parameters was as follows: particle size (5.7%), exposure time (13%), coating (binary) (4.7%), and concentration (76.6%).

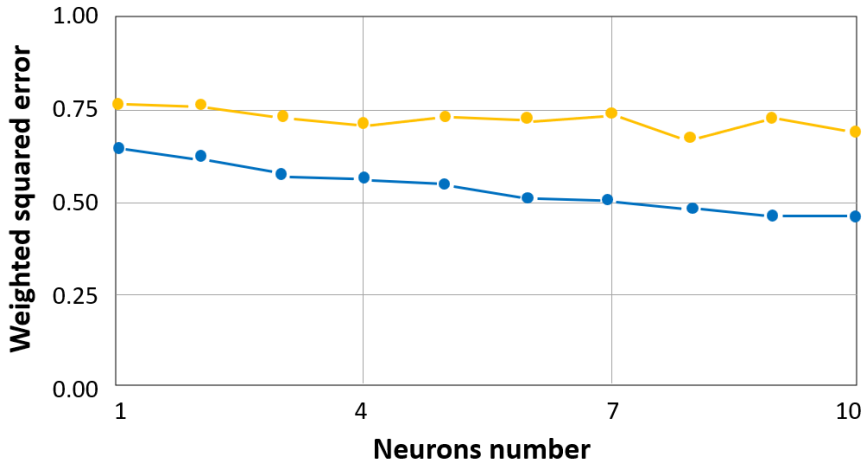

Figure 4.6. The training (blue) and selection (yellow) errors as a function of the number of neurons

4.3.1. Supporting Tables and Figures Associated with This Chapter

Table S1. Effect sizes for ANOVA Models

Attribute	**Cell Viability** **Eta-squared***
Coating category	0.06 (0.05 – 0.08)
Exposure concentration	0.33 (0.31 – 0.35)
Cell morphology	0.02 (0.01 – 0.03)
Cell nature (heathy or cancer cell line)	0.01 (0.01 – 0.02)
Cell source (species)	0.01 (0.00 – 0.01)
Cell source (tissue/organ)	0.05 (0.04 – 0.06)
Cytotoxicity assay	0.05 (0.04 – 0.06)

(Eta-squared is calculated by dividing the sum of squares of an effect for one variable, SS_{effect}, by the total sum of squares in the ANOVA model, SS_{total}) * 0.01: small effect size; 0.06: medium effect size; 0.14 or higher: large effect size

Table S2. Tukey's Post Hoc test results (results with statistical significance are reported only)

Parameter	**Group 1**	**Group 2**	**Mean Difference (Group2-Group1)**	***HSD-test***
Coating	Algea extract	Nanoparticles w/o polymer	29.49	*6.41**
		Peptide, protein or DNA	41.18	*8.95**
		Phospholipid	22.77	*4.95**
		Small molecule mixture w/o nanoparticle	36.81	*8.00**
		Small molecule	24.92	*5.42**
	Bacteria	Nanoparticles w/o polymer	23.42	*5.09**
		Peptide, protein or DNA	35.10	*7.63**
		Small molecule mixture w/o nanoparticle	30.74	*6.68**
	Peptide, protein or DNA	Fungi	-24.01	*5.22**
		Plant extract	-27.61	*6.00**
		Polymer	-23.85	*5.19**
		Small molecule w/o polymer	-41.16	*9.39**
		Uncoated	-29.23	*6.36**
		Surfactant	-22.07	*4.80**
	Small molecule mixture w/o nanoparticle	Plant extract	-23.25	*5.06**
		Small molecule w/o polymer	-38.80	*8.44**
		Uncoated	-24.87	*5.41**
	Small molecule w/o polymer	Nanoparticles w/o polymer	31.48	*6.85**
		Phospholipid	24.76	*5.38**
		Small molecule	26.91	*5.85**

(cont. on next page)

Table S2. (cont.)

Cell morphology	Endothelial	Epithelial	-9.06	*4.00**
	Epithelial	Lymphoblast	14.53	*6.42**
	Lymphoblast	Neuronal	-9.30	*4.11**
Cell source (species)	Bovine	Dog	45.45	*5.76**
		Monkey	39.18	*4.97**
	Hamster	Dog	50.40	*6.39**
		Monkey	44.13	*5.60**
Cell source (tissue/organ)	Ascites	Bone	-9.02	*4.93**
		Brain	-14.6	*7.98**
		Breast	-26.55	*14.51**
		Colon	-16.48	*9.00**
		Embryo	-30.91	*16.90**
		Kidney	-12.32	*6.84**
		Liver	-16.05	*8.78**
		Lung	-12.52	*6.84**
		Skin	-21.08	*11.52**
		Urinary	-25.22	*13.79**
	Blood	Brain	-11.84	*6.47**
		Breast	-23.79	*13.00**
		Colon	-13.72	*7.50**
		Embryo	-28.15	*15.39**
		Kidney	-9.56	*5.23**
		Liver	-13.29	*7.27**
		Lung	-9.76	*5.33**
		Skin	-18.31	*10.01**
		Urinary	-22.46	*12.28**
	Bone	Breast	-17.52	*9.58**
		Embryo	-21.89	*11.97**
		Skin	-12.05	*6.59**
		Urinary	-16.20	*8.85**
	Brain	Breast	-11.94	*6.53**
		Embryo	-16.31	*8.92**
		Urinary	-10.61	*5.80**
	Breast	Colon	10.07	*5.51**
		Kidney	14.23	*7.78**
		Liver	10.50	*5.74**
		Lung	14.03	*7.67**
		Other	19.60	*10.72**

(cont. on next page)

Table S2. (cont.)

Cell source (tissue/organ)	Colon	Embryo	-14.43	*7.89**
		Other	-9.53	*5.21**
		Urinary	-8.73	*4.78**
	Embryo	Kidney	18.59	*10.16**
		Liver	14.86	*8.12**
		Lung	18.40	*10.06**
		Other	23.97	*13.10**
		Skin	9.84	*5.38**
	Kidney	Skin	-8.75	*4.78**
		Urinary	-12.89	*7.05**
	Liver	Other	9.11	*4.98**
		Urinary	-9.16	*5.01**
	Other	Skin	-14.13	*7.28**
		Urinary	-18.27	*9.99**
	Lung	Urinary	-12.70	*6.94**
Test indicator	Dye inclusion or exclusion	Other	23.22	*7.93**
		Tetrazolium	12.88	*4.38**
	Other	LDH activity	-20.37	*6.92**
		Resazurin	-12.50	*4.25**

Table S3. Pearson correlation results

	$d_{TEM/SEM}$	***d_{DLS}***	***Zeta***	***Conc.***	***Duration***	***Viability***
$d_{TEM/SEM}$	---					
d_{DLS}	0.27 *<0.001*	-- -				
Zeta	*-0.08* *0.002*	-0.03 *0.194*	-- -			
Conc.	0.03 *0.085*	0.04 *0.050*	-0.09 *<0.001*	-- -		
Duration	0.018 *0.257*	-0.20 *<0.001*	-0.06 *<0.001*	0.01 *0.342*	---	
Viability	*-0.06* *<0.001*	0.01 *0.564*	-0.05 *0.012*	**-0.37** *<0.001*	-0.09 *<0.001*	---

Table S4. The optimal ANN model performance metrics

Metric	Description	Value
Classification	Ratio of cases correctly classified	0.825
Error rate	Ratio of cases misclassified	0.175
Sensitivity	Portion of real positive which are predicted	0.808
Specificity	Portion of real negative which are predicted	0.834
Precision	Portion of predicted positive which are real	0.719
F1 score	Harmonic mean of precision and sensitivity	0.760
AUC	The area under the receiver operating	0.877

4.3.2. Supporting Figures Associated with This Chapter

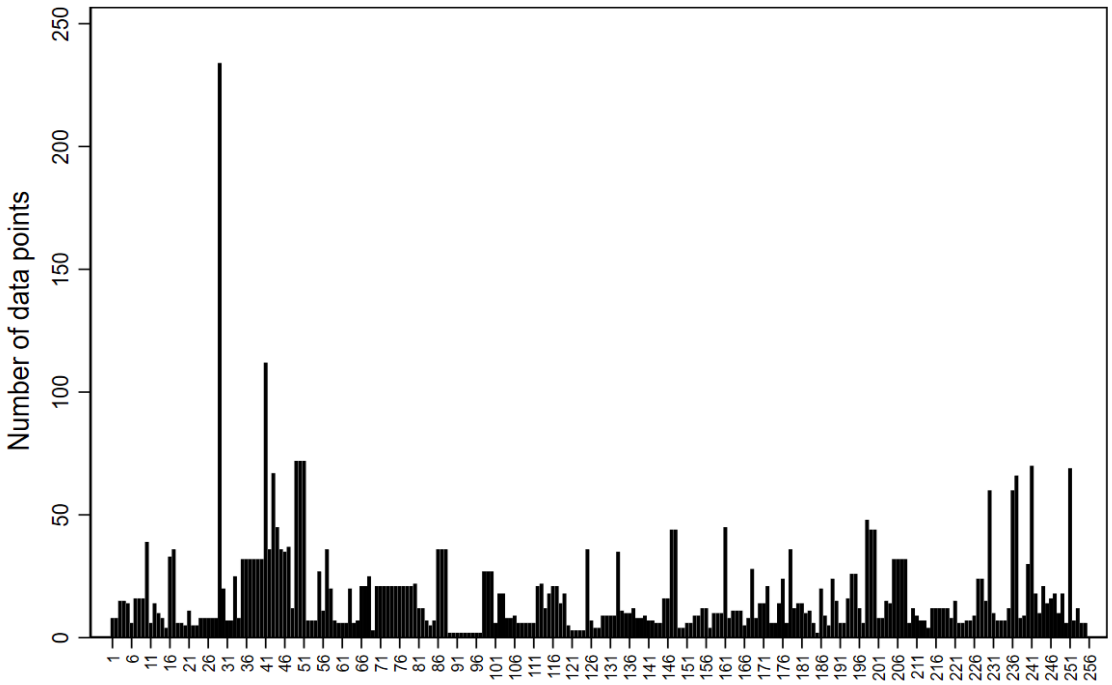

Figure S1. Number of data points per individual nanoparticle included in meta-analysis.

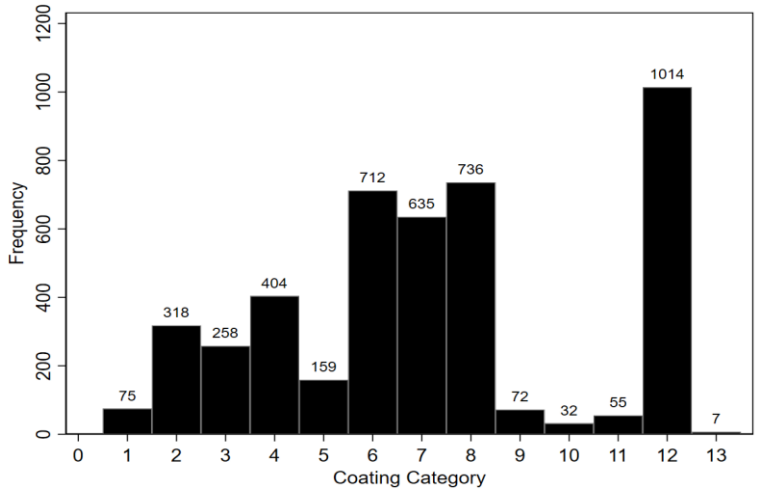

Figure S2. Frequency of data points per coating category.

1: Algae; 2: Bacteria; 3: Fungi; 4: Nanoparticles with or without polymer; 5: Peptide, protein or DNA; 6: Plant extract; 7:Polymer; 8: Small molecule; 9: Small molecule mixture with or without NP; 10: Small molecule with or without polymer; 11: Surfactant with or without polymer; 12: Uncoated; 13: Phospholipid

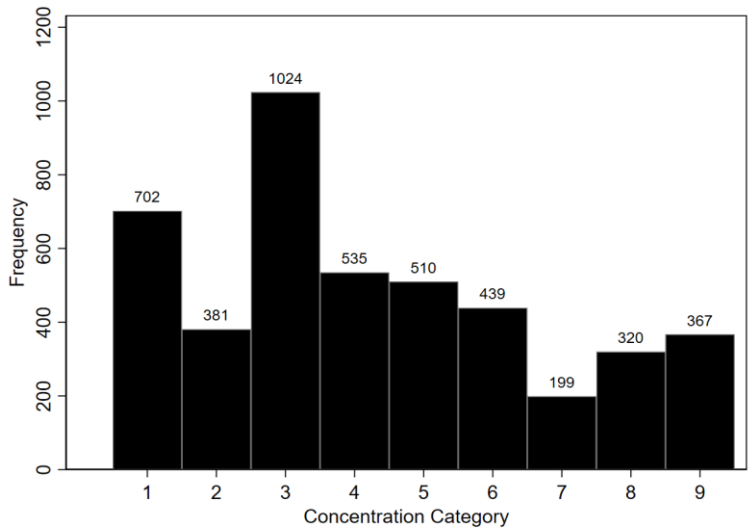

Figure S3. Frequency of data points per concentration category.

1: 0 µg/mL (untreated control); 2: 0 – 1 µg/mL; 3: 1 – 10 µg/mL; 4: 10 – 20 µg/mL; 5: 20 – 40 µg/mL; 6: 40 – 60 µg/mL; 7: 60 – 100 µg/mL; 8: 100 – 200 µg/mL; 9: >200 µg/mL

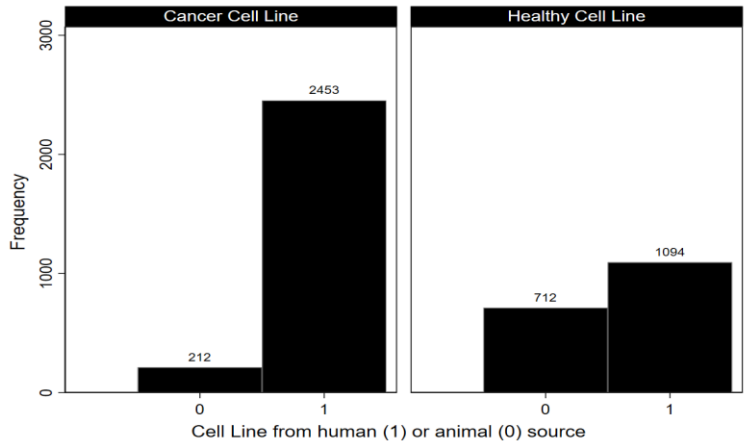

Figure S4. Frequency of data points per cell source (animal or human), grouped by cell nature (cancer or healthy).

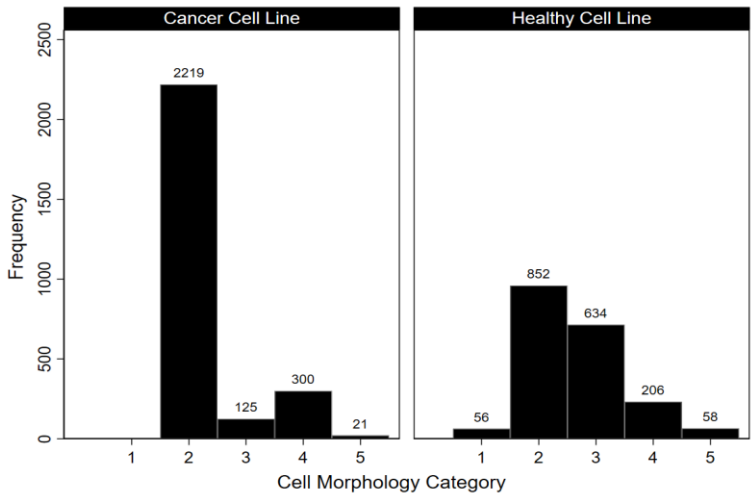

Figure S5. Frequency of data points per cell morphology category.

1: Endothelial; 2: Epithelial; 3: Fibroblast, 4: Lymphoblast; 5: Neuronal), grouped by cell nature (cancer or healthy

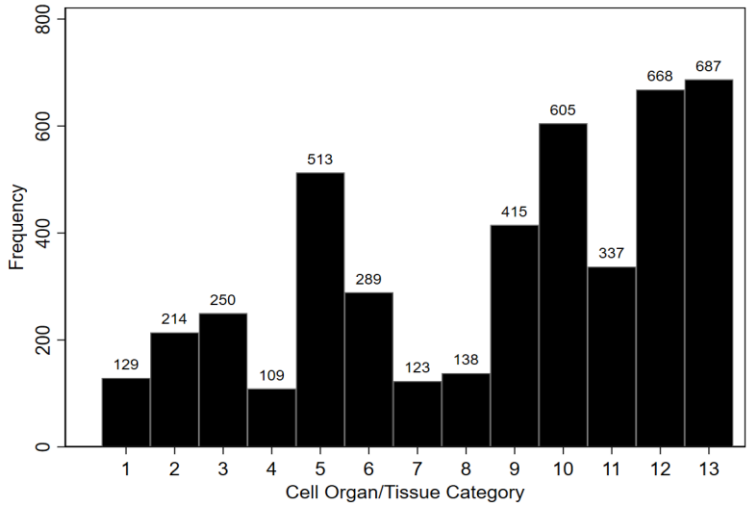

Figure S6. Frequency of data points per cell organ/tissue category.

1: Ascites; 2: Blood; 3: Bone; 4: Brain; 5: Breast; 6: Colon; 7: Embryo; 8: Kidney; 9: Liver; 10: Lung; 11: Others, 12: Skin; 13: Urinary systems

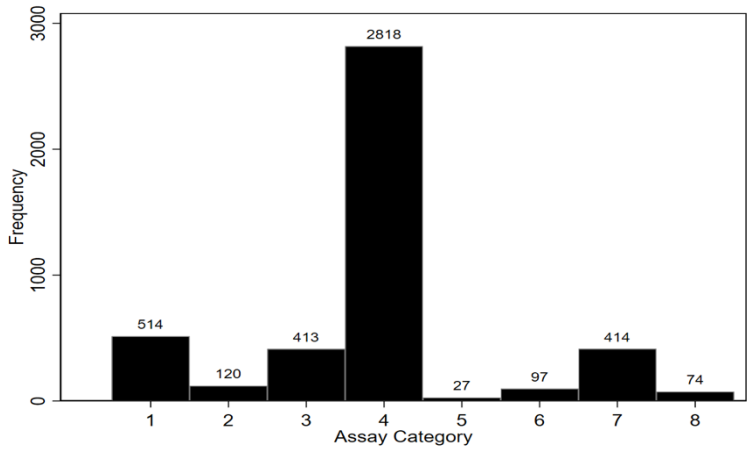

Figure S7. Frequency of data points per assay category.

1: Dye-based; 2: LDH; 3: MTS; 4: MTT; 5:Others; 6: Presto Blue; 7: WST1/8; 8: XTT

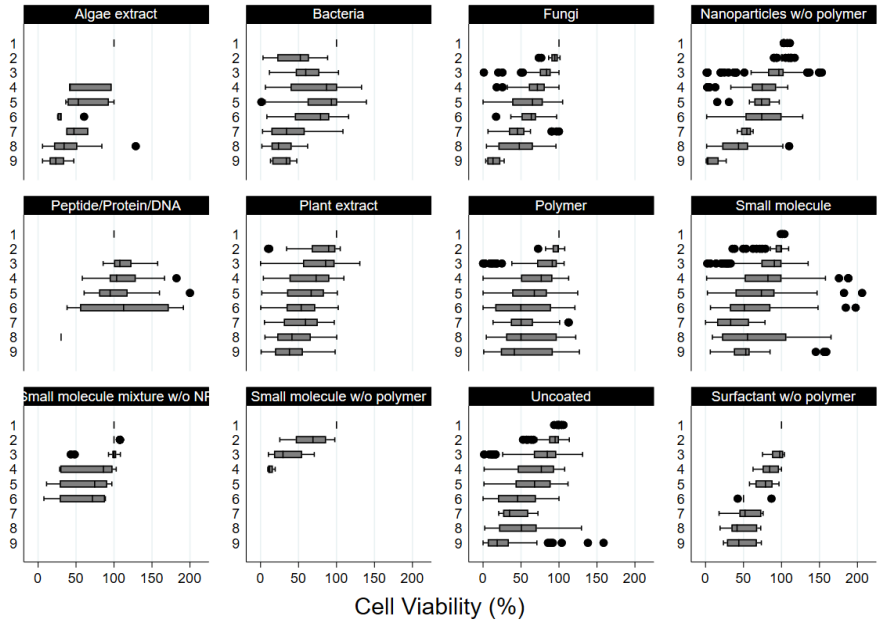

Figure S8. Box plot of changes in cell viability (%) as a function of NP exposure concentration category.

1: 0 µg/mL (untreated control); 2: 0 – 1 µg/mL; 3: 1 – 10 µg/mL; 4: 10 – 20 µg/mL; 5: 20 – 40 µg/mL; 6: 40 – 60 µg/mL; 7: 60 – 100 µg/mL; 8: 100 – 200 µg/mL; 9: >200 µg/mL, grouped by NP coating category. Circles outside the plot represent outliers beyond the 10th and 90th percentiles.

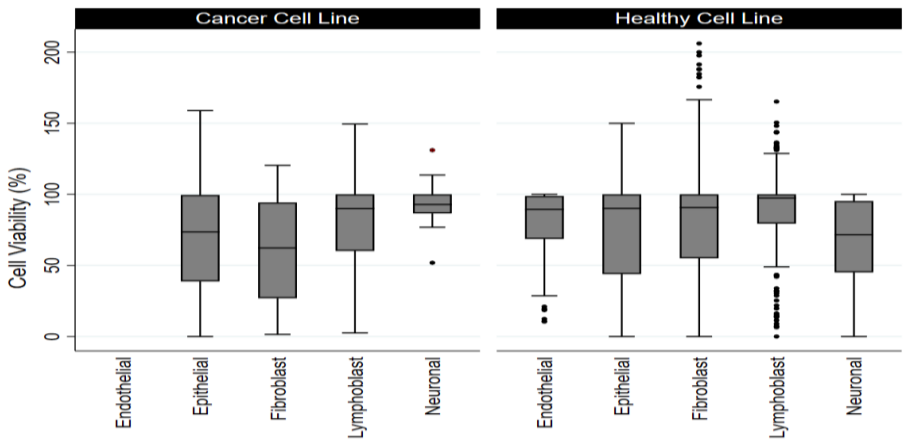

Figure S9. Box plot of changes in cell viability (%) as a function of cell morphology, grouped by cell nature (cancer or healthy).

Circles outside the plot represent outliers beyond the 10th and 90th percentiles.

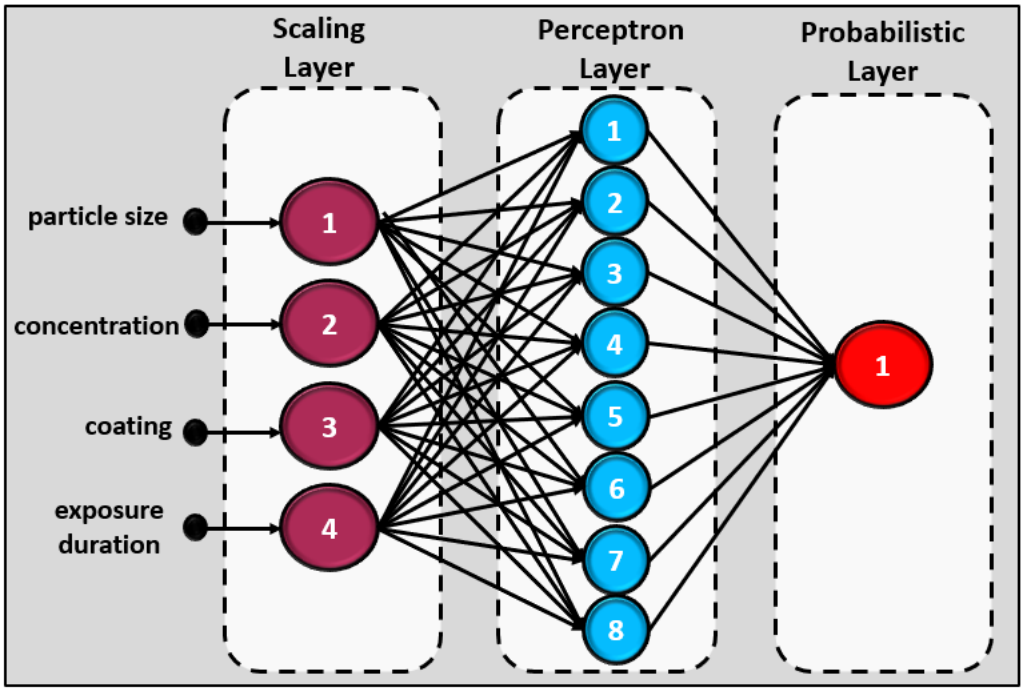

Figure S10. The structure of the ANN Model

4.4. Discussion

This study aggregated a large pool of data to build on previous work demonstrating the importance of machine learning algorithms to generate accurate predictions of NP cytotoxicity. First, five supervised classification algorithms were compared: Decision Tree, Random Forest, k-Nearest Neighbor, Naive Bayes, and Logistic Regression. Each classifier was trained multiple times using different input features and subsets of the collected data chosen based on coating material or concentration range. Algorithms were evaluated using out-of-sample validations. The highest accuracy (84%) in the models trained with the complete data (n=1515 data points excluding missing cases and untreated cell controls) was achieved when applying Random Forest, Decision Tree, and k-Nearest Neighbor, with the precision being generally higher for the Decision Tree model. An added advantage of the classification models with a tree-like structure of conditional statements is the simplicity and ease of interpretation. To further simplify the tree's interpretation without overloading

information, we used an informative visualization approach where the inner nodes and leaf nodes were combined with detailed histograms and pie chart representations of toxic and nontoxic classes, respectively [291].

Surprisingly, the performance of neural network models trained with the same dataset was not statistically very different than tree-based models, suggesting that increased sophistication in machine learning algorithms does not always translate into better predictions. Similar findings where tree-based ensemble models demonstrated superior performance for both classification and regression tasks were reported in many other studies [292-294]. An additional machine learning technique to consider would be gradient boosting and its advanced implementations, such as XGBoost Tree, which works by iteratively adding weak classifiers to an ensemble, with each model trying to compensate for the weaknesses of its predecessor [295, 296].

Predictive models were developed for the cytotoxic potential of nanosilver. Each model used a combination of NP-related (particle size, zeta potential, concentration, and coating), cell-related (nature, origin, organ/tissue source, age, and morphology), and assay-related (type, indicator, and duration) parameters, which have been related to the viability of nanosilver-treated cells. It is worth mentioning that the key physicochemical features of NPs such as particle size, shape, aggregation state, and zeta potential are dynamic, changing as a function of environmental conditions, biological interactions, and time [297, 298]. In particular, the surfaces of NPs become immediately coated by macromolecules (e.g., proteins and lipids) in the physiological environment, and this newly-formed layer masks physicochemical characteristics of pristine (as-received or as-manufactured) NPs. Therefore, linking intrinsic NP characteristics to their biological activity measured *in vitro* requires a deeper understanding of how the adsorbed biomolecule layer (so-called protein corona layer) changes the key NP characteristics under realistic exposure conditions and how these changes are reflected in their biological identity/behavior.

The accuracy of models including all features did not exceed the chance level, suggesting that the performance of machine learning models could have suffered due to the inclusion of redundant attributes. The features included in best-performing models were NP concentration, exposure duration, coating, zeta potential, and particle size, with the first two being relatively more influential. This finding highlights the importance of using relevant exposure conditions when characterizing the potential health effects of NPs on human health. The use of unrealistically high concentrations or exposure durations can

magnify the severity of the induced effect and prevent most of the beneficial uses of NPs, while lower values of those parameters could mask potentially harmful effects. As included in the screening strategies of NPs, designing nanotoxicity testing parameters in line with the anticipated human exposure levels is critical to avoid over/underestimating the actual risks [86, 299].

The major strength of this work is the aggregation of a large pool of data (n=162 independent studies) on which machine learning models are trained, which is a larger training data size than much of the previous work [277, 300, 301]. The included studies differed in terms of experimental protocols followed, which provide a reasonable estimate of the applicability of developed classification models. Another strength is the implementation of various machine learning algorithms to minimize errors in cytotoxicity prediction. The main limitation of this study is the absence of physicochemical characterization data measured under conditions that closely mimic the relevant physiological environment and the resulting difficulty of linking intrinsic NP characteristics to observed biological activity. A further limitation was the high number of missing values in zeta potential measurements, which was partly dealt with by excluding the entire data record from analysis if any single parameter was missing. Finally, it is important not to interpret the reported models as definite, foolproof or fixed as they potentially reflect the assumptions, biases, and errors of the data sources and need to be updated regularly as the new data become available. One area of future work is to incorporate new data when it is generated and to validate the computational findings with systemically designed experimental observations.

4.5. Conclusion

There are several challenges to overcome before the potential of nano-enabled products can truly be realized, starting with the development of a complete understanding of nanosafety-related concepts. Systematic reviews and statistical procedures are increasingly adopted in health risk assessments to decide whether a NP is a viable candidate for medical applications. By statistically and strategically combining evidence from multiple studies in the nanotoxicity domain, it is possible to generate accurate

estimations of the actual risks posed by NPs. In this work, we investigated the relationship between both NP- (concentration, size, zeta potential, and coating) and assay-related (cell type, test indicator, exposure duration, etc.) parameters and the cytotoxic response of silver NPs using a meta-analytic dataset encompassing over 4477 data points from 162 studies. Heterogeneity within the collected data was explored by performing subgroup analyses and visualizations. Beyond looking at hidden patterns within the subgroup of studies, we developed machine learning models that can predict the cytotoxicity of silver NPs with high classification accuracies (>0.84). While the scope of this analysis is limited to cytotoxicity, similar data-driven models can also be developed for different toxicity endpoints (e.g., NP-induced genotoxicity or oxidative stress) or well-defined regions of chemical space. Such meta-analytic approaches represent a major step toward including safety at the earliest possible stage of NM development, the so-called *safe-by-design* (SbyD) concept.

CHAPTER 5

IDENTIFYING FACTORS CONTROLLING CELLULAR UPTAKE OF GOLD NANOPARTICLES BY MACHINE LEARNING

5.1. Background

There is strong interest to improve the therapeutic potential of gold nanoparticles (GNPs) while ensuring their safe development. The utility of GNPs in medicine requires a molecular-level understanding of how GNPs interact with biological systems. Despite considerable research efforts devoted to monitoring the internalization of GNPs, there is still insufficient understanding of the factors responsible for the variability in GNP uptake in different cell types. Data-driven models are useful for identifying the sources of this variability. Here, we trained multiple machine learning models on 2077 data points for 193 individual NPs from 59 independent studies to predict cellular uptake level of GNPs and compared different algorithms for their efficacies of prediction. The five ensemble learners (Xgboost, random forest, bootstrap aggregation, gradient boosting, light gradient boosting machine) made the best predictions of GNP uptake, accounting for 80-90% of the variance in the test data. The models identified particle size, zeta potential, GNP concentration and exposure duration as the most important drivers of cellular uptake. We expect this proof-of-concept study will foster the more effective use of accumulated cellular uptake data for GNPs and minimize any methodological bias in individual studies that may lead to under- or over-estimation of cellular internalization rates.

5.1.1. GNPs and Cellular Uptake

NP are defined as a materials with at least one dimension < 100 nm [13, 302]. Their small size and high surface to volume ratios elicit novel characteristics relative to bulk materials that find applications in a diverse areas such as electronics, energy, agriculture, and the healthcare industry [303]. Today, thousands of commercial products contain NPs while many others are produced using nano-enabled tools [304]. The use of nanotechnology in healthcare applications has led to the development of new diagnostic molecules and drugs with improved functionality and therapeutic outputs [305, 306].

In the field of medicine, the most important problems are driven by processes at the molecular/nanoscale level. Consequently, nanoscale diagnostics and therapeutics allow fine-tuning of material properties to target specific cells or tissues [306, 307]. For example, nanoscale silica, lipids, polymers, metallics and carbon nanotubes are sometimes administered intravenously to target diseased cells, and kill them selectively [308]. Although several types of NP are commonly used in medical applications, gold NPs (GNPs) are of particular diagnostic and therapeutic interest due to their useful optical properties [309].

GNPs can be synthesized from other forms of gold by laser ablation or chemically by using reducing and stabilizing agents [310, 311]. Nano-sized gold displays useful characteristics not seen in bulk gold, making them especially useful for medical applications such as bioimaging, drug and gene delivery, targeting, photothermal therapy, and radiotherapy [312]. Their surfaces can be easily modified for specific cell targeting applications to improve disease management and to treat conditions not responsive to available medications [313]. Furthermore, colloidal GNPs exhibit so-called surface plasmon resonance (SPR), a particular interaction between light and matter when a specific wavelength of light is applied [314], making them promising agents for hyperthermic cancer treatments and medical imaging [315].

GNPs can function as delivery vehicles, therapeutics, or theranostics (diagnostics and therapeutics combined), a promising, relatively new concept for medicine [316]. When used for targeted drug delivery and release, GNPs are generally composed of a nano-size gold core with a surface monolayer containing the drugs and/or other (e.g., targeting) molecules [317, 318]. Drug-loaded GNPs are commonly combined with targeting agents to

provide safety for healthy bystander cells. Once bound to disease cells, they are taken up through different uptake mechanisms depending on their size and shape [319, 320].

GNPs have diverse sizes, shapes, surface coatings, functionalities, and charges. Earlier work suggested (incorrectly) that positively charged GNPs were always more toxic than negatively charge ones because they could disrupt the negatively charged cell membrane [321, 322]. Another common early misconception was that small NPs were more toxic than larger ones [323]. While it is true that particle size and surface characteristics are important determinants of cellular uptake and the fate of translocated NPs in the body, it was simplistic to associate certain NP sizes or morphologies with a specific internalization rates or toxicity profiles [324]. An important research challenge in nanomedicine is therefore deciphering how to control cellular internalization and safe uptake of NPs by altering the shape, size, and surface properties [243, 298, 325].

There is increasing evidence that morphology and surface charge modulate cellular uptake of GNPs, but most investigations have produced inconclusive and inconsistent results [326-328]. To better leverage value of this existing literature data resource and to resolve controversies arising from inconsistent findings in prior research, it is helpful to create a pooled (or *absolute*) estimate by combining findings from separate studies and critically appraising total bodies of evidence. While many meta-analytic studies report NP cytotoxicity, none focus on the cellular uptake profile of the NPs. Here, we present a meta-analysis of cellular uptake by combining data on intracellular uptake of GNPs from the period 2010–2023. We hypothesize that cellular uptake rate of GNPs can be predicted from their characteristics (e.g., particle size, shape, concentration, surface charge, and coating) and experimental conditions (e.g., cell type and morphology, and exposure duration and concentration). We trained multiple machine learning models on these features that aimed to predict cellular uptake on GNPs and compared them for their efficacies of prediction.

5.2. Methods

5.2.1. Literature Search and Data Extraction

A systematic literature search was undertaken using SCOPUS and Google Scholar search engines (Figure 5.1). The search was restricted to English-language articles published between 2000 and 2023. Combinations of the following keywords were used for the article search: gold; nano*; ICP*; cell; uptake. This yielded an initial pool of 100+ peer-reviewed studies, 91 of which were manually filtered by: (i) the core of the studied NP must be gold; (ii) cellular uptake data must be available; and (iii) the unit of cellular uptake must be convertible to pg Au/cell. A total of 2077 data points from 59 studies remained after cleaning and formatting and were included in the meta-analysis.

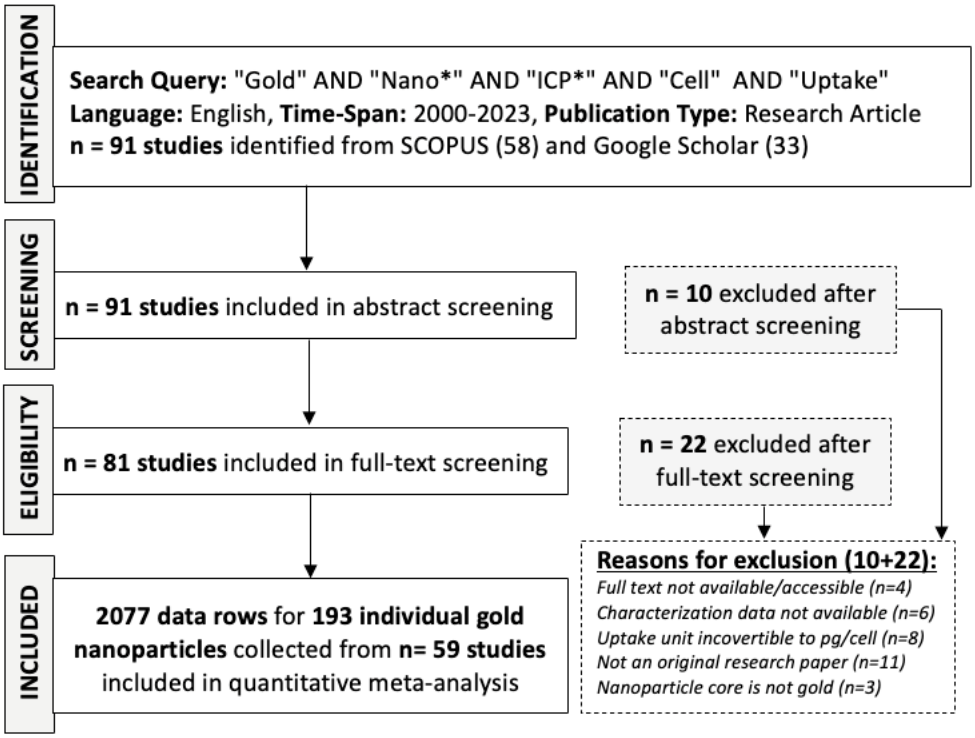

Figure 5.1. Data search and selection procedure

5.2.2. Data Cleaning and Pre-processing

The raw dataset included 2077 rows, each corresponding to a single cellular uptake measurement, and 25 columns summarizing NP properties and *in vitro* test conditions. Surface-coated GNPs were divided into 10 categories according to the coating material (e.g., polymer, protein, small-molecule, metal, peptide, DNA, albumin etc.). A (base 10) log transformation was applied to the cellular uptake data that was converted to pg Au per cell. The final dataset was randomly divided into training (75%) and test set (25%). Parameters with high correlation values (>0.7) were identified, and only one of the correlated pairs was included in the modelling process.

5.2.3. Descriptive Statistics

One-way analysis of variance (ANOVA) was used to determine how strongly each of the categorical parameters describing NP, cell line, or assay characteristics was related to cellular uptake level. A box plot was used to display the distribution and skewness of the cellular uptake data. ANOVA and box plot visualization were performed using STATA/IC statistical software (version 16.1; StataCorp). Significance was reported at $p < 0.05$ and $p < 0.001$ levels.

5.2.4. Machine Learning

Five ensemble learners, a general meta-approach to machine learning that improves predictive performance by combining the predictions from multiple models, were employed in this study: XGBoost (XGB), random forest (RF), bootstrap aggregation (BA), gradient boosting (GB) and light gradient boosting machine (LGB). In XGB (*extreme gradient boosting trees*), each tree within the scheme boosts the attributes to correct the errors of the previous tree [329]. RF is a version of ensemble learning that

provides improvement over bagged decision trees by training individual models in parallel and creating a diverse group of ensemble members [330]. BA, also called *bagging*, fits a decision tree on a number of subsets of training data chosen at random with replacement [331]. GB is a family of models that are added to the ensemble sequentially such that each new models tries to minimize the prediction error of the previous one [332]. LGB is a gradient boosting framework that differs from XGBoost in tree construction (i.e. trees are grown leaf-wise rather than level-wise) [333].

In this study, the response variable was the log-transformed cellular uptake level, while the predictors were physicochemical characteristics of GNPs and assay conditions. The Random Forest Regressor, Bagging Regressor, Gradient Boosting Regressor, and Hist Gradient Boosting Regressor, implemented in Python's sklearn.ensemble module, were used with standard settings to construct RF, BA, GB and LGB models. The XGBoost package was utilized to construct the XGB model. 25% of the data were reserved as a test set to compare the performance of models and the best performing ones were selected based on the R-squared (R^2) value and measures of dispersion (e.g., mean absolute error (MAE) and root mean square error (RMSE)) for the test set predictions. To understand the role of the different parameters in the cellular uptake predictions, the Scikit "feature importance" function implemented in Python was used. The performance of ensemble regressors was compared with 13 other linear and nonlinear machine learning algorithms implemented in Python libraries. The versions were Python 3.8.10 and Scikit-learn 1.0.2.

Of the nonlinear ML methods, decision trees (DT) are classifiers that are easy to interpret but are ill-posed (a small change in data can lead to a large change in optimal tree structure), and are often relatively inaccurate compared to ensemble methods like RF [334, 335]. The k-nearest neighbors (k-NN) method is fast and nonparametric regression method but suffers from sensitivity to the local structure of the data [336]. The support vector machine (SVM) is a machine learning method that maps inputs into high-dimensional feature spaces but it is prone to overfitting [337]. Adaboost is a type of linear regression where the normal quadratic cost function is replaced by an exponential function [338]. Bayesian ridge regression is a type of linear regression where Bayes rule is used to regularize the regression to control the complexity of the linear model [339]. Ridge regression, beneficial when there is multicollinearity in the features, is a special case of Bayesian regression [340]. Stochastic gradient descent regression is a linear modelling algorithm in which the gradient (calculated from the entire data set) is approximated by a

stochastic estimate of it (calculated from a randomly selected subset of the data) [341]. It is particularly useful for very large data sets. The Theil–Sen estimator robustly fits a line to sample points (simple linear regression) by choosing the median of the slopes of all lines through pairs of points [342, 343]. Compared to ordinary least squares regression, it is insensitive to outliers, can be used when residuals are not normally distributed, can be more accurate than simple linear regression for skewed and heteroskedastic data, and competes well with least squares for normally distributed data. Tweedie, Huber, and Poisson regression (log-linear) models are all forms of generalized linear regression that deal with non-Normal or skewed data distributions in different ways [344].

Artificial neural networks (ANN) are one of the most popular algorithms in machine learning [284-286]. The processing units of ANNs are called layers: input, output, and hidden. Each layer contains a number of neurons or nodes that contain transfer functions that transform the data they receive. The input layer contains with the same number of nodes as inputs, each of which contain a linear transfer function. The output layer contains a single node that predicts the final output. This node generally has a linear transfer function for regression and a sigmoidal transfer function for classification. The hidden layers perform most of the computations required to generate the model and contain a variable number of nodes with (usually) nonlinear transfer functions. Each node has an associated weight and activation threshold above which the data is sent to the next network layer. A range of activation functions (e.g., sigmoid or the Rectified Linear Unit (ReLU) function) can be used to compress the weighted sums into the interval of 0–1 in ANN models. The most common algorithm used to train neural networks (i.e., find which weights and biases minimize a specific cost function) is called backpropagation. Here, *errors in predicting the output* are propagated backwards from output to input nodes. In this study, the backpropagation algorithm was used for reducing the network error. Different numbers of hidden layers and nodes in those hidden layers, different activation functions (ReLU, tanh, sigmoid, linear, eLU), batch sizes (32, 64 and 128), and learning rates (0.0001-0.01) were compared based on measures of dispersion (MAE, RMSE) for the test set predictions. The hyperparameters used to train models are given in Table S1.

5.3. Results and Discussion

A summary of the data 2077 records from 193 independent studies remaining after applying the inclusion criteria is provided in Table 5.1. Characteristics of collected data are presented in Figure S11-S18.

Table 5.1. Dataset description

Parameter	Type	Range
Nanoparticle Characteristics		
$NP_{Size\ by}$	Numerical	3 – 205 nm
$NP_{Size\ by\ DLS}$	Numerical	3 – 1070 nm
$NP_{Zeta\ potential}$	Numerical	-75 – +65.5
NP_{Shape}	Categorical	Spherical (72%), Rod (17%), Shell (5%), Cubic (2%), Triangular (2%), Star (1%)
$NP_{Coating}$	Categorical	Uncoated (10%), Polymer (20.9%), Protein (5.2%), Small molecules (37%), Metallic (1.7%) Polymer_protein (11.5%), Peptide_antibody (1.7%),
Viability Assay		
$Cell_{Viability}$	Numerical	0 – 150%
$Exposure_{Time}$	Numerical	1 – 96h
$Exposure_{Con.}$	Numerical	0 – 10000 μg/mL
ICP-based Uptake Assay		
$Cell_{uptake}$	Numerical	0 – 518 pg Au/cell
$Cell_{Morphology}$	Categorical	Epithelial (85.4%), Macrophage (7.9%), Fibroblast (4.3%), Endothelial (1.3%), Neuron (0.7%), Multi–
$Cell_{Condition}$	Categorical	Healthy (68%), Cancer (32%)
$Cell_{Source}$	Categorical	Human (87.3%), Mouse (10.7%), Rat (1.2%), Monkey (0.4%), Dog (0.4%)

(cont. on next page)

Table 5.1. (cont.)

$Cell_{Organ/System}$	*Categorical*	*Circulatory (2%), Reproductive (38.1%), Digestive (34.5%), Nervous (1.5%), Embryonic (1.8%), Excretory (13.8%), Integumentary (4.1%), Respiratory (3.1),*
$Exposure_{Time}$	Numerical	0h (4%), 1h (7%), 2h (5%), 3h (5.5%), 4h (7.5%), 6h (7%), 8h (6.3%), 12h (10.3%), 16h (3.2%), 24h (32%), 36h (0.3%), 48h (2.2%), 72 (1.5%), 96h (0.2%)
$Exposure_{Con.}$	Numerical	0 – 1000 µg/mL
$Assay_{Type}$	Categorical	ICP_MS (72.9%), ICP_AES (15%), ICP_OES (11.1%), ICP_AAS (1%)

5.3.1. Statistical Analyses

A series of one-way ANOVAs were conducted to understand how the categorical variables modulated cellular uptake (Table S2). The variation of cellular uptake with NP shape and surface modification was statistically significant ($p < 0.001$). Coating of GNP surfaces with protein or small molecules (e.g., Thiol and DMSA) resulted in higher gold mass in exposed cells while albumin coating led to decrease in cellular internalization of GNPs. This is consistent with the results of Li et al. [345] who showed that albumin pre-coating on GNPs led to a lower intracellular Au mass when compared to pristine GNPs. The number of internalized GNPs was slightly higher in cancer cells compared to healthy ones ($p=0.05$), and particularly low in healthy fibroblasts. This is also consistent with the findings of Bromma et al., who reported that the cancer cells (HeLa and MDA-MB-231) had a higher uptake compared to normal fibroblasts cells [346]. When comparing the cellular internalization of GNPs with different shape configurations, the highest uptake was found for gold nanoshells (Table S2). The results of univariate analysis suggest that the interplay between GNP properties and cellular internalization profile is complex and requires a multivariate, nonlinear modelling approach.

5.3.2. Regression Machine Learning Models

Next, we trained regression models using ensemble regression, discrete nonlinear regression, and linear regression methods and used them to predict cellular uptake level of GNPs in the test set.

R^2 (coefficient of determination), root mean squared error (RMSE), and mean absolute error (MAE) values for prediction of training and test sets were calculated. Measures of dispersion such as RMSE and MAE are preferred when comparing the quality of model predictions [347]. We used MAE as the primary metric for comparing models because it is less influenced by a few large outliers than is RMSE [348].

Table 5.2 shows the relative performance of regression models fall broadly into three classes when assessed by the MAE of the test set predictions. The three classes are models based on ensemble learning (MAE 0.3-0.5), those estimated by discrete nonlinear methods (MAE 0.5-0.7), and those generated by linear methods (MAE 0.9-1.0). Clearly, the nonlinear ensemble learning methods are superior to the other two classes of methods, also indicating substantial nonlinearity on the relationship between GNP features and uptake. Best agreement overall between the test set predictions and measurements for GNP uptake was found for XGBoost (MAE:0.31), closely followed by random forest (MAE:0.37) and bagging aggregate (MAE:0.38).

Plots of cellular uptake measurements (x-axis) against the predicted values (y-axis) for XGBoost and four other ensemble models are shown in Fig. 5.2 and Fig. S19, respectively. The diagonal lines on the plots represent the best-fit regression line through the data.

5.3.3. Feature Importance and Model Interpretation

Fig. 5.3 displays the impurity-based importance scores of GNP characteristics and experimental parameters for predicting cellular uptake.

Table 5.2. Performance of regression algorithms

Algorithm	R^2		*RMSE*		*MAE*	
	Train	*Test*	*Train*	*Test*	*Train*	*Test*
Ensemble learners						
XGBoost	0.99	0.88	0.08	0.50	0.05	**0.31**
Random Forest	0.97	0.83	0.23	0.58	0.14	**0.37**
Bootstrap Aggregation (bagging)	0.97	0.82	0.25	0.60	0.15	**0.38**
Light Gradient Boosting	0.94	0.81	0.34	0.63	0.23	**0.41**
Gradient Boosting	0.81	0.71	0.62	0.78	0.46	**0.56**
Class mean ± SD	0.94±0.06	0.81±0.06	0.30±0.18	0.62±0.09	0.21±0.14	**0.41**±0.08
Discrete nonlinear methods						
Decision Tree	0.89	0.69	0.47	0.80	0.32	**0.53**
K-Nearest Neighbors	0.69	0.57	0.81	0.94	0.56	**0.66**
BPNN (ReLu, 4 neurons in hidden layer)	0.74	0.57	0.63	0.89	0.60	**0.68**
Support Vector Regression (RBF kernel)	0.59	0.47	0.92	1.04	0.61	**0.70**
Class mean ± SD	0.73±0.13	0.58±0.09	0.71±0.20	0.92±0.10	0.52± 0.14	**0.64**±0.08
Linear methods						
AdaBoost	0.41	0.39	1.11	1.11	0.95	**0.96**
BayesianRidge	0.35	0.29	1.17	1.20	0.90	**0.92**
Stochastic Gradient Descent	0.35	0.29	1.17	1.20	0.89	**0.91**
Ridge with Cross-Validation	0.35	0.29	1.16	1.20	0.89	**0.92**
Generalized Additive Models	0.42	0.27	1.09	1.22	0.85	**0.96**
Huber Regression	0.33	0.26	1.18	1.24	0.87	**0.91**
Support Vector Regression (linear	0.32	0.25	1.19	1.24	0.86	**0.90**
Poisson Regression	0.28	0.24	1.22	1.25	1.00	**1.01**
Tweedie Regression	0.26	0.22	1.24	1.27	1.02	**1.03**
Theil – Sen Regression	0.19	0.16	1.34	1.33	0.97	**0.96**
Class mean ± SD	0.33±0.07	0.27±0.06	1.19±0.07	1.23±0.06	0.92±0.06	**0.95**±0.04

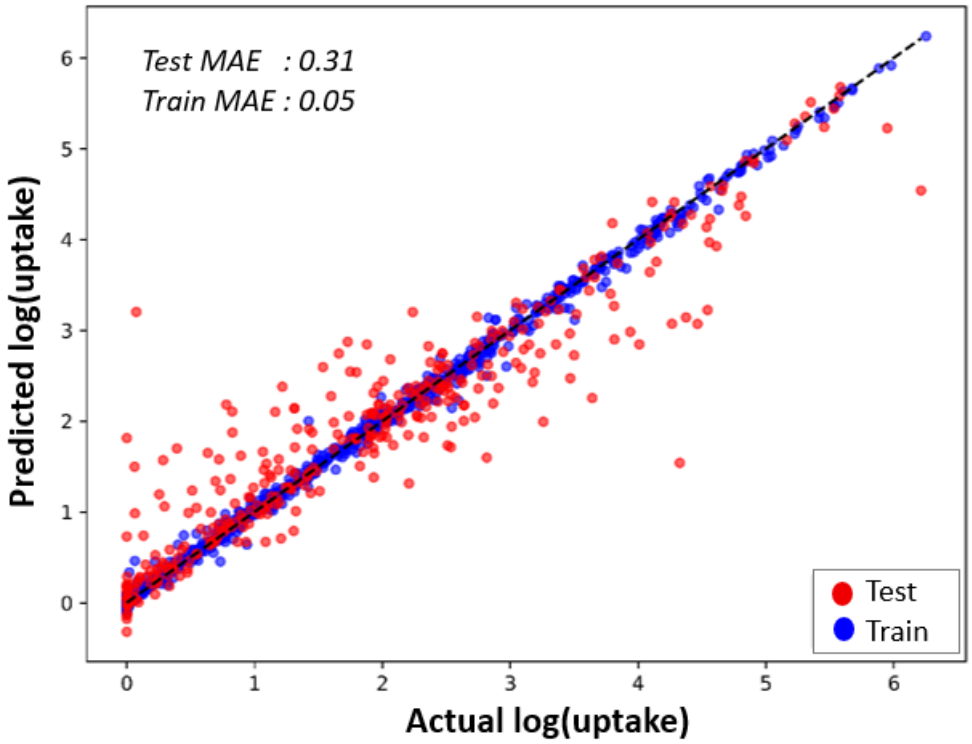

Figure 5.2. Scatterplot of measured cellular uptake (x-axis) against predictions (y-axis) for XGBoost ensemble model.

The agreement between feature importances calculated by the ensemble learners is good considering that for nonlinear models, feature importance is a local rather than global model property. As expected, exposure concentration and time were among the strongest predictors of cellular uptake. The positive relationship between uptake level and exposure concentration was consistent for all cells but prolonged exposure not always resulted in increased uptake. As reported elsewhere [349], we observed that different cell lines displayed unique GNP uptake profiles. For example, the time required for maximal GNP uptake ranged between 3-24h for HepG2, HeLa, A549 and SKOV3 cells, and the cell lines maintained either a similar amount or less internalized GNPs after this point.

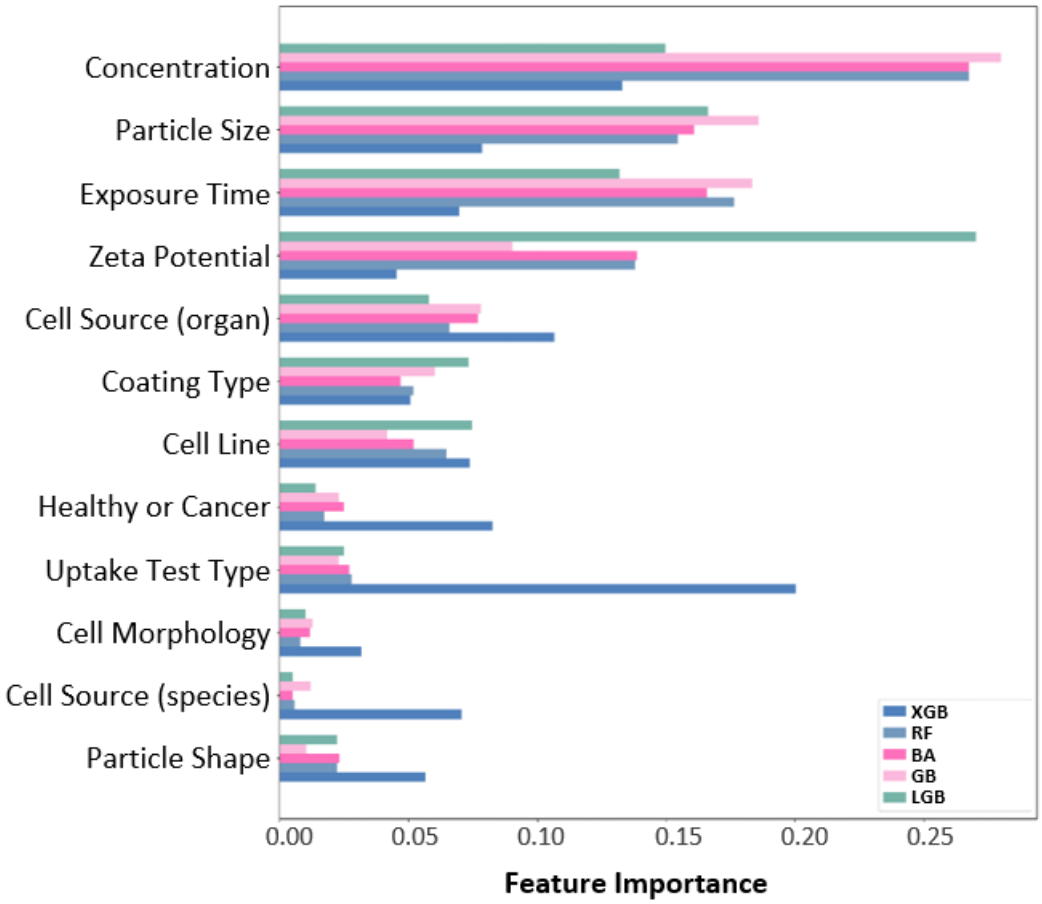

Figure 5.3. Bar chart showing the impurity-based importance of features included in ensemble regression models.

XGB: XGBoost, RF: Random Forest, BA: Bootstrap Aggregation, GB: Gradient Boosting, LGB: Light Gradient Boosting.

The diameter of GNPs, the zeta potential and type of surface coating material were the key physicochemical properties modulating cellular uptake. The direct relationship between GNP size and cellular uptake was shown in many studies [350-352]. Surface modification, in some cases, improves dispersion characteristics of NPs, which, in return, reduces the uptake of large-sized aggregates [345].

As expected, zeta potential was another important design parameter when engineering GNPs for efficient cellular uptake. Zeta potential indicates the overall surface charge in a colloidal dispersion and directly controls the likelihood of adhesion to the plasma membrane and cellular uptake [353, 354]. Earlier studies arguably suggested that cationic NPs had higher ability to interact with the negatively charged cellular membrane compared to anionic ones [355, 356]. Later research suggested that cellular uptake of NPs involves highly regulated mechanisms

with complex interactions, not simply Coulomb-driven electrostatic interactions [357, 358]. For examples, GNPs that had a positive zeta potential in pristine form may no longer be cationic in the cellular media due to protein adsorption to their surfaces. Type of ICP-based uptake test, cell line and the organ it represented were among top seven important predictors, suggesting the importance of cell culture configurations in cellular uptake studies.

5.3.4. Supporting Figures Associated with This Chapter

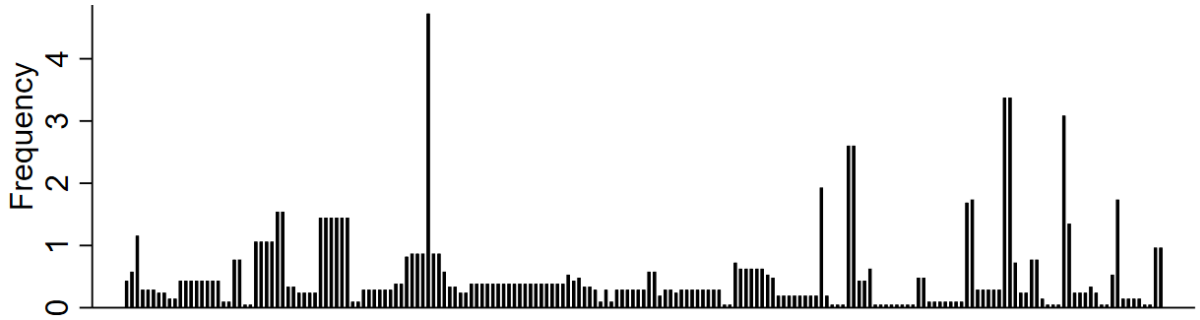

Figure S11. Percent frequency of data points per individual GNP included in meta-analysis.

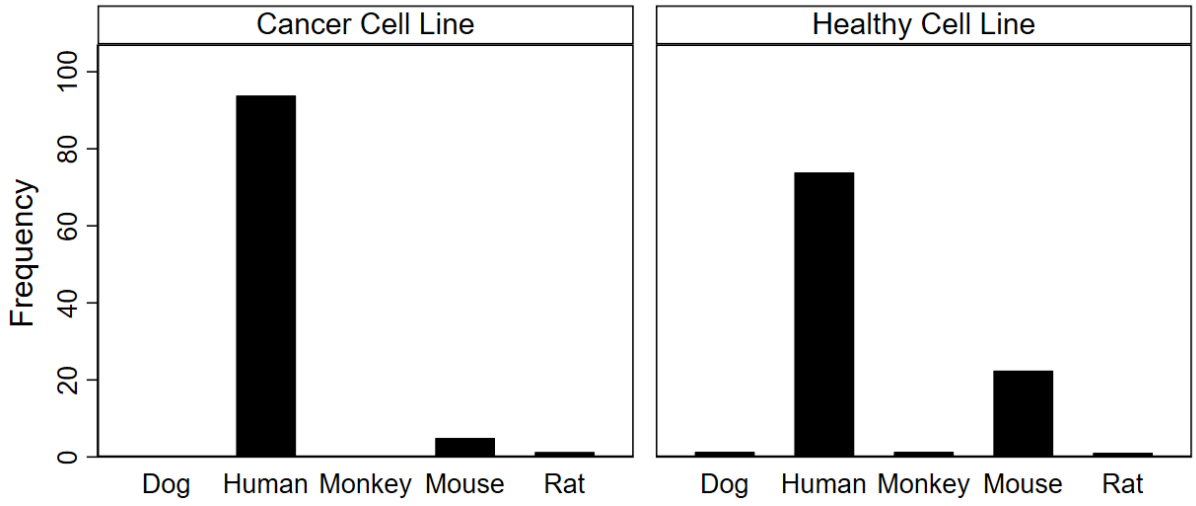

Figure S12. Percent frequency of data points per cell source, grouped by cell nature

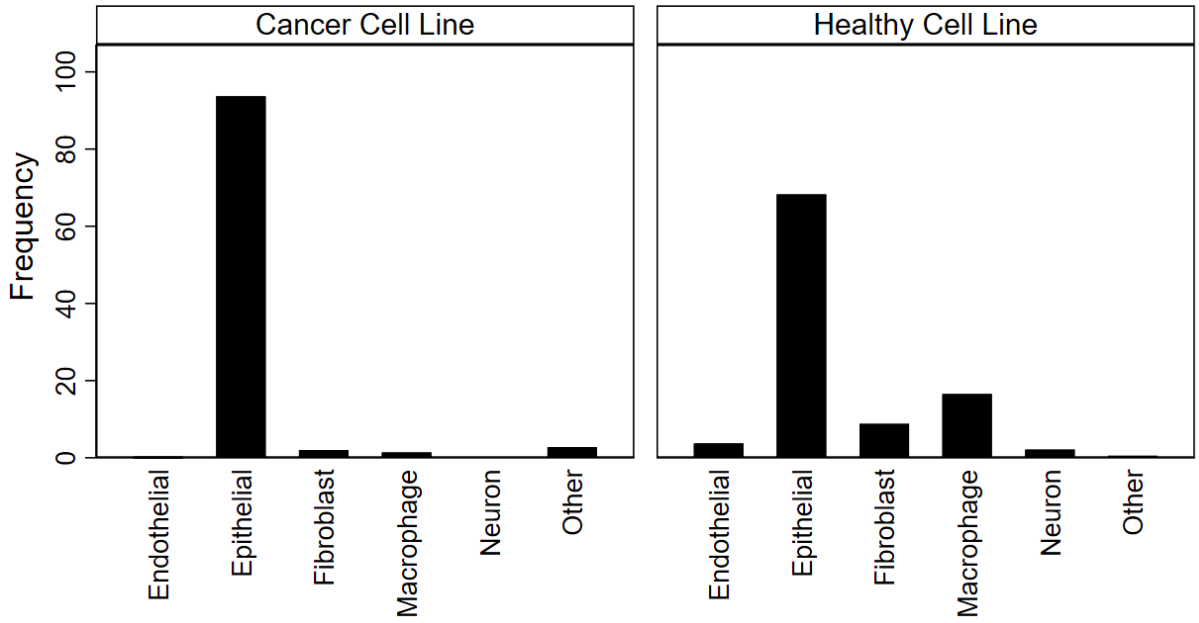

Figure S13. Percent frequency of data points per cell morphology, grouped by cell nature

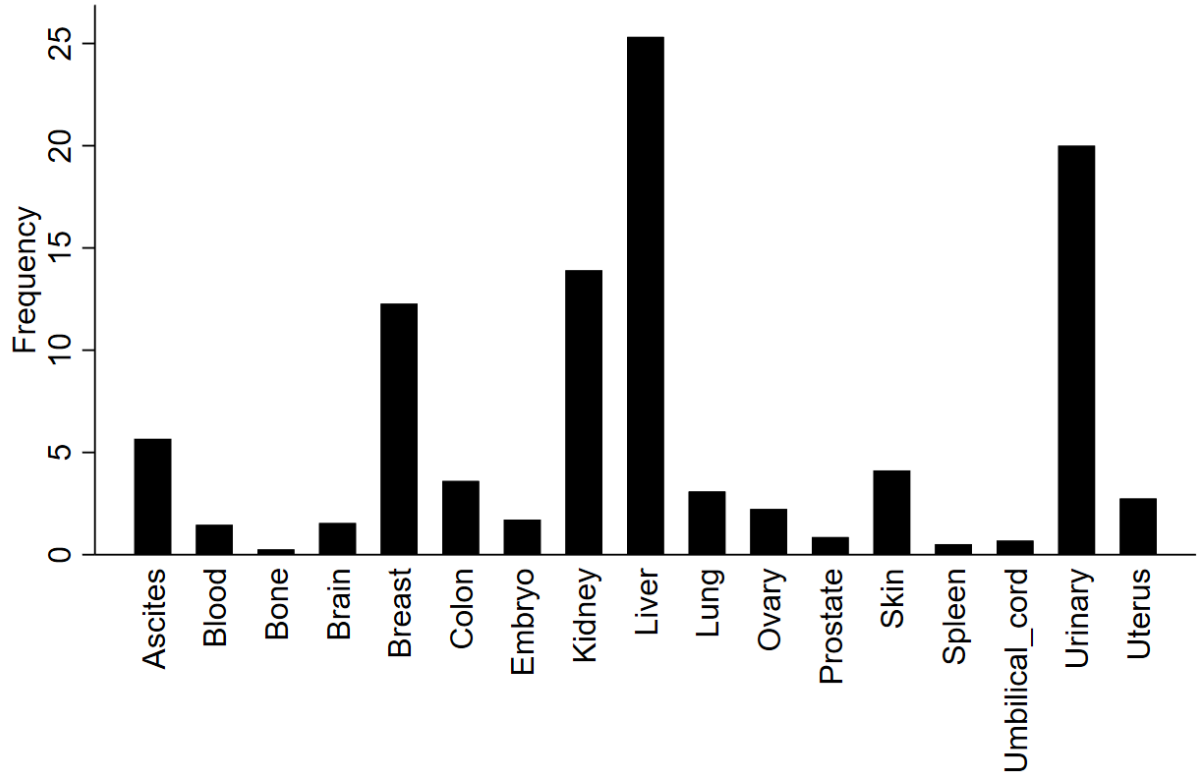

Figure S14. Percent frequency of data points per cell organ/tissue category

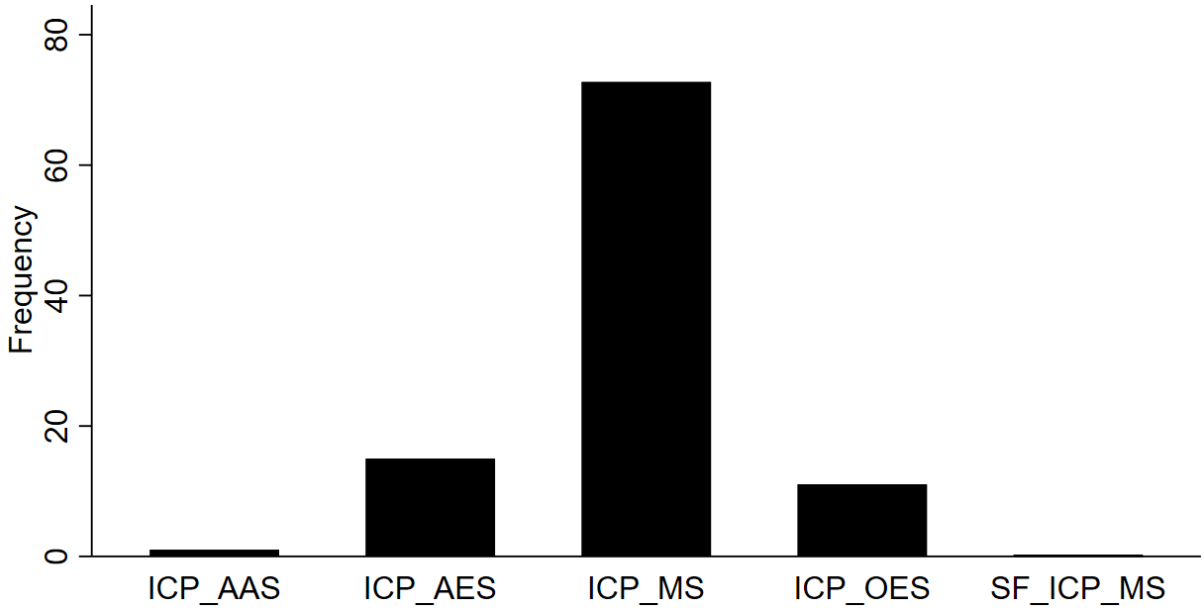

Figure S15. Percent frequency of data points per assay category

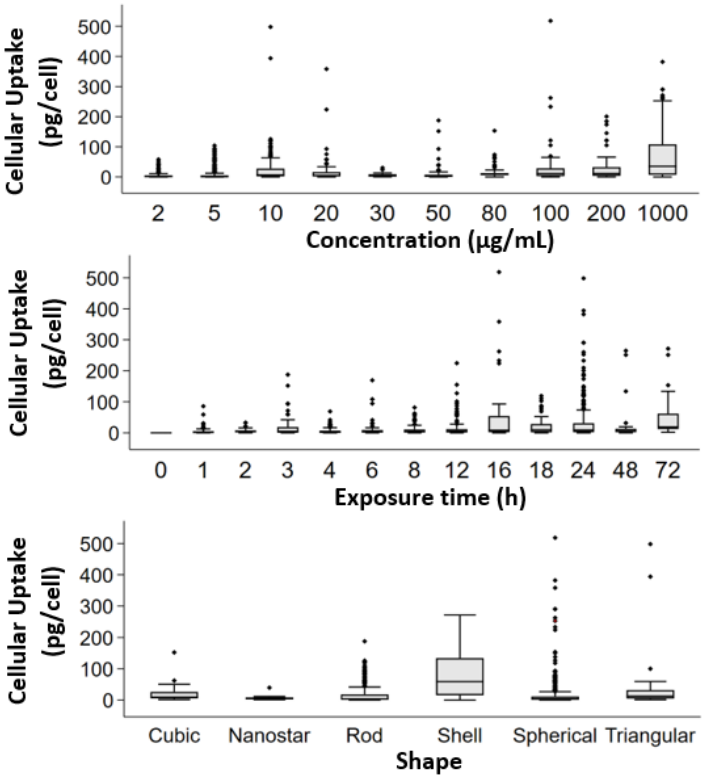

Figure S16. Box plot of changes in cellular uptake as a function of NP exposure concentration, exposure time or NP shape.

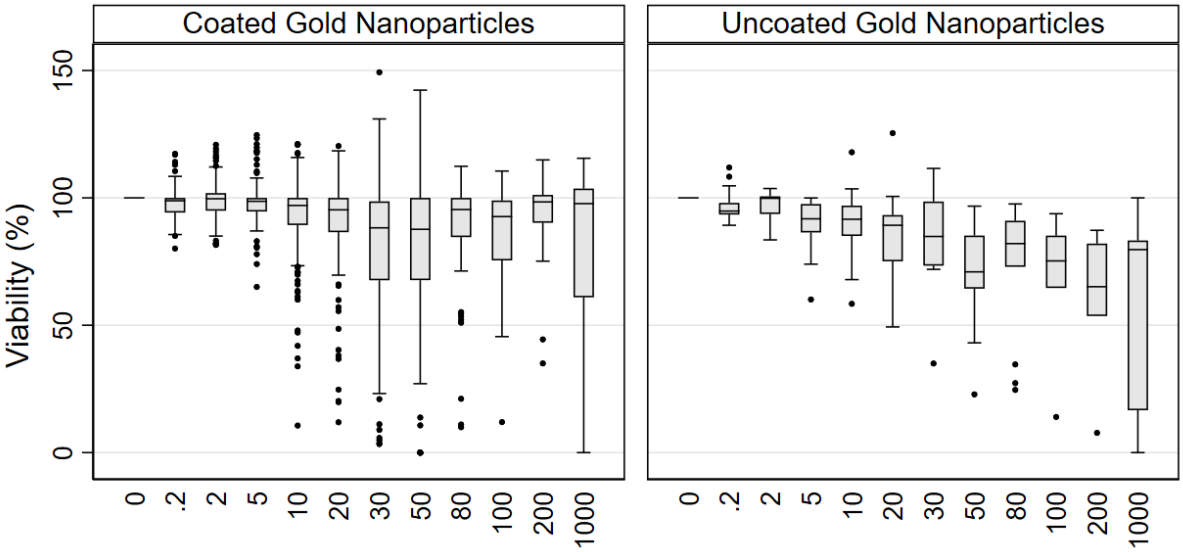

Figure S17. Box plot of changes in cell viability (%) as a function of NP exposure concentration (0-1000 µg/mL), grouped by NP coating.

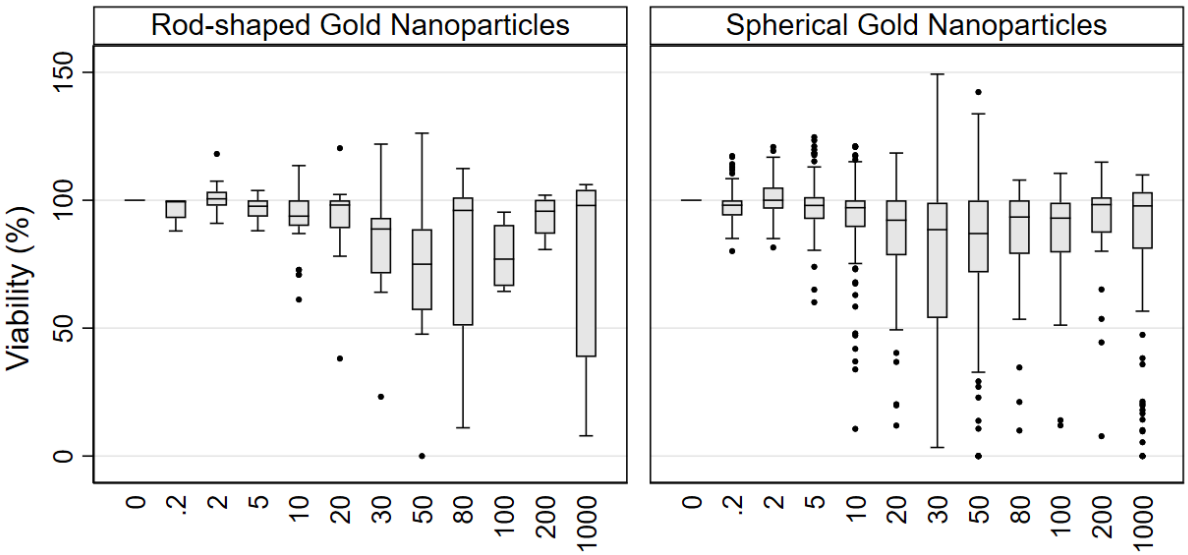

Figure S18. Box plot of changes in cell viability (%) as a function of NP exposure concentration (0-1000 µg/mL), grouped by NP shape.

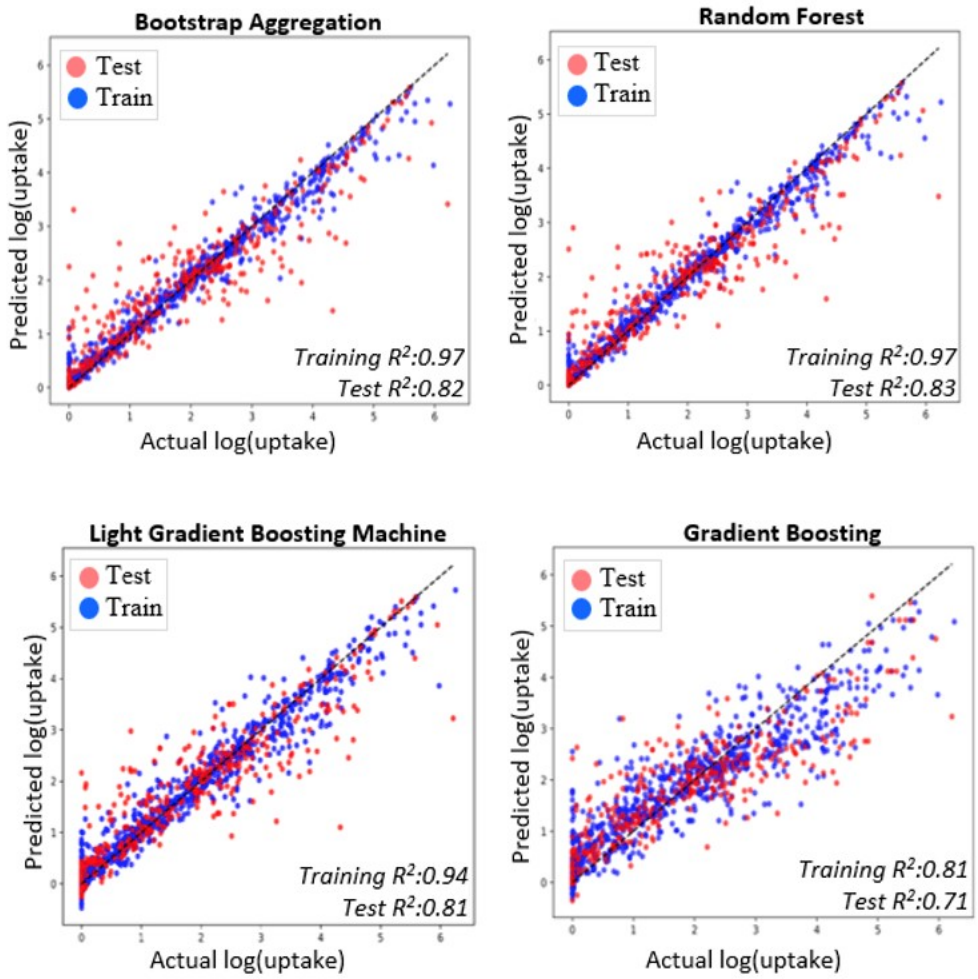

Figure S19. Scatterplots of measured cellular uptake (x-axis) against predictions (y-axis) for each ensemble model.

Table S5. Hyperparameters used for regression models.

Algorithm	*Parameters*
XGBoost	{'objective': 'reg:squarederror', 'base_score': None, 'booster': None, 'callbacks': None, 'colsample_bylevel': None, 'colsample_bynode': None, 'colsample_bytree': 0.9, 'early_stopping_rounds': None, 'enable_categorical': False, 'eval_metric': None, 'feature_types': None, 'gamma': None, 'gpu_id': None, 'grow_policy': None, 'importance_type': None, 'interaction_constraints': None, 'learning_rate': 0.1, 'max_bin': None, 'max_cat_threshold': None, 'max_cat_to_onehot': None, 'max_delta_step': None, 'max_depth': 7, 'max_leaves': None, 'min_child_weight': None, 'missing': nan, 'monotone_constraints': None, 'n_estimators': 200, 'n_jobs': None, 'num_parallel_tree': None, 'predictor': None, 'random_state': 42, 'reg_alpha': None, 'reg_lambda': None, 'sampling_method': None, 'scale_pos_weight': None, 'subsample': 0.8, 'tree_method': None, 'validate_parameters': None, 'verbosity': None}
Random Forest	{'bootstrap': True, 'ccp_alpha': 0.0, 'criterion': 'squared_error', 'max_depth': None, 'max_features': 1.0, 'max_leaf_nodes': None, 'max_samples': None, 'min_impurity_decrease': 0.0, 'min_samples_leaf': 1, 'min_samples_split': 2, 'min_weight_fraction_leaf': 0.0, 'n_estimators': 100, 'n_jobs': None, 'oob_score': False, 'random_state': 42, 'verbose': 0, 'warm_start': False}
Bootstrap Aggregation (bagging)	{'base_estimator': 'deprecated', 'bootstrap': True, 'bootstrap_features': False, 'estimator': None, 'max_features': 1.0, 'max_samples': 1.0, 'n_estimators': 30, 'n_jobs': None, 'oob_score': False, 'random_state': 42, 'verbose': 0, 'warm_start': False}
Light Gradient Boosting	{'boosting_type': 'gbdt', 'class_weight': None, 'colsample_bytree': 1.0, 'importance_type': 'split', 'learning_rate': 0.1, 'max_depth': -1, 'min_child_samples': 20, 'min_child_weight': 0.001, 'min_split_gain': 0.0, 'n_estimators': 100, 'n_jobs': None, 'num_leaves': 31, 'objective': None, 'random_state': None, 'reg_alpha': 0.0, 'reg_lambda': 0.0, 'subsample': 1.0, 'subsample_for_bin': 200000, 'subsample_freq': 0}
Gradient Boosting	{'alpha': 0.9, 'ccp_alpha': 0.0, 'criterion': 'friedman_mse', 'init': None, 'learning_rate': 0.1, 'loss': 'squared_error', 'max_depth': 3, 'max_features': None, 'max_leaf_nodes': None, 'min_impurity_decrease': 0.0, 'min_samples_leaf': 1, 'min_samples_split': 2, 'min_weight_fraction_leaf': 0.0, 'n_estimators': 100, 'n_iter_no_change': None, 'random_state': 42, 'subsample': 1.0, 'tol': 0.0001, 'validation_fraction': 0.1, 'verbose': 0, 'warm_start': False}
Decision Tree	{'ccp_alpha': 0.0, 'criterion': 'friedman_mse', 'max_depth': 9, 'max_features': None, 'max_leaf_nodes': None, 'min_impurity_decrease': 0.0, 'min_samples_leaf': 2, 'min_samples_split': 2, 'min_weight_fraction_leaf': 0.0, 'random_state': 42, 'splitter': 'best'}
K-Nearest Neighbors	{'algorithm': 'auto', 'leaf_size': 30, 'metric': 'minkowski', 'metric_params': None, 'n_jobs': None, 'n_neighbors': 5, 'p': 2, 'weights': 'uniform'}
Backpropagation Artificial Neural Network	{num_hidden_layer:4, activation_function:ReLu, batch_size:32, learning_rate:0.01, number_of_epochs:100, dropout rate:0.2, optimizer: Adam, loss_function: mean_squared_error}
Support Vector Regression (nonlinear)	{'C': 1.0, 'cache_size': 200, 'coef0': 0.0, 'degree': 3, 'epsilon': 0.1, 'gamma': 'scale', 'kernel': 'rbf', 'max_iter': -1, 'shrinking': True, 'tol': 0.001, 'verbose': False}

(cont. on next page)

Table S5 (cont.)

Support Vector Regression (linear)	{'C': 1.0, 'cache_size': 200, 'coef0': 0.0, 'degree': 3, 'epsilon': 0.1, 'gamma': 'scale', 'kernel': 'linear', 'max_iter': -1, 'shrinking': True, 'tol': 0.001, 'verbose': False}
AdaBoost	{'base_estimator': 'deprecated', 'estimator': None, 'learning_rate': 1.0, 'loss': 'linear', 'n_estimators': 50, 'random_state': 42}
BayesianRidge	{'alpha_1': 1e-06, 'alpha_2': 1e-06, 'alpha_init': None, 'compute_score': False, 'copy_X': True, 'fit_intercept': True, 'lambda_1': 1e-06, 'lambda_2': 1e-06, 'lambda_init': None, 'n_iter': 300, 'tol': 0.001, 'verbose': False}
Stochastic Gradient Descent	{'alpha': 0.0001, 'average': False, 'early_stopping': False, 'epsilon': 0.1, 'eta0': 0.01, 'fit_intercept': True, 'l1_ratio': 0.15, 'learning_rate': 'invscaling', 'loss': 'squared_error', 'max_iter': 1000, 'n_iter_no_change': 5, 'penalty': 'l2', 'power_t': 0.25, 'random_state': None, 'shuffle': True, 'tol': 0.001, 'validation_fraction': 0.1, 'verbose': 0, 'warm_start': False}
Ridge with Cross-Validation	{'alpha_per_target': False, 'alphas': (0.1, 1.0, 10.0), 'cv': None, 'fit_intercept': True, 'gcv_mode': None, 'scoring': None, 'store_cv_values': False}
Generalised Additive Models	{'terms': 's(0) + s(1) + intercept'}
Huber Regression	{'alpha': 0.0001, 'epsilon': 1.35, 'fit_intercept': True, 'max_iter': 100, 'tol': 1e-05, 'warm_start': False}
Poisson Regression	{'alpha': 1.0, 'fit_intercept': True, 'max_iter': 100, 'solver': 'lbfgs', 'tol': 0.0001, 'verbose': 0, 'warm_start': False}
Tweedie Regression	{'alpha': 1.0, 'fit_intercept': True, 'link': 'auto', 'max_iter': 100, 'power': 0.0, 'solver': 'lbfgs', 'tol': 0.0001, 'verbose': 0, 'warm_start': False}
Theil – Sen Regression	{'copy_X': True, 'fit_intercept': True, 'max_iter': 300, 'max_subpopulation': 10000.0, 'n_jobs': None, 'n_subsamples': None, 'random_state': None, 'tol': 0.001, 'verbose': False}

Table S6. One-way ANOVA results

Parameter	**N**	**Cellular Uptake** pg Au per cell	***p-value***
Modifier type			
Uncoated	97	16 ± 23	*<0.001*
Polymer	170	20 ± 58	
Small molecule	470	29 ± 60	
Protein	19	26 ± 40	
Polymer&Protein	134	6 ± 12	
Peptide/Antibody	34	16 ± 16	
Metal	7	22 ± 38	
DNA	176	12 ± 20	
Albumin	49	4 ± 9	
Other	11	15 ± 10	
Shape			
Spherical	780	14 ± 38	*<0.001*
Rod	237	18 ± 30	
Shell	75	83 ± 79	
Cubic	37	20 ± 27	
Nanostar	12	8 ± 10	
Triangular	26	52 ± 119	
Cell Morphology			
Endothelial	15	13 ± 12	*<0.001*
Epithelial	998	17 ± 38	
Fibroblast	49	12 ± 24	
Macrophage	73	45 ± 78	
Neuron	8	0.2 ± 0.1	
Others	24	101 ± 140	
Cell Condition			
Healthy	375	16 ± 46	*0.05*
Cancer	792	22 ± 47	

5.4. Conclusion

In recent years, lipid-based, polymeric, and inorganic NPs have been engineered to navigate intracellular barriers and overcome the limitations of conventional drug delivery systems. Gold is one of the most studied inorganic NPs that is particularly suitable for mediating the release of therapeutically active compounds. The addition of GNP to the treatment cycle as a means of transport increases cellular uptake by target

cells while causing no or minimal toxicity to normal tissues. The intrinsic characteristics of GNPs greatly affect their cellular internalization rate and therapeutic potential. Several *in vitro* studies have demonstrated that spherical GNPs internalize better than nanorods [319, 359, 360], but others show an opposite effect [361]. Similarly, there are studies suggesting that GNPs of 50 nm have the maximum uptake [362, 363], whereas other studies report that GNPs in the range of 10-25 nm are more easily taken up by cells [364]. In addition to NP characteristics such as size, shape, surface chemistry, and charge, the fate of GNPs within the cell is affected by a number of experimental parameters (e.g., exposure conditions) and cell configurations (e.g., cell type, source organ/tissue and morphology) [365].

Machine learning models are very useful *in silico* tools for predicting the cellular uptake level of GNPs and for elucidating factors that control their cellular uptake. Here, we used SCOPUS and Google Scholar databases to identify 59 studies that met data inclusion requirements. The performance of ensemble regressors in predicting cellular uptake was compared with other linear and nonlinear machine learning algorithms. The XGBoost ensemble model performed the best, explaining 88% of the variance in cellular uptake of GNPs for the test set. Several important trends in the data were identified. First, GNPs functionalized with PVA, DMSA, or thiol internalize more than uncoated GNPs. 90% of the GNPs included in this study had a particle size of <90 nm and we found a positive relationship between GNP size and cellular uptake in this size range. There was no (or very slight) size-dependent increase in uptake level beyond this point. Gold nanoshells had the highest uptake, particularly in cancer cell lines. Parameters that directly control dispersion characteristics of GNPs such as zeta potential and surface modification were also identified as important drivers of cellular uptake.

The major strength of this work is the use of a relatively large dataset (n=193 individual gold core NPs from 59 independent studies) to train machine learning models. Although there are computational studies focused on predicting the cellular uptake of NPs [48, 366-368], none of them used a compiled dataset. The clear advantage of nonlinear ensemble machine learning methods over other discrete nonlinear and linear methods was also a useful outcome from this work. The major limitation is the absence of characterization data measured under biologically relevant conditions and the resulting difficulty of relating medium-dependent NP characteristics to measured cellular uptake level.

The results presented here show the power of machine learning tools to make accurate predictions of cellular uptake behaviour of GNPs. The lack of conclusion on the

role of protein corona formation in mediating cellular uptake behaviour was not due to a limitation of our meta-analysis but rather highlights an important deficiency in published studies that fail to account for NP-protein interactions [245]. With further developments in nanometrology (i.e., a subfield of metrology that is concerned with the science of measurement at the nanoscale level), the quality of generated data in nanosafety and the accuracy of computational models trained on them is likely to improve.

CHAPTER 6

CONCLUSION

NPs, possessing at least one dimension within the range of 1-100 nm, exhibit distinct physical and chemical properties significantly different from those of macro-scale particles. For instance, the increased surface area of NPs predisposes them to more intensive interactions. While the NPs of natural sources have existed in nature since the origin of life on Earth, one of the first intentionally synthesized NPs was arguably the gold particles (10-100 nm) produced through chemical reactions by Michael Faraday in 1857 [369]. The unique optical properties and reactivity exhibited by gold NPs could be regarded as a significant breakthrough in the field. The lack of widespread usage of the term 'NM' until the 20th Century might have delayed the universal acceptance of this discovery in the scientific community. The lecture titled "**There is Plenty of Room at the Bottom**" by Richard Feynman marked a pivotal moment, establishing the field of nanotechnology within the scientific arena. The synthesis of the fullerene (C60) molecule in 1985 by Robert Curl, Richard Smalley, and Harold Kroto represents a seminal work in this field, despite ongoing debates regarding its classification as either a particle or a complex molecule [370, 371]. The discovery of fullerene has subsequently led to an exponential increase in the production of various nanotechnology products.

Together with the quantum effects that begin to dominate the behaviour of matter at the nano-scale, the increased surface area of NPs makes them highly suitable for a variety of novel and advanced applications. Today, the applications of NMs are extensive and can be categorized as follows:

Food and Beverages: NMs are employed to enhance the taste, texture, and shelf-life of food and beverages. Examples include nano-encapsulated food colorings, antimicrobial packaging agents, and clarified fruit juices utilizing cellulose nanofibers.

Cosmetics and Personal Care: In sunscreens, lotions, and makeup products, NMs are used for UV protection, controlled release, and improved properties, frequently utilizing titanium dioxide, zinc oxide, and silica NPs.

Clothing: Nanotechnology is applied in the development of self-cleaning fabrics, enhancing water and dirt resistance, wrinkle prevention, and antimicrobial properties, often employing silver NPs.

Electronics and Home Appliances: NMs such as quantum dots and cerium oxide are used in batteries, displays, solar panels, and other electronic components to improve efficiency, lifespan, and conductivity.

Medicine and Health: Various NMs have been developed for drug delivery, diagnostic imaging agents, and biosensors, including liposomal carriers and iron oxide NPs.

The ambiguity in defining, regulating, categorizing, and standardizing NMs (so-called *nano ambiguities*) complicates the precise determination of the number of NMs present on the market. This study is premised on the potential of NMs, coupled with the notion that "**There is Plenty of RISK at the Bottom**" emphasizing the need for comprehensive risk assessment.

A decade ago, the main problem hampering efforts to understand and explain the effects of NMs on human health and the environment was the lack of consistent and reliable data. The last decade witnessed the generation of a large volume of nano-safety data, which were then gradually uploaded to various databases. The efforts to generate data in the field have later been replaced with converting them into a uniformly recorded and publicly accessible format, resulting in the generation of various data repositories such as eNanoMapper, Toxbank, Cananolab, S2Nano Data, and Nano Health-Environment Commented Database. As a first step, the available databases were searched but numerous forms of database-related problems were encountered. The main challenges encountered in these databases include:

- Inaccessibility (due to outdated or closed URLs),
- Subscription fees,
- Lack of suitable data for model development,
- Incompatibility in the formats of stored data,
- Co-storage of textual and numerical data in the same cells,

- Difficulty in extracting comparable data from different studies due to variations in experimental designs,
- Absence of raw data within the systems.

Then, an extensive literature review was carried out using different scientific search engines. This step revealed a substantial volume of scientific work related to NMs. Key observations from these studies include:

- A tendency to share only graphically transformed data rather than raw data.
- Repetition of similar tests with the same NMs by different researchers.
- Despite the abundance of data, a lack of sufficient meta-analytical studies in this area.

To overcome these challenges, the following steps were undertaken:

- Conducting an extensive literature review to identify potential gaps,
- Accessing academic sources through targeted keyword searches,
- Manually converting graphical data into numerical formats and storing data in a standardized format,
- Cleaning the data with various exclusion and inclusion criteria,
- Preparing and visualizing the data, applying transformations and scaling, when necessary,
- Identifying the heterogeneity of the dataset,
- Developing models ranging from simple to complex using various machine learning algorithms and attempting to predict targeted endpoints,
- Visualizing, interpreting, and documenting the model,
- Storing and publishing the raw data, developed models, and codes used for these models as open-source resources.

The aim of this study is to use computational power to complement and extend existing knowledge on NM safety and to maximize the use of accumulated nanotoxicity data. The overarching goal is to support the safe(r)-by-design concept which requires an

early integration of the safety component into the design plan of NMs by means of structural manipulation strategies. In the first study, we assessed the correlation between the toxicity of zinc oxide NPs and both internal (i.e., intrinsic NM properties) and external (i.e., cellular system and assay-related features) parameters. Overall, a negative correlation between cell viability and exposure dose/duration was found, meaning that the higher concentration of NPs and extended exposure to them caused an increase in the cytotoxicity level. Particle size measured by SEM/TEM or DLS was positively correlated with cell viability, with increasing particle size leading to an increase in the percentage of viable cells. Another important parameter was surface characteristics. Variations in coatings were observed to alter cell viability. Next, a decision tree was constructed that identified a NP concentration of 20 μg/ml and a particle size of 10 nm to be critical thresholds differentiating cytotoxic responses. The primary mechanism of action of zinc oxide NPs has been identified as the generation of reactive oxygen species in various studies. It is speculated that high concentrations and small sizes of particles increase their internalization by cells, and the increase in exposure time, along with the increase in reactive oxygen species formation, may lead to a decrease in cell viability.

The second case study was focused on maximizing the use of individual risk assessments with potentially biased estimates of toxicological effects. A large pool of data on the cytotoxicity of nanosilver was collected and modeled to unravel potential triggers of toxicity, by leveraging the power of a meta-analytic dataset and machine-learning approaches. Such machine learning-assisted efforts are critical to developing commercially viable and safe nanosilver-containing products in the ever-expanding nano-biomaterials market. The main conclusions of the exploratory analysis are summarized below:

- Descriptive statistics, effect size, and heterogeneity analyses demonstrated statistically significant differences between various categories and the endpoint of cell viability.
- Similar to the zinc oxide study, concentration, size, and exposure time emerged as significant factors in cell viability.
- Coating of silver NPs with organic macromolecules such as proteins or DNA was found to increase cell viability,
- The use of green synthesis approaches involving plant extracts, bacteria, or algae significantly reduced cell viability (attributed to substances from

the extracts and microorganisms adhering to the NPs, acting as surface-modifying agents).

- Similarly, silver NPs were found to exhibit a slightly higher cytotoxic effect on cancer cells compared to healthy cells.

In the modeling part, the collated dataset was divided into 15 different sub-sections (varying concentration ranges, different coatings, data integrity, etc.) and analyzed using five different machine learning algorithms (Decision Tree (DT), Logistic Regression (LR), Gaussian Naive Bayes (GNB), K-Nearest Neighbors (KNN), Random Forest (RF)). Validation metrics such as accuracy, precision, sensitivity, and area under the curve were calculated and used to compare the performance of developed models. The highest accuracy was achieved with the decision tree model trained on the dataset excluding missing and zero concentration values. Visualization of the optimal decision tree facilitated the determination of thresholds for potential toxicity, including zeta potential, concentration, particle size, and exposure time. Analysis of the dataset with Artificial Neural Networks (ANN) revealed that coating was another significant parameter driving the toxicity of silver NPs.

Nano-sized gold displays useful characteristics not seen in bulk gold, making them especially useful for medical applications such as drug/gene delivery and targeting. Their surfaces can be easily modified for specific cell-targeting applications to improve disease management and to treat conditions not responsive to available medications. Once bound to disease cells, they are taken up through different uptake mechanisms depending on their size and shape. The potential cellular uptake mechanisms of NPs are shown in Figure 6.1. (adapted from [372] and [353]). An important research challenge here is deciphering how to control cellular internalization and safe uptake of gold NPs by altering the shape, size, and surface properties in different cell configurations.

To resolve controversies arising from inconsistent findings in prior research and to critically appraise total bodies of evidence, multiple machine learning models were trained on a large pool of literature data to predict the cellular uptake level of gold NPs. A total of 18 different machine learning algorithms (ensemble learners, discrete nonlinear methods, and linear methods) were tested. To the best of our knowledge, this is the first meta-analytic study that focuses on predicting the cellular uptake profile of the NPs (i.e., existing meta-analytic studies report NPs' cellular toxicity but not cellular uptake). Analysis of the size effect and heterogeneity of the collected dataset showed that

variations in cellular uptake of NPs were mainly caused by the shape of the NP and surface modifications. Surface modifications with small molecules increased cellular uptake, while protein-based coatings reduced it. Similar trends were observed in cell viability studies involving zinc oxide and silver NPs. This supports the possibility of a negative correlation between cellular uptake and cell viability. In the cellular uptake study, the predictive capacities of various regression-based machine learning algorithms were examined. A total of 19 models were trained (10 linear methods, 4 discrete nonlinear methods, and 5 ensemble learning methods), and the best results across all metrics (R^2, RMSE, MAE) were achieved with ensemble learning methods. The critical drivers of cellular uptake were particle size, zeta potential, concentration, and exposure duration.

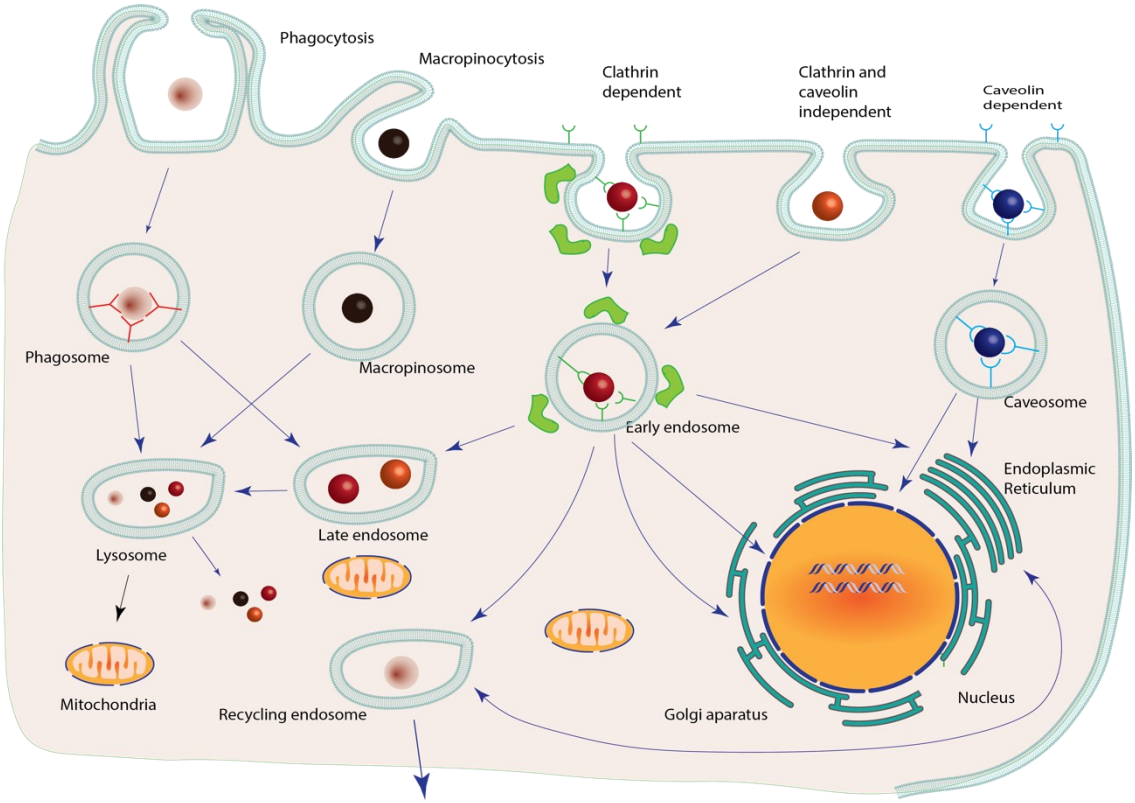

Figure 6.1. Cellular internalization mechanisms of nanoparticles.

Overall, this thesis aims to contribute to Safer-By-Design strategies that are critical to developing commercially viable and safe NMs. The results obtained here are expected to foster the more effective use of accumulated data on NPs and enable the optimization of experimental parameters when engineering NPs for biomedical applications.

The models developed in this thesis demonstrate that such complex interactions can only be modeled with equally complex algorithms. The findings suggest that the typical approach of toxicity evaluation which is solely based on the core of materials should be expanded as different dimensions of physicochemical features and experimental procedures directly affect their *in vitro* toxicity.

6.1. Future Work

While the critical role of size, shape, and surface chemistry in determining NM behavior has been pronounced for almost two decades now, there remain substantial gaps in our understanding. The observation that different coatings on the analyzed NMs in this thesis (zinc oxide, silver, and gold) have distinct effects, particularly the decrease in toxicity and altered cellular uptake associated with protein coatings, suggests a close link between protein interactions and NM behavior. As proteins can modify NM surfaces, influencing their toxicity and cellular uptake, and can also form a dynamic protein corona (Figure 2.3.) that significantly alters their characteristics, this interaction undoubtedly plays a crucial role in determining their overall behavior. Furthermore, just as NMs can enter the body through various routes like inhalation, digestion, and oral uptake, their cellular entry mechanisms are also diverse, as illustrated in Figure 6.1. This underscores the necessity for future research to prioritize the rigorous modeling of the protein corona structure, integrating this crucial information into our understanding of NM-biological interactions. By doing so, we can pave the way for the systematic design of inherently safer and more efficacious NMs with wider applicability across various fields.

The structure and composition of adsorbed protein corona provide an important resource for understanding the interactions of NMs with the cell. However, the measurement and identification of corona proteins is currently a time- and cost-intensive analysis, often requiring the isolation of proteins from NP surfaces. Researchers have been interested in developing computational models to predict NP corona in diverse environments by leveraging the relatively small number of experimental studies. Findlay and coworkers proposed one of the first predictive models of protein corona formation on NM surfaces [373]. They developed a random forest model that related characteristics of

proteins (e.g. isoelectric point, protein weight and abundance, percent of positively and negatively charged amino acids), NMs (e.g., particle size and surface charge), and solvent (e.g., salt concentration) to protein corona formation. Duan et al. combined a similar set of protein descriptors (e.g., the isoelectric point, molecular weight, grand average of hydropathy, and percentage of negative/positive/aromatic amino acids) with novel NM descriptors (e.g., the fluorescence changes upon protein binding) to build predictive models for corona formation [374]. Ban et al. used a pool of qualitative (e.g., NP type, shape, core, modification, dispersion medium, incubation plasma source, and culture) and quantitative (e.g., particle size, dispersion medium pH and concentration, charge, polydispersity index, NP and plasma concentration, incubation time and temperature, centrifugation speed, time, temperature and repetitions) descriptors to predict the functional protein compositions of coronas [375]. Movadi and coworkers used a set of experimental descriptors including surface area, primary and hydrodynamic particle size, density, zeta potential, and polydispersity index to predict the percentage of nine particular proteins adsorbed on the surface of four different NPs (CeO_2, Si-CeO_2, $BaSO_4$, and ZnO) [376]. The initial attempts to predict protein corona formation and composition were severely hampered by the scarcity of large and robust datasets on NP-protein interactions and the lack of interpretable nano-specific descriptors. The key to the future success of computational predictions of protein corona on NPs rests squarely on the availability of high-quality NP-protein corona datasets and a suite of computable descriptors that accurately represent biologically relevant features of NPs. The availability of such datasets will improve the accuracy of protein corona predictions by enabling the development of machine learning-based platforms that unveil different aspects of how proteins interact with NPs.

The exploration of atoms through quantum mechanical calculations (QMC) offers us a valuable perspective in assessing the risks and behaviors of NMs. These calculations are not just theoretical exercises; they provide us with practical insights into the atomic structure and behaviors, revealing the nuances of electron configurations, bonding patterns, and charge distributions. From these insights, we can draw meaningful connections to the safety profiles of NMs. By correlating the theoretical data with empirical findings on aspects like toxicity, cellular uptake and genotoxicity, it is possible to develop predictive models. These models have the potential to identify NMs that might pose risks before they are widely used, contributing to the creation of safer alternatives.

Building upon these insights from quantum mechanics, the behavior of NMs in biological environments can be predicted. By integrating these calculations into predictive models, one can simulate how NMs interact with biomolecules, providing a clearer picture of their uptake, transport, and potential impact on cellular functions. This holds significant promise for the future of nanomedicine, particularly in the areas of drug delivery and bioimaging. In Fig. 6.2, six gold atoms in different starting orientations (left; front-F, right-R) and their relaxed positions after QMC simulations are shown (right, F and R). The observed atomic orientation under these experimental conditions potentially correlates with the (111) planes of the face-centered cubic crystal structure of gold. By varying the number of atoms and the proposed experimental conditions (e.g., temperature), the possible geometry of final products can be predicted. By comparing these predictions with the developed models, the simulations can iteratively be refined until safer structures are obtained.

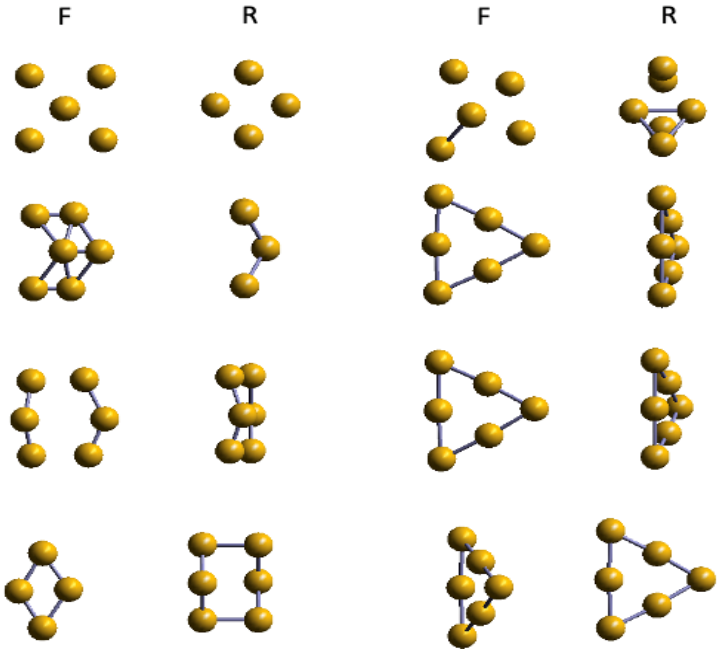

Figure 6.2. Molecular dynamics study on six gold atoms with different starting positions

Moving beyond individual elements like gold, the true power of quantum mechanical calculations lies in its ability to decipher the complex behaviors underlying the diverse world of NMs. By performing such calculations, it is possible to uncover a rich spectrum of novel descriptors that define and predict the complicated interaction of these materials with their environment. This deeper understanding, encompassing factors beyond the traditional ones like size, shape, composition, and surface charges, would illuminate the nuanced interplay between NMs and their surroundings, directly impacting their efficacy, toxicity, and overall performance. Studies within this scope can lead to the development of experimental conditions with the necessary precision to allow for the very accurate determination of the properties of NMs. While quantum mechanical descriptors provide information about the electronic structure and mechanical properties of NPs which can help predict their behaviors such as chemical reactivity, stability, and biological activity, it is important to note that the computational costs of such calculations increase with decreasing size of particles. In addition to high computational costs, there are also other difficulties associated with computing quantum mechanical descriptors for NPs, such as limited applicability to ultra-fine NPs, the high error introduced by approximations/simplifications and the choice of basis set representing the wavefunctions of electrons, solvent and dispersion effects, and lack of experimental validation. Once these issues are addressed quantum mechanical descriptors can provide a better understanding of the mechanistic behaviors of NPs.

Given the complexity of NMs, it becomes apparent that traditional molecular representation approaches fall short in capturing their unique properties. Traditional methods such as SMILES and InChI, while effective for standard chemical structures, struggle to adapt to the diverse and dynamic nature of nanoscale materials. This limitation poses a significant challenge in the field of Chemoinformatic, where accurate representation of these materials is essential for understanding their behaviour and interactions in biological systems. As we delve deeper into the field of nanotechnology, the need to develop more advanced and refined representation systems that can effectively encompass the complexities of NMs becomes increasingly evident. This need marks a critical turning point in our discovery and understanding of nanostructures and ushers in an era of research focused on renewing and improving the way we represent and comprehend these small but powerful entities.

In chemoinformatics, the data scientist is confronted with a fundamental question concerning how to represent and store chemical entities on a computer. One of the most

common machine-readable chemical representations is the concept of a molecular graph, showing the geometric arrangement of atoms within a molecule. Two other widely-used chemical structure file formats are simplified input line entry system (SMILES) and molfile. The SMILES is a line notation representing atoms, bonds and their connectivity. Molfile is a connection table containing information about the atoms, bonds, connectivity and coordinates of a molecule. An alternative identifier that provides unique labels for well-defined chemical structures is the International Chemical Identifier (InChI) which converts a chemical structure (in connection table format) into a series of ASCII characters. Similarly, the Chemical Abstracts Service (CAS) number is a numerical identifier that is uniquely assigned to a chemical compound when it enters the CAS registry database. While these chemical 'naming' approaches are suited for well-defined structures, the complex chemistry of nanostructures makes their use problematic in nano-domain. In particular, conventional naming procedures, such as connection tables, graphic visualizations, line notations or other descriptive forms, are incapable of providing unique labels for compositionally similar NMs of different sizes, shapes, or coatings. Clearly, there is a strong need for better machine-readable and machine-actionable representations of nanostructures. This need has been partly addressed by the development of *nano* extensions to the standard SMILES and InChI notations [377, 378]. However, not all questions on how these extended identifiers will be used to represent biologically relevant features of NMs have been answered as yet.

Consistent substance identification and naming is critically important for the development of NM databases with cheminformatics functionalities including searching by names, chemical structures, substructures or chemical patterns. Having an agreed set of rules and language to represent the molecular identity of nanoscale substances is also important to simplify the development of interpretable descriptors that encode relevant structural properties of NMs and to quantitatively represent nanostructure diversity. Computed theoretical descriptors are arguably the most important element in various cheminformatics applications, including similarity searching, clustering and predictive modelling. While the definition of 'similar' can vary a lot in structural context, the core principle of *machine learning* in chemical domain is the expectation that structurally similar compound will have similar biological activities. Producing materials in nanoscale often results in novel characteristics that differ from those of the bulk form. Traditional descriptors are often able only to indicate physico-chemical aspects that are independent of the particle size or the physiological environment The novelty of nano-

characteristics calls for new kind of descriptors that are able to encode structures and interactions at the nanoscale. Molecular descriptors are commonly used in studies of molecular similarity to quantify the degree of structural overlap. However, almost all existing theoretical descriptors currently used are not nano-specific, meaning they are incapable of reliably discriminating between different-size forms of the same chemical substance. Development of novel descriptors that capture the specificity of nanoscale properties and the changes they undergo in different biological environments remains a challenging task and will be an area of active research for some time. Further development and adaptation of spectra-derived descriptors to NPs and the extraction of structural information from their microscopic images would greatly facilitate meaningful representation of nanostructures.

Predictive models of NPs can provide better understanding of the complex interactions between nanoscale entities and biological systems only if the descriptors used to train the model are interpretable and able to distinguish between ordinary and nanosized particles. Therefore, special attention must be given to the interpretability as well as efficacy of nano-descriptors so that they can be used to develop models that are both predictive and explanatory. To systematically overcome these challenges, further investigation is needed in following research areas:

- ✓ Development of efficient ways to represent nanostructures in machine-readable and machine-actionable format,
- ✓ Development of nanostructure descriptors that are (1) easy to compute and interpret, (2) compact enough to represent large sets of structures, (3) generalizable to multi-dimensional nanostructures and (4) able to represent physically and biologically relevant properties of NMs,
- ✓ Development of accessible, self-updating and domain-specific NM databases that impose specific requirements on the quality and reporting format of the data to be included,
- ✓ Development of computational tools that allows for integration of heterogenous data sources, transformation of data into a form that can be used in NM modeling and implementation of data analysis in a single environment,
- ✓ Development of globally-harmonized nano-hazard classification systems that can distinguish the more toxic NMs from the less toxic or

non-toxic ones, and hence, aid in the selection of NMs for synthesis and detailed toxicity testing.

It is clear that there are many areas that require in-depth study in the field of NM safety. To achieve the targeted success in these areas, it is necessary to strengthen interdisciplinary communication, accelerate the flow of data between theoretical and experimental working groups, and cyclically nourish every stakeholder with the obtained results. Thus, eventually, common denominators (the highlighted points above) that seemed very challenging for small molecules a few decades ago can also be achieved for NMs, and the synthesis of inherently safer materials, which is one of the ultimate goals, can be successfully accomplished

REFERENCES

1. Kokila, G.; Mallikarjunaswamy, C.; Ranganatha, V. L., A review on synthesis and applications of versatile nanomaterials. *Inorganic and Nano-Metal Chemistry* **2022**, 1-30.

2. Bratovcic, A., Different applications of nanomaterials and their impact on the environment. *SSRG International Journal of Material Science and Engineering* **2019,** *5* (1), 1-7.

3. Bradford, S. A.; Shen, C.; Kim, H.; Letcher, R. J.; Rinklebe, J.; Ok, Y. S.; Ma, L., Environmental applications and risks of nanomaterials: An introduction to CREST publications during 2018–2021. *Critical Reviews in Environmental Science and Technology* **2022,** *52* (21), 3753-3762.

4. Khan, I.; Saeed, K.; Khan, I., Nanoparticles: Properties, applications and toxicities. *Arabian journal of chemistry* **2019,** *12* (7), 908-931.

5. Council, N. R., Small wonders, endless frontiers: A review of the National Nanotechnology Initiative. **2002**.

6. Dawson, K. A.; Yan, Y., Current understanding of biological identity at the nanoscale and future prospects. *Nature nanotechnology* **2021,** *16* (3), 229-242.

7. Nature_nanoscience https://www.nature.com/subjects/nanoscience-and-technology (accessed 07.11.2023).

8. Braun, T.; Schubert, A.; Zsindely, S., Nanoscience and nanotecnology on the balance. *Scientometrics* **1997,** *38*, 321-325.

9. Roco, M. C., The long view of nanotechnology development: the National Nanotechnology Initiative at 10 years. Springer: **2011**; Vol. 13, pp 427-445.

10. Colvin, V. L., The potential environmental impact of engineered nanomaterials. *Nature biotechnology* **2003,** *21* (10), 1166-1170.

11. Hochella Jr, M. F.; Mogk, D. W.; Ranville, J.; Allen, I. C.; Luther, G. W.; Marr, L. C.; McGrail, B. P.; Murayama, M.; Qafoku, N. P.; Rosso, K. M., Natural, incidental, and engineered nanomaterials and their impacts on the Earth system. *Science* **2019,** *363* (6434), eaau8299.

12. Kennedy, A.; Brame, J.; Rycroft, T.; Wood, M.; Zemba, V.; Weiss Jr, C.; Hull, M.; Hill, C.; Geraci, C.; Linkov, I., A definition and categorization system for advanced materials: The foundation for risk-informed environmental health and safety testing. *Risk Analysis* **2019,** *39* (8), 1783-1795.

13. Auffan, M.; Rose, J.; Bottero, J.-Y.; Lowry, G. V.; Jolivet, J.-P.; Wiesner, M. R., Towards a definition of inorganic nanoparticles from an environmental, health and safety perspective. *Nature nanotechnology* **2009,** *4* (10), 634-641.

14. Bi, H.; Chen, Z.; Guo, L.; Zhang, Y.; Zeng, X.; Xu, L., Fabrication, modification and application of lipid nanotubes. *Chemistry and Physics of Lipids* **2022**, 105242.

15. Doke, S. K.; Dhawale, S. C., Alternatives to animal testing: A review. *Saudi Pharmaceutical Journal* **2015,** *23* (3), 223-229.

16. Knudsen, T. B.; Keller, D. A.; Sander, M.; Carney, E. W.; Doerrer, N. G.; Eaton, D. L.; Fitzpatrick, S. C.; Hastings, K. L.; Mendrick, D. L.; Tice, R. R., FutureTox II: in vitro data and in silico models for predictive toxicology. *Toxicological Sciences* **2015,** *143* (2), 256-267.

17. Höfer, T.; Gerner, I.; Gundert-Remy, U.; Liebsch, M.; Schulte, A.; Spielmann, H.; Vogel, R.; Wettig, K., Animal testing and alternative approaches for the human health risk assessment under the proposed new European chemicals regulation. *Archives of toxicology* **2004,** *78*, 549-564.

18. Adler, S.; Basketter, D.; Creton, S.; Pelkonen, O.; Van Benthem, J.; Zuang, V.; Andersen, K. E.; Angers-Loustau, A.; Aptula, A.; Bal-Price, A., Alternative (non-animal) methods for cosmetics testing: current status and future prospects—2010. *Archives of toxicology* **2011,** *85*, 367-485.

19. Halappanavar, S.; Nymark, P.; Krug, H. F.; Clift, M. J.; Rothen-Rutishauser, B.; Vogel, U., Non-animal strategies for toxicity assessment of nanoscale materials: Role of adverse outcome pathways in the selection of endpoints. *Small* **2021,** *17* (15), 2007628.

20. Fröhlich, E.; Salar-Behzadi, S., Toxicological assessment of inhaled nanoparticles: role of in vivo, ex vivo, in vitro, and in silico studies. *International journal of molecular sciences* **2014,** *15* (3), 4795-4822.

21. Louisse, J.; Beekmann, K.; Rietjens, I. M., Use of physiologically based kinetic modeling-based reverse dosimetry to predict in vivo toxicity from in vitro data. *Chemical Research in Toxicology* **2017,** *30* (1), 114-125.

22. Singh, K. P.; Gupta, S., Nano-QSAR modeling for predicting biological activity of diverse nanomaterials. *RSC Advances* **2014,** *4* (26), 13215-13230.

23. Oksel Karakus, C.; Bilgi, E.; Winkler, D. A., Biomedical nanomaterials: applications, toxicological concerns, and regulatory needs. *Nanotoxicology* **2021,** *15* (3), 331-351.

24. Ball, N.; Bars, R.; Botham, P. A.; Cuciureanu, A.; Cronin, M. T.; Doe, J. E.; Dudzina, T.; Gant, T. W.; Leist, M.; van Ravenzwaay, B., A framework for chemical safety assessment incorporating new approach methodologies within REACH. *Archives of Toxicology* **2022,** *96* (3), 743-766.

25. Schultz, T.; Amcoff, P.; Berggren, E.; Gautier, F.; Klaric, M.; Knight, D.; Mahony, C.; Schwarz, M.; White, A.; Cronin, M., A strategy for structuring and reporting a read-across prediction of toxicity. *Regulatory Toxicology and Pharmacology* **2015,** *72* (3), 586-601.

26. Drasler, B.; Sayre, P.; Steinhäuser, K. G.; Petri-Fink, A.; Rothen-Rutishauser, B., In vitro approaches to assess the hazard of nanomaterials. *NanoImpact* **2017,** *8*, 99-116.

27. Stone, V.; Gottardo, S.; Bleeker, E. A.; Braakhuis, H.; Dekkers, S.; Fernandes, T.; Haase, A.; Hunt, N.; Hristozov, D.; Jantunen, P., A framework for grouping and read-across of nanomaterials-supporting innovation and risk assessment. *Nano Today* **2020,** *35*, 100941.

28. OECD, Guidance on Grouping of Chemicals, Second Edition. **2017**.

29. Escher, S. E.; Kamp, H.; Bennekou, S. H.; Bitsch, A.; Fisher, C.; Graepel, R.; Hengstler, J. G.; Herzler, M.; Knight, D.; Leist, M., Towards grouping concepts based on new approach methodologies in chemical hazard assessment: the read-across approach of the EU-ToxRisk project. *Archives of toxicology* **2019,** *93*, 3643-3667.

30. OECD, Guidance on grouping of chemicals. Series on Testing and Assessment No. 194. Organisation for Economic Co-operation and Development Paris, France: **2014**.

31. Gajewicz, A.; Rasulev, B.; Dinadayalane, T. C.; Urbaszek, P.; Puzyn, T.; Leszczynska, D.; Leszczynski, J., Advancing risk assessment of engineered nanomaterials: application of computational approaches. *Advanced drug delivery reviews* **2012,** *64* (15), 1663-1693.

32. Basketter, D.; Clewell, H.; Kimber, I.; Rossi, A.; Blaauboer, B.; Burrier, R.; Daneshian, M.; Eskes, C.; Goldberg, A.; Hasiwa, N., A roadmap for the development of alternative (non-animal) methods for systemic toxicity testing. **2012**.

33. Fourches, D.; Pu, D.; Tropsha, A., Exploring quantitative nanostructure-activity relationships (QNAR) modeling as a tool for predicting biological effects of manufactured nanoparticles. *Combinatorial Chemistry & High Throughput Screening* **2011,** *14* (3), 217-225.

34. Mech, A.; Rasmussen, K.; Jantunen, P.; Aicher, L.; Alessandrelli, M.; Bernauer, U.; Bleeker, E.; Bouillard, J.; Di Prospero Fanghella, P.; Draisci, R., Insights into possibilities for grouping and read-across for nanomaterials in EU chemicals legislation. *Nanotoxicol.* **2019,** *13* (1), 119-141.

35. Patlewicz, G.; Ball, N.; Becker, R. A.; Booth, E. D.; Cronin, M. T.; Kroese, D.; Steup, D.; Van Ravenzwaay, B.; Hartung, T., Read-across approaches–misconceptions, promises and challenges ahead. *ALTEX-Alternatives to animal experimentation* **2014,** *31* (4), 387-396.

36. Ball, N.; Cronin, M. T.; Shen, J.; Blackburn, K.; Booth, E. D.; Bouhifd, M.; Donley, E.; Egnash, L.; Hastings, C.; Juberg, D. R., T4 report: Toward good read-across practice (GRAP) guidance. *Altex* **2016,** *33* (2), 149.

37. Schultz, T. W.; Richarz, A.-N.; Cronin, M. T., Assessing uncertainty in read-across: questions to evaluate toxicity predictions based on knowledge gained from case studies. *Computational Toxicology* **2019,** *9*, 1-11.

38. Rovida, C.; Barton-Maclaren, T.; Benfenati, E.; Caloni, F.; Chandrasekera, P. C.; Chesne, C.; Cronin, M. T.; De Knecht, J.; Dietrich, D. R.; Escher, S. E., Internationalization of read-across as a validated new approach method (NAM) for regulatory toxicology. *Altex* **2020,** *37* (4), 579.

39. Patlewicz, G.; Ball, N.; Booth, E. D.; Hulzebos, E.; Zvinavashe, E.; Hennes, C., Use of category approaches, read-across and (Q) SAR: general considerations. *Regulatory Toxicology and Pharmacology* **2013,** *67* (1), 1-12.

40. Forest, V., Experimental and Computational Nanotoxicology-Complementary Approaches for Nanomaterial Hazard Assessment. *Nanomaterials (Basel)* **2022,** *12* (8).

41. Halappanavar, S.; Ede, J. D.; Mahapatra, I.; Krug, H. F.; Kuempel, E. D.; Lynch, I.; Vandebriel, R. J.; Shatkin, J. A., A methodology for developing key events to advance nanomaterial-relevant adverse outcome pathways to inform risk assessment. *Nanotoxicology* **2021,** *15* (3), 289-310.

42. Halappanavar, S.; Ede, J. D.; Shatkin, J. A.; Krug, H. F., A systematic process for identifying key events for advancing the development of nanomaterial relevant adverse outcome pathways. *NanoImpact* **2019,** *15*, 100178.

43. Nel, A.; Xia, T.; Meng, H.; Wang, X.; Lin, S.; Ji, Z.; Zhang, H., Nanomaterial toxicity testing in the 21st century: use of a predictive toxicological approach and high-throughput screening. *Accounts of chemical research* **2013,** *46* (3), 607-621.

44. George, S.; Xia, T.; Rallo, R.; Zhao, Y.; Ji, Z.; Lin, S.; Wang, X.; Zhang, H.; France, B.; Schoenfeld, D., Use of a high-throughput screening approach coupled with in vivo zebrafish embryo screening to develop hazard ranking for engineered nanomaterials. *ACS nano* **2011,** *5* (3), 1805-1817.

45. Potyrailo, R.; Rajan, K.; Stoewe, K.; Takeuchi, I.; Chisholm, B.; Lam, H., Combinatorial and high-throughput screening of materials libraries: review of state of the art. *ACS combinatorial science* **2011,** *13* (6), 579-633.

46. Singh, A. V.; Laux, P.; Luch, A.; Sudrik, C.; Wiehr, S.; Wild, A.-M.; Santomauro, G.; Bill, J.; Sitti, M., Review of emerging concepts in nanotoxicology: Opportunities and challenges for safer nanomaterial design. *Toxicology Mechanisms and Methods* **2019,** *29* (5), 378-387.

47. Basei, G.; Hristozov, D.; Lamon, L.; Zabeo, A.; Jeliazkova, N.; Tsiliki, G.; Marcomini, A.; Torsello, A., Making use of available and emerging data to predict the hazards of engineered nanomaterials by means of in silico tools: A critical review. *NanoImpact* **2019,** *13*, 76-99.

48. Winkler, D. A.; Burden, F. R.; Yan, B.; Weissleder, R.; Tassa, C.; Shaw, S.; Epa, V. C., Modelling and predicting the biological effects of nanomaterials. *SAR and QSAR in Environmental Research* **2014,** *25* (2), 161-172.

49. Oksel, C.; Ma, C. Y.; Liu, J. J.; Wilkins, T.; Wang, X. Z., Literature review of (Q) SAR modelling of nanomaterial toxicity. *Modelling the toxicity of nanoparticles* **2017**, 103-142.

50. Dearden, J. C., The history and development of quantitative structure-activity relationships (QSARs). In *Oncology: breakthroughs in research and practice*, IGI Global: **2017**; pp 67-117.

51. Samek, W.; Binder, A.; Montavon, G.; Lapuschkin, S.; Müller, K.-R., Evaluating the visualization of what a deep neural network has learned. *IEEE transactions on neural networks and learning systems* **2016,** *28* (11), 2660-2673.

52. Singh, A. V.; Ansari, M. H. D.; Rosenkranz, D.; Maharjan, R. S.; Kriegel, F. L.; Gandhi, K.; Kanase, A.; Singh, R.; Laux, P.; Luch, A., Artificial intelligence and machine learning in computational nanotoxicology: unlocking and empowering nanomedicine. *Advanced Healthcare Materials* **2020,** *9* (17), 1901862.

53. Afantitis, A.; Melagraki, G.; Isigonis, P.; Tsoumanis, A.; Varsou, D. D.; Valsami-Jones, E.; Papadiamantis, A.; Ellis, L.-J. A.; Sarimveis, H.; Doganis, P., NanoSolveIT Project: Driving nanoinformatics research to develop innovative and integrated tools for in silico nanosafety assessment. *Computational and Structural Biotechnology Journal* **2020,** *18*, 583-602.

54. Ma, C. Y.; Buontempo, F. V.; Wang, X. Z., Inductive data mining: automatic generation of decision trees from data for QSAR modelling and process historical data analysis. In *Computer Aided Chemical Engineering*, Elsevier: **2008**; Vol. 25, pp 581-586.

55. Priyanka; Kumar, D., Decision tree classifier: a detailed survey. *International Journal of Information and Decision Sciences* **2020,** *12* (3), 246-269.

56. Ban, Z.; Zhou, Q.; Sun, A.; Mu, L.; Hu, X., Screening priority factors determining and predicting the reproductive toxicity of various nanoparticles. *Environmental science & technology* **2018,** *52* (17), 9666-9676.

57. Yu, H.; Zhao, Z.; Cheng, F., Predicting and investigating cytotoxicity of nanoparticles by translucent machine learning. *Chemosphere* **2021,** *276*, 130164.

58. Roy, J.; Roy, K., Assessment of toxicity of metal oxide and hydroxide nanoparticles using the QSAR modeling approach. *Environmental Science: Nano* **2021,** *8* (11), 3395-3407.

59. Papa, E.; Doucet, J.; Doucet-Panaye, A., Linear and non-linear modelling of the cytotoxicity of TiO2 and ZnO nanoparticles by empirical descriptors. *SAR and QSAR in Environmental Research* **2015,** *26* (7-9), 647-665.

60. Keri, G.; Toth, I., Molecular pathomechanisms and new trends in drug research. CRC Press: **2003**.

61. Scior, T.; Medina-Franco, J.; Do, Q.-T.; Martínez-Mayorga, K.; Yunes Rojas, J.; Bernard, P., How to recognize and workaround pitfalls in QSAR studies: a critical review. *Current medicinal chemistry* **2009,** *16* (32), 4297-4313.

62. Keri, G.; Toth, I., Molecular pathomechanisms and new trends in drug research. CRC Press: **2002**.

63. Eriksson, L.; Johansson, E., Multivariate design and modeling in QSAR. *Chemometrics and intelligent laboratory systems* **1996,** *34* (1), 1-19.

64. Rosipal, R.; Trejo, L. J., Kernel partial least squares regression in reproducing kernel hilbert space. *The Journal of Machine Learning Research* **2002,** *2*, 97-123.

65. Qin, S. J.; McAvoy, T. J., Nonlinear PLS modeling using neural networks. *Computers & Chemical Engineering* **1992,** *16* (4), 379-391.

66. Hasegawa, K.; Miyashita, Y.; Funatsu, K., GA Strategy for Variable Selection in QSAR Studies: GA-Based PLS Analysis of Calcium Channel Antagonists⊥. *Journal of Chemical Information and Computer Sciences* **1997,** *37* (2), 306-310.

67. Winkler, D. A.; Le, T. C., Performance of Deep and Shallow Neural Networks, the Universal Approximation Theorem, Activity Cliffs, and QSAR. *Molecular Informatics* **2016**.

68. Jalali-Heravi, M.; Parastar, F., Use of artificial neural networks in a QSAR study of anti-HIV activity for a large group of HEPT derivatives. *Journal of chemical information and computer sciences* **2000,** *40* (1), 147-154.

69. Habibi-Yangjeh, A.; Danandeh-Jenagharad, M.; Nooshyar, M., Application of artificial neural networks for predicting the aqueous acidity of various phenols using QSAR. *Journal of molecular modeling* **2006,** *12* (3), 338-347.

70. Jalali-Heravi, M.; Asadollahi-Baboli, M.; Shahbazikhah, P., QSAR study of heparanase inhibitors activity using artificial neural networks and Levenberg–Marquardt algorithm. *European journal of medicinal chemistry* **2008,** *43* (3), 548-556.

71. Ventura, C.; Latino, D. A.; Martins, F., Comparison of Multiple Linear Regressions and Neural Networks based QSAR models for the design of new antitubercular compounds. *European journal of medicinal chemistry* **2013,** *70*, 831-845.

72. Guyon, I.; Elisseeff, A., An introduction to variable and feature selection. *The Journal of Machine Learning Research* **2003,** *3*, 1157-1182.

73. Zurada, J. M.; Malinowski, A.; Cloete, I. In *Sensitivity analysis for minimization of input data dimension for feedforward neural network*, Circuits and Systems, 1994. ISCAS'94., 1994 IEEE International Symposium on, **1994**; pp 447-450.

74. Chen, Y.; Alba, M.; Tieu, T.; Tong, Z.; Minhas, R. S.; Rudd, D.; Voelcker, N. H.; Cifuentes-Rius, A.; Elnathan, R., Engineering micro–nanomaterials for biomedical translation. *Advanced NanoBiomed Research* **2021,** *1* (9), 2100002.

75. Singh, A. V.; Rosenkranz, D.; Ansari, M. H. D.; Singh, R.; Kanase, A.; Singh, S. P.; Johnston, B.; Tentschert, J.; Laux, P.; Luch, A., Artificial intelligence

and machine learning empower advanced biomedical material design to toxicity prediction. *Advanced Intelligent Systems* **2020,** *2* (12), 2000084.

76. Balci, O., Verification, validation, and testing. *Handbook of simulation* **1998,** *10* (8), 335-393.

77. Subramanian, N. A.; Palaniappan, A., NanoTox: development of a parsimonious in silico model for toxicity assessment of metal-oxide nanoparticles using physicochemical features. *ACS omega* **2021,** *6* (17), 11729-11739.

78. Utembe, W.; Clewell, H.; Sanabria, N.; Doganis, P.; Gulumian, M., Current approaches and techniques in physiologically based pharmacokinetic (PBPK) modelling of nanomaterials. *Nanomaterials* **2020,** *10* (7), 1267.

79. Carlander, U.; Moto, T. P.; Desalegn, A. A.; Yokel, R. A.; Johanson, G., Physiologically based pharmacokinetic modeling of nanoceria systemic distribution in rats suggests dose-and route-dependent biokinetics. *International Journal of Nanomedicine* **2018**, 2631-2646.

80. Vinken, M., The adverse outcome pathway concept: a pragmatic tool in toxicology. *Toxicology* **2013,** *312*, 158-165.

81. Ankley, G. T.; Bennett, R. S.; Erickson, R. J.; Hoff, D. J.; Hornung, M. W.; Johnson, R. D.; Mount, D. R.; Nichols, J. W.; Russom, C. L.; Schmieder, P. K., Adverse outcome pathways: a conceptual framework to support ecotoxicology research and risk assessment. *Environmental Toxicology and Chemistry* **2010,** *29* (3), 730-741.

82. Lai, R. W.; Yeung, K. W.; Yung, M. M.; Djurišić, A. B.; Giesy, J. P.; Leung, K. M., Regulation of engineered nanomaterials: current challenges, insights and future directions. *Environmental Science and Pollution Research* **2018,** *25*, 3060-3077.

83. Halappanavar, S.; Van Den Brule, S.; Nymark, P.; Gaté, L.; Seidel, C.; Valentino, S.; Zhernovkov, V.; Høgh Danielsen, P.; De Vizcaya, A.; Wolff, H., Adverse outcome pathways as a tool for the design of testing strategies to support the safety assessment of emerging advanced materials at the nanoscale. *Particle and Fibre Toxicology* **2020,** *17* (1), 1-24.

84. Oberdörster, G.; Oberdörster, E.; Oberdörster, J., Nanotoxicology: an emerging discipline evolving from studies of ultrafine particles. *Environ. Health Persp.* **2005,** *113* (7), 823-839.

85. Linkov, I.; Satterstrom, F. K., Nanomaterial risk assessment and risk management. In *Real-time and deliberative decision making*, Springer: **2008**; pp 129-157.

86. Oksel, C.; Subramanian, V.; Semenzin, E.; Ma, C. Y.; Hristozov, D.; Wang, X. Z.; Hunt, N.; Costa, A.; Fransman, W.; Marcomini, A., Evaluation of existing control measures in reducing health and safety risks of engineered nanomaterials. *Environ. Sci. Nano* **2016,** *3* (4), 869-882.

87. Savolainen, K.; Alenius, H.; Norppa, H.; Pylkkänen, L.; Tuomi, T.; Kasper, G., Risk assessment of engineered nanomaterials and nanotechnologies—a review. *Toxicol.* **2010,** *269* (2-3), 92-104.

88. Yokel, R. A.; MacPhail, R. C., Engineered nanomaterials: exposures, hazards, and risk prevention. *J. Occup. Med. Toxicol.* **2011,** *6* (1), 7.

89. Donaldson, K.; Poland, C. A., Nanotoxicity: challenging the myth of nano-specific toxicity. *Curr. Opin. Biotechnol.* **2013,** *24* (4), 724-734.

90. Kim, B. Y.; Rutka, J. T.; Chan, W. C., Nanomedicine. *New Engl. J. Med.* **2010,** *363* (25), 2434-2443.

91. Riehemann, K.; Schneider, S. W.; Luger, T. A.; Godin, B.; Ferrari, M.; Fuchs, H., Nanomedicine—challenge and perspectives. *Angew. Chem. Int. Ed.* **2009,** *48* (5), 872-897.

92. Wagner, V.; Dullaart, A.; Bock, A.-K.; Zweck, A., The emerging nanomedicine landscape. *Nat. Biotechnol.* **2006,** *24* (10), 1211-1217.

93. Grand View Research, I. Nanomedicine Market Analysis by Products, Application, Nanomolecule & Segment Forecasts. https://www.grandviewresearch.com/industry-analysis/nanomedicine-market (accessed 18 March).

94. Resnik, D. B., How Should Engineered Nanomaterials Be Regulated for Public and Environmental Health? *AMA J. Ethics* **2019,** *21* (4), 363-369.

95. Beaudrie, C. E.; Kandlikar, M.; Gregory, R.; Long, G.; Wilson, T., Nanomaterial risk screening: a structured approach to aid decision making under uncertainty. *Environ. Sys. Decis.* **2015,** *35* (1), 88-109.

96. Falkner, R.; Jaspers, N., Regulating nanotechnologies: risk, uncertainty and the global governance gap. *Glob. Environ. Polit.* **2012,** *12* (1), 30-55.

97. Heidmann, I.; Milde, J., Communication about scientific uncertainty: how scientists and science journalists deal with uncertainties in nanoparticle research. *Environ. Sci. Eur.* **2013,** *25* (1), 25.

98. Maynard, A. D., A decade of uncertainty. *Nat. Nanotech.* **2014,** *9* (3), 159.

99. Gao, X.; Lowry, G. V., Progress towards standardized and validated characterizations for measuring physicochemical properties of manufactured nanomaterials relevant to nano health and safety risks. *NanoImpact* **2018,** *9*, 14-30.

100. Kuempel, E. D.; Geraci, C. L.; Schulte, P. A., Risk assessment and risk management of nanomaterials in the workplace: translating research to practice. *Ann. Occup. Hyg.* **2012,** *56* (5), 491-505.

101. Duvall, M.; Wyatt, A., Regulation of nanotechnology and nanomaterials at EPA and around the world: Recent developments and context. *Washington, DC: Beveridge & Diamond, PC* **2011**.

102. Park, H.-G.; Yeo, M.-K., Nanomaterial regulatory policy for human health and environment. *Mol. Cell. Toxicol.* **2016,** *12* (3), 223-236.

103. Rasmussen, K.; González, M.; Kearns, P.; Sintes, J. R.; Rossi, F.; Sayre, P., Review of achievements of the OECD Working Party on Manufactured Nanomaterials' Testing and Assessment Programme. From exploratory testing to test guidelines. *Regul. Toxicol. Pharmacol.* **2016,** *74*, 147-160.

104. Rauscher, H.; Rasmussen, K.; Sokull-Klüttgen, B., Regulatory aspects of nanomaterials in the EU. *Chem. Ingen. Techn.* **2017,** *89* (3), 224-231.

105. Rauscher, H.; Roebben, G.; Mech, A.; Gibson, N.; Kestens, V.; Linsinger, T.; Sintes, J. R., An overview of concepts and terms used in the European Commission's definition of nanomaterial. *Chem. Ing. Tech.* **2019**, 224-231.

106. Hansen, S. F.; Michelson, E. S.; Kamper, A.; Borling, P.; Stuer-Lauridsen, F.; Baun, A., Categorization framework to aid exposure assessment of nanomaterials in consumer products. *Ecotoxicol.* **2008,** *17* (5), 438-447.

107. Gebel, T.; Foth, H.; Damm, G.; Freyberger, A.; Kramer, P.-J.; Lilienblum, W.; Röhl, C.; Schupp, T.; Weiss, C.; Wollin, K.-M., Manufactured nanomaterials: categorization and approaches to hazard assessment. *Arch. Toxicol.* **2014,** *88* (12), 2191-2211.

108. Godwin, H.; Nameth, C.; Avery, D.; Bergeson, L. L.; Bernard, D.; Beryt, E.; Boyes, W.; Brown, S.; Clippinger, A. J.; Cohen, Y., Nanomaterial categorization for assessing risk potential to facilitate regulatory decision-making. ACS Publications: **2015**.

109. Dolez, P. I., Nanomaterials definitions, classifications, and applications. In *Nanoengineering*, Elsevier: **2015**; pp 3-40.

110. Roubert, F.; Beuzelin-Ollivier, M.-G.; Hofmann-Amtenbrink, M.; Hofmann, H.; Hool, A., "Nanostandardization" in action: implementing standardization processes in a multidisciplinary nanoparticle-based research and development project. *NanoEthics* **2016,** *10* (1), 41-62.

111. Commission, E., Regulation (EC) No 1907/2006 of the European Parliament and of the Council of 18 December 2006 concerning the Registration, Evaluation, Authorisation and Restriction of Chemicals (REACH), establishing a European Chemicals Agency, amending Directive 1999/45/EC and repealing Council Regulation (EEC) No 793/93 and Commission Regulation (EC) No 1488/94 as well as Council Directive 76/769/EEC and Commission Directives 91/155/EEC, 93/67/EEC, 93/105/EC and 2000/21/EC. *Offic. J. Eur. Union* **2006,** *396*, 1-849.

112. REACH, E., Commission Regulation (EU) 2018/1881 of 3 December 2018 amending Regulation (EC) No 1907/2006 of the European Parliament and of the Council on the Registration, Evaluation, Authorisation and Restriction of Chemicals (REACH) as regards Annexes I, III, VI, VII, VIII, IX, X, XI, and XII to address nanoforms of substances. *Offic. J. Eur. Union* **2018,** *308*, 1-20.

113. ECHA Nanomaterials. https://echa.europa.eu/regulations/nanomaterials (accessed 18 March).

114. Krug, H. F., Nanosafety research—are we on the right track? *Angew. Chem. Int. Ed.* **2014,** *53* (46), 12304-12319.

115. Guadagnini, R.; Halamoda Kenzaoui, B.; Walker, L.; Pojana, G.; Magdolenova, Z.; Bilanicova, D.; Saunders, M.; Juillerat-Jeanneret, L.; Marcomini, A.; Huk, A., Toxicity screenings of nanomaterials: challenges due to interference with assay processes and components of classic in vitro tests. *Nanotoxicol.* **2015,** *9* (sup1), 13-24.

116. Docter, D.; Strieth, S.; Westmeier, D.; Hayden, O.; Gao, M.; Knauer, S. K.; Stauber, R. H., No king without a crown–impact of the nanomaterial-protein corona on nanobiomedicine. *Nanomed.* **2015,** *10* (3), 503-519.

117. Walkey, C. D.; Chan, W. C., Understanding and controlling the interaction of nanomaterials with proteins in a physiological environment. *Chem. Soc. Rev.* **2012,** *41* (7), 2780-2799.

118. Farrera, C.; Fadeel, B., It takes two to tango: Understanding the interactions between engineered nanomaterials and the immune system. *Eur. J. Pharmaceut. Biopharmaceut.* **2015,** *95*, 3-12.

119. Yan, L.; Zhao, F.; Wang, J.; Zu, Y.; Gu, Z.; Zhao, Y., A Safe-by-Design Strategy towards Safer Nanomaterials in Nanomedicines. *Adv. Mater.* **2019,** *31* (45), 1805391.

120. Sayes, C. M.; Warheit, D. B., Characterization of nanomaterials for toxicity assessment. *Wiley Interdisc. Rev. Nanomed. Nanobiotechnol.* **2009,** *1* (6), 660-670.

121. Powers, K. W.; Palazuelos, M.; Moudgil, B. M.; Roberts, S. M., Characterization of the size, shape, and state of dispersion of nanoparticles for toxicological studies. *Nanotoxicol.* **2007,** *1* (1), 42-51.

122. Boverhof, D. R.; David, R. M., Nanomaterial characterization: considerations and needs for hazard assessment and safety evaluation. *Anal. Bioanal. Chem.* **2010,** *396* (3), 953-961.

123. Wongrakpanich, A.; Mudunkotuwa, I. A.; Geary, S. M.; Morris, A. S.; Mapuskar, K. A.; Spitz, D. R.; Grassian, V. H.; Salem, A. K., Size-dependent cytotoxicity of copper oxide nanoparticles in lung epithelial cells. *Environ. Sci. Nano* **2016,** *3* (2), 365-374.

124. Gliga, A. R.; Skoglund, S.; Wallinder, I. O.; Fadeel, B.; Karlsson, H. L., Size-dependent cytotoxicity of silver nanoparticles in human lung cells: the role of cellular uptake, agglomeration and Ag release. *Partic. Fibre Toxicol.* **2014,** *11* (1), 11.

125. Pan, Y.; Neuss, S.; Leifert, A.; Fischler, M.; Wen, F.; Simon, U.; Schmid, G.; Brandau, W.; Jahnen-Dechent, W., Size-dependent cytotoxicity of gold nanoparticles. *Small* **2007,** *3* (11), 1941-1949.

126. Napierska, D.; Thomassen, L. C.; Rabolli, V.; Lison, D.; Gonzalez, L.; Kirsch-Volders, M.; Martens, J. A.; Hoet, P. H., Size-dependent cytotoxicity of monodisperse silica nanoparticles in human endothelial cells. *Small* **2009,** *5* (7), 846-853.

127. Di Bucchianico, S.; Fabbrizi, M. R.; Misra, S. K.; Valsami-Jones, E.; Berhanu, D.; Reip, P.; Bergamaschi, E.; Migliore, L., Multiple cytotoxic and genotoxic effects induced in vitro by differently shaped copper oxide nanomaterials. *Mutagen.* **2013,** *28* (3), 287-299.

128. Zhang, B.; Lung, P. S.; Zhao, S.; Chu, Z.; Chrzanowski, W.; Li, Q., Shape dependent cytotoxicity of PLGA-PEG nanoparticles on human cells. *Sci. Rep.* **2017,** *7* (1), 1-8.

129. Niu, M.; Zhong, H.; Shao, H.; Hong, D.; Ma, T.; Xu, K.; Chen, X.; Han, J.; Sun, J., Shape-dependent genotoxicity of mesoporous silica nanoparticles and cellular mechanisms. *J. Nanosci. Nanotechnol.* **2016,** *16* (3), 2313-2318.

130. Woźniak, A.; Malankowska, A.; Nowaczyk, G.; Grześkowiak, B. F.; Tuśnio, K.; Słomski, R.; Zaleska-Medynska, A.; Jurga, S., Size and shape-dependent cytotoxicity profile of gold nanoparticles for biomedical applications. *J. Mater. Sci. Mater. Med.* **2017,** *28* (6), 92.

131. Yang, X.; Gondikas, A. P.; Marinakos, S. M.; Auffan, M.; Liu, J.; Hsu-Kim, H.; Meyer, J. N., Mechanism of silver nanoparticle toxicity is dependent on dissolved silver and surface coating in Caenorhabditis elegans. *Environ. Sci. Technol.* **2012,** *46* (2), 1119-1127.

132. Hoshino, A.; Fujioka, K.; Oku, T.; Suga, M.; Sasaki, Y. F.; Ohta, T.; Yasuhara, M.; Suzuki, K.; Yamamoto, K., Physicochemical properties and cellular toxicity of nanocrystal quantum dots depend on their surface modification. *Nano Lett.* **2004,** *4* (11), 2163-2169.

133. El Badawy, A. M.; Silva, R. G.; Morris, B.; Scheckel, K. G.; Suidan, M. T.; Tolaymat, T. M., Surface charge-dependent toxicity of silver nanoparticles. *Environ. Sci. Technol.* **2011,** *45* (1), 283-287.

134. Warheit, D. B., How meaningful are the results of nanotoxicity studies in the absence of adequate material characterization? *Toxicol. Sci.* **2008,** *101* (2), 183-185.

135. He, C.; Hu, Y.; Yin, L.; Tang, C.; Yin, C., Effects of particle size and surface charge on cellular uptake and biodistribution of polymeric nanoparticles. *Biomater.* **2010,** *31* (13), 3657-3666.

136. Greish, K.; Thiagarajan, G.; Herd, H.; Price, R.; Bauer, H.; Hubbard, D.; Burckle, A.; Sadekar, S.; Yu, T.; Anwar, A., Size and surface charge significantly influence the toxicity of silica and dendritic nanoparticles. *Nanotoxicol.* **2012,** *6* (7), 713-723.

137. Tsoi, K. M.; MacParland, S. A.; Ma, X.-Z.; Spetzler, V. N.; Echeverri, J.; Ouyang, B.; Fadel, S. M.; Sykes, E. A.; Goldaracena, N.; Kaths, J. M., Mechanism of hard-nanomaterial clearance by the liver. *Nature materials* **2016,** *15* (11), 1212-1221.

138. Choi, H. S.; Ashitate, Y.; Lee, J. H.; Kim, S. H.; Matsui, A.; Insin, N.; Bawendi, M. G.; Semmler-Behnke, M.; Frangioni, J. V.; Tsuda, A., Rapid translocation of nanoparticles from the lung airspaces to the body. *Nature biotechnology* **2010,** *28* (12), 1300-1303.

139. Buckley, A.; Warren, J.; Hodgson, A.; Marczylo, T.; Ignatyev, K.; Guo, C.; Smith, R., Slow lung clearance and limited translocation of four sizes of inhaled iridium nanoparticles. *Particle and fibre toxicology* **2017,** *14* (1), 5.

140. Haute, D. V.; Berlin, J. M., Challenges in realizing selectivity for nanoparticle biodistribution and clearance: lessons from gold nanoparticles. *Therapeutic delivery* **2017,** *8* (9), 763-774.

141. Ahmed, K. B. R.; Nagy, A. M.; Brown, R. P.; Zhang, Q.; Malghan, S. G.; Goering, P. L., Silver nanoparticles: Significance of physicochemical properties and assay interference on the interpretation of in vitro cytotoxicity studies. *Toxicol. in Vitro* **2017,** *38*, 179-192.

142. Wang, G.; Zhang, J.; Dewilde, A. H.; Pal, A. K.; Bello, D.; Therrien, J. M.; Braunhut, S. J.; Marx, K. A., Understanding and correcting for carbon nanotube interferences with a commercial LDH cytotoxicity assay. *Toxicol.* **2012,** *299* (2-3), 99-111.

143. Geys, J.; Nemery, B.; Hoet, P. H., Assay conditions can influence the outcome of cytotoxicity tests of nanomaterials: better assay characterization is needed to compare studies. *Toxicol. in Vitro* **2010,** *24* (2), 620-629.

144. Ong, K. J.; MacCormack, T. J.; Clark, R. J.; Ede, J. D.; Ortega, V. A.; Felix, L. C.; Dang, M. K.; Ma, G.; Fenniri, H.; Veinot, J. G., Widespread nanoparticle-assay interference: implications for nanotoxicity testing. *PLoS One* **2014,** *9* (3).

145. Brunner, T. J.; Wick, P.; Manser, P.; Spohn, P.; Grass, R. N.; Limbach, L. K.; Bruinink, A.; Stark, W. J., In vitro cytotoxicity of oxide nanoparticles: comparison to asbestos, silica, and the effect of particle solubility. *Environ. Sci. Technol.* **2006,** *40* (14), 4374-4381.

146. Hu, X.; Cook, S.; Wang, P.; Hwang, H.-m., In vitro evaluation of cytotoxicity of engineered metal oxide nanoparticles. *Sci. Total Environ.* **2009,** *407* (8), 3070-3072.

147. Dobrovolskaia, M. A.; Germolec, D. R.; Weaver, J. L., Evaluation of nanoparticle immunotoxicity. *Nat. Nanotech.* **2009,** *4* (7), 411-414.

148. Smith, M. J.; Brown, J. M.; Zamboni, W. C.; Walker, N. J., From immunotoxicity to nanotherapy: the effects of nanomaterials on the immune system. *Toxicol. Sci.* **2014,** *138* (2), 249-255.

149. Gonzalez, L.; Sanderson, B.; Kirsch-Volders, M., Adaptations of the in vitro MN assay for the genotoxicity assessment of nanomaterials. *Mutagen.* **2011,** *26* (1), 185-191.

150. Doak, S.; Manshian, B.; Jenkins, G.; Singh, N., In vitro genotoxicity testing strategy for nanomaterials and the adaptation of current OECD guidelines. *Mutat. Res. Genet. Toxicol. Environ. Mutagen.* **2012,** *745* (1-2), 104-111.

151. Qiao, Y.; An, J.; Ma, L., Single cell array based assay for in vitro genotoxicity study of nanomaterials. *Anal. Chem.* **2013,** *85* (8), 4107-4112.

152. Manke, A.; Wang, L.; Rojanasakul, Y., Mechanisms of nanoparticle-induced oxidative stress and toxicity. *BioMed Res. Int.* **2013,** *2013*.

153. Lehman, S. E.; Morris, A. S.; Mueller, P. S.; Salem, A. K.; Grassian, V. H.; Larsen, S. C., Silica nanoparticle-generated ROS as a predictor of cellular toxicity: mechanistic insights and safety by design. *Environ. Sci. Nano* **2016,** *3* (1), 56-66.

154. Kodali, V.; Thrall, B. D., Oxidative stress and nanomaterial-cellular interactions. In *Studies on Experimental Toxicology and Pharmacology*, Springer: **2015**; pp 347-367.

155. Oksel, C.; Ma, C. Y.; Liu, J. J.; Wilkins, T.; Wang, X. Z., (Q) SAR modelling of nanomaterial toxicity: A critical review. *Particuology* **2015,** *21*, 1-19.

156. Winkler, D. A., Role of Artificial Intelligence and Machine Learning in Nanosafety. *Small* **2020**, e2001883.

157. Tantra, R.; Oksel, C.; Puzyn, T.; Wang, J.; Robinson, K. N.; Wang, X. Z.; Ma, C. Y.; Wilkins, T., Nano (Q) SAR: Challenges, pitfalls and perspectives. *Nanotoxicol.* **2015,** *9* (5), 636-642.

158. Lison, D.; Vietti, G.; van den Brule, S., Paracelsus in nanotoxicology. *Partic. Fibre Toxicol.* **2014,** *11* (1), 35.

159. Cohen, J. M.; DeLoid, G. M.; Demokritou, P., A critical review of in vitro dosimetry for engineered nanomaterials. *Nanomed.* **2015,** *10* (19), 3015-3032.

160. Delmaar, C. J.; Peijnenburg, W. J.; Oomen, A. G.; Chen, J.; de Jong, W. H.; Sips, A. J.; Wang, Z.; Park, M. V., A practical approach to determine dose metrics for nanomaterials. *Environ. Toxicol. Chem.* **2015,** *34* (5), 1015-1022.

161. DeLoid, G. M.; Cohen, J. M.; Pyrgiotakis, G.; Pirela, S. V.; Pal, A.; Liu, J.; Srebric, J.; Demokritou, P., Advanced computational modeling for in vitro nanomaterial dosimetry. *Partic. Fibre Toxicol.* **2015,** *12* (1), 32.

162. Oksel, C.; Ma, C.; Wang, X., Current situation on the availability of nanostructure–biological activity data. *SAR QSAR Environ. Res.* **2015,** *26* (2), 79-94.

163. Miernicki, M.; Hofmann, T.; Eisenberger, I.; von der Kammer, F.; Praetorius, A., Legal and practical challenges in classifying nanomaterials according to regulatory definitions. *Nat Nanotechnol* **2019,** *14* (3), 208-216.

164. Robertson, D.; Williams, G. H., Clinical and translational science: principles of human research. Academic Press: **2009**.

165. Mohammed, L.; Gomaa, H. G.; Ragab, D.; Zhu, J., Magnetic nanoparticles for environmental and biomedical applications: A review. *Particuology* **2017,** *30*, 1-14.

166. Arias, L. S.; Pessan, J. P.; Vieira, A. P. M.; de Lima, T. M. T.; Delbem, A. C. B.; Monteiro, D. R., Iron Oxide Nanoparticles for Biomedical Applications: A Perspective on Synthesis, Drugs, Antimicrobial Activity, and Toxicity. *Antibiotics-Basel* **2018,** *7* (2).

167. Burdusel, A. C.; Gherasim, O.; Grumezescu, A. M.; Mogoanta, L.; Ficai, A.; Andronescu, E., Biomedical Applications of Silver Nanoparticles: An Up-to-Date Overview. *Nanomaterials* **2018,** *8* (9).

168. Elahi, N.; Kamali, M.; Baghersad, M. H., Recent biomedical applications of gold nanoparticles: A review. *Talanta* **2018,** *184*, 537-556.

169. Han, X. J.; Xu, K.; Taratula, O.; Farsad, K., Applications of nanoparticles in biomedical imaging. *Nanoscale* **2019,** *11* (3), 799-819.

170. Maiti, D.; Tong, X. M.; Mou, X. Z.; Yang, K., Carbon-Based Nanomaterials for Biomedical Applications: A Recent Study. *Frontiers in Pharmacology* **2019,** *9*.

171. Alcaraz, J. P.; Menassol, G.; Penven, G.; Thelu, J.; El Ichi, S.; Zebda, A.; Cinquin, P.; Martin, D. K., Challenges for the Implantation of Symbiotic Nanostructured Medical Devices. *Applied Sciences-Basel* **2020,** *10* (8).

172. Makvandi, P.; Wang, C. Y.; Zare, E. N.; Borzacchiello, A.; Niu, L. N.; Tay, F. R., Metal-Based Nanomaterials in Biomedical Applications: Antimicrobial Activity and Cytotoxicity Aspects. *Advanced Functional Materials* **2020,** *30* (22).

173. Park, W.; Shin, H.; Choi, B.; Rhim, W. K.; Na, K.; Han, D. K., Advanced hybrid nanomaterials for biomedical applications. *Progress in Materials Science* **2020,** *114*.

174. Nakamura, Y.; Mochida, A.; Choyke, P. L.; Kobayashi, H., Nanodrug delivery: is the enhanced permeability and retention effect sufficient for curing cancer? *Bioconj. Chem.* **2016,** *27* (10), 2225-2238.

175. Fan, Z.; Sun, L.; Huang, Y.; Wang, Y.; Zhang, M., Bioinspired fluorescent dipeptide nanoparticles for targeted cancer cell imaging and real-time monitoring of drug release. *Nat. Nanotech.* **2016,** *11* (4), 388-394.

176. Gao, X.; Cui, Y.; Levenson, R. M.; Chung, L. W.; Nie, S., In vivo cancer targeting and imaging with semiconductor quantum dots. *Nat. Biotechnol.* **2004,** *22* (8), 969-976.

177. Cheng, C.-C.; Liao, Z.-S.; Huang, J.-J.; Lee, D.-J.; Chen, J.-K., Supramolecular polymer micelles as universal tools for constructing high-performance fluorescent nanoparticles. *Dye. Pig.* **2017,** *137*, 284-292.

178. Cheng, C.-C.; Huang, J.-J.; Muhable, A. A.; Liao, Z.-S.; Huang, S.-Y.; Lee, S.-C.; Chiu, C.-W.; Lee, D.-J., Supramolecular fluorescent nanoparticles

functionalized with controllable physical properties and temperature-responsive release behavior. *Polym. Chem.* **2017,** *8* (15), 2292-2298.

179. Pecher, J.; Huber, J.; Winterhalder, M.; Zumbusch, A.; Mecking, S., Tailor-made conjugated polymer nanoparticles for multicolor and multiphoton cell imaging. *Biomacromol.* **2010,** *11* (10), 2776-2780.

180. Zhang, X.; Zhang, X.; Yang, B.; Zhang, Y.; Liu, M.; Liu, W.; Chen, Y.; Wei, Y., Fabrication of water-dispersible and biocompatible red fluorescent organic nanoparticles via PEGylation of aggregate induced emission enhancement dye and their cell imaging applications. *Coll. Surf. B* **2014,** *113*, 435-441.

181. Caponetti, V.; Trzcinski, J. W.; Cantelli, A.; Tavano, R.; Papini, E.; Mancin, F.; Montalti, M., Self-assembled biocompatible fluorescent nanoparticles for bioimaging. *Front. Chem.* **2019,** *7*, 168.

182. Winter, P. M.; Caruthers, S. D.; Kassner, A.; Harris, T. D.; Chinen, L. K.; Allen, J. S.; Lacy, E. K.; Zhang, H.; Robertson, J. D.; Wickline, S. A., Molecular imaging of angiogenesis in nascent Vx-2 rabbit tumors using a novel αvβ3-targeted nanoparticle and 1.5 tesla magnetic resonance imaging. *Cancer Res.* **2003,** *63* (18), 5838-5843.

183. Zhang, Z.; Mascheri, N.; Dharmakumar, R.; Fan, Z.; Paunesku, T.; Woloschak, G.; Li, D., Superparamagnetic iron oxide nanoparticle-labeled cells as an effective vehicle for tracking the GFP gene marker using magnetic resonance imaging. *Cytother.* **2009,** *11* (1), 43-51.

184. Mi, P.; Kokuryo, D.; Cabral, H.; Wu, H.; Terada, Y.; Saga, T.; Aoki, I.; Nishiyama, N.; Kataoka, K., A pH-activatable nanoparticle with signal-amplification capabilities for non-invasive imaging of tumour malignancy. *Nat. Nanotech.* **2016,** *11* (8), 724.

185. Rahmer, J.; Antonelli, A.; Sfara, C.; Tiemann, B.; Gleich, B.; Magnani, M.; Weizenecker, J.; Borgert, J., Nanoparticle encapsulation in red blood cells enables blood-pool magnetic particle imaging hours after injection. *Phys. Med. Biol.* **2013,** *58* (12), 3965.

186. Park, I.-K.; Ng, C.-P.; Wang, J.; Chu, B.; Yuan, C.; Zhang, S.; Pun, S. H., Determination of nanoparticle vehicle unpackaging by MR imaging of a T2 magnetic relaxation switch. *Biomater.* **2008,** *29* (6), 724-732.

187. Romero-Aburto, R.; Narayanan, T. N.; Nagaoka, Y.; Hasumura, T.; Mitcham, T. M.; Fukuda, T.; Cox, P. J.; Bouchard, R. R.; Maekawa, T.; Kumar, D. S., Fluorinated graphene oxide; a new multimodal material for biological applications. *Adv. Mater.* **2013,** *25* (39), 5632-5637.

188. Yu, Y.; Yang, T.; Sun, T., New insights into the synthesis, toxicity and applications of gold nanoparticles in CT imaging and treatment of cancer. *Nanomed.* **2020,** *15* (11), 1127-1145.

189. Chhour, P.; Naha, P. C.; O'Neill, S. M.; Litt, H. I.; Reilly, M. P.; Ferrari, V. A.; Cormode, D. P., Labeling monocytes with gold nanoparticles to track their recruitment in atherosclerosis with computed tomography. *Biomater.* **2016,** *87*, 93-103.

190. Keshavarz, M.; Moloudi, K.; Paydar, R.; Abed, Z.; Beik, J.; Ghaznavi, H.; Shakeri-Zadeh, A., Alginate hydrogel co-loaded with cisplatin and gold nanoparticles for computed tomography image-guided chemotherapy. *J. Biomater. Appl.* **2018,** *33* (2), 161-169.

191. Lin, W.; Zhang, X.; Qian, L.; Yao, N.; Pan, Y.; Zhang, L., Doxorubicin-loaded unimolecular micelle-stabilized gold nanoparticles as a theranostic nanoplatform for tumor-targeted chemotherapy and computed tomography imaging. *Biomacromol.* **2017,** *18* (12), 3869-3880.

192. Kim, D.; Park, S.; Lee, J. H.; Jeong, Y. Y.; Jon, S., Antibiofouling polymer-coated gold nanoparticles as a contrast agent for in vivo X-ray computed tomography imaging. *J. Am. Chem. Soc.* **2007,** *129* (24), 7661-7665.

193. Peng, C.; Zheng, L.; Chen, Q.; Shen, M.; Guo, R.; Wang, H.; Cao, X.; Zhang, G.; Shi, X., PEGylated dendrimer-entrapped gold nanoparticles for in vivo blood pool and tumor imaging by computed tomography. *Biomater.* **2012,** *33* (4), 1107-1119.

194. Devaraj, N. K.; Keliher, E. J.; Thurber, G. M.; Nahrendorf, M.; Weissleder, R., 18F labeled nanoparticles for in vivo PET-CT imaging. *Bioconj. Chem.* **2009,** *20* (2), 397-401.

195. Glaus, C.; Rossin, R.; Welch, M. J.; Bao, G., In vivo evaluation of 64Cu-labeled magnetic nanoparticles as a dual-modality PET/MR imaging agent. *Bioconj. Chem.* **2010,** *21* (4), 715-722.

196. Zhao, Y.; Pang, B.; Luehmann, H.; Detering, L.; Yang, X.; Sultan, D.; Harpstrite, S.; Sharma, V.; Cutler, C. S.; Xia, Y., Gold Nanoparticles Doped with 199Au Atoms and Their Use for Targeted Cancer Imaging by SPECT. *Adv. Healthc. Mater.* **2016,** *5* (8), 928-935.

197. Sampath, L.; Kwon, S.; Hall, M. A.; Price, R. E.; Sevick-Muraca, E. M., Detection of Cancer Metastases with a Dual-labeled Near-Infrared/Position Emission Tomography Imaging Agent. *Transl. Oncol.* **2010,** *3* (5), 307-IN1.

198. Thakor, A. S.; Jokerst, J. V.; Ghanouni, P.; Campbell, J. L.; Mittra, E.; Gambhir, S. S., Clinically approved nanoparticle imaging agents. *J. Nucl. Med.* **2016,** *57* (12), 1833-1837.

199. Gunasekaran, T.; Nigusse, T.; Dhanaraju, M. D., Silver nanoparticles as real topical bullets for wound healing. *J. Am. Coll. Clin. Wound Special.* **2011,** *3* (4), 82-96.

200. Santos, L. M.; Stanisic, D.; Menezes, U. J.; Mendonça, M. A.; Barral, T. D.; Seyffert, N.; Azevedo, V.; Durán, N.; Meyer, R.; Tasic, L., Biogenic silver nanoparticles as a post-surgical treatment for Corynebacterium pseudotuberculosis infection in small ruminants. *Front. Microbiol.* **2019,** *10*, 824.

201. Cochis, A.; Azzimonti, B.; Della Valle, C.; De Giglio, E.; Bloise, N.; Visai, L.; Cometa, S.; Rimondini, L.; Chiesa, R., The effect of silver or gallium doped titanium against the multidrug resistant Acinetobacter baumannii. *Biomater.* **2016,** *80*, 80-95.

202. Gao, A.; Hang, R.; Huang, X.; Zhao, L.; Zhang, X.; Wang, L.; Tang, B.; Ma, S.; Chu, P. K., The effects of titania nanotubes with embedded silver oxide nanoparticles on bacteria and osteoblasts. *Biomater.* **2014,** *35* (13), 4223-4235.

203. Kuehl, R.; Brunetto, P. S.; Woischnig, A.-K.; Varisco, M.; Rajacic, Z.; Vosbeck, J.; Terracciano, L.; Fromm, K. M.; Khanna, N., Preventing implant-associated infections by silver coating. *Antimicrob. Agents Chemother.* **2016,** *60* (4), 2467-2475.

204. Khezerlou, A.; Alizadeh-Sani, M.; Azizi-Lalabadi, M.; Ehsani, A., Nanoparticles and their antimicrobial properties against pathogens including bacteria, fungi, parasites and viruses. *Microb. Pathogen.* **2018,** *123*, 505-526.

205. Winkler, D. A., Computational Modelling of Magnetic Nanoparticle Properties and In Vivo Responses. *Curr. Med. Chem.* **2017,** *24* (5), 483-496.

206. Nazir, S.; Hussain, T.; Ayub, A.; Rashid, U.; MacRobert, A. J., Nanomaterials in combating cancer: therapeutic applications and developments. *Nanomedicine: Nanotechnology, Biology and Medicine* **2014,** *10* (1), 19-34.

207. Chen, J.; Ning, C.; Zhou, Z.; Yu, P.; Zhu, Y.; Tan, G.; Mao, C., Nanomaterials as photothermal therapeutic agents. *Progress in materials science* **2019,** *99*, 1-26.

208. Barreto, J. A.; O'Malley, W.; Kubeil, M.; Graham, B.; Stephan, H.; Spiccia, L., Nanomaterials: applications in cancer imaging and therapy. *Advanced materials* **2011,** *23* (12), H18-H40.

209. Ji, T.; Zhao, Y.; Ding, Y.; Nie, G., Using functional nanomaterials to target and regulate the tumor microenvironment: diagnostic and therapeutic applications. *Advanced Materials* **2013,** *25* (26), 3508-3525.

210. Buchholz, K., Science–or not? The status and dynamics of biotechnology. *Biotechnol. J.* **2007,** *2* (9), 1154-1168.

211. Fahey, M.; Indelicato, P. A., Bone tunnel enlargement after anterior cruciate ligament replacement. *Am. J. Sports Med.* **1994,** *22* (3), 410-414.

212. Clark, R. A.; Ghosh, K.; Tonnesen, M. G., Tissue engineering for cutaneous wounds. *J. Investig. Dermatol.* **2007,** *127* (5), 1018-1029.

213. Hynes, R. O., The extracellular matrix: not just pretty fibrils. *Science* **2009,** *326* (5957), 1216-1219.

214. Holmes, B.; Fang, X.; Zarate, A.; Keidar, M.; Zhang, L. G., Enhanced human bone marrow mesenchymal stem cell chondrogenic differentiation in electrospun constructs with carbon nanomaterials. *Carbon* **2016,** *97*, 1-13.

215. Fathi-Achachelouei, M.; Knopf-Marques, H.; Riberio de Silva, C. E.; Barthès, J. G. D.; Bat, E.; Tezcaner, A.; Vrana, N. E., Use of nanoparticles in tissue engineering and regenerative medicine. *Front. Bioengin. Biotechnol.* **2019,** *7*, 113.

216. Fleischer, S.; Dvir, T., Tissue engineering on the nanoscale: lessons from the heart. *Curr. Opin. Biotechnol.* **2013,** *24* (4), 664-671.

217. Hasan, A.; Morshed, M.; Memic, A.; Hassan, S.; Webster, T. J.; Marei, H. E.-S., Nanoparticles in tissue engineering: Applications, challenges and prospects. *Int. J. Nanomed.* **2018,** *13*, 5637.

218. Chen, F.; Zhu, Y.; Wu, J.; Huang, P.; Cui, D., Nanostructured Calcium Phosphates: Preparation and Their Application in Biomedicine. *Nano Biomed. Eng.* **2012,** *4* (1).

219. Barba, A.; Maazouz, Y.; Diez-Escudero, A.; Rappe, K.; Espanol, M.; Montufar, E. B.; Öhman-Mägi, C.; Persson, C.; Fontecha, P.; Manzanares, M.-C., Osteogenesis by foamed and 3D-printed nanostructured calcium phosphate scaffolds: Effect of pore architecture. *Acta Biomater.* **2018,** *79*, 135-147.

220. Markstedt, K.; Mantas, A.; Tournier, I.; Martínez Ávila, H. c.; Hagg, D.; Gatenholm, P., 3D bioprinting human chondrocytes with nanocellulose–alginate bioink for cartilage tissue engineering applications. *Biomacromol.* **2015,** *16* (5), 1489-1496.

221. You, S.; Li, J.; Zhu, W.; Yu, C.; Mei, D.; Chen, S., Nanoscale 3D printing of hydrogels for cellular tissue engineering. *J. Mater. Chem. B* **2018,** *6* (15), 2187-2197.

222. LaFleur, L.; Yager, P., Medical biosensors. In *Biomaterials Science*, Elsevier: **2013**; pp 996-1006.

223. Mohanty, S. P.; Kougianos, E., Biosensors: a tutorial review. *IEEE Potent.* **2006,** *25* (2), 35-40.

224. Sireesha, M.; Jagadeesh Babu, V.; Kranthi Kiran, A. S.; Ramakrishna, S., A review on carbon nanotubes in biosensor devices and their applications in medicine. *Nanocompos.* **2018,** *4* (2), 36-57.

225. Balasubramanian, K.; Burghard, M., Biosensors based on carbon nanotubes. *Anal. Bioanal. Chem.* **2006,** *385* (3), 452-468.

226. Hofferber, E. M.; Stapleton, J. A.; Iverson, N. M., Single Walled Carbon Nanotubes as Optical Sensors for Biological Applications. *J. Electrochem. Soc.* **2020,** *167* (3), 037530.

227. Zhu, J.-J.; Li, J.-J.; Cheng, F.-F., Quantum Dot-Fluorescence-Based Biosensing. In *Quantum Dots for DNA Biosensing*, Springer: **2013**; pp 25-51.

228. Azimzadeh, M.; Rahaie, M.; Nasirizadeh, N.; Ashtari, K.; Naderi-Manesh, H., An electrochemical nanobiosensor for plasma miRNA-155, based on graphene oxide and gold nanorod, for early detection of breast cancer. *Biosens. Bioelect.* **2016,** *77*, 99-106.

229. Liu, G.; Wang, J.; Kim, J.; Jan, M. R.; Collins, G. E., Electrochemical coding for multiplexed immunoassays of proteins. *Anal. Chem.* **2004,** *76* (23), 7126-7130.

230. Qu, B.; Chu, X.; Shen, G.; Yu, R., A novel electrochemical immunosensor based on colabeled silica nanoparticles for determination of total prostate specific antigen in human serum. *Talanta* **2008,** *76* (4), 785-790.

231. Loiseau, A.; Asila, V.; Boitel-Aullen, G.; Lam, M.; Salmain, M.; Boujday, S., Silver-based plasmonic nanoparticles for and their use in biosensing. *Biosensors* **2019,** *9* (2), 78.

232. Paradise, J., Regulating Nanomedicine at the Food and Drug Administration. *AMA J. Ethics* **2019,** *21* (4), E347-355.

233. Vassey, M. J.; Figueredo, G. P.; Scurr, D. J.; Vasilevich, A. S.; Vermeulen, S.; Carlier, A.; Luckett, J.; Beijer, N. R. M.; Williams, P.; Winkler, D. A.; de Boer, J.; Ghaemmaghami, A. M.; Alexander, M. R., Immune Modulation by Design: Using Topography to Control Human Monocyte Attachment and Macrophage Differentiation. *Adv. Sci.* **2020,** *7* (11), 1903392.

234. Hulla, J.; Sahu, S.; Hayes, A., Nanotechnology: History and future. *Human & experimental toxicology* **2015,** *34* (12), 1318-1321.

235. Mobasser, S.; Firoozi, A. A., Review of nanotechnology applications in science and engineering. *J Civil Eng Urban* **2016,** *6* (4), 84-93.

236. Lu, J.; Chen, Z.; Ma, Z.; Pan, F.; Curtiss, L. A.; Amine, K., The role of nanotechnology in the development of battery materials for electric vehicles. *Nature nanotechnology* **2016,** *11* (12), 1031-1038.

237. Safari, J.; Zarnegar, Z., Advanced drug delivery systems: Nanotechnology of health design A review. *Journal of Saudi Chemical Society* **2014,** *18* (2), 85-99.

238. Sudha, P. N.; Sangeetha, K.; Vijayalakshmi, K.; Barhoum, A., Nanomaterials history, classification, unique properties, production and market. In *Emerging applications of nanoparticles and architecture nanostructures*, Elsevier: **2018**; pp 341-384.

239. Uikey, P.; Vishwakarma, K., Review of zinc oxide (ZnO) nanoparticles applications and properties. *International Journal of Emerging Technology in Computer Science & Electronics* **2016,** *21* (2), 239-242.

240. Osmond, M. J.; Mccall, M. J., Zinc oxide nanoparticles in modern sunscreens: an analysis of potential exposure and hazard. *Nanotoxicology* **2010,** *4* (1), 15-41.

241. Smijs, T. G.; Pavel, S., Titanium dioxide and zinc oxide nanoparticles in sunscreens: focus on their safety and effectiveness. *Nanotechnology, science and applications* **2011**, 95-112.

242. Newman, M. D.; Stotland, M.; Ellis, J. I., The safety of nanosized particles in titanium dioxide–and zinc oxide–based sunscreens. *Journal of the American Academy of Dermatology* **2009,** *61* (4), 685-692.

243. Tran, L.; Bañares, M. A.; Rallo, R., *Modelling the toxicity of nanoparticles*. Springer: **2017**.

244. Lewinski, N.; Colvin, V.; Drezek, R., Cytotoxicity of nanoparticles. *small* **2008,** *4* (1), 26-49.

245. Tomak, A.; Cesmeli, S.; Hanoglu, B. D.; Winkler, D.; Oksel Karakus, C., Nanoparticle-protein corona complex: understanding multiple interactions between environmental factors, corona formation, and biological activity. *Nanotoxicology* **2021,** *15* (10), 1331-1357.

246. Turan, N. B.; Erkan, H. S.; Engin, G. O.; Bilgili, M. S., Nanoparticles in the aquatic environment: Usage, properties, transformation and toxicity—A review. *Process safety and environmental protection* **2019,** *130*, 238-249.

247. Shin, S. W.; Song, I. H.; Um, S. H., Role of physicochemical properties in nanoparticle toxicity. *Nanomaterials* **2015,** *5* (3), 1351-1365.

248. Lewis, R. J. In *An introduction to classification and regression tree (CART) analysis*, Annual meeting of the society for academic emergency medicine in San Francisco, California, Citeseer: **2000**.

249. Steinberg, D., CART: classification and regression trees. In *The top ten algorithms in data mining*, Chapman and Hall/CRC: **2009**; pp 193-216.

250. Timofeev, R., Classification and regression trees (CART) theory and applications. *Humboldt University, Berlin* **2004,** *54*.

251. Sirelkhatim, A.; Mahmud, S.; Seeni, A.; Kaus, N. H. M.; Ann, L. C.; Bakhori, S. K. M.; Hasan, H.; Mohamad, D., Review on zinc oxide nanoparticles: antibacterial activity and toxicity mechanism. *Nano-micro letters* **2015,** *7*, 219-242.

252. Baek, M.; Kim, M.; Cho, H.; Lee, J.; Yu, J.; Chung, H.; Choi, S. In *Factors influencing the cytotoxicity of zinc oxide nanoparticles: particle size and surface charge*, Journal of Physics: Conference Series, IOP Publishing: **2011**; p 012044.

253. Cierech, M.; Wojnarowicz, J.; Kolenda, A.; Krawczyk-Balska, A.; Prochwicz, E.; Woźniak, B.; Łojkowski, W.; Mierzwińska-Nastalska, E., Zinc oxide nanoparticles cytotoxicity and release from newly formed PMMA–ZnO nanocomposites designed for denture bases. *Nanomaterials* **2019,** *9* (9), 1318.

254. Zhang, Y.; Nguyen, K. C.; Lefebvre, D. E.; Shwed, P. S.; Crosthwait, J.; Bondy, G. S.; Tayabali, A. F., Critical experimental parameters related to the cytotoxicity of zinc oxide nanoparticles. *Journal of nanoparticle research* **2014,** *16*, 1-13.

255. Valdiglesias, V.; Costa, C.; Kiliç, G.; Costa, S.; Pásaro, E.; Laffon, B.; Teixeira, J. P., Neuronal cytotoxicity and genotoxicity induced by zinc oxide nanoparticles. *Environment international* **2013,** *55*, 92-100.

256. Kang, T.; Guan, R.; Song, Y.; Lyu, F.; Ye, X.; Jiang, H., Cytotoxicity of zinc oxide nanoparticles and silver nanoparticles in human epithelial colorectal adenocarcinoma cells. *LWT-Food Science and Technology* **2015,** *60* (2), 1143-1148.

257. Ickrath, P.; Wagner, M.; Scherzad, A.; Gehrke, T.; Burghartz, M.; Hagen, R.; Radeloff, K.; Kleinsasser, N.; Hackenberg, S., Time-dependent toxic and genotoxic effects of zinc oxide nanoparticles after long-term and repetitive exposure to human mesenchymal stem cells. *International journal of environmental research and public health* **2017,** *14* (12), 1590.

258. Khan, M.; Naqvi, A. H.; Ahmad, M., Comparative study of the cytotoxic and genotoxic potentials of zinc oxide and titanium dioxide nanoparticles. *Toxicology Reports* **2015,** *2*, 765-774.

259. Sharma, V.; Anderson, D.; Dhawan, A., Zinc oxide nanoparticles induce oxidative stress and genotoxicity in human liver cells (HepG2). *Journal of Biomedical Nanotechnology* **2011,** *7* (1), 98-99.

260. Park, B., Current and future applications of nanotechnology. *Issues Environ. Sci. Technol* **2007,** *24*, 1-19.

261. Eigler, D. M.; Schweizer, E. K., Positioning single atoms with a scanning tunnelling microscope. *Nature* **1990,** *344* (6266), 524-526.

262. Jagaran, K.; Singh, M., Nanomedicine for neurodegenerative disorders: Focus on Alzheimer's and Parkinson's diseases. *International Journal of Molecular Sciences* **2021,** *22* (16), 9082.

263. Reidy, B.; Haase, A.; Luch, A.; Dawson, K. A.; Lynch, I., Mechanisms of silver nanoparticle release, transformation and toxicity: a critical review of current knowledge and recommendations for future studies and applications. *Materials* **2013,** *6* (6), 2295-2350.

264. Clement, J. L.; Jarrett, P. S., Antibacterial silver. *Metal-based drugs* **1994,** *1* (5-6), 467-482.

265. Martínez-Gutierrez, F.; Thi, E. P.; Silverman, J. M.; de Oliveira, C. C.; Svensson, S. L.; Hoek, A. V.; Sánchez, E. M.; Reiner, N. E.; Gaynor, E. C.; Pryzdial, E. L., Antibacterial activity, inflammatory response, coagulation and cytotoxicity effects of silver nanoparticles. *Nanomedicine: Nanotechnology, Biology and Medicine* **2012,** *8* (3), 328-336.

266. Ferdous, Z.; Nemmar, A., Health impact of silver nanoparticles: a review of the biodistribution and toxicity following various routes of exposure. *International journal of molecular sciences* **2020,** *21* (7), 2375.

267. Stensberg, M. C.; Wei, Q.; McLamore, E. S.; Porterfield, D. M.; Wei, A.; Sepúlveda, M. S., Toxicological studies on silver nanoparticles: challenges and

opportunities in assessment, monitoring and imaging. *Nanomedicine* **2011,** *6* (5), 879-898.

268. Liao, C.; Li, Y.; Tjong, S. C., Bactericidal and cytotoxic properties of silver nanoparticles. *International journal of molecular sciences* **2019,** *20* (2), 449.

269. Zhang, T.; Wang, L.; Chen, Q.; Chen, C., Cytotoxic potential of silver nanoparticles. *Yonsei medical journal* **2014,** *55* (2), 283-291.

270. Freshney, R. I., Cytotoxicity. Culture of animal cells: a manual of basic technique **2005**.

271. Mello, D. F.; Trevisan, R.; Rivera, N.; Geitner, N. K.; Di Giulio, R. T.; Wiesner, M. R.; Hsu-Kim, H.; Meyer, J. N., Caveats to the use of MTT, neutral red, Hoechst and Resazurin to measure silver nanoparticle cytotoxicity. *Chemico-biological interactions* **2020,** *315*, 108868.

272. Gu, Q.; Cuevas, E.; Ali, S. F.; Paule, M. G.; Krauthamer, V.; Jones, Y.; Zhang, Y., An alternative in vitro method for examining nanoparticle-induced cytotoxicity. *International Journal of Toxicology* **2019,** *38* (5), 385-394.

273. Oh, S.-J.; Kim, H.; Liu, Y.; Han, H.-K.; Kwon, K.; Chang, K.-H.; Park, K.; Kim, Y.; Shim, K.; An, S. S. A., Incompatibility of silver nanoparticles with lactate dehydrogenase leakage assay for cellular viability test is attributed to protein binding and reactive oxygen species generation. *Toxicology Letters* **2014,** *225* (3), 422-432.

274. Liang, L.; Cui, M.; Zhang, M.; Zheng, P.; Deng, Z.; Gao, S.; Wang, X.; Zhang, X.; Wang, C.; Liu, Y., Nanoparticles' interference in the evaluation of in vitro toxicity of silver nanoparticles. *RSC Advances* **2015,** *5* (82), 67327-67334.

275. Karakus, C. O.; Winkler, D. A., Overcoming roadblocks in computational roadmaps to the future for safe nanotechnology. *Nano Futures* **2021,** *5* (2), 022002.

276. Semenzin, E.; Subramanian, V.; Pizzol, L.; Zabeo, A.; Fransman, W.; Oksel, C.; Hristozov, D.; Marcomini, A., Controlling the risks of nano-enabled products through the life cycle: The case of nano copper oxide paint for wood protection and nano-pigments used in the automotive industry. *Environment international* **2019,** *131*, 104901.

277. Labouta, H. I.; Asgarian, N.; Rinker, K.; Cramb, D. T., Meta-analysis of nanoparticle cytotoxicity via data-mining the literature. *ACS nano* **2019,** *13* (2), 1583-1594.

278. Liu, L.; Zhang, Z.; Cao, L.; Xiong, Z.; Tang, Y.; Pan, Y., Cytotoxicity of phytosynthesized silver nanoparticles: A meta-analysis by machine learning algorithms. *Sustainable Chemistry and Pharmacy* **2021,** *21*, 100425.

279. Sharma, H.; Kumar, S., A survey on decision tree algorithms of classification in data mining. *International Journal of Science and Research (IJSR)* **2016,** *5* (4), 2094-2097.

280. Gupta, B.; Rawat, A.; Jain, A.; Arora, A.; Dhami, N., Analysis of various decision tree algorithms for classification in data mining. *International Journal of Computer Applications* **2017,** *163* (8), 15-19.

281. Hao, J.; Ho, T. K., Machine learning made easy: a review of scikit-learn package in python programming language. *Journal of Educational and Behavioral Statistics* **2019,** *44* (3), 348-361.

282. Kramer, O.; Kramer, O., Scikit-learn. *Machine learning for evolution strategies* **2016**, 45-53.

283. Yuan, Y.; Wu, L.; Zhang, X., Gini-Impurity index analysis. *IEEE Transactions on Information Forensics and Security* **2021,** *16*, 3154-3169.

284. Wang, S.-C.; Wang, S.-C., Artificial neural network. *Interdisciplinary computing in java programming* **2003**, 81-100.

285. Jain, A. K.; Mao, J.; Mohiuddin, K. M., Artificial neural networks: A tutorial. *Computer* **1996,** *29* (3), 31-44.

286. Krogh, A., What are artificial neural networks? *Nature biotechnology* **2008,** *26* (2), 195-197.

287. Uzair, M.; Jamil, N. In *Effects of hidden layers on the efficiency of neural networks*, 2020 IEEE 23rd international multitopic conference (INMIC), IEEE: **2020**; pp 1-6.

288. Stathakis, D., How many hidden layers and nodes? *International Journal of Remote Sensing* **2009,** *30* (8), 2133-2147.

289. Richardson, J. T., Eta squared and partial eta squared as measures of effect size in educational research. *Educational research review* **2011,** *6* (2), 135-147.

290. Byrd, J.; Lipton, Z. In *What is the effect of importance weighting in deep learning?*, International conference on machine learning, PMLR: **2019**; pp 872-881.

291. Le, T. T.; Moore, J. H., treeheatr: an R package for interpretable decision tree visualizations. *Bioinformatics* **2021,** *37* (2), 282-284.

292. O'Driscoll, R.; Turicchi, J.; Hopkins, M.; Duarte, C.; Horgan, G. W.; Finlayson, G.; Stubbs, R. J., Comparison of the validity and generalizability of machine learning algorithms for the prediction of energy expenditure: validation study. *JMIR mHealth and uHealth* **2021,** *9* (8), e23938.

293. Wolpert, D. H.; Macready, W. G., No free lunch theorems for optimization. *IEEE transactions on evolutionary computation* **1997,** *1* (1), 67-82.

294. Stephens, D.; Diesing, M., A comparison of supervised classification methods for the prediction of substrate type using multibeam acoustic and legacy grain-size data. *PloS one* **2014,** *9* (4), e93950.

295. Wang, S.; Liu, S.; Zhang, J.; Che, X.; Yuan, Y.; Wang, Z.; Kong, D., A new method of diesel fuel brands identification: SMOTE oversampling combined with XGBoost ensemble learning. *Fuel* **2020,** *282*, 118848.

296. He, Z.; Armaghani, D. J.; Masoumnezhad, M.; Khandelwal, M.; Zhou, J.; Murlidhar, B. R., A combination of expert-based system and advanced decision-tree algorithms to predict air-overpressure resulting from quarry blasting. *Natural Resources Research* **2021,** *30*, 1889-1903.

297. Akhter, M. H.; Khalilullah, H.; Gupta, M.; Alfaleh, M. A.; Alhakamy, N. A.; Riadi, Y.; Md, S., Impact of protein corona on the biological identity of nanomedicine: understanding the fate of nanomaterials in the biological milieu. *Biomedicines* **2021,** *9* (10), 1496.

298. Tantra, R.; Oksel, C.; Robinson, K.; Sikora, A.; Wang, X.; Wilkins, T., A method for assessing nanomaterial dispersion quality based on principal component analysis of particle size distribution data. *Particuology* **2015,** *22*, 30-38.

299. Oberdörster, G.; Maynard, A.; Donaldson, K.; Castranova, V.; Fitzpatrick, J.; Ausman, K.; Carter, J.; Karn, B.; Kreyling, W.; Lai, D., Principles for characterizing the potential human health effects from exposure to nanomaterials: elements of a screening strategy. *Particle and fibre toxicology* **2005,** *2* (1), 1-35.

300. Kad, A.; Pundir, A.; Arya, S. K.; Puri, S.; Khatri, M., Meta-analysis of in-vitro cytotoxicity evaluation studies of zinc oxide nanoparticles: Paving way for safer innovations. *Toxicology in Vitro* **2022**, 105418.

301. Shirokii, N.; Din, Y.; Petrov, I.; Seregin, Y.; Sirotenko, S.; Razlivina, J.; Serov, N.; Vinogradov, V., Quantitative Prediction of Inorganic Nanomaterial Cellular Toxicity via Machine Learning. *Small* **2023**, 2207106.

302. Mohanraj, V.; Chen, Y., Nanoparticles-a review. *Tropical journal of pharmaceutical research* **2006,** *5* (1), 561-573.

303. Stark, W. J.; Stoessel, P. R.; Wohlleben, W.; Hafner, A., Industrial applications of nanoparticles. *Chemical Society Reviews* **2015,** *44* (16), 5793-5805.

304. Nargis, M.; Raju Ahmed, A. B. I., Emerging Nanomaterials in Drug Delivery and Therapy. *Emerging Nanomaterials and Their Impact on Society in the 21st Century* **2023,** *135*, 125-151.

305. Avasthi, A.; Caro, C.; Pozo-Torres, E.; Leal, M. P.; García-Martín, M. L., Magnetic nanoparticles as MRI contrast agents. *Surface-modified Nanobiomaterials for Electrochemical and Biomedicine Applications* **2020**, 49-91.

306. Saeedi, M.; Eslamifar, M.; Khezri, K.; Dizaj, S. M., Applications of nanotechnology in drug delivery to the central nervous system. *Biomedicine & pharmacotherapy* **2019,** *111*, 666-675.

307. Raj, S.; Khurana, S.; Choudhari, R.; Kesari, K. K.; Kamal, M. A.; Garg, N.; Ruokolainen, J.; Das, B. C.; Kumar, D. In *Specific targeting cancer cells with*

nanoparticles and drug delivery in cancer therapy, Seminars in cancer biology, Elsevier: **2021**; pp 166-177.

308. Hazis, N. U. A.; Aneja, N.; Rajabalaya, R.; David, S. R., Systematic patent review of nanoparticles in drug delivery and cancer therapy in the last decade. *Recent Advances in Drug Delivery and Formulation* **2021,** *15* (1), 59.

309. Sibuyi, N. R. S.; Moabelo, K. L.; Fadaka, A. O.; Meyer, S.; Onani, M. O.; Madiehe, A. M.; Meyer, M., Multifunctional gold nanoparticles for improved diagnostic and therapeutic applications: a review. *Nanoscale Research Letters* **2021,** *16*, 1-27.

310. Hammami, I.; Alabdallah, N. M., Gold nanoparticles: Synthesis properties and applications. *Journal of king Saud university-science* **2021,** *33* (7), 101560.

311. Patil, T.; Gambhir, R.; Vibhute, A.; Tiwari, A. P., Gold nanoparticles: Synthesis methods, functionalization and biological applications. *Journal of Cluster Science* **2023,** *34* (2), 705-725.

312. Hu, X.; Zhang, Y.; Ding, T.; Liu, J.; Zhao, H., Multifunctional gold nanoparticles: a novel nanomaterial for various medical applications and biological activities. *Frontiers in Bioengineering and Biotechnology* **2020,** *8*, 990.

313. Zhao, P.; Li, N.; Astruc, D., State of the art in gold nanoparticle synthesis. *Coordination Chemistry Reviews* **2013,** *257* (3-4), 638-665.

314. Amendola, V.; Pilot, R.; Frasconi, M.; Maragò, O. M.; Iatì, M. A., Surface plasmon resonance in gold nanoparticles: a review. *Journal of Physics: Condensed Matter* **2017,** *29* (20), 203002.

315. Vines, J. B.; Yoon, J.-H.; Ryu, N.-E.; Lim, D.-J.; Park, H., Gold nanoparticles for photothermal cancer therapy. *Frontiers in chemistry* **2019,** *7*, 167.

316. Daraee, H.; Eatemadi, A.; Abbasi, E.; Fekri Aval, S.; Kouhi, M.; Akbarzadeh, A., Application of gold nanoparticles in biomedical and drug delivery. *Artificial cells, nanomedicine, and biotechnology* **2016,** *44* (1), 410-422.

317. Arvizo, R.; Bhattacharya, R.; Mukherjee, P., Gold nanoparticles: opportunities and challenges in nanomedicine. *Expert opinion on drug delivery* **2010,** *7* (6), 753-763.

318. Han, G.; Ghosh, P.; De, M.; Rotello, V. M., Drug and gene delivery using gold nanoparticles. *Nanobiotechnology* **2007,** *3* (1), 40.

319. Chithrani, B. D.; Chan, W. C., Elucidating the mechanism of cellular uptake and removal of protein-coated gold nanoparticles of different sizes and shapes. *Nano letters* **2007,** *7* (6), 1542-1550.

320. Rothen-Rutishauser, B.; Kuhn, D. A.; Ali, Z.; Gasser, M.; Amin, F.; Parak, W. J.; Vanhecke, D.; Fink, A.; Gehr, P.; Brandenberger, C., Quantification of gold nanoparticle cell uptake under controlled biological conditions and adequate resolution. *Nanomedicine* **2014,** *9* (5), 607-621.

321. Alkilany, A. M.; Lohse, S. E.; Murphy, C. J., The gold standard: gold nanoparticle libraries to understand the nano–bio interface. *Accounts of chemical research* **2013,** *46* (3), 650-661.

322. Goodman, C. M.; McCusker, C. D.; Yilmaz, T.; Rotello, V. M., Toxicity of gold nanoparticles functionalized with cationic and anionic side chains. *Bioconjugate chemistry* **2004,** *15* (4), 897-900.

323. Karlsson, H. L.; Gustafsson, J.; Cronholm, P.; Möller, L., Size-dependent toxicity of metal oxide particles—a comparison between nano-and micrometer size. *Toxicology letters* **2009,** *188* (2), 112-118.

324. Foged, C.; Brodin, B.; Frokjaer, S.; Sundblad, A., Particle size and surface charge affect particle uptake by human dendritic cells in an in vitro model. *International journal of pharmaceutics* **2005,** *298* (2), 315-322.

325. Gong, N.; Chen, S.; Jin, S.; Zhang, J.; Wang, P. C.; Liang, X.-J., Effects of the physicochemical properties of gold nanostructures on cellular internalization. *Regenerative biomaterials* **2015,** *2* (4), 273-280.

326. Ahmad, S.; Zamry, A. A.; Tan, H.-T. T.; Wong, K. K.; Lim, J.; Mohamud, R., Targeting dendritic cells through gold nanoparticles: A review on the cellular uptake and subsequent immunological properties. *Molecular immunology* **2017,** *91*, 123-133.

327. Matczuk, M.; Ruzik, L.; Aleksenko, S. S.; Keppler, B. K.; Jarosz, M.; Timerbaev, A. R., Analytical methodology for studying cellular uptake, processing and localization of gold nanoparticles. *Analytica Chimica Acta* **2019,** *1052*, 1-9.

328. Giljohann, D. A.; Seferos, D. S.; Daniel, W. L.; Massich, M. D.; Patel, P. C.; Mirkin, C. A., Gold nanoparticles for biology and medicine. *Angewandte Chemie International Edition* **2010,** *49* (19), 3280-3294.

329. Chen, T.; He, T.; Benesty, M.; Khotilovich, V.; Tang, Y.; Cho, H.; Chen, K.; Mitchell, R.; Cano, I.; Zhou, T., Xgboost: extreme gradient boosting. *R package version 0.4-2* **2015,** *1* (4), 1-4.

330. Qi, Y., Random forest for bioinformatics. *Ensemble machine learning: Methods and applications* **2012**, 307-323.

331. Breiman, L., Bagging predictors. *Machine learning* **1996,** *24*, 123-140.

332. Bentéjac, C.; Csörgő, A.; Martínez-Muñoz, G., A comparative analysis of gradient boosting algorithms. *Artificial Intelligence Review* **2021,** *54*, 1937-1967.

333. Fan, J.; Ma, X.; Wu, L.; Zhang, F.; Yu, X.; Zeng, W., Light Gradient Boosting Machine: An efficient soft computing model for estimating daily reference evapotranspiration with local and external meteorological data. *Agricultural water management* **2019,** *225*, 105758.

334. Bakushinsky, A.; Goncharsky, A., *Ill-posed problems: theory and applications*. Springer Science & Business Media: **2012**; Vol. 301.

335. Ali, J.; Khan, R.; Ahmad, N.; Maqsood, I., Random forests and decision trees. *International Journal of Computer Science Issues (IJCSI)* **2012,** *9* (5), 272.

336. Zhang, L.; Liu, Q.; Yang, W.; Wei, N.; Dong, D., An improved k-nearest neighbor model for short-term traffic flow prediction. *Procedia-Social and Behavioral Sciences* **2013,** *96*, 653-662.

337. Burden, F. R.; Winkler, D. A., Relevance vector machines: sparse classification methods for QSAR. *Journal of chemical information and modeling* **2015,** *55* (8), 1529-1534.

338. Shrestha, D. L.; Solomatine, D. P., Experiments with AdaBoost. RT, an improved boosting scheme for regression. *Neural computation* **2006,** *18* (7), 1678-1710.

339. Assaf, A. G.; Tsionas, M.; Tasiopoulos, A., Diagnosing and correcting the effects of multicollinearity: Bayesian implications of ridge regression. *Tourism Management* **2019,** *71*, 1-8.

340. Duzan, H.; Shariff, N. S. B. M., Ridge regression for solving the multicollinearity problem: review of methods and models. *Journal of Applied Science* **2015**.

341. Jain, P.; Kakade, S. M.; Kidambi, R.; Netrapalli, P.; Sidford, A. In *Accelerating stochastic gradient descent for least squares regression*, Conference On Learning Theory, PMLR: **2018**; pp 545-604.

342. Dang, X.; Peng, H.; Wang, X.; Zhang, H., Theil-sen estimators in a multiple linear regression model. *Olemiss Edu* **2008**.

343. Wang, X.; Yu, Q., Unbiasedness of the Theil–Sen estimator. *Nonparametric Statistics* **2005,** *17* (6), 685-695.

344. Nakagawa, S.; Johnson, P. C.; Schielzeth, H., The coefficient of determination R 2 and intra-class correlation coefficient from generalized linear mixed-effects models revisited and expanded. *Journal of the Royal Society Interface* **2017,** *14* (134), 20170213.

345. Li, T.; Wang, Y.; Wang, M.; Zheng, L.; Dai, W.; Jiao, C.; Song, Z.; Ma, Y.; Ding, Y.; Zhang, Z., Impact of albumin pre-coating on gold nanoparticles uptake at single-cell level. *Nanomaterials* **2022,** *12* (5), 749.

346. Bromma, K.; Bannister, A.; Kowalewski, A.; Cicon, L.; Chithrani, D. B., Elucidating the fate of nanoparticles among key cell components of the tumor microenvironment for promoting cancer nanotechnology. *Cancer Nanotechnology* **2020,** *11* (1), 1-16.

347. Alexander, D.; Tropsha, A.; Winkler, D., Beware of R2: correct statistical usage in QSAR and QSPR studies. *J. Chem. Inf. Model.* **2015,** *55*, 1316-1322.

348. Willmott, C. J., On the validation of models. *Physical geography* **1981,** *2* (2), 184-194.

349. Marquis, B. J.; Maurer-Jones, M. A.; Braun, K. L.; Haynes, C. L., Amperometric assessment of functional changes in nanoparticle-exposed immune cells: varying Au nanoparticle exposure time and concentration. *Analyst* **2009,** *134* (11), 2293-2300.

350. Ryan, J. A.; Overton, K. W.; Speight, M. E.; Oldenburg, C. N.; Loo, L.; Robarge, W.; Franzen, S.; Feldheim, D. L., Cellular uptake of gold nanoparticles passivated with BSA− SV40 large T antigen conjugates. *Analytical chemistry* **2007,** *79* (23), 9150-9159.

351. Jewell, C. M.; Jung, J. M.; Atukorale, P. U.; Carney, R. P.; Stellacci, F.; Irvine, D. J., Oligonucleotide Delivery by Cell-Penetrating "Striped" Nanoparticles. *Angewandte Chemie* **2011,** *123* (51), 12520-12523.

352. Jiang, Y.; Huo, S.; Mizuhara, T.; Das, R.; Lee, Y.-W.; Hou, S.; Moyano, D. F.; Duncan, B.; Liang, X.-J.; Rotello, V. M., The interplay of size and surface functionality on the cellular uptake of sub-10 nm gold nanoparticles. *ACS nano* **2015,** *9* (10), 9986-9993.

353. Donahue, N. D.; Acar, H.; Wilhelm, S., Concepts of nanoparticle cellular uptake, intracellular trafficking, and kinetics in nanomedicine. *Advanced drug delivery reviews* **2019,** *143*, 68-96.

354. Hunter, R. J., Zeta potential in colloid science: principles and applications. Academic press: **2013**; Vol. 2.

355. Chertok, B.; David, A. E.; Yang, V. C., Polyethyleneimine-modified iron oxide nanoparticles for brain tumor drug delivery using magnetic targeting and intra-carotid administration. *Biomaterials* **2010,** *31* (24), 6317-6324.

356. Vigderman, L.; Manna, P.; Zubarev, E. R., Quantitative replacement of cetyl trimethylammonium bromide by cationic thiol ligands on the surface of gold nanorods and their extremely large uptake by cancer cells. *Angewandte Chemie* **2012,** *124* (3), 660-665.

357. Ayala, V.; Herrera, A. P.; Latorre-Esteves, M.; Torres-Lugo, M.; Rinaldi, C., Effect of surface charge on the colloidal stability and in vitro uptake of carboxymethyl dextran-coated iron oxide nanoparticles. *Journal of nanoparticle research* **2013,** *15* (8), 1874.

358. Xie, Y.; Qiao, H.; Su, Z.; Chen, M.; Ping, Q.; Sun, M., PEGylated carboxymethyl chitosan/calcium phosphate hybrid anionic nanoparticles mediated hTERT siRNA delivery for anticancer therapy. *Biomaterials* **2014,** *35* (27), 7978-7991.

359. Schaeublin, N. M.; Braydich-Stolle, L. K.; Maurer, E. I.; Park, K.; MacCuspie, R. I.; Afrooz, A. N.; Vaia, R. A.; Saleh, N. B.; Hussain, S. M., Does shape matter? Bioeffects of gold nanomaterials in a human skin cell model. *Langmuir* **2012,** *28* (6), 3248-3258.

360. Arnida; Malugin, A.; Ghandehari, H., Cellular uptake and toxicity of gold nanoparticles in prostate cancer cells: a comparative study of rods and spheres. *Journal of Applied Toxicology: An International Journal* **2010,** *30* (3), 212-217.

361. Zhang, L.; Su, H.; Wang, H.; Li, Q.; Li, X.; Zhou, C.; Xu, J.; Chai, Y.; Liang, X.; Xiong, L., Tumor chemo-radiotherapy with rod-shaped and spherical gold nano probes: shape and active targeting both matter. *Theranostics* **2019,** *9* (7), 1893.

362. Chithrani, D. B.; Jelveh, S.; Jalali, F.; Van Prooijen, M.; Allen, C.; Bristow, R. G.; Hill, R. P.; Jaffray, D. A., Gold nanoparticles as radiation sensitizers in cancer therapy. *Radiation research* **2010,** *173* (6), 719-728.

363. Chithrani, B. D.; Ghazani, A. A.; Chan, W. C., Determining the size and shape dependence of gold nanoparticle uptake into mammalian cells. *Nano letters* **2006,** *6* (4), 662-668.

364. Zhang, X.-D.; Wu, D.; Shen, X.; Chen, J.; Sun, Y.-M.; Liu, P.-X.; Liang, X.-J., Size-dependent radiosensitization of PEG-coated gold nanoparticles for cancer radiation therapy. *Biomaterials* **2012,** *33* (27), 6408-6419.

365. Behzadi, S.; Serpooshan, V.; Tao, W.; Hamaly, M. A.; Alkawareek, M. Y.; Dreaden, E. C.; Brown, D.; Alkilany, A. M.; Farokhzad, O. C.; Mahmoudi, M., Cellular uptake of nanoparticles: journey inside the cell. *Chemical society reviews* **2017,** *46* (14), 4218-4244.

366. Fourches, D.; Pu, D.; Tassa, C.; Weissleder, R.; Shaw, S. Y.; Mumper, R. J.; Tropsha, A., Quantitative nanostructure− activity relationship modeling. *ACS nano* **2010,** *4* (10), 5703-5712.

367. Alafeef, M.; Srivastava, I.; Pan, D., Machine learning for precision breast cancer diagnosis and prediction of the nanoparticle cellular internalization. *ACS sensors* **2020,** *5* (6), 1689-1698.

368. Ali, R.; Balamurali, M.; Varamini, P., Deep Learning-Based Artificial Intelligence to Investigate Targeted Nanoparticles' Uptake in TNBC Cells. *International Journal of Molecular Sciences* **2022,** *23* (24), 16070.

369. Faraday, M., X. The Bakerian Lecture.—Experimental relations of gold (and other metals) to light. *Philosophical transactions of the Royal Society of London* **1857,** (147), 145-181.

370. Kroto, H. W.; Heath, J. R.; O'Brien, S. C.; Curl, R. F.; Smalley, R. E., C60: Buckminsterfullerene. *nature* **1985,** *318* (6042), 162-163.

371. Feynman, R., There's plenty of room at the bottom. In *Feynman and computation*, CRC Press: **2018**; pp 63-76.

372. Augustine, R.; Hasan, A.; Primavera, R.; Wilson, R. J.; Thakor, A. S.; Kevadiya, B. D., Cellular uptake and retention of nanoparticles: Insights on particle properties and interaction with cellular components. *Materials Today Communications* **2020,** *25*, 101692.

373. Findlay, M. R.; Freitas, D. N.; Mobed-Miremadi, M.; Wheeler, K. E., Machine learning provides predictive analysis into silver nanoparticle protein corona formation from physicochemical properties. *Environmental Science: Nano* **2018,** *5* (1), 64-71.

374. Duan, Y.; Coreas, R.; Liu, Y.; Bitounis, D.; Zhang, Z.; Parviz, D.; Strano, M.; Demokritou, P.; Zhong, W., Prediction of protein corona on nanomaterials by machine learning using novel descriptors. *NanoImpact* **2020,** *17*, 100207.

375. Ban, Z.; Yuan, P.; Yu, F.; Peng, T.; Zhou, Q.; Hu, X., Machine learning predicts the functional composition of the protein corona and the cellular recognition of nanoparticles. *Proceedings of the National Academy of Sciences* **2020,** *117* (19), 10492-10499.

376. Movahedi, M.; Zare-Mirakabad, F.; Ramazani, A.; Konduru, N.; Arab, S. S. In *Computational Analysis of Nanoparticle Features on Protein Corona Composition in Biological Nanoparticle-Protein Interactions*, 5th Conference on Knowledge Based Engineering and Innovation (KBEI), IEEE: **2019**; pp 776-781.

377. Toropov, A. A.; Toropova, A. P., Quasi-SMILES and nano-QFAR: United model for mutagenicity of fullerene and MWCNT under different conditions. *Chemosphere* **2015,** *139*, 18-22.

378. Lynch, I.; Afantitis, A.; Exner, T.; Himly, M.; Lobaskin, V.; Doganis, P.; Maier, D.; Sanabria, N.; Papadiamantis, A. G.; Rybinska-Fryca, A., Can an InChI for nano address the need for a simplified representation of complex nanomaterials across experimental and nanoinformatics studies? *Nanomaterials* **2020,** *10* (12), 2493.

APPENDICES

FUNDAMENTAL CODES THROUGHOUT THE THESIS

Importing Libraries

```
!pip install dtreeviz #For decision tree visualization
import dtreeviz
import sys
import os
import dtreeviz.trees
import pandas as pd
import numpy as np
import pandas as pd
import matplotlib.pyplot as plt
```

The Packages Below Are Used For Decision Trees

```
from sklearn.tree import DecisionTreeClassifier
from sklearn.model_selection import train_test_split
from sklearn import metrics
from sklearn.tree import DecisionTreeClassifier
from sklearn.metrics import accuracy_score
from sklearn import tree
from sklearn.utils import shuffle
from sklearn.model_selection import train_test_split
from sklearn.metrics import (
    confusion_matrix,
    accuracy_score,
    precision_score,
    recall_score,
```

```
    f1_score
)
from sklearn.utils import shuffle
```

The Packages Below Are Used For Classifiers Other Than Decision Trees.

```
from sklearn.linear_model import LogisticRegression
from sklearn.naive_bayes import GaussianNB
from sklearn.neighbors import KNeighborsClassifier
from sklearn.ensemble import RandomForestClassifier
from sklearn.metrics import accuracy_score, precision_score, recall_score, f1_score
from sklearn.model_selection import train_test_split
```

To Read and Assign Dataset to a Dataframe

```
df = pd.read_csv('/path_of_your_dataset/dataset_name.csv',sep=',',decimal='.')
```

To see column names

```
df.columns
```

To see dataframe's head and tail

```
df
```

To assign a new dataframe that only contains the requested columns, use the following code

```
df2=df[['column_name1','column_name2','column_name3','column_name4','column_na
me7',]]
```

```
        #In this thesis, the bioactivity threshold value is determined as 50.
```

```
        #Therefore, those with cytotoxicity values of 50 or less are labeled as toxic,
        #and those above 50 are labeled as non-toxic. By updating the following code
        #according to your own threshold values, you can add these categories to a new
column.

        #For example, you can consider the values between 90% and 110% as non-toxic,
        #above 110% as proliferative, and between 50% and 90% as intermediate toxicity.
        #You can add these values to a list called "bioactivity_threshold" and
        #then append it to the "toxicology_class" column.

#numeric_column_name is Cell_viability for our raw dataset
bioactivity_threshold = []
for i in df2.numeric_column_name:
  if float(i) >= 90 and float(i)<= 110:
    bioactivity_threshold.append("nontoxic")
  if float(i)>50 and float(i)<90:
    bioactivity_threshold.append('nontoxic')
  elif float(i) <= 50:
    bioactivity_threshold.append("toxic")
  elif float(i)>110:
    bioactivity_threshold.append("nontoxic")
bioactivity_class = pd.Series(bioactivity_threshold, name='toxicology_class')
df3 = pd.concat([df2, bioactivity_class], axis=1)
df4=df3[df3.toxicology_class.notna()]
df5=df4[df4.Cell_viability.notna()]
df5

        #Since categorical and binary data are more useful for classification algorithms,
        #we can create a new column called 'toxicology_category' using the data in the
        #'toxicology_class' column we previously created and
        #add it to a new dataframe called df6 using the following code:

class_cat = []
for i in df5.toxicology_class:
```

```
  if i=='toxic':
    class_cat.append("0")
  if i=='nontoxic':
    class_cat.append("1")

class_category = pd.Series(class_cat, name='toxicology_category')
df6 = pd.concat([df5, class_category], axis=1)
df6

#As an alternative, you can use this code

df6 = pd.get_dummies(df5, drop_first=True) # to create categorical versions of all columns including toxicology_class
```

To drop unwanted rows you can use the code below:

```
df5.drop(df5.loc[df5['Concentration_category']==1].index, inplace=True) #in this article concentration divided into 9 different category, not to create bias from untreated cells we preferred to drop those raws.
```

To discard NA values

```
#If you have numeric rows with NA values, you can discard them
#by writing the relevant column name in the following code.
df6 = df5[df5.colum_name.notna()]
```

Separating Target Columns

```
#Since toxicology_class_toxic will be the endpoint we used in the article, we can separate it from the dataframe and
#assign it to a different variable for later use in classification.
encoded_x = df6.drop('toxicology_class_toxic', axis=1)
encoded_y=df6['toxicology_class_toxic']
```

To see distributions in dataframe:

```
item_counts = df6["toxicology_class_toxic"].value_counts()
item_counts
```

Analyzes

```
#After completing the preparation process,
#We can start the analysis on the dataframe with the following codes

shuffled = shuffle(df6) #To shuffle the dataframe in a way that does not create bias:
feature_cols = ['Feautre_column1','Feature_column2', 'Feature_column3', 'Feature_column4']
X = shuffled[feature_cols] # Features

y = shuffled.toxicology_class_toxic # Target variable
X_train, X_test, y_train, y_test = train_test_split(X, y, test_size=0.3, random_state = 12345, stratify = y)
        # 70% training and 30% test,
        #stratify=y ensures that the target binary variable (such as toxic=0, non-toxic=1) is distributed
        #in the test and train sets in the same proportion as it is distributed
        #throughout the entire dataframestratify=y ensures random split of data
```

To create Decision Tree classifier object

```
clf = DecisionTreeClassifier(max_depth=5, min_samples_leaf=15) #you can change the depth and leaf number
```

Train Decision Tree Classifer

```
clf = clf.fit(X_train,y_train)
```

```
y_pred = clf.predict(X_test)
print("Accuracy:",metrics.accuracy_score(y_test, y_pred))
```

To get metrics

```
precision = precision_score(y_test, y_pred)
recall = recall_score(y_test, y_pred)
f1score = f1_score(y_test, y_pred)
accuracy = accuracy_score(y_test, y_pred)
print('Precision: ',precision)
print('Recall: ', recall)
print('f1score: ', f1score)

shuffled.to_csv('<path_to_computer>/shuffled_dataset.csv')
```

Visualization

```
#TO CREATE PLOT THAT SHOWS FEATURE IMPORTANCE WITH VALUES
```

Create plot

```
fig, ax = plt.subplots()
```

Create plot title

```
ax.set_title("Feature Importance")
```

Add bars

```
bars = ax.bar(range(X.shape[1]), importances[indices])
```

Add feature names as x-axis labels

```
ax.set_xticks(range(X.shape[1]))
ax.set_xticklabels(names, rotation=90
```

Show values on bar

```
for bar in bars:
    height = bar.get_height()
    ax.text(bar.get_x() + bar.get_width() / 2, height, round(height, 2), ha="center", va="bottom")
```

Save Plots

```
plt.savefig('featureDT1_valued.svg', format='svg')
```

See plot

```
plt.show()
```

Parameter Check

```
#To see whether the included feature used in the model use the code below
```

Define the feature columns and target variable

```
feature_cols = ['Feature1', 'Feature2', 'Feature3', 'Feature4']
X = shuffled[feature_cols]
y = shuffled['target_variable']
```

Split the dataset into training and testing sets

```
X_train, X_test, y_train, y_test = train_test_split(X, y, test_size=0.3, random_state=12345, stratify=y)
```

Train the decision tree classifier

```
clf = DecisionTreeClassifier(max_depth=5, min_samples_leaf=15, random_state=0)
clf.fit(X_train, y_train)
```

Get the features used in the decision tree

```
used_features = set()
for feature, threshold, _, _ in zip(clf.tree_.feature, clf.tree_.threshold, clf.tree_.children_left, clf.tree_.children_right):
    if feature >= 0:
        used_features.add(feature_cols[feature])

print("Features used in the decision tree:")
print(used_features)
```

To get area under curves for different classifier

Instantiate the classifiers and make a list

```
classifiers = [LogisticRegression(random_state=1234),
               GaussianNB(),
               KNeighborsClassifier(),
               DecisionTreeClassifier(random_state=1234),
               RandomForestClassifier(random_state=1234)]
```

Define a result table as a DataFrame

```
result_table = pd.DataFrame(columns=['classifiers', 'fpr','tpr','auc'])
```

Train the models and record the results

```
for cls in classifiers:
    model = cls.fit(X_train, y_train)
    yproba = model.predict_proba(X_test)[::,1]

    fpr, tpr, _ = roc_curve(y_test,  yproba)
    auc = roc_auc_score(y_test, yproba)

    result_table = result_table.append({'classifiers':cls.__class__.__name__,
                                        'fpr':fpr,
                                        'tpr':tpr,
                                        'auc':auc}, ignore_index=True)
```

Set name of the classifiers as index labels

```
result_table.set_index('classifiers', inplace=True)
```

To visualize the ROC curve

```
fig = plt.figure(figsize=(8,6))

for i in result_table.index:
    plt.plot(result_table.loc[i]['fpr'],
             result_table.loc[i]['tpr'],
             label="{}, AUC={:.3f}".format(i, result_table.loc[i]['auc']))

plt.plot([0,1], [0,1], color='orange', linestyle='--')
```

```
plt.xticks(np.arange(0.0, 1.1, step=0.1))
plt.xlabel("Flase Positive Rate", fontsize=15)

plt.yticks(np.arange(0.0, 1.1, step=0.1))
plt.ylabel("True Positive Rate", fontsize=15)

plt.title('ROC Curve Analysis', fontweight='bold', fontsize=15)
plt.legend(prop={'size':13}, loc='lower right')

plt.savefig('roc_curve.svg', format='svg')
plt.show()
```

To compare classifiers

Define feature columns and target variable

```
feature_cols = ['Feature1', 'Feature2', 'Feature3', 'Feature4']
target_col = 'target_variable'
```

Split data into training and test sets

```
X_train, X_test, y_train, y_test = train_test_split(X, y, test_size=0.3, random_state=12345, stratify=y)
```

Define models

```
models = [
    ('Logistic Regression', LogisticRegression()),
    ('Gaussian Naive Bayes', GaussianNB()),
    ('K-Nearest Neighbors', KNeighborsClassifier()),
    ('Random Forest', RandomForestClassifier()),
    ("Decision Tree", DecisionTreeClassifier(max_depth=5, min_samples_leaf=15))
]
```

Evaluate models

```
results = []
for name, model in models:
    model.fit(X_train, y_train)
    y_pred = model.predict(X_test)
    accuracy = round(accuracy_score(y_test, y_pred), 2)
    precision = round(precision_score(y_test, y_pred), 2)
    recall = round(recall_score(y_test, y_pred), 2)
    f1score = round(f1_score(y_test, y_pred), 2)
    results.append((name, accuracy, precision, recall, f1score))
```

Convert results to dataframe

```
results_df = pd.DataFrame(results, columns=['Model', 'Accuracy', 'Precision', 'Recall', 'F1 Score'])
```

Display results as table

```
print(results_df)
```

Save table as image

```
fig, ax = plt.subplots(figsize=(10, 5))
ax.axis('off')
ax.axis('tight')
ax.table(cellText=results_df.values,colLabels=results_df.columns, loc='center')
plt.savefig('path_to_computer/Comparison.svg', dpi=900, bbox_inches='tight')
```

To visualize decision tree

```
%config InlineBackend.figure_format = 'retina' # Make visualizations look good
%config InlineBackend.figure_format = 'svg'
```

```
%matplotlib inline

if 'google.colab' in sys.modules:
  !pip install -q dtreeviz
import pandas as pd
from sklearn.tree import DecisionTreeClassifier, DecisionTreeRegressor

import dtreeviz
dataset=shuffled
random_state = 12345
stratify=y # get reproducible trees
features = ['Concentration','Size_nm', 'Exposure_time_h', 'Coat_categorical']
target = "toxicology_class_toxic"

tree_classifier = DecisionTreeClassifier(max_depth=4, random_state=random_state)
tree_classifier.fit(dataset[features].values, dataset[target].values)
viz_model = dtreeviz.model(tree_classifier,
                    X_train=dataset[features], y_train=dataset[target],
                    feature_names=features,
                    target_name=target,class_names=["nontoxic", "toxic"])
viz_model.rtree_feature_space3D
viz_model.view(fancy=True)
#viz_model.view(fancy=False) #you can activate if you want a more detailed visualization

v = viz_model.view()     # render as SVG into internal object
v.show()                 # pop up window
v.save("/path_to_your_computer/decisiontree.svg")  # optionally save as svg
```

BPNN – ANN

The snippet below consists back propagation neural networ with sigmoid activation function with 2-3 neurons and linear output activation function. You can also

use this code the compare different activation functions namely 'relu', 'tanh', 'sigmoid', 'linear', 'elu', 'leaky_relu' and graph the best results of each run with defined regression metrics.

Importing necessary libraries

```
import pandas as pd
import numpy as np
import time
import matplotlib.pyplot as plt
import tensorflow as tf
from sklearn.preprocessing import StandardScaler, LabelEncoder
from sklearn.model_selection import train_test_split
from sklearn.metrics import r2_score
from tensorflow.keras.models import Sequential
from tensorflow.keras.layers import Dense, Dropout, LeakyReLU,
Activation
from tensorflow.keras.optimizers import Adam
from tensorflow.keras.callbacks import EarlyStopping,
LearningRateScheduler, Callback
```

Main Code

```
print("..............Reading the Dataset and Dataset Pre-
Processing ..............")
start_time = time.time()
```

Loading the dataset

```
# Adjust your path accordingly
data = pd.read_csv('path_to_your_data')
```

Transforming the target variable by applying a logarithmic function to make the distribution more symmetric.

```
data['Target_log'] = np.log(data['Target'] + 1)
```

Data preparation by dropping irrelevant columns

```
X = data.drop(columns=['List_of_columns_to_drop'])
y = data['Target_log']  # Specifying the target variable
```

Encoding categorical variables

```
for col in X.select_dtypes(include='object').columns:
    le = LabelEncoder()
    X[col] = le.fit_transform(X[col])
```

Train-test split

```
X_train, X_test, y_train, y_test = train_test_split(X, y,
test_size=0.3, random_state=42)
```

Scaling

```
scaler = StandardScaler()
X_train = scaler.fit_transform(X_train)
X_test = scaler.transform(X_test)

y_train = y_train.values.reshape(-1, 1)
y_test = y_test.values.reshape(-1, 1)

end_time = time.time()
total_time = end_time - start_time
print("Time Cost for Pre-processing and Reading the Dataset: %f
seconds \n " % total_time)
```

BPNN Model

```
def build_bpnn_model(input_dim):
```

```
    model = Sequential()
    model.add(Dense(128, activation=activation_function,
input_dim=input_dim))  # Input layer
    model.add(Dense(3, activation='sigmoid'))  # Hidden layer with
2-3 neurons and sigmoid activation
    model.add(Dense(1, activation='linear'))  # Output layer with
linear activation
    model.compile(optimizer=Adam(learning_rate=0.001),
loss='mean_squared_error', metrics=['mae'])
    return model
class R2Callback(Callback):
    def __init__(self, train_data, validation_data):
        super(R2Callback, self).__init__()
        self.train_data = train_data
        self.validation_data = validation_data
        self.train_r2s = []
        self.validation_r2s = []

    def on_epoch_end(self, epoch, logs=None):
        y_train_pred = self.model.predict(self.train_data[0])
        train_r2 = r2_score(self.train_data[1], y_train_pred)
        self.train_r2s.append(train_r2)
        y_val_pred = self.model.predict(self.validation_data[0])
        val_r2 = r2_score(self.validation_data[1], y_val_pred)
        self.validation_r2s.append(val_r2)
        print(f" - train_r2: {train_r2:.4f} - val_r2:
{val_r2:.4f}")

activation_functions = ['relu', 'tanh', 'sigmoid', 'linear', 'elu',
'leaky_relu']
histories = {}
r2_callbacks = {}
results = []

for activation_function in activation_functions:
    print(f"Training BPNN model with {activation_function}
activation function")
    ann_model = build_ann_model(x_train.shape[1],
activation_function)
```

```
    early_stop = EarlyStopping(monitor='val_loss', patience=10)
    r2_callback = R2Callback(train_data=(x_train, y_train),
validation_data=(x_test, y_test))
    history = ann_model.fit(x_train, y_train, epochs=100,
batch_size=32, validation_data=(x_test, y_test),
callbacks=[early_stop, r2_callback], verbose=1)
    histories[activation_function] = history
    r2_callbacks[activation_function] = r2_callback
    results.append({
        'Model': f'BPNN_{activation_function}',
        'Final Train Loss': history.history['loss'][-1],
        'Final Validation Loss': history.history['val_loss'][-1],
        'Final Train MAE': history.history['mae'][-1],
        'Final Validation MAE': history.history['val_mae'][-1],
        'Final Train R²': r2_callback.train_r2s[-1],
        'Final Validation R²': r2_callback.validation_r2s[-1]
    })
```

Visualization

```
plt.figure(figsize=(20, 15))

for i, activation_function in enumerate(activation_functions):
    plt.subplot(3, len(activation_functions), i + 1)
    plt.plot(histories[activation_function].history['loss'],
label='Train Loss')
    plt.plot(histories[activation_function].history['val_loss'],
label='Validation Loss')
    plt.title(f'{activation_function} Loss')
    plt.xlabel('Epoch')
    plt.ylabel('Loss')
    plt.legend()

    plt.subplot(3, len(activation_functions), i + 1 +
len(activation_functions))
    plt.plot(histories[activation_function].history['mae'],
label='Train MAE')
    plt.plot(histories[activation_function].history['val_mae'],
label='Validation MAE')
```

```
    plt.title(f'{activation_function} MAE')
    plt.xlabel('Epoch')
    plt.ylabel('MAE')
    plt.legend()

    plt.subplot(3, len(activation_functions), i + 1 + 2 *
len(activation_functions))
    plt.plot(r2_callbacks[activation_function].train_r2s,
label='Train R²')
    plt.plot(r2_callbacks[activation_function].validation_r2s,
label='Validation R²')
    plt.title(f'{activation_function} R²')
    plt.xlabel('Epoch')
    plt.ylabel('R²')
    plt.legend()

plt.tight_layout()
plt.show()

results_df = pd.DataFrame(results)
print("Tabulated Results: ")
print(results_df)
```

Instead of running a BPNN algorithm in which some layer informations already defined, you can run the below ANN code to search the best hperparameters for each activation functions. If your local machine is struggleing to run the code because the intense computation needed, use the example code which is revised for the tanh activation algorithm. You can use that code for other activation functions too by changing the name of the activaiton functions.

```
class R2Callback(Callback):
    def __init__(self, train_data, validation_data):
        super(R2Callback, self).__init__()
        self.train_data = train_data
        self.validation_data = validation_data
        self.train_r2s = []
        self.validation_r2s = []
```

```
    def on_epoch_end(self, epoch, logs=None):
        X_train, y_train = self.train_data
        X_val, y_val = self.validation_data
        y_train_pred = self.model.predict(X_train)
        y_val_pred = self.model.predict(X_val)
        train_r2 = r2_score(y_train, y_train_pred)
        val_r2 = r2_score(y_val, y_val_pred)
        self.train_r2s.append(train_r2)
        self.validation_r2s.append(val_r2)

print(".............Reading the Dataset and Dataset Pre-
Processing .............")
start_time = time.time()
# Adjust your path accordingly
# Loading the dataset
data = pd.read_csv('path_to_your_data')

# Transforming the target variable by applying a logarithmic
function to make the distribution more symmetric
data['Target_log'] = np.log(data['Target'] + 1)

# Data preparation by dropping irrelevant columns
X = data.drop(columns=['List_of_columns_to_drop'])
y = data['Target_log']  # Specifying the target variable

# Encoding categorical variables
for col in X.select_dtypes(include='object').columns:
    le = LabelEncoder()
    X[col] = le.fit_transform(X[col])

# Train-test split
X_train, X_test, y_train, y_test = train_test_split(X, y,
test_size=0.3, random_state=42)

# Scaling
scaler = StandardScaler()
X_train = scaler.fit_transform(X_train)
X_test = scaler.transform(X_test)
```

```
def build_model(input_dim, num_hidden_layers, activation='relu',
is_leaky_relu=False):
    model = Sequential()
    model.add(Dense(128, input_dim=input_dim))
    if is_leaky_relu:
        model.add(LeakyReLU(alpha=0.01))
    else:
        model.add(Activation(activation))
    model.add(Dropout(0.2))

    for _ in range(num_hidden_layers - 1):
        model.add(Dense(64))
        if is_leaky_relu:
            model.add(LeakyReLU(alpha=0.01))
        else:
            model.add(Activation(activation))
        model.add(Dropout(0.2))

    model.add(Dense(32, activation=activation))
    model.add(Dense(1, activation='linear'))
    model.compile(optimizer=Adam(learning_rate=0.001),
loss='mean_squared_error', metrics=['mae'])
    return model

# Hyperparameters
activation_functions = ['relu', 'tanh', 'sigmoid', 'linear', 'elu',
'leaky_relu']
num_hidden_layers_list = [1, 2, 3, 4, 5]
additional_learning_rates = [0.01, 0.0001]
additional_batch_sizes = [32, 128]

early_stop = EarlyStopping(monitor='val_loss', patience=15,
restore_best_weights=True)

best_val_r2 = float('-inf')
results = []

for activation_function in activation_functions:
```

```
    for num_hidden_layers in num_hidden_layers_list:
        for batch_size in [32, 64] + additional_batch_sizes:
            for learning_rate in [0.001] +
additional_learning_rates:
                print(f"Training model with
activation_function={activation_function},
num_hidden_layers={num_hidden_layers}, batch_size={batch_size},
learning_rate={learning_rate}")

                r2_callback = R2Callback(train_data=(X_train,
y_train), validation_data=(X_test, y_test))
                lr_schedule_callback = LearningRateScheduler(lambda
epoch, lr: lr if epoch < 10 else lr * 0.9)

                is_leaky_relu = activation_function == 'leaky_relu'
                ann_model = build_model(X_train.shape[1],
num_hidden_layers, activation_function, is_leaky_relu)
                ann_model.optimizer.lr.assign(learning_rate)

                history = ann_model.fit(X_train, y_train,
epochs=100, batch_size=batch_size,
                        validation_data=(X_test, y_test),
verbose=1,
                        callbacks=[r2_callback,
lr_schedule_callback, early_stop])

                final_train_r2 = r2_callback.train_r2s[-1] if
r2_callback.train_r2s else float('-inf')
                final_val_r2 = r2_callback.validation_r2s[-1] if
r2_callback.validation_r2s else float('-inf')

                results.append({
                    'Activation Function': activation_function,
                    'Number of Hidden Layers': num_hidden_layers,
                    'Batch Size': batch_size,
                    'Learning Rate': learning_rate,
                    'Final Train Loss': history.history['loss'][-1]
if 'loss' in history.history else float('nan'),
```

```
                    'Final Validation Loss':
history.history['val_loss'][-1] if 'val_loss' in history.history
else float('nan'),
                    'Final Train MAE': history.history['mae'][-1]
if 'mae' in history.history else float('nan'),
                    'Final Validation MAE':
history.history['val_mae'][-1] if 'val_mae' in history.history else
float('nan'),
                    'Final Train R²': final_train_r2,
                    'Final Validation R²': final_val_r2
                })

results_df = pd.DataFrame(results)
print(results_df)

# Plot the best model
if best_model:
    activation_function, num_hidden_layers, history, r2_callback =
best_model
    metrics = ['loss', 'mae', 'R²']
    num_metrics = len(metrics)
    fig, axs = plt.subplots(1, num_metrics, figsize=(5 *
num_metrics, 5))

    train_metrics = [history.history['loss'],
history.history['mae'], history.history['train_r2']]
    val_metrics = [history.history['val_loss'],
history.history['val_mae'], history.history['val_r2']]

    for i, metric in enumerate(metrics):
        axs[i].plot(train_metrics[i], label=f'Train {metric}')
        axs[i].plot(val_metrics[i], label=f'Validation {metric}')

axs[i].set_title(f'{activation_function}_{num_hidden_layers}hidden
{metric}')
        axs[i].set_xlabel('Epoch')
        axs[i].set_ylabel(metric)
        axs[i].legend()
```

```
    plt.tight_layout()
    # Saving the plot in PNG format with 1000 dpi
    plt.savefig(f"{save_directory}best_model_plot.png", dpi=1000)
    # Saving the plot in TIFF format with 1000 dpi
    plt.savefig(f"{save_directory}best_model_plot.tiff", dpi=1000)
    plt.show()

save_directory
```

Individual Activation Functions, change the activation function which is "sigmoid" here to the name of the activation function you want to investigate.

```
class R2Callback(Callback):
    def __init__(self, train_data, validation_data):
        super(R2Callback, self).__init__()
        self.train_data = train_data
        self.validation_data = validation_data

    def on_epoch_end(self, epoch, logs=None):
        X_train, y_train = self.train_data
        X_val, y_val = self.validation_data
        y_train_pred = self.model.predict(X_train)
        y_val_pred = self.model.predict(X_val)
        train_r2 = r2_score(y_train, y_train_pred)
        val_r2 = r2_score(y_val, y_val_pred)
        logs['train_r2'] = train_r2
        logs['val_r2'] = val_r2

print(".............Reading the Dataset and Dataset Pre-
Processing .............")
start_time = time.time()
# Adjust your path accordingly
# Loading the dataset
data = pd.read_csv('path_to_your_data')
```

```
# Transforming the target variable by applying a logarithmic
function to make the distribution more symmetric
data['Target_log'] = np.log(data['Target'] + 1)

# Data preparation by dropping irrelevant columns
X = data.drop(columns=['List_of_columns_to_drop'])
y = data['Target_log']  # Specifying the target variable

# Encoding categorical variables
for col in X.select_dtypes(include='object').columns:
    le = LabelEncoder()
    X[col] = le.fit_transform(X[col])

# Train-test split
X_train, X_test, y_train, y_test = train_test_split(X, y,
test_size=0.3, random_state=42)

# Scaling
scaler = StandardScaler()
X_train = scaler.fit_transform(X_train)
X_test = scaler.transform(X_test)

def build_model(input_dim, num_hidden_layers,
activation='sigmoid'):
    model = Sequential()
    model.add(Dense(128, input_dim=input_dim))

    if activation == 'leaky_relu':
        model.add(LeakyReLU(alpha=0.01))
    else:
        model.add(Activation(activation))

    model.add(Dropout(0.2))

    for _ in range(num_hidden_layers - 1):
        model.add(Dense(64))

        if activation == 'leaky_relu':
            model.add(LeakyReLU(alpha=0.01))
```

```
        else:
            model.add(Activation(activation))

        model.add(Dropout(0.2))

    model.add(Dense(32, activation=activation))
    model.add(Dense(1, activation='linear'))
    model.compile(optimizer=Adam(learning_rate=0.001),
loss='mean_squared_error', metrics=['mae'])
    return model

activation_functions = ['sigmoid']
num_hidden_layers_list = [1, 2, 3, 4, 5]
additional_batch_sizes = [32, 128]
additional_learning_rates = [0.01, 0.0001]

early_stop = EarlyStopping(monitor='val_loss', patience=15,
restore_best_weights=True)
best_val_r2 = float('-inf')
best_model = None
results = []

for activation_function in activation_functions:
    for num_hidden_layers in num_hidden_layers_list:
        for batch_size in [32, 64] + additional_batch_sizes:
            for learning_rate in [0.001] +
additional_learning_rates:
                print(f"Training model with
activation_function={activation_function},
num_hidden_layers={num_hidden_layers}, batch_size={batch_size},
learning_rate={learning_rate}")

                r2_callback = R2Callback(train_data=(X_train,
y_train), validation_data=(X_test, y_test))
                lr_schedule_callback = LearningRateScheduler(lambda
epoch, lr: lr if epoch < 10 else lr * 0.9)

                ann_model = build_model(X_train.shape[1],
num_hidden_layers, activation_function)
```

```
                ann_model.optimizer.lr.assign(learning_rate)

                history = ann_model.fit(X_train, y_train,
epochs=100, batch_size=batch_size, validation_data=(X_test,
y_test), verbose=1,
                                        callbacks=[r2_callback,
lr_schedule_callback, early_stop])
                # Print metrics after the first training iteration
to verify the results.
                print("Train Loss:", history.history['loss'][0])
                print("Validation Loss:",
history.history['val_loss'][0])
                print("Train MAE:", history.history['mae'][0])
                print("Validation MAE:",
history.history['val_mae'][0])
                print("Train R²:", history.history['train_r2'][0])
                print("Validation R²:",
history.history['val_r2'][0])
                final_val_r2 = history.history['val_r2'][-1] if
'val_r2' in history.history else float('-inf')

                if final_val_r2 > best_val_r2:
                    best_val_r2 = final_val_r2
                    best_model = (activation_function,
num_hidden_layers, history, r2_callback)

                results.append({
                    'Activation Function': activation_function,
                    'Number of Hidden Layers': num_hidden_layers,
                    'Batch Size': batch_size,
                    'Learning Rate': learning_rate,
                    'Final Train Loss': history.history['loss'][-1]
if 'loss' in history.history else float('nan'),
                    'Final Validation Loss':
history.history['val_loss'][-1] if 'val_loss' in history.history
else float('nan'),
                    'Final Train MAE': history.history['mae'][-1]
if 'mae' in history.history else float('nan'),
```

```
                    'Final Validation MAE':
history.history['val_mae'][-1] if 'val_mae' in history.history else
float('nan'),
                    'Final Train R²': history.history['train_r2'][-
1] if 'train_r2' in history.history else float('nan'),
                    'Final Validation R²': final_val_r2
                })

results_df = pd.DataFrame(results)
print(results_df)

# Define a directory to save the plots
save_directory = "/saving_directory_for_plots/"


# Plot the best model
if best_model:
    activation_function, num_hidden_layers, history, r2_callback =
best_model
    metrics = ['loss', 'mae', 'R²']
    num_metrics = len(metrics)
    fig, axs = plt.subplots(1, num_metrics, figsize=(5 *
num_metrics, 5))

    train_metrics = [history.history['loss'],
history.history['mae'], history.history['train_r2']]
    val_metrics = [history.history['val_loss'],
history.history['val_mae'], history.history['val_r2']]

    for i, metric in enumerate(metrics):
        axs[i].plot(train_metrics[i], label=f'Train {metric}')
        axs[i].plot(val_metrics[i], label=f'Validation {metric}')

axs[i].set_title(f'{activation_function}_{num_hidden_layers}hidden
{metric}')
        axs[i].set_xlabel('Epoch')
        axs[i].set_ylabel(metric)
        axs[i].legend()
```

```
    plt.tight_layout()
    # Saving the plot in PNG format with 1000 dpi
    plt.savefig(f"{save_directory}best_model_plot.png", dpi=1000)
    # Saving the plot in TIFF format with 1000 dpi
    plt.savefig(f"{save_directory}best_model_plot.tiff", dpi=1000)
    plt.show()

save_directory
```

After running each code, you can save the results_df dataframe to csv file to check the results. You can also save the plots for the best results too.

```
results_df.to_csv('path_to_saving_directory/file_name.csv',
index=False)
```

Regression Future Importance and Residuals

```
!pip install catboost
!pip install pygam

import pandas as pd
import numpy as np
import warnings
from sklearn.linear_model import (HuberRegressor, RANSACRegressor,
TheilSenRegressor,
                                  OrthogonalMatchingPursuit,
PoissonRegressor,
                                  TweedieRegressor, RidgeCV, Lasso,
                                  ElasticNet, SGDRegressor,
BayesianRidge)
from sklearn.kernel_ridge import KernelRidge
from sklearn.model_selection import GridSearchCV, train_test_split
from sklearn.preprocessing import StandardScaler, LabelEncoder
from sklearn.metrics import r2_score
from sklearn.ensemble import (RandomForestRegressor,
GradientBoostingRegressor,
                              AdaBoostRegressor, BaggingRegressor,
StackingRegressor)
```

```
from sklearn.tree import DecisionTreeRegressor
from sklearn.svm import SVR
from sklearn.neighbors import KNeighborsRegressor
from sklearn.gaussian_process import GaussianProcessRegressor
from xgboost import XGBRegressor
from lightgbm import LGBMRegressor
from pygam import LinearGAM, s, f

warnings.simplefilter(action='ignore', category=Warning)

warnings.simplefilter(action='ignore', category=Warning)

# Load the dataset
data = pd.read_csv('path_to_your_file/file_name.csv')

# Log-transform the target variable
data['Cellular_Uptake_pg_Au_cell_log'] =
np.log(data['Cellular_Uptake_pg_Au_cell'] + 1)

# Data preparation, you can change the column names to adjust your
dataset
always_drop_columns = ['Row_number', 'row_number',
'Cell_source_system', 'Particle_ID', 'Coating_type',
'Coating_category', 'Coating category new','NP_mass_pg',
'Reference_DOI', 'Cellular_Uptake_pg_Au_cell_log',
'Cellular_uptake_number_of_NP', 'Cellular_Uptake_pg_Au_cell']
X = data.drop(columns=always_drop_columns + ['Coating_type',
'Coating_category', 'Coating category new'])
y = data['Cellular_Uptake_pg_Au_cell_log']

# Encoding categorical variables
for col in X.select_dtypes(include='object').columns:
    le = LabelEncoder()
    X[col] = le.fit_transform(X[col])

# Train-test split
X_train, X_test, y_train, y_test = train_test_split(X, y,
test_size=0.3, random_state=42)
```

```
# Scaling
scaler = StandardScaler()
X_train = scaler.fit_transform(X_train)
X_test = scaler.transform(X_test)

# Hyperparameters for tuning, use this part to ensure which
hyperparameters are better for that individual regressor
"""rf_params = {
    'n_estimators': [50, 100, 150],
    'max_depth': [None, 10, 20, 30],
    'min_samples_split': [2, 5, 10],
    'min_samples_leaf': [1, 2, 4]
}

xgb_params = {
    'learning_rate': [0.01, 0.05, 0.1],
    'n_estimators': [100, 150, 200],
    'max_depth': [3, 5, 7],
    'subsample': [0.8, 0.9, 1],
    'colsample_bytree': [0.8, 0.9, 1]
}

bagging_params = {
    'n_estimators': [10, 20, 30],
    'max_samples': [0.5, 0.8, 1.0],
    'max_features': [0.5, 0.8, 1.0]
}

dt_params = {
    'criterion': ['mse', 'friedman_mse', 'mae'],
    'splitter': ['best', 'random'],
    'max_depth': [None, 10, 20, 30],
    'min_samples_split': [2, 5, 10],
    'min_samples_leaf': [1, 2, 4]
}

# GridSearchCV for each model
rf_grid = GridSearchCV(RandomForestRegressor(random_state=42),
rf_params, cv=5, n_jobs=-1)
```

```
rf_grid.fit(X_train, y_train)
print("Best parameters for Random Forest:", rf_grid.best_params_)

xgb_grid = GridSearchCV(XGBRegressor(random_state=42), xgb_params,
cv=5, n_jobs=-1)
xgb_grid.fit(X_train, y_train)
print("Best parameters for XGBoost:", xgb_grid.best_params_)

bagging_grid = GridSearchCV(BaggingRegressor(random_state=42),
bagging_params, cv=5, n_jobs=-1)
bagging_grid.fit(X_train, y_train)
print("Best parameters for Bagging:", bagging_grid.best_params_)

dt_grid = GridSearchCV(DecisionTreeRegressor(random_state=42),
dt_params, cv=5, n_jobs=-1)
dt_grid.fit(X_train, y_train)
print("Best parameters for Decision Tree:",
dt_grid.best_params_)"""

# Define and train various regressors with the training data, the
hyperparameters in this code has been determined by running the
codes between the """grid search""" statements

regressors = {
    'Random Forest': RandomForestRegressor(n_estimators=100,
max_depth=None, min_samples_leaf=1, min_samples_split=2,
random_state=42),
    'Gradient Boosting':
GradientBoostingRegressor(random_state=42),
    'AdaBoost': AdaBoostRegressor(random_state=42),
    'Bagging': BaggingRegressor(n_estimators=30, max_features=1.0,
max_samples=1.0, random_state=42),
    'Decision Tree':
DecisionTreeRegressor(criterion='friedman_mse', max_depth=9,
min_samples_leaf=2, min_samples_split=2, splitter='best',
random_state=42),
    'Support Vector': SVR(),
    'K-Neighbors': KNeighborsRegressor(),
    'RidgeCV': RidgeCV(),
```

```
    'Lasso': Lasso(),
    'ElasticNet': ElasticNet(),
    'SGD': SGDRegressor(),
    'Gaussian Process': GaussianProcessRegressor(),
    'BayesianRidge': BayesianRidge(),
    'XGBoostRegressor': XGBRegressor(colsample_bytree=0.9,
learning_rate=0.1, max_depth=7, n_estimators=200, subsample=0.8,
random_state=42),
    'LightGBMRegressor': LGBMRegressor(),
    'SVR_poly': SVR(kernel='poly'),
    'SVR_sigmoid': SVR(kernel='sigmoid'),
    'SVR_rbf': SVR(kernel='rbf'),
    'HuberRegressor': HuberRegressor(),
    'RANSACRegressor': RANSACRegressor(),
    'TheilSenRegressor': TheilSenRegressor(),
    'KernelRidge': KernelRidge(),
    'OMP': OrthogonalMatchingPursuit(),
    'PoissonRegressor': PoissonRegressor(),
    'TweedieRegressor': TweedieRegressor()
}
results_log_transformed = []
for model_name, model in regressors.items():
    model.fit(X_train, y_train)
    y_train_pred = model.predict(X_train)
    y_test_pred = model.predict(X_test)
    r2_train = r2_score(y_train, y_train_pred)
    r2_test = r2_score(y_test, y_test_pred)
    results_log_transformed.append({
        'Model': model_name,
        'Train R2 Score': r2_train,
        'Test R2 Score': r2_test
    })

# Training and evaluating GAM separately
gam = LinearGAM(s(0) + s(1) + f(2)).fit(X_train, y_train)
gam_train_pred = gam.predict(X_train)
gam_test_pred = gam.predict(X_test)
results_log_transformed.append({
    'Model': 'GAM',
```

```
    'Train R2 Score': r2_score(y_train, gam_train_pred),
    'Test R2 Score': r2_score(y_test, gam_test_pred)
})
# Perform stacking using top models and append results to
results_log_transformed,

stacked_models = []

for i in [2, 3, 4]:
    # Filter out already stacked models
    top_models = sorted([r for r in results_log_transformed if
r['Model'] not in stacked_models],
                        key=lambda x: x['Test R2 Score'],
reverse=True)[:i]

    estimators = [(model['Model'], regressors[model['Model']]) for
model in top_models]

    stacking_regressor = StackingRegressor(estimators=estimators,
cv=5)
    stacking_regressor.fit(X_train, y_train)
    stacked_train_pred = stacking_regressor.predict(X_train)
    stacked_test_pred = stacking_regressor.predict(X_test)

    stacked_r2_train = r2_score(y_train, stacked_train_pred)
    stacked_r2_test = r2_score(y_test, stacked_test_pred)

    stacked_model_name = f'StackingRegressor_Top{i}'
    results_log_transformed.append({
        'Model': stacked_model_name,
        'Train R2 Score': stacked_r2_train,
        'Test R2 Score': stacked_r2_test
    })
    stacked_models.append(stacked_model_name)

results_df =
pd.DataFrame(results_log_transformed).sort_values(by='Test R2
Score', ascending=False)
print(results_df)
```

```
#by running this code snippet it is achiavable to get test and
train R^2's of both individual and stacked models.
```

Since the R^2 values of the stacked models did not improve much, only individual regressors had been chosen to plot feature importances. The selection of algorithms for visualization was made by manually sorting the R^2 values. If you want to do this through code, you can modify your snippet with the line below.

IMPORTANT NOTE: Not every algorithm may contain the feature importance attribute.

```
# Extract the names of the top-performing models
top_models = sorted(results_log_transformed, key=lambda x: x['Test
R2 Score'], reverse=True)[:4]  # Top 4 models
top_model_names = [model['Model'] for model in top_models if
model['Model'] in regressors and
hasattr(regressors[model['Model']], 'feature_importances_')]

# Define positions of bars for each model
positions = np.array(range(len(sorted_idx)))

# Plotting bars
for idx, name in enumerate(top_model_names):
    values = importances[name]
    plt.barh(positions + width*idx, values[sorted_idx],
color=colors[idx], label=name, height=width)
```

Feature Importance Visualization

```
plt.figure(figsize=(15, 12))

# Define the models you want to plot according to R^2's you got
from running the code above
models_to_plot = ['XGBoostRegressor', 'Random Forest', 'Bagging',
'Gradient Boosting', 'LightGBMRegressor']
```

```
# Colors for the models
colors = ['#5081bc', '#7298bc', '#fe70bc', '#fab8dc', '#76b4a8']

# Normalize feature importances, the scale of the feature
importances for LightGBMRegressor is different from others so
normalizing would be a good option
for name, importance_values in importances.items():
    importances[name] = importance_values /
np.sum(importance_values)

# Define positions of bars for each model
positions = np.array(range(len(sorted_idx)))

# Calculate width of a bar
width = 0.15

# Adjust the positions array to ensure bars are side-by-side
positions = positions - (width * len(models_to_plot) / 2)

# Plotting bars
for idx, name in enumerate(models_to_plot):
    values = importances[name]
    plt.barh(positions + width*idx, values[sorted_idx],
color=colors[idx], label=name, height=width, align='center')

# Updating y-ticks to be in the center of grouped bars
plt.yticks(positions + width*(len(models_to_plot) - 1)/2,
X.columns[sorted_idx])

plt.xlabel('Importance', fontsize=14)
plt.ylabel('Features', fontsize=14)
plt.title('Feature Importances\n', fontsize=16)
plt.legend(loc='best', fontsize=14)
plt.tight_layout()

# Directory to save the plot
output_directory =
"path_for_saving_the_feature_importance_bar_graphs"
```

```
# Save the plot in PNG and TIFF formats, do not forget 1000 dpi for
tiff could take large amount of space in your memory so adjust the
resolution properly
plt.savefig(f"{output_directory}/Feature_Importances_results.png",
format='png', dpi=1000)
plt.savefig(f"{output_directory}/Feature_Importances_results.tiff",
format='tiff', dpi=1000)

plt.show()
```

Residuals Visualization

```
plt.figure(figsize=(15, 12))

# Define the models you want to plot according to R^2's you got
from running the code above
models_to_plot = ['XGBoostRegressor', 'Random Forest', 'Bagging',
'Gradient Boosting', 'LightGBMRegressor']

# Colors for the models
colors = ['#5081bc', '#7298bc', '#fe70bc', '#fab8dc', '#76b4a8']

# Normalize feature importances, the scale of the feature
importances for LightGBMRegressor is different from others so
normalizing would be a good option
for name, importance_values in importances.items():
    importances[name] = importance_values /
np.sum(importance_values)

# Define positions of bars for each model
positions = np.array(range(len(sorted_idx)))

# Calculate width of a bar
width = 0.15

# Adjust the positions array to ensure bars are side-by-side
positions = positions - (width * len(models_to_plot) / 2)
```

```
# Plotting bars
for idx, name in enumerate(models_to_plot):
    values = importances[name]
    plt.barh(positions + width*idx, values[sorted_idx],
color=colors[idx], label=name, height=width, align='center')

# Updating y-ticks to be in the center of grouped bars
plt.yticks(positions + width*(len(models_to_plot) - 1)/2,
X.columns[sorted_idx])

plt.xlabel('Importance', fontsize=14)
plt.ylabel('Features', fontsize=14)
plt.title('Feature Importances\n', fontsize=16)
plt.legend(loc='best', fontsize=14)
plt.tight_layout()

# Directory to save the plot
output_directory =
"path_for_saving_the_feature_importance_bar_graphs"

# Save the plot in PNG and TIFF formats, do not forget 1000 dpi for
tiff could take large amount of space in your memory so adjust the
resolution properly
plt.savefig(f"{output_directory}/Feature_Importances_results.png",
format='png', dpi=1000)
plt.savefig(f"{output_directory}/Feature_Importances_results.tiff",
format='tiff', dpi=1000)

plt.show()
```

Regression Feature Importance with Hyper Parameters

```
!pip install catboost
!pip install pygam
```

The code snippet below is to get permutation importance graphs of both train and test sets individually for the defined models to plot. You can change the models_to_plot

variable according to your model or define a sorting criteria to choose the models to be graphed.

```
import pandas as pd  # Importing pandas library for data
manipulation and analysis
import numpy as np  # Importing numpy library for numerical
operations
import warnings  # Importing warnings to manage warnings during the
runtime
import os  # Importing os for operating system dependent
functionalities

# Importing necessary classes and functions from sklearn for model
building, preprocessing, and evaluation
from sklearn.model_selection import train_test_split
from sklearn.preprocessing import StandardScaler, LabelEncoder
from sklearn.metrics import r2_score
from sklearn.ensemble import RandomForestRegressor,
GradientBoostingRegressor, BaggingRegressor
from xgboost import XGBRegressor
from sklearn.inspection import permutation_importance
import matplotlib.pyplot as plt  # Importing matplotlib for
plotting graphs

# Loading the dataset
data = pd.read_csv('path_to_your_data')

# Transforming the target variable by applying a logarithmic
function to make the distribution more symmetric
data['Target_log'] = np.log(data['Target'] + 1)

# Data preparation by dropping irrelevant columns
X = data.drop(columns=['List_of_columns_to_drop'])
y = data['Target_log']  # Specifying the target variable

# Encoding categorical variables
for col in X.select_dtypes(include='object').columns:
```

```
    le = LabelEncoder()
    X[col] = le.fit_transform(X[col])

# Train-test split
X_train, X_test, y_train, y_test = train_test_split(X, y,
test_size=0.3, random_state=42)

# Scaling
scaler = StandardScaler()
X_train = scaler.fit_transform(X_train)
X_test = scaler.transform(X_test)

# Best parameters
rf_best_params = {'max_depth': None, 'min_samples_leaf': 1,
'min_samples_split': 2, 'n_estimators': 100}
xgb_best_params = {'colsample_bytree': 0.9, 'learning_rate': 0.1,
'max_depth': 7, 'n_estimators': 200, 'subsample': 0.8}
bagging_best_params = {'max_features': 1.0, 'max_samples': 1.0,
'n_estimators': 30}
dt_best_params = {'criterion': 'friedman_mse', 'max_depth': 9,
'min_samples_leaf': 2, 'min_samples_split': 2, 'splitter': 'best'}

# Create a dictionary of models
regressors = {
    'Random Forest': RandomForestRegressor(n_estimators=100,
max_depth=None, min_samples_leaf=1, min_samples_split=2,
random_state=42),
    'Gradient Boosting':
GradientBoostingRegressor(random_state=42),
    'AdaBoost': AdaBoostRegressor(random_state=42),
    'Bagging': BaggingRegressor(n_estimators=30, max_features=1.0,
max_samples=1.0, random_state=42),
    'Decision Tree':
DecisionTreeRegressor(criterion='friedman_mse', max_depth=9,
min_samples_leaf=2, min_samples_split=2, splitter='best',
random_state=42),
    'Support Vector': SVR(),
    'K-Neighbors': KNeighborsRegressor(),
    'RidgeCV': RidgeCV(),
```

```
    'Lasso': Lasso(),
    'ElasticNet': ElasticNet(),
    'SGD': SGDRegressor(),
    'Gaussian Process': GaussianProcessRegressor(),
    'BayesianRidge': BayesianRidge(),
    'XGBoostRegressor': XGBRegressor(colsample_bytree=0.9,
learning_rate=0.1, max_depth=7, n_estimators=200, subsample=0.8,
random_state=42),
    'LightGBMRegressor': LGBMRegressor(),
    'SVR_poly': SVR(kernel='poly'),
    'SVR_sigmoid': SVR(kernel='sigmoid'),
    'SVR_rbf': SVR(kernel='rbf'),
    'HuberRegressor': HuberRegressor(),
    'RANSACRegressor': RANSACRegressor(),
    'TheilSenRegressor': TheilSenRegressor(),
    'KernelRidge': KernelRidge(),
    'OMP': OrthogonalMatchingPursuit(),
    'PoissonRegressor': PoissonRegressor(),
    'TweedieRegressor': TweedieRegressor()
}
# Fit models and extract permutation importances
perm_importances = {}  # Initializing the dictionary
def plot_permutation_importance(model, X_train, y_train, X_test,
y_test, title='', save_path=''):
    # Compute permutation importance for training set
    result_train = permutation_importance(model, X_train, y_train,
n_repeats=10, random_state=42, n_jobs=2)
    sorted_idx_train = result_train.importances_mean.argsort()

    # Compute permutation importance for test set
    result_test = permutation_importance(model, X_test, y_test,
n_repeats=10, random_state=42, n_jobs=2)
    sorted_idx_test = result_test.importances_mean.argsort()

    # Convert the results to DataFrame for better visualization
    importances_train =
pd.DataFrame(result_train.importances[sorted_idx_train].T,
columns=X.columns[sorted_idx_train])
```

```
    importances_test =
pd.DataFrame(result_test.importances[sorted_idx_test].T,
columns=X.columns[sorted_idx_test])

    fig, ax = plt.subplots(nrows=2, ncols=1, figsize=(12, 12))

    # Plotting for training set
    importances_train.plot.box(vert=False, whis=10, ax=ax[0])
    ax[0].set_title(f"Permutation Importances (train set) -
{title}")
    ax[0].axvline(x=0, color="k", linestyle="--")
    ax[0].set_xlabel("Decrease in accuracy score")

    # Plotting for test set
    importances_test.plot.box(vert=False, whis=10, ax=ax[1])
    ax[1].set_title(f"Permutation Importances (test set) -
{title}")
    ax[1].axvline(x=0, color="k", linestyle="--")
    ax[1].set_xlabel("Decrease in accuracy score")

    plt.tight_layout()
    plt.show()
    if save_path:
        png_path = os.path.join(save_path,
f"{title}_Permutation_Importance.png")
        tiff_path = os.path.join(save_path,
f"{title}_Permutation_Importance.tiff")
#decrease the dpi if the resolution is larger than it should be
        fig.savefig(png_path, dpi=1000)
        fig.savefig(tiff_path, dpi=1000)

    plt.close(fig)  # close the figure

# Create directories if they don't exist
save_directory = "path_to_save_directory"
if not os.path.exists(save_directory):
    os.makedirs(save_directory)
    # Models to visualize
```

```
models_to_plot = ['XGBoostRegressor', 'Random Forest', 'Bagging',
'Gradient Boosting',"LightGBMRegressor"]
# Fit the models and visualize
for name in models_to_plot:
    model = regressors[name]
    model.fit(X_train, y_train)
    plot_permutation_importance(model, X_train, y_train, X_test,
y_test, title=name, save_path=save_directory)
```

To graph feature importances of which train set and test set located in one graph you can use the snippet below.

```
import pandas as pd  # Importing pandas library for data
manipulation and analysis
import numpy as np  # Importing numpy library for numerical
operations
import warnings  # Importing warnings to manage warnings during the
runtime
import os  # Importing os for operating system dependent
functionalities

# Importing necessary classes and functions from sklearn for model
building, preprocessing, and evaluation
from sklearn.model_selection import train_test_split
from sklearn.preprocessing import StandardScaler, LabelEncoder
from sklearn.metrics import r2_score
from sklearn.ensemble import RandomForestRegressor,
GradientBoostingRegressor, BaggingRegressor
from xgboost import XGBRegressor
from sklearn.inspection import permutation_importance
import matplotlib.pyplot as plt  # Importing matplotlib for
plotting graphs

# Loading the dataset
data = pd.read_csv('path_to_your_data')
```

```
# Transforming the target variable by applying a logarithmic
function to make the distribution more symmetric
data['Target_log'] = np.log(data['Target'] + 1)

# Data preparation by dropping irrelevant columns
X = data.drop(columns=['List_of_columns_to_drop'])
y = data['Target_log']  # Specifying the target variable

# Encoding categorical variables
for col in X.select_dtypes(include='object').columns:
    le = LabelEncoder()
    X[col] = le.fit_transform(X[col])

# Train-test split
X_train, X_test, y_train, y_test = train_test_split(X, y,
test_size=0.3, random_state=42)

# Scaling
scaler = StandardScaler()
X_train = scaler.fit_transform(X_train)
X_test = scaler.transform(X_test)

# Best parameters
rf_best_params = {'max_depth': None, 'min_samples_leaf': 1,
'min_samples_split': 2, 'n_estimators': 100}
xgb_best_params = {'colsample_bytree': 0.9, 'learning_rate': 0.1,
'max_depth': 7, 'n_estimators': 200, 'subsample': 0.8}
bagging_best_params = {'max_features': 1.0, 'max_samples': 1.0,
'n_estimators': 30}
dt_best_params = {'criterion': 'friedman_mse', 'max_depth': 9,
'min_samples_leaf': 2, 'min_samples_split': 2, 'splitter': 'best'}

# Create a dictionary of models
regressors = {
    'Random Forest': RandomForestRegressor(n_estimators=100,
max_depth=None, min_samples_leaf=1, min_samples_split=2,
random_state=42),
    'Gradient Boosting':
GradientBoostingRegressor(random_state=42),
```

```
    'AdaBoost': AdaBoostRegressor(random_state=42),
    'Bagging': BaggingRegressor(n_estimators=30, max_features=1.0,
max_samples=1.0, random_state=42),
    'Decision Tree':
DecisionTreeRegressor(criterion='friedman_mse', max_depth=9,
min_samples_leaf=2, min_samples_split=2, splitter='best',
random_state=42),
    'Support Vector': SVR(),
    'K-Neighbors': KNeighborsRegressor(),
    'RidgeCV': RidgeCV(),
    'Lasso': Lasso(),
    'ElasticNet': ElasticNet(),
    'SGD': SGDRegressor(),
    'Gaussian Process': GaussianProcessRegressor(),
    'BayesianRidge': BayesianRidge(),
    'XGBoostRegressor': XGBRegressor(colsample_bytree=0.9,
learning_rate=0.1, max_depth=7, n_estimators=200, subsample=0.8,
random_state=42),
    'LightGBMRegressor': LGBMRegressor(),
    'SVR_poly': SVR(kernel='poly'),
    'SVR_sigmoid': SVR(kernel='sigmoid'),
    'SVR_rbf': SVR(kernel='rbf'),
    'HuberRegressor': HuberRegressor(),
    'RANSACRegressor': RANSACRegressor(),
    'TheilSenRegressor': TheilSenRegressor(),
    'KernelRidge': KernelRidge(),
    'OMP': OrthogonalMatchingPursuit(),
    'PoissonRegressor': PoissonRegressor(),
    'TweedieRegressor': TweedieRegressor()
}
# Fit models and extract permutation importances
perm_importances = {}  # Initializing the dictionary
from matplotlib.lines import Line2D

def plot_overlapped_permutation_importance(model, X_train, y_train,
X_test, y_test, title='', save_path=''):
    # Compute permutation importance for training set
    result_train = permutation_importance(model, X_train, y_train,
n_repeats=10, random_state=42, n_jobs=2)
```

```
    sorted_idx_train = result_train.importances_mean.argsort()

    # Compute permutation importance for test set
    result_test = permutation_importance(model, X_test, y_test,
n_repeats=10, random_state=42, n_jobs=2)
    sorted_idx_test = result_test.importances_mean.argsort()

    # Convert the results to DataFrame for better visualization
    importances_train =
pd.DataFrame(result_train.importances[sorted_idx_train].T,
columns=X.columns[sorted_idx_train])
    importances_test =
pd.DataFrame(result_test.importances[sorted_idx_test].T,
columns=X.columns[sorted_idx_test])

    fig, ax = plt.subplots(figsize=(12, 12))

    # Plotting for training set
    importances_train.boxplot(ax=ax, vert=False,
positions=np.arange(len(importances_train.columns))*2.0-0.4,
widths=0.4, boxprops=dict(color='blue'),
medianprops=dict(color='blue'), whiskerprops=dict(color='blue'),
capprops=dict(color='blue'))

    # Plotting for test set
    importances_test.boxplot(ax=ax, vert=False,
positions=np.arange(len(importances_test.columns))*2.0+0.4,
widths=0.4, boxprops=dict(color='red'),
medianprops=dict(color='red'), whiskerprops=dict(color='red'),
capprops=dict(color='red'))

    # Tweaking the plot appearance
    ax.set_yticks(np.arange(len(importances_train.columns))*2.0)
    ax.set_yticklabels(importances_train.columns)
    ax.axvline(x=0, color="k", linestyle="--")
    ax.set_xlabel("Decrease in accuracy score")
    ax.set_title(f"Overlapped Permutation Importances - {title}")
    ax.grid(False)
    # Custom legend
```

```
    custom_lines = [Line2D([0], [0], color="blue", lw=4),
Line2D([0], [0], color="red", lw=4)]
    ax.legend(custom_lines, ['Train', 'Test'], loc="lower right")

    plt.tight_layout()
    plt.show()

    if save_path:
        png_path = os.path.join(save_path,
f"{title}_Overlapped_Permutation_Importance3.png")
        tiff_path = os.path.join(save_path,
f"{title}_Overlapped_Permutation_Importance3.tiff")

        fig.savefig(png_path, dpi=1000)
        fig.savefig(tiff_path, dpi=1000)

    plt.close(fig)  # close the figure
# Create directories if they don't exist
save_directory = "path_to_save_directory"
if not os.path.exists(save_directory):
    os.makedirs(save_directory)
    # Models to visualize
models_to_plot = ['XGBoostRegressor', 'Random Forest', 'Bagging',
'Gradient Boosting',"LightGBMRegressor"]
# Fit the models and visualize
for name in models_to_plot:
    model = regressors[name]
    model.fit(X_train, y_train)
    plot_permutation_importance(model, X_train, y_train, X_test,
y_test, title=name, save_path=save_directory)
```

You can use the code below to get hyperparameters of all models that is used for the regression.In addition to test and train R^2 values you can obtain other regression metrics such as MAE, MSE, RMSE, MAPE with the code below.

```
import pandas as pd
import numpy as np
```

```
import warnings
from sklearn.linear_model import (HuberRegressor, RANSACRegressor,
TheilSenRegressor,
                                  OrthogonalMatchingPursuit,
PoissonRegressor,
                                  TweedieRegressor, RidgeCV, Lasso,
                                  ElasticNet, SGDRegressor,
BayesianRidge)
from sklearn.kernel_ridge import KernelRidge
from sklearn.model_selection import GridSearchCV, train_test_split
from sklearn.preprocessing import StandardScaler, LabelEncoder
from sklearn.metrics import r2_score, mean_squared_error,
mean_absolute_error
from sklearn.ensemble import (RandomForestRegressor,
GradientBoostingRegressor,
                              AdaBoostRegressor, BaggingRegressor,
StackingRegressor)
from sklearn.tree import DecisionTreeRegressor
from sklearn.svm import SVR
from sklearn.neighbors import KNeighborsRegressor
from sklearn.gaussian_process import GaussianProcessRegressor
from xgboost import XGBRegressor
from lightgbm import LGBMRegressor
from pygam import LinearGAM, s, f

# Define a function to calculate Mean Absolute Percentage Error
def mean_absolute_percentage_error(y_true, y_pred):
    y_true, y_pred = np.array(y_true), np.array(y_pred)
    return np.mean(np.abs((y_true - y_pred) / (y_true + 1e-6))) *
100

# Loading the dataset
data = pd.read_csv('path_to_your_data')

# Transforming the target variable by applying a logarithmic
function to make the distribution more symmetric
data['Target_log'] = np.log(data['Target'] + 1)

# Data preparation by dropping irrelevant columns
```

```
X = data.drop(columns=['List_of_columns_to_drop'])
y = data['Target_log']  # Specifying the target variable

# Encode categorical features
for col in X.select_dtypes(include='object').columns:
    le = LabelEncoder()
    X[col] = le.fit_transform(X[col])

# Split the dataset into train and test sets
X_train, X_test, y_train, y_test = train_test_split(X, y,
test_size=0.3, random_state=42)

# Standardize the features
scaler = StandardScaler()
X_train = scaler.fit_transform(X_train)
X_test = scaler.transform(X_test)

# Define a dictionary with models
regressors = {
    'Random Forest': RandomForestRegressor(n_estimators=100,
max_depth=None, min_samples_leaf=1, min_samples_split=2,
random_state=42),
    'Gradient Boosting':
GradientBoostingRegressor(random_state=42),
    'AdaBoost': AdaBoostRegressor(random_state=42),
    'Bagging': BaggingRegressor(n_estimators=30, max_features=1.0,
max_samples=1.0, random_state=42),
    'Decision Tree':
DecisionTreeRegressor(criterion='friedman_mse', max_depth=9,
min_samples_leaf=2, min_samples_split=2, splitter='best',
random_state=42),
    'Support Vector': SVR(),
    'K-Neighbors': KNeighborsRegressor(),
    'RidgeCV': RidgeCV(),
    'Lasso': Lasso(),
    'ElasticNet': ElasticNet(),
    'SGD': SGDRegressor(),
    'Gaussian Process': GaussianProcessRegressor(),
    'BayesianRidge': BayesianRidge(),
```

```
    'XGBoostRegressor': XGBRegressor(colsample_bytree=0.9,
learning_rate=0.1, max_depth=7, n_estimators=200, subsample=0.8,
random_state=42),
    'LightGBMRegressor': LGBMRegressor(),
    'SVR_poly': SVR(kernel='poly'),
    'SVR_sigmoid': SVR(kernel='sigmoid'),
    'SVR_rbf': SVR(kernel='rbf'),
    'HuberRegressor': HuberRegressor(),
    'SVR_linear': SVR(kernel='linear'),
    'RANSACRegressor': RANSACRegressor(),
    'TheilSenRegressor': TheilSenRegressor(),
    'KernelRidge': KernelRidge(),
    'OMP': OrthogonalMatchingPursuit(),
    'PoissonRegressor': PoissonRegressor(),
    'TweedieRegressor': TweedieRegressor()
}

# Initialize lists to store results
results = []
stacked_results = []

# Fit models and evaluate performance
# Extend the script to save hyperparameters of each model
for model_name, model in regressors.items():
    model.fit(X_train, y_train)
    y_train_pred = model.predict(X_train)
    y_test_pred = model.predict(X_test)

    # Extract hyperparameters of the model
    hyperparameters = model.get_params()

    # Calculate metrics and store them along with hyperparameters
in the results list
    results.append({
        'Model': model_name,
        'Hyperparameters': hyperparameters,  # Save hyperparameters
as a nested dictionary
        'Train R2 Score': r2_score(y_train, y_train_pred),
        'Test R2 Score': r2_score(y_test, y_test_pred),
```

```
        'Train MSE': mean_squared_error(y_train, y_train_pred),
        'Train RMSE': np.sqrt(mean_squared_error(y_train,
y_train_pred)),
        'Train MAE': mean_absolute_error(y_train, y_train_pred),
        'Train MAPE': mean_absolute_percentage_error(y_train,
y_train_pred),
        'Test MSE': mean_squared_error(y_test, y_test_pred),
        'Test RMSE': np.sqrt(mean_squared_error(y_test,
y_test_pred)),
        'Test MAE': mean_absolute_error(y_test, y_test_pred),
        'Test MAPE': mean_absolute_percentage_error(y_test,
y_test_pred)
    })
# Define and fit a GAM model
gam = LinearGAM(s(0) + s(1)).fit(X_train, y_train)
gam_train_pred = gam.predict(X_train)
gam_test_pred = gam.predict(X_test)

# Also, save the hyperparameters of the GAM model
gam_hyperparameters = {'terms': str(gam.terms)}  # Extract relevant
hyperparameters or configurations

results.append({
    'Model': 'GAM',
    'Hyperparameters': gam_hyperparameters,
    'Train R2 Score': r2_score(y_train, gam_train_pred),
    'Test R2 Score': r2_score(y_test, gam_test_pred),
    'Train MSE': mean_squared_error(y_train, gam_train_pred),
    'Train RMSE': np.sqrt(mean_squared_error(y_train,
gam_train_pred)),
    'Train MAE': mean_absolute_error(y_train, gam_train_pred),
    'Train MAPE': mean_absolute_percentage_error(y_train,
gam_train_pred),
    'Test MSE': mean_squared_error(y_test, gam_test_pred),
    'Test RMSE': np.sqrt(mean_squared_error(y_test,
gam_test_pred)),
    'Test MAE': mean_absolute_error(y_test, gam_test_pred),
    'Test MAPE': mean_absolute_percentage_error(y_test,
gam_test_pred)
```

```
})

# For stacked models, you can save the names of the models being
stacked as hyperparameters
for stacked_model in stacked_results:
    model_names = [estimator[0] for estimator in
stacking_regressor.estimators_]
    stacked_model['Hyperparameters'] = {'Models': model_names}

# Save results to DataFrames and then to CSV or Excel
results_df = pd.DataFrame(results)
stacked_results_df = pd.DataFrame(stacked_results)
results_df.to_csv('path_to_save_your_results/results_with_hyperpara
meters.csv', index=False)
stacked_results_df.to_csv('path_to_save_your_results_of_stacked_mod
els/stacked_results_with_hyperparameters.csv', index=False)
```

Box Plots

You can adjust the code below to get different box plots.

```
# Importing required libraries
import seaborn as sns  # For data visualization
import matplotlib.pyplot as plt  # For plotting graphs
import pandas as pd  # For handling dataframes

# Load the dataset from the specified path
data = pd.read_csv('path_to_your_file/file_name.csv')

# Log-transforming the target variable to adjust the scale and make
the distribution more normal
data['Cellular_Uptake_pg_Au_cell_log'] =
np.log(data['Cellular_Uptake_pg_Au_cell'] + 1)

# Correcting typo in 'Certain_column' column if exists
if 'Wrong_typo' in data['Certain_column'].values:
    data['Certain_column'] = data['Certain_column
'].replace('Wrong_typo', 'Corrected_typo')
```

```
# Simplifying labels for 'Coating_subgrouped'; While collecting
data, much more definitive column or row names could be exist,
before visualize them it is better to simplify.
label_replacements = {
    'Albumin_containing': 'Albumin',
    'DNA_modified_DNA': 'DNA',
    'Small_molecule': 'Small molecule',
    'Polymeric_protein': 'Polymer and protein',
    'Metallic_metal_oxide': 'Metal',
    'Peptide_antibody': 'Peptide'
}
data['Coating_subgrouped'].replace(label_replacements,
inplace=True)

# Defining bins for 'Concentration' and 'Exposure Time' since there
should be lots of different individual concentration and exposure
time values,
# Same approach can be used for other continuous variables
concentration_bins = [0, 2, 5, 10, 20, 30, 50, 80, 100, 200, 1000]
exposure_bins = [0, 1, 2, 3, 4, 6, 8, 12, 16, 18, 24, 48, 72]

# Creating new categorical variables representing the bins with
labels as the upper limit of the bins
data['Concentration_Binned'] = pd.cut(data['Concentration_µg/ml'],
bins=concentration_bins, labels=concentration_bins[1:], right=True,
include_lowest=True)
data['Exposure_Binned'] = pd.cut(data['Exposure_time_h'],
bins=exposure_bins, labels=exposure_bins[1:], right=True,
include_lowest=True)

# Specifying the output directory to save the plots
output_directory = "output_directory_to_save_results/Box_plots"

# Define a constant width for each box in the box plots; otherwise
the widths will vary depending on the variables
box_width = 0.3
```

```
# Defining a function to create and save box plots with specified
parameters
def create_and_save_box_plot(x, y, data, xlabel, title, filename):
    plt.figure(figsize=(12, 6))  # Setting figure size
    sns.boxplot(x=x, y=y, data=data, color='#e1e1e0',
width=box_width)  # Creating a box plot with a constant width for
each box with certain color
    plt.title(title, fontsize=20)  # Setting title and font size
    plt.xlabel(xlabel, fontsize=20)  # Setting x-label and font
size
    plt.ylabel('Cellular Uptake (pg Au/cell)\n', fontsize=20)  #
Setting y-label and font size
    plt.xticks(rotation=45, fontsize=20)  # Adjusting x-axis tick
labels' rotation and font size
    plt.yticks(fontsize=20)  # Adjusting y-axis tick labels' font
size
    plt.tight_layout()  # Adjusting layout to prevent clipping
    plt.savefig(f"{output_directory}/{filename}2.png",
format='png', dpi=1000)  # Saving the plot in PNG format with
specified dpi
    plt.show()  # Displaying the plot

# Creating and saving box plots for various variables against
cellular uptake
create_and_save_box_plot('Concentration_Binned',
'Cellular_Uptake_pg_Au_cell', data, 'Concentration (µg/ml)\n',
'Cellular Uptake vs Concentration\n',
'Concentration_Box_Plot_Not_Transformed')
create_and_save_box_plot('Exposure_Binned',
'Cellular_Uptake_pg_Au_cell', data, 'Exposure Duration (hours)\n',
'Cellular Uptake vs Exposure Duration\n',
'Exposure_Box_Plot_Not_Transformed')
create_and_save_box_plot('Coating_category',
'Cellular_Uptake_pg_Au_cell', data, 'Coating Category\n', 'Cellular
Uptake vs Coating Category\n',
'Coating_Category_Box_Plot_Not_Transformed')
create_and_save_box_plot('Shape', 'Cellular_Uptake_pg_Au_cell',
data, 'Shape\n', 'Cellular Uptake vs Shape\n',
'Shape_Box_Plot_Not_Transformed')
```

```
create_and_save_box_plot('Coating_subgrouped',
'Cellular_Uptake_pg_Au_cell', data, 'Coating Subgrouped', 'Cellular
Uptake vs Coating Subgrouped\n',
'Coating_Subgrouped_Box_Plot_Not_Transformed')
```

GitHub

In order to achieve publicly available data and code repository you may create files and folder in GitHub platform. Below you can find the steps to upload your codes and files to a publicly available repository.
https://github.com/BilgiEyup

1. Open the terminal and give your folders destination.
   cd /path_to_your_Github_folder
2. Initialize a new Git repository; if you have already a repository you may pass these steps
   git init

3. From remote you can open a repository as shown in below

   git remote add origin https://github.com/Your_Profile_Name/The_name_of_the_folders_you_want_to_create.git

4. Fetch the latest version of the remote repository

   git fetch origin main

5. Create ne branch

   git checkout main

6. Merge the folders in your local space with the git folders

   git merge origin/main

7. Add the changes within the your local folders to the git folders

   git add .

8. Commit your changes

   git commit -m "Added new content from Github_folder"

9. Push the changes to GitHub repository

   git push origin main

10. You may have been asked to enter your Github profile informations.

Link for the GitHub Repository Created for This Thesis

Either you can visit it from https://github.com/BilgiEyup or you can scan the QRcode below and navigate through the repository.

Link to GitHub Repository with Uploaded Dataset

In this thesis, the datasets utilized encompass nearly ten thousand rows. Due to the extensive volume of data, it has not been feasible to include all raw data within the thesis document. For comprehensive review and further analysis, interested parties are invited to access the complete datasets. These are available through the link and QR codes provided below, which direct to the thesis' GitHub repository

Either you can visit it from https://github.com/BilgiEyup/Data_Sets or you can scan the QRcode below and navigate through the repository.

Format of the Datasets

In Table S8, the first 35 rows of the gold nanomaterials dataset are presented. The complete datasets can be downloaded from the GitHub repositories, the links to which are provided above.

Table S7. First 35 rows for Gold dataset

Row_number	Particle_ID	Coating_presence	Coating_type	Coating_category	TEM_SEM_Diameter_nm	DLS_diameter_nm	Concentration_mg/ml
1	1	Uncoated	Uncoated	Uncoated	25	NA	0.00
2	1	Uncoated	Uncoated	Uncoated	25	NA	50.00
3	1	Uncoated	Uncoated	Uncoated	25	NA	50.00
4	1	Uncoated	Uncoated	Uncoated	25	NA	50.00
5	1	Uncoated	Uncoated	Uncoated	25	NA	0.00
6	1	Uncoated	Uncoated	Uncoated	25	NA	50.00
7	1	Uncoated	Uncoated	Uncoated	25	NA	50.00
8	1	Uncoated	Uncoated	Uncoated	25	NA	50.00
9	2	Coated	Acaica_Gum_(Polysaccaride)	Polymer	25	NA	0.00
10	2	Coated	Acaica_Gum_(Polysaccaride)	Polymer	25	NA	50.00
11	2	Coated	Acaica_Gum_(Polysaccaride)	Polymer	25	NA	50.00
12	2	Coated	Acaica_Gum_(Polysaccaride)	Polymer	25	NA	50.00
13	2	Coated	Acaica_Gum_(Polysaccaride)	Polymer	25	NA	0.00
14	2	Coated	Acaica_Gum_(Polysaccaride)	Polymer	25	NA	50.00
15	2	Coated	Acaica_Gum_(Polysaccaride)	Polymer	25	NA	50.00
16	2	Coated	Acaica_Gum_(Polysaccaride)	Polymer	25	NA	50.00
17	3	Coated	Human_Serum_Albumin	Peptide/Protein/DNA	NA	10	0.00
18	3	Coated	Human_Serum_Albumin	Peptide/Protein/DNA	NA	10	10.00
19	3	Coated	Human_Serum_Albumin	Peptide/Protein/DNA	NA	10	15.00
20	3	Coated	Human_Serum_Albumin	Peptide/Protein/DNA	NA	10	30.00
21	3	Coated	Human_Serum_Albumin	Peptide/Protein/DNA	NA	10	50.00
22	3	Coated	Human_Serum_Albumin	Peptide/Protein/DNA	NA	10	0.00
23	3	Coated	Human_Serum_Albumin	Peptide/Protein/DNA	NA	10	10.00
24	3	Coated	Human_Serum_Albumin	Peptide/Protein/DNA	NA	10	15.00
25	3	Coated	Human_Serum_Albumin	Peptide/Protein/DNA	NA	10	30.00
26	3	Coated	Human_Serum_Albumin	Peptide/Protein/DNA	NA	10	50.00
27	3	Coated	Human_Serum_Albumin	Peptide/Protein/DNA	NA	10	0.00
28	3	Coated	Human_Serum_Albumin	Peptide/Protein/DNA	NA	10	10.00
29	3	Coated	Human_Serum_Albumin	Peptide/Protein/DNA	NA	10	15.00
30	3	Coated	Human_Serum_Albumin	Peptide/Protein/DNA	NA	10	30.00
31	3	Coated	Human_Serum_Albumin	Peptide/Protein/DNA	NA	10	50.00
32	4	Coated	Citrate	Small_molecule	5.2	5	0.00
33	4	Coated	Citrate	Small_molecule	5.2	5	10.00
34	4	Coated	Citrate	Small_molecule	5.2	5	15.00
35	4	Coated	Citrate	Small_molecule	5.2	5	30.00

(cont. on next page)

Table S8. (cont.)

Row_number	Cell_viability (%)	Zeta_potential_mV	Cells	Cell_nature	Cell_origin	Cell_source	Cell_species	Cell_morphology
1	100.00	NA	mESC	Healthy	Cell line	Animal	Mouse	Epithelial
2	60.83	NA	mESC	Healthy	Cell line	Animal	Mouse	Epithelial
3	37.34	NA	mESC	Healthy	Cell line	Animal	Mouse	Epithelial
4	29.88	NA	mESC	Healthy	Cell line	Animal	Mouse	Epithelial
5	100.00	NA	MEF	Healthy	Cell line	Animal	Mouse	Fibroblast
6	56.81	NA	MEF	Healthy	Cell line	Animal	Mouse	Fibroblast
7	52.15	NA	MEF	Healthy	Cell line	Animal	Mouse	Fibroblast
8	42.84	NA	MEF	Healthy	Cell line	Animal	Mouse	Fibroblast
9	100.00	NA	mESC	Healthy	Cell line	Animal	Mouse	Epithelial
10	40.32	NA	mESC	Healthy	Cell line	Animal	Mouse	Epithelial
11	26.15	NA	mESC	Healthy	Cell line	Animal	Mouse	Epithelial
12	16.07	NA	mESC	Healthy	Cell line	Animal	Mouse	Epithelial
13	100.00	NA	MEF	Healthy	Cell line	Animal	Mouse	Fibroblast
14	53.84	NA	MEF	Healthy	Cell line	Animal	Mouse	Fibroblast
15	23.80	NA	MEF	Healthy	Cell line	Animal	Mouse	Fibroblast
16	22.09	NA	MEF	Healthy	Cell line	Animal	Mouse	Fibroblast
17	100.00	-56	HDFa	Healthy	Primary cells	Human	Human	Fibroblast
18	91.27	-56	HDFa	Healthy	Primary cells	Human	Human	Fibroblast
19	93.46	-56	HDFa	Healthy	Primary cells	Human	Human	Fibroblast
20	71.99	-56	HDFa	Healthy	Primary cells	Human	Human	Fibroblast
21	72.37	-56	HDFa	Healthy	Primary cells	Human	Human	Fibroblast
22	100.00	-56	HDFa	Healthy	Primary cells	Human	Human	Fibroblast
23	182.26	-56	HDFa	Healthy	Primary cells	Human	Human	Fibroblast
24	166.53	-56	HDFa	Healthy	Primary cells	Human	Human	Fibroblast
25	159.84	-56	HDFa	Healthy	Primary cells	Human	Human	Fibroblast
26	152.84	-56	HDFa	Healthy	Primary cells	Human	Human	Fibroblast
27	100.00	-56	HDFa	Healthy	Primary cells	Human	Human	Fibroblast
28	151.35	-56	HDFa	Healthy	Primary cells	Human	Human	Fibroblast
29	158.92	-56	HDFa	Healthy	Primary cells	Human	Human	Fibroblast
30	200.00	-56	HDFa	Healthy	Primary cells	Human	Human	Fibroblast
31	191.35	-56	HDFa	Healthy	Primary cells	Human	Human	Fibroblast
32	100.00	-49	HDFa	Healthy	Primary cells	Human	Human	Fibroblast
33	92.86	-49	HDFa	Healthy	Primary cells	Human	Human	Fibroblast
34	85.71	-49	HDFa	Healthy	Primary cells	Human	Human	Fibroblast
35	81.43	-49	HDFa	Healthy	Primary cells	Human	Human	Fibroblast

Table S8. (cont.)

Row_number	Cell_age	Cell_organ_tissue_source	Exposure_time_h	Viability_test	Test_indicator	Reference_DOI
1	Embryonic	Embryo	0	MTT	Tetrazolium_salt	doi:10.1016/j.taap.2008.09.015
2	Embryonic	Embryo	24	MTT	Tetrazolium_salt	doi:10.1016/j.taap.2008.09.015
3	Embryonic	Embryo	48	MTT	Tetrazolium_salt	doi:10.1016/j.taap.2008.09.015
4	Embryonic	Embryo	72	MTT	Tetrazolium_salt	doi:10.1016/j.taap.2008.09.015
5	Embryonic	Embryo	0	MTT	Tetrazolium_salt	doi:10.1016/j.taap.2008.09.015
6	Embryonic	Embryo	24	MTT	Tetrazolium_salt	doi:10.1016/j.taap.2008.09.015
7	Embryonic	Embryo	48	MTT	Tetrazolium_salt	doi:10.1016/j.taap.2008.09.015
8	Embryonic	Embryo	72	MTT	Tetrazolium_salt	doi:10.1016/j.taap.2008.09.015
9	Embryonic	Embryo	0	MTT	Tetrazolium_salt	doi:10.1016/j.taap.2008.09.015
10	Embryonic	Embryo	24	MTT	Tetrazolium_salt	doi:10.1016/j.taap.2008.09.015
11	Embryonic	Embryo	48	MTT	Tetrazolium_salt	doi:10.1016/j.taap.2008.09.015
12	Embryonic	Embryo	72	MTT	Tetrazolium_salt	doi:10.1016/j.taap.2008.09.015
13	Embryonic	Embryo	0	MTT	Tetrazolium_salt	doi:10.1016/j.taap.2008.09.015
14	Embryonic	Embryo	24	MTT	Tetrazolium_salt	doi:10.1016/j.taap.2008.09.015
15	Embryonic	Embryo	48	MTT	Tetrazolium_salt	doi:10.1016/j.taap.2008.09.015
16	Embryonic	Embryo	72	MTT	Tetrazolium_salt	doi:10.1016/j.taap.2008.09.015
17	Embryonic	Skin_epidermis	6	MTS	Tetrazolium_salt	doi.org/10.1007/s11051-012-1374-7
18	Embryonic	Skin_epidermis	6	MTS	Tetrazolium_salt	doi.org/10.1007/s11051-012-1374-7
19	Embryonic	Skin_epidermis	6	MTS	Tetrazolium_salt	doi.org/10.1007/s11051-012-1374-7
20	Embryonic	Skin_epidermis	6	MTS	Tetrazolium_salt	doi.org/10.1007/s11051-012-1374-7
21	Embryonic	Skin_epidermis	6	MTS	Tetrazolium_salt	doi.org/10.1007/s11051-012-1374-7
22	Embryonic	Skin_epidermis	24	MTS	Tetrazolium_salt	doi.org/10.1007/s11051-012-1374-7
23	Embryonic	Skin_epidermis	24	MTS	Tetrazolium_salt	doi.org/10.1007/s11051-012-1374-7
24	Embryonic	Skin_epidermis	24	MTS	Tetrazolium_salt	doi.org/10.1007/s11051-012-1374-7
25	Embryonic	Skin_epidermis	24	MTS	Tetrazolium_salt	doi.org/10.1007/s11051-012-1374-7
26	Embryonic	Skin_epidermis	24	MTS	Tetrazolium_salt	doi.org/10.1007/s11051-012-1374-7
27	Embryonic	Skin_epidermis	48	MTS	Tetrazolium_salt	doi.org/10.1007/s11051-012-1374-7
28	Embryonic	Skin_epidermis	48	MTS	Tetrazolium_salt	doi.org/10.1007/s11051-012-1374-7
29	Embryonic	Skin_epidermis	48	MTS	Tetrazolium_salt	doi.org/10.1007/s11051-012-1374-7
30	Embryonic	Skin_epidermis	48	MTS	Tetrazolium_salt	doi.org/10.1007/s11051-012-1374-7
31	Embryonic	Skin_epidermis	48	MTS	Tetrazolium_salt	doi.org/10.1007/s11051-012-1374-7
32	Embryonic	Skin_epidermis	6	MTS	Tetrazolium_salt	doi.org/10.1007/s11051-012-1374-7
33	Embryonic	Skin_epidermis	6	MTS	Tetrazolium_salt	doi.org/10.1007/s11051-012-1374-7
34	Embryonic	Skin_epidermis	6	MTS	Tetrazolium_salt	doi.org/10.1007/s11051-012-1374-7
35	Embryonic	Skin_epidermis	6	MTS	Tetrazolium_salt	doi.org/10.1007/s11051-012-1374-7

PUBLICATIONS

The research articles that have resulted from this thesis are given below, followed by conference papers, presentations, and reward:

Journals:

Eyup BILGI, David A. WINKLER & Ceyda OKSEL KARAKUS (2023) Identifying factors controlling cellular uptake of gold nanoparticles by machine learning, Journal of Drug Targeting, DOI: 10.1080/1061186X.2023.2288995

Eyup BILGI, Ceyda ÖKSEL KARAKUŞ. Machine learning-assisted prediction of the toxicity of silver nanoparticles: a meta-analysis. *J Nanopart Res* **25**, 157 (2023). DOI:10.1007/s11051-023-05806-2

Ceyda ÖKSEL KARAKUS, **Eyup BILGI** & David A. WINKLER (2021) Biomedical nanomaterials: applications, toxicological concerns, and regulatory needs, Nanotoxicology, 15:3, 331-351, DOI: 10.1080/17435390.2020.1860265

Conference Paper:

Eyup BILGI & Ceyda ÖKSEL KARAKUŞ. Machine-learning assisted insights into cytotoxicity of zinc oxide nanoparticles (accepted).

Conference Presentations

Eyup BILGI & Ceyda ÖKSEL KARAKUŞ (2022). Computational nanotoxicology: a case study with silver and zinc nanomaterials. Toxicology Letters. DOI:10.1016/j.toxlet.2022.07.304

Eyup BILGI & Ceyda ÖKSEL KARAKUŞ (2023). Machine-learning assisted insights into cytotoxicity of zinc oxide nanoparticles, NanoSafe2023, June 5-9th 2023.

Awards

International Congress of Toxicology 2022 EUROTOX Travel Bursary (Free registration and 500 Euro on site award) for the application for "Computational nanotoxicology: a case study with silver and zinc nanomaterials."

VITA

Eyüp Bilgi

Education and Work Experiences

- 2017 –2023: **PhD**, IZTECH, Material Science and Engineering
- 2012 – 2015: **MSc**, Ege University Department of Biomedical Technologies
- 2008 – 2012: **BSc**, Ege University Department of Bioengineering
- 2017 – Still Continued: Research Assistant at Izmir Institute of Technology
- 2015 – 2021: Founder and Manager at Bilgi Biotechnological Products LLC.
- 2014 – 2015: Research Assistant at Adana Science and Technology University

Selected Publications

- Kale, İ., Kırdök, O., **Bilgi, E**., et. al. (2023). DOI:10.1007/978-3-031-24942-6_16
- E. Alperay Tarim, Muge Anil Inevi, Ilayda Ozkan, Seren Kecili, **Eyup Bilgi et. al.**.(2023) DOI: 10.1007/s10544-023-00649-z.
- **Bilgi, E.**, Homan Gokce, E., Bayir, E. *et al.* (2023). DOI:10.1007/s10570-021-04106-z
- Karakoyun, Ç., Küçüksolak, M., **Bilgi, E.**, Doğan, G., Çömlekçi, Y. E., & Bedir, E. (2021). DOI: 10.1016/j.phytol.2020.12.003
- Bayir, E**., Bilgi, E.,** Hames, E. E., & Sendemir, A. (2019). DOI:10.1007/s10570-019-02763-9
- ÜRKMEZ, A. Ş., Bayir, E., **BİLGİ, E**., & ÖZEN, M. Ö. (2017). DOI:10.3906/biy-1608-61
- **E. Bilgi,** E. Bayir, A. Sendemir-Urkmez, E. E. Hames-Kocabas (2016):DOI: /10.1016/j.ijbiomac.2016.02.052
- E. Bayir, **E. Bilgi,** A. Sendemir-Urkmez, E. E. Hames-Kocabas (2015) DOI: 10.3109/15368378.2013.853671